



Wiles, Alan Andrew (2013) *Redox active molecules with molecular electronics and synthetic applications*. PhD thesis.

<http://theses.gla.ac.uk/4878/>

Copyright and moral rights for this work are retained by the author

A copy can be downloaded for personal non-commercial research or study, without prior permission or charge

This work cannot be reproduced or quoted extensively from without first obtaining permission in writing from the author

The content must not be changed in any way or sold commercially in any format or medium without the formal permission of the author

When referring to this work, full bibliographic details including the author, title, awarding institution and date of the thesis must be given

Glasgow Theses Service

<http://theses.gla.ac.uk/>

theses@ gla.ac.uk

**REDOX ACTIVE MOLECULES
WITH MOLECULAR ELECTRONICS AND SYNTHETIC APPLICATIONS**

Thesis submitted in fulfilment of the requirements

**For the degree of
Doctor of Philosophy**

**School of Chemistry
College of Science and Engineering
University of Glasgow**

August 2013

Alan Andrew Wiles

**The School of Chemistry
Joseph Black Building
University of Glasgow
Glasgow
G12 8QQ**

ABSTRACT:

REDOX ACTIVE MOLECULES WITH MOLECULAR ELECTRONICS AND SYNTHETIC APPLICATIONS.

Alan Andrew Wiles, Doctor of Philosophy, The University of Glasgow, 2013

Redox active molecules are ubiquitous to nature and have properties that make them coveted targets for applications in areas of synthesis as well as for the development of materials. This thesis describes the synthesis and characterisation of several flavin donor-acceptor dyads designed around an oligothiophene donor backbone and a flavin acceptor moiety. These show potential applications as optoelectronic materials. It also describes the synthesis of a ferrocene-flavin tetracyanobutadiene super-acceptor compound which showed preliminary evidence of non-linear-optic effects. Finally, a novel method was developed to investigate the redox umpolung activated reactions of vinylferrocene. The vinyl group of vinylferrocene was activated by polarity inversion of ferrocene to ferrocenium and was able to undergo Diels-Alder cycloadditions with cyclobutadiene and furan, as well as, Markovnikov addition of thiols. These reactions were then used to explore the use of vinylferrocene as a redox auxiliary and as a redox active tag in polymers and have the potential to be used in nanoparticles as well as biological systems.

TABLE OF CONTENT:

Abstract	p. 2
List of tables	p. 8
List of figures and schemes	p. 9
Acknowledgements	p. 16
Declaration	p. 17
Definitions and abbreviations	p. 18
<u>CHAPTER I: GENERAL INTRODUCTION</u>	p. 20
1. Flavins	p. 20
1.1. <u>History of Flavins:</u>	p. 20
1.2. <u>Properties:</u>	p. 22
1.3. <u>Applications:</u>	p. 26
1.3.1. <u>Flavins in synthesis and catalysis:</u>	p. 27
1.3.2. <u>Flavins as molecular devices:</u>	p. 30
<u>-Optical probes:</u>	p. 30
<u>-Molecular machines:</u>	p. 33
<u>-Molecular electronic devices:</u>	p. 34
2. Ferrocene	p. 38
2.1. <u>History of ferrocene:</u>	p. 38
2.2. <u>Reactions of ferrocene:</u>	p. 39
2.3. <u>Properties:</u>	p. 39
2.3.1. <u>Electrochemistry:</u>	p. 39
2.3.2. <u>Electron richness:</u>	p. 40

Redox active molecules with molecular electronics and synthetic applications

2.4. <u>Applications:</u>	p. 40
2.4.1. <u>Ferrocene as a catalyst:</u>	p. 41
2.4.2. <u>Application in medicinal chemistry:</u>	p. 42
2.4.3. <u>Materials:</u>	p. 43
<u>CHAPTER II: SYNTHESIS AND CHARACTERISATION OF</u>	p. 47
<u>8-ETHYL-6,7-BISTHIOPHENE-THIOPTERIDINE-2,4-(3H,8H)-DIONE</u>	
<u>AND ITS DERIVATIVES AS MATERIALS FOR OPTOELECTRONIC</u>	
<u>APPLICATIONS.</u>	
1. Introduction	p. 47
1.1. <u>The photovoltaic (PV) effect:</u>	p. 47
1.2. <u>Overview of PV in the global market:</u>	p. 49
1.3. <u>Emerging organic photovoltaics:</u>	p. 50
1.3.1. <u>Dye-sensitised solar cells (DSSC):</u>	p. 52
1.3.2. <u>Quantum dot solar cells (QDSC):</u>	p. 54
1.3.3. <u>Organic/polymer solar cells (OPV):</u>	p. 55
<u>-Device architecture:</u>	p. 55
<u>-Mode of action:</u>	p. 56
<u>-Active layer materials:</u>	p. 57
2. Aims	p. 62
3. Results and discussion	p. 66
3.1. <u>Synthesis of 8-ethyl-6,7-bisthiophene-thiopteridine-2,4-(3H,8H)-</u>	p. 66
<u>dione 47:</u>	
3.1.1. <u>Synthesis of 3,4-dinitro-2,5-dibromothiophene 50:</u>	p. 66

Redox active molecules with molecular electronics and synthetic applications

3.1.2. <u>Synthesis of 3',4'-dinitro-[2,2',5',2'']-terthiophene 51:</u>	p. 67
3.1.3. <u>Reduction of nitro groups:</u>	p. 68
3.1.4. <u>Synthesis N-Ethyl-[2,2',5',2'']-terthiophene-3',4'-diamine 54:</u>	p. 69
<u>-Acylation and reduction:</u>	p. 70
<u>-Direct alkylation:</u>	p. 71
3.1.5. <u>Alloxan condensation:</u>	p. 72
3.2. <u>Analysis and characterisation of compound 47:</u>	p. 73
3.3. <u>Synthesis and characterisation of flavin dyads for optoelectronic applications:</u>	p. 74
3.4. <u>Analysis and characterisation:</u>	p. 77
<u>-UV-vis spectroscopy:</u>	p. 77
<u>-Voltammetry studies:</u>	p. 78
<u>-Optoelectronic data:</u>	p. 79
4. Conclusions	p. 82
5. Future work	p. 83
CHATER III: SYNTHESIS AND CHARACTERISATION OF 8-(3'-FERROCENE-1',1',4',4'-TETRACIANO BUTADIENE)-10-ISOBUTYL FLAVIN AS AN ORGANIC ELECTRON SUPER-ACCEPTOR.	p. 85
1. Introduction	p. 85
2. Aims	p. 92
3. Results and discussion	p. 94
3.1. <u>First approach:</u>	p. 94
3.2. <u>Synthesis of N-(5-chloro-2-nitro-phenyl)isobutyramide 80:</u>	p. 95

Redox active molecules with molecular electronics and synthetic applications

3.3. <u>Synthesis of <i>N</i>-(2-nitro-4-ethynylferrocene-phenyl)isobutyramide 81:</u>	p. 96
3.4. <u>Synthesis of 8-ethynylferrocene-10-isobutyl-benzopteridine-2,4(3<i>H</i>, 10<i>H</i>) dione 72:</u>	p. 98
3.5. <u>Synthesis of 2-(ferrocene)-3-[8-(10-isobutyl-benzopteridine-2,4(3<i>H</i>, 10<i>H</i>)dione)]-1,4-butadiene-1,1,5,5-tetracarbonitrile 71:</u>	p. 100
3.6. <u>Analysis and Characterisation:</u>	p. 100
<u>-UV-vis spectroscopy:</u>	p. 101
<u>-Cyclic voltammetry studies:</u>	p. 102
<u>-Optical and electronic data:</u>	p. 103
4. Conclusions	p. 104
5. Future work	p. 105
CHAPTER IV: NEW REDOX UMPOLUNG MEDIATED REACTIONS OF VINYLFERROCENE.	p. 108
1. Introduction	p. 108
1.1. <u>Umpolung chemistry: concept and history</u>	p. 108
1.2. <u>Synthetic examples of umpolung chemistry:</u>	p. 109
1.2.1. <u>Examples of umpolung by chemical conversion:</u>	p. 110
<u>-Chemistry of dithianes:</u>	p. 110
<u>-<i>N</i>-Heterocyclic carbenes and organocatalysis:</u>	p. 111
1.3. <u>Redox umpolung (Ferrocene):</u>	p. 112
2. Aims	p. 116
2.1. <u>Cycloadditions:</u>	p. 117

Redox active molecules with molecular electronics and synthetic applications

2.2. <u>Umpolung nucleophilic additions:</u>	p. 119
3. Results and discussion	p. 121
3.1. <u>Reduction of ferrocium hexafluorophosphate 18 PF₆:</u>	p. 121
3.2. <u>Umpolung controled cycloaddition of vinylferrocene 19:</u>	p. 122
3.2.1. <u>Cycloadditions with cyclopentadiene 92:</u>	p. 123
<u>-Control reaction without oxidising agent:</u>	p. 123
<u>-Optimisation of conditions:</u>	p. 123
<u>-Characterisation of products:</u>	p. 125
3.2.2. <u>Cycloadditions with furan 95:</u>	p. 129
3.2.3. <u>Oxidation and reduction of vinylferrocene 19 in absence of a diene:</u>	p. 130
3.3. <u>Reactions of 6-ferrocene-bicyclo[2.2.1]hept-2-ene 93:</u>	p. 133
3.3.1. <u>Ferrocene as a redox auxiliary:</u>	p. 133
<u>-Synthesis of 1-cyclopentane-bicyclo[2.2.1]heptane 104:</u>	p. 135
3.3.2. <u>Ring opening metathesis-cross metathesis (ROM-CM):</u>	p. 137
3.3.3. <u>Ring opening metathesis polymerisation (ROMP):</u>	p. 141
3.4. <u>Umpolung controlled nucleophilic additions:</u>	p. 142
3.4.1. <u>Control reaction without oxidising agent:</u>	p. 142
3.4.2. <u>Umpolung activated reactions of vinylferrocene 19 with thiols:</u>	p. 143
4. Conclusions	p. 150
5. Future work	p. 151
CHAPTER V: EXPERIMENTAL	p. 153
Apendices	p. 175
References	p. 190

LIST OF TABLES AND GRAPH:

Table 1: Table of commercial PV module efficiencies. ⁶⁵	p. 50
Table 2: Optimisation of dinitro reduction.	p. 69
Table 3: Summary of electrochemical and optical data. (x: data unavailable)	p. 80
Table 4: Optimisation of amide formation.	p. 95
Table 5: Optimisation of Sonogashira cross-coupling conditions.	p. 98
Table 6: Optimisation of TCNE reaction.	p. 100
Table 7: Summary of electrochemical and optical data.	p. 103
Table 8: Various conditions for the blank reaction of vinylferrocene 19 and cyclopentadiene 92 .	p. 123
Table 9: Optimisation of the reaction of 19 with cyclopentadiene 92 (Cp). Endo product was the major isomer in all cases generally 11:1 ratio. All reaction carried several times and were performed on a 100 mg scale of vinylferrocene.	p. 125
Table 10: Optimisation of ROM-CM conditions. a: catalyst added in one portion; b: catalyst dissolved in toluene and added in two portions, 1 hour apart; c: catalyst and 93 dissolved in toluene (0.01 and 0.1 mol.L ⁻¹ respectively), added in six portions over 1 hour.	p. 140
Table 11: Optimisation of the reaction of vinylferrocene 19 with thiols (RSH). All reaction performed on a 50 mg scale of vinylferrocene.	p. 149
Graph 1: Graph representing the best research in PV technology by efficiency over time. ⁶⁵	p. 51

LIST OF FIGURES AND SCHEEMES:

Figures:

- Fig. 1: Structure of riboflavin **1**. p. 21
- Fig. 2: Structure of FAD **2** and FMN **3** riboflavin cofactors. p. 22
- Fig. 3: General structure of pteridine **4** and isoalloxazine **5**. p. 22
- Fig. 4: Structures of the nine redox states of flavins. p. 23
- Fig. 5: Structures of flavins showing substitution sites at C(7) and C(8) and the three-way H-bonding interaction with DAP. p. 25
- Fig. 6: Structures showing the influence of π -stacking on the binding constant of the three-way H-bonding interaction of flavins. p. 25
- Fig. 7: Structure of a flavin system with intramolecular H-Bonding and π -stacking interactions.^{20e} p. 26
- Fig. 8: Structures of isoalloxazines showing possible substitution sites. p. 26
- Fig. 9: Flavin peroxide **7b**. p. 28
- Fig. 10: Example of the Dakin oxidation using a flavin peroxide catalyst. p. 29
- Fig. 11: *N*(5)-Ethylflavinium ion **8**. p. 29
- Fig. 12: Cartoon depicting the “on” and “off” positions of the flavin luminescence affected by π -stacking interactions with SWNT. p. 30
- Fig. 13: *N*(10)-Isobutylflavin **9** p. 31
- Fig. 14: Structure of stimuli responsive polymers **10** containing a flavin probe. p. 32
- Fig. 15: Structure of ABFL **11** and MABFL **12**. p. 32
- Fig. 16: Flavin based rotaxane **13** (left) and catenane **14** (right). p. 33
- Fig. 17: Scanning electron microscopy micrographs of assemblies formed with c) ABFL and d) MABFL. p. 35
- Fig. 18: Structure of flavin **15** and porphyrin **16**. p. 36
- Fig. 19: Schematic of the QD-polymer assembly between Thy-QD and DAT-polymer. p. 37
- Fig. 20: Schematic of the QD-polymer assembly between Thy-QD and DAP-Flavin-polymer. p. 37

Redox active molecules with molecular electronics and synthetic applications

- Fig. 21: Alfrey-Price e values of vinylferrocene **19**, *p*-*N,N*-dimethylamino styrene **20** and 1,1'-dianysylethylene **21**. p. 40
- Fig. 22: Structure of dppf **22**. p. 41
- Fig. 23: 1,1'-type (left) and 1,2-type (right) ferrocenyl ligands. p. 42
- Fig. 24: Structure of josiphos **23**. p. 42
- Fig. 25: Structure of Ferrocerone **24**. p. 42
- Fig. 26: Structures of Ferroquine **25** and Chloroquine **26**. p. 43
- Fig. 27: Structure of Ferrocifen **27** and Tamoxifen **28**. p. 43
- Fig. 28: Structure of a ferrocene-[60]fullerene **29**.⁵² p. 44
- Fig. 29: Structure of a ferrocene-[60]fullerene dyads **31** and **32**.⁵⁵ p. 45
- Fig. 30: Structure of a ferrocene-phosphorus **30**.^{56a} p. 45
- Fig. 31: Typical silicon PV cell cartoon representation.⁶¹ p. 48
- Fig. 32: Representation of solar radiation power against wavelength.⁶² p. 49
- Fig. 33: Schematic representation of the composition and the operating principle of a DSSC.⁶⁶ p. 52
- Fig. 34: Structure of "black dye" **33**. p. 53
- Fig. 35: Structure of YD2-o-C8 **34** and Y123 **35**. p. 53
- Fig. 36: Representation of device architectures, bilayer (left) and bulk heterojunction (right). p. 56
- Fig. 37: Charge transfer process in a bi-layer device.⁷⁷ p. 57
- Fig. 38: Charge transfer process at the molecular orbital level, favourable staggered orbitals (right), disfavoured non staggered orbitals (left). p. 58
- Fig. 39: Structures of CuPc **36** and C₆₀ **37**. p. 58
- Fig. 40: Structures of alternative donor materials with acceptor partner and recorded efficiency. p. 59
- Fig. 41: Structure of P3HT **41**. p. 60
- Fig. 42: Structures of IC₆₀BA **42**, PBDTT-DPP **43** and PC₇₁BM **44**. p. 61
- Fig. 43: Structure of compound **45**. p. 62
- Fig. 44: X-ray structure of flavin **46**. p. 63
- Fig. 45: Structure of compound **47**. p. 63
- Fig. 46: Structure of sexi-thiophene target **48**. p. 64
- Fig. 47: Structure of compound **55**. p. 65

Redox active molecules with molecular electronics and synthetic applications

- Fig. 48: Di-acylated **58** and di-alkylated **59** terthiophene products p. 71
(T=thiophene).
- Fig. 49: X-ray structure of compound **47**. p. 73
- Fig. 50: Resonance structures of **47** showing conjugation of the “in-plane” p. 73
thiophene.
- Fig. 51: Comparison of absorption spectra of **47** and **44** (5×10^{-5} M, in DCM). p. 74
- Fig. 52: Structure of compound **61**. p. 75
- Fig. 53: X-ray crystals of monobrominated flavins **46** and **56**. p. 76
- Fig. 54: Structures of the oligothiophene dimers **48**, **62** and **63**. p. 76
- Fig. 55: Comparison of absorption spectra of **47**, **48**, **62** and **63** (1×10^{-5} M, in p. 77
DCM).
- Fig. 56: CV traces of **47** (t3, black), **48** (t6, red), **62** (t7, blue) and **63** (t8, green) p. 78
with corresponding $E_{1/2}$ values (1×10^{-5} M, in Acetonitrile).
- Fig. 57: Square wave voltammetry traces of **47** (t3, black), **48** (t6, red), **62** (t7, p. 79
blue) and **63** (t8, green) with corresponding E_{diff} values (1×10^{-5} M, in
Acetonitrile).
- Fig. 58: DFT calculations of HOMO/LUMO levels for heptathiophene dimer p. 81
62. Calculations performed on Spartan '08, B3LYP exchange-correlation
function with Basis Set 6-31G*
- Fig. 59: Structure of future oligothiophene dimers with $n \leq 3$. p. 84
- Fig. 60: Structure of future dimers with extended non conjugated thiophene p. 84
side chains, with $n \leq 2$.
- Fig. 61: Structures of TCNE **64** and TCNQ **65**. p. 85
- Fig. 62: Structure of generic cyanoethene. p. 86
- Fig. 63: Structure of generic tetracyanbutadiene. p. 86
- Fig. 64: X-ray structure of push-pull TCBD compounds showing non-planarity. p. 87
- Fig. 65: Structure of compound **66**. p. 89
- Fig. 66: Structure of cyanocarbazole organic acceptors **67**. p. 89
- Fig. 67: Structure of cyanocarbon polymer triads as organic donors **68**. p. 90
- Fig. 68: Structure of TCBD-OPV compound **69**. p. 90
- Fig. 69: Structure of TCBD functionalised conjugated polymer **70**. p. 91
- Fig. 70: Structure of TCBD-flavin **71** and its precursor ferrocene-flavin **72**. p. 93

Redox active molecules with molecular electronics and synthetic applications

Fig. 71: Resonance structure of compound 72 .	p. 93
Fig. 72: Structure of reseo flavin 73 .	p. 93
Fig. 73: Structures of two regioisomers 75 and 78 .	p. 95
Fig. 74: Absorption spectra of 72 in different polarity solvents (all samples were recorded at 1×10^{-5} M)	p. 101
Fig. 75: Absorption spectra of 72 and 71 (1×10^{-5} M in DCM).	p. 102
Fig. 76: CV traces of 72 (black), 71 (red) with corresponding $E_{1/2}$ values (1×10^{-5} M, in Acetonitrile).	p. 103
Fig. 77: HOMO and LUMO level representation of 72 and 71 with respect to ITO and aluminium.	p. 106
Fig. 78: Structure of the C(7) substituted TCBD flavin 84 .	p. 106
Fig. 79: Structure of products of TCNQ 65 and F4-TCNQ 85 addition to 72 .	p. 107
Fig. 80: Structure of potential extended conjugation flavin-ferrocene TCBD compound ($1 \leq n \leq 3$).	p. 107
Fig. 81: Reactivity of a carbonyl group.	p. 108
Fig. 82: Structure of Spirastrellolide A Methyl Ester 86 .	p. 111
Fig. 83: Structure of ferrocene modified H-G II catalyst 87 .	p. 113
Fig. 84: Recycling cycle of ferrocene-phosphine unit.	p. 114
Fig. 85: Structure of ferrocene appended cholesterol “super-gelator” 88 .	p. 115
Fig. 86: Structure of ferrocene appended cholesterol “super-gelator” 89 .	p. 116
Fig. 87: Structure of dicyclopentadiene 94 .	p. 124
Fig. 88: <i>Endo</i> preference because of SOO and <i>endo/exo</i> products.	p. 126
Fig. 89: NMR spectrum of compound 93 .	p. 127
Fig. 90: NOE interaction in compound 93 .	p. 127
Fig. 91a: Comparison of the NMR of 93 (red) and the product of entry 2 (blue).	p. 128
Fig. 91b: Comparison of the NMR of 93 (red) and the product of entry 2 (blue).	p. 129
Fig. 92: NMR of compound 98 .	p. 131
Fig. 93: Structure of compound 98 .	p. 131
Fig. 94: Structure of compound 99 .	p. 132
Fig. 95: General structure of prostaglandins 100 $R^1 = H, O, OH, R^2 = H, O, OH$.	p. 134
Fig. 96: NMR spectrum of compound 104 .	p. 137
Fig. 97: Structures of <i>E</i> -stilbene 108 and 1-ferrocene-polybornene 109 .	p. 138

Redox active molecules with molecular electronics and synthetic applications

Fig. 98: Structure of compound 112 .	p. 139
Fig. 99: Desired product for the hydrogenation of 112 .	p. 140
Fig. 100: Potential product of the ferrocene hydrogenation of 112 .	p. 141
Fig. 101: Structures of the charge/discharge polymers developed by Masuda and co-workers.	p. 142
Fig. 102: Structure of 1-ferrocene-polnorbornene 109 .	p. 142
Fig. 103: Structures of compound 116 and compound 120 .	p. 144
Fig. 104: Structure of compound 121 (R= C ₆ H ₁₃).	p. 145

Schemes:

Scheme 1: Aerobic organocatalytic Baeyer-Villiger reaction.	p. 28
Scheme 2: Preparation of ferrocene 17 .	p. 38
Scheme 3: Functionalisation of ferrocene 17 .	p. 39
Scheme 4: Chemical oxidation of ferrocene 17 to ferrocenium 18 .	p. 40
Scheme 5: Proposed strategy for the synthesis of 47 .	p. 65
Scheme 6: Synthetic strategy toward sexi-thiophene dimer 48 .	p. 66
Scheme 7: Stille coupling catalytic cycle.	p. 68
Scheme 8: Acylation mechanism (T=thiophene).	p. 70
Scheme 9: Intramolecular <i>N</i> -cyclisation mechanism (T=thiophene).	p. 70
Scheme 10: Proposed mechanism of alloxan condensation.	p. 72
Scheme 11: Alkylation of the N(3) terminus of 47 .	p. 75
Scheme 12: Summary of the synthesis of targets 47 , 48 , 62 , 63 .	p. 82
Scheme 13: Formation of TCBD via cyclodutene intermediate.	p. 86
Scheme 14: Proposed reaction mechanism for the formation of TCBDs.	p. 88
Scheme 15: Synthetic pathway of super-acceptors.	p. 92
Scheme 16: Proposed synthetic approach towards 72 .	p. 94
Scheme 17: Alternative synthetic route to 72 .	p. 95
Scheme 18: Proposed catalytic cycle of Sonogashira cross-coupling. (R= aryl; R'= alkyl, aryl...;X= halide)	p. 97
Scheme 19: Final strategy towards synthesis of 72 .	p. 99

Redox active molecules with molecular electronics and synthetic applications

Scheme 20: Possible side products if nitro group is reduced before the amide group.	p. 99
Scheme 21: Summary of the synthesis of targets 72 and 71 .	p. 105
Scheme 22: Formation of enolate governed by reactivity of carbonyl groups (E= electrophile).	p. 108
Scheme 23: Conjugated reactivity and Michael addition (Nu= nucleophile).	p. 109
Scheme 24: Use of thioacetals to change the reactivity of carbonyls towards electrophiles (E= electrophile).	p. 109
Scheme 25: Key reactions of dithianes.	p. 110
Scheme 26: Key synthetic step toward 86 .	p. 111
Scheme 27: Generic schemes of NHC and enamine-iminium umpolung catalytic proceses.	p. 112
Scheme 28: Chemical oxidation and reduction of ferrocene 17 .	p. 116
Scheme 29: Redox Umpolung controlled reactions of vinylferrocene 19 .	p. 117
Scheme 30: Standard [4+2] Diels-Alder cycloaddition.	p. 117
Scheme 31: Ideal Diels-Alder configuration and reverse demand configuration.	p. 118
Scheme 32: Reverse demand Diel-Alder cycloaddition of vinylferrocene 19 and acryloylferrocene 90 with 1,2,3,4-tetrahalo-5,5-dimethoxy cyclopentadienes 91 .	p. 118
Scheme 33: Scope of thiol-click reactions.	p. 120
Scheme 34: Potential outcome of umpolung activated nucleophilic addition.	p. 121
Scheme 35: The template reaction for method development, cycloaddition with cyclopentadiene 92 .	p. 123
Scheme 36: Umpolung controled Diels-Alder reaction of vinylferrocene 19 and furan 95 .	p. 129
Scheme 37: Proposed mechanism for the formation of compound 98 .	p. 131
Scheme 38a: First proposed mechanism for the formation of compound 99 .	p. 132
Scheme 38b: Second proposed mechanism for the formation of compound 99 .	p. 133
Scheme 39: Stereospecific hydrogenation of ferrocene.	p. 135
Scheme 40: Redox auxiliary synthesis.	p. 135
Scheme 41: Hydrogenation of 93 to 105 .	p. 136
Scheme 42: Hydrogenation of 105 to 104 .	p. 136

Redox active molecules with molecular electronics and synthetic applications

Scheme 43: Hydrogenation conditions of 105 to 104 .	p. 136
Scheme 44: ROM-CM of 6-ferrocene-bicyclo[2.2.1]hept-2-ene 93 .	p. 138
Scheme 45: ROM-CM reaction with ethylene to maximise intermediate 111 lifetime.	p. 139
Scheme 46: Blank reaction of vinylferrocene 19 with hexanethiol 115 .	p. 143
Scheme 47: Reaction of vinylferrocene 19 and octanethiol 118 entry 1.	p. 143
Scheme 48: Proposed reaction progression for the formation of 1,2-bis-octanesulfide-ethylferrocene 119 .	p. 144
Scheme 49: Proposed reaction progression for the formation of compound 121 .	p. 145
Scheme 50: Reaction of vinylferrocene 19 and hexanethiol 115 entry 3 (thiol added before FeCl ₃).	p. 146
Scheme 51: Proposed mechanism for the formation of compound 120 .	p. 147
Scheme 52: Reaction of vinylferrocene 19 with butanedisulfide 122 .	p. 147
Scheme 53: Proposed mechanism for the formation of compound 120 .	p. 147
Scheme 54: Proposed reaction mechanism for the Markovnikov thiol addition.	p. 148
Scheme 55: Proposed reaction mechanism for the Michael-like Markovnikov thiol addition.	p. 149
Scheme 56: Umpolung activated reactions of vinylferrocene 19 .	p. 150
Scheme 57: Reductive hydrogenation of ferrocene.	p. 150
Scheme 58: Umpolung activated cycloadditions of vinylferrocene 19 .	p. 151
Scheme 59: Reductive hydrogenation of the thiol addition products.	p. 152
Scheme 60: Umpolung activated reductive hydrogenation of ferrocene.	p. 152

ACKNOWLEDGEMENTS:

I would like to thank the God of the Bible, because without my faith I would not have been able to accomplish anything. I want to thank my wife Eleanor Wiles who's constant support has been invaluable. Further thanks is extended to my friends and family for their support.

I want to thank Professor Graeme Cooke for the opportunity to learn and work under his supervision. All the members of the Cooke research group, past and present, in particular Dr. Brian Fitzpatrick for his work carried out on the Flavin-thiophene dyads (Chapter 2) and Mrs Helen Smith for her friendship and support in the lab.

Further thanks needs to go to Mr Jim Tweedy for the operation of the mass spectrometry facility, and to the rest of the technicians and staff at the school of chemistry.

DECLARATION:

I declare that, except where explicit reference is made to the contribution of others, that this dissertation is the result of my own work and has not been submitted for any other degree at the University of Glasgow or any other institution.

DEFINITIONS AND ABBREVIATIONS:

ABFL: 8-[[*p*-[*bis*(Ethyl)amino]phenyl]azo]-isobutylflavin

AM 1.5 light: Air mass solar energy; a simulation of atmospheric solar radiations

BHJ: Bulk heterojunction

C₆₀: Fullerene

COSY: Homonuclear correlation spectroscopy

CuPc: Copper phthalocyanine

CV: Cyclic voltammetry DAP: Diaminopyridine

DAT: Diaminotriazine

DCM: Dichloromethane

dppf: 1,1'-*bis*(Diphenylphosphino)ferrocene

DSSC: Dye-sensitised solar cell

DEPT: Distortionless enhancement by polarization transfer

DFT: Density functional theory EDTA: Ethylenediaminetetraacetic acid

DMA: 4-(*N,N*-Dimethylamino)phenylacetylenes

FAD/FADH₂: Flavin adenine dinucleotide

FDA: Food and Drug Administration

FMN/FMNH₂: Flavin mononucleotide

FRET: Fluorescence resonance energy transfer

H-G II: Hoveyda-Grubbs 2nd generation catalyst

HOMO: Highest occupied molecular orbital

HPLC: High performance liquid chromatography

HTL: Hole transport layer

HSQC: Heteronuclear single-quantum correlation spectroscopy

IC_nBA: *bis*-Indene-C_n

ICT: Intramolecular charge transfer

IR: Infra-red spectroscopy ITO: Indium tin oxide

LUMO: Lowest unoccupied molecular orbital

MABFL: 3-Methyl-8-[[*p*-[*bis*(ethyl)amino]phenyl]azo]-isobutylflavin

MCM-41: Mobil Composition of Matter, a type of mesoporous molecular sieve.

Redox active molecules with molecular electronics and synthetic applications

MPA: Mercaptopropionic acid

NHC: *N*-Heterocyclic carbene

NLO: Non-linear optics / non-linear optical

NMR: Nuclear magnetic resonance spectroscopy

OLED: Organic light emitting diode

OPV: Organic solar cell

QD: Quantum dot

QDSC: Quantum dot solar cell

P3HT: Poly(3-hexylthiophene)

PC_nBM: Phenyl-C_n-butyric acid methyl ester

PBDTT-DPP: Poly{2,6'-4,8-di(5-ethylhexylthienyl)benzo[1,2-b;3,4-b]dithiophene-alt-5-dibutyloctyl-3,6-bis(5-bromothiophen-2-yl)pyrrolo[3,4-c]pyrrole-1,4-dione}

PEDOT:PSS: Poly(3,4-ethylenedioxythiophene):poly(styrenesulfonate)

PV: Photovoltaic

TCBD: Tetracyano-butadienes

TCNE: Tetracyanoethene

TCNQ: 7,7,8,8-Tetracyanoquinodimethane

TFA: Trifluoroacetic acid

THF: Tetrahydrofuran UV-Vis: UV-visible spectroscopy

ROM-CM: Ring opening metathesis - cross metathesis

ROMP: Ring opening metathesis polymerisation

SCE: Standard Calomel electrode

SWNT: Single-walled carbon nanotube

CHAPTER I: GENERAL INTRODUCTION

Redox active molecules are ubiquitous to nature and are involved throughout the processes of life.¹ For this reason, considerable effort has been spent in the scientific community to synthesise model systems in order to understand the processes of redox systems.² Greater understanding always leads to more focused research, for instance, redox enzymes have become part of a chemist's portfolio of reagents as catalysts for an increasing number of syntheses.³ In the same way, synthetic redox molecules are now being investigated for the implementation as biomimetic enzymatic systems which could have applications in medicinal chemistry.⁴ A second benefit that comes from understanding these processes is that it also opens the way towards new applications of redox active molecules. Redox molecules are now being used for applications in synthesis, in catalysis, and in materials, where their properties form a key part of their function. This thesis describes the use of naturally occurring (flavins) redox active molecules in the preparation of materials with potential optoelectronic application as well as the use of ferrocene in the development of a new method which utilises the redox properties of ferrocene to promote known synthetic reactions.

2. Flavins

2.1. History of Flavins:

In 1879, Blyth isolated a yellow pigment from the whey of cow's milk and named it lactochrome.⁵ Little did he know that he had successfully isolated one of the most common proteins in nature. Several years later, in the 1920's and 30's, the interest in the yellow pigment with greenish fluorescence flourished and led to its isolation from a wide variety of sources. At the same time it was found to be part of the vitamin B

Chapter I: General Introduction

complex.⁶ Richard Kuhn⁷ and Paul Karrer⁸ almost simultaneously elucidated and proved by synthesis the structure of what is now known as riboflavin **1** (Figure 1).

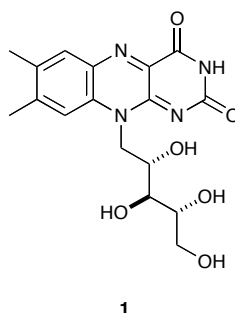


Fig. 1: Structure of riboflavin **1**.

Riboflavin **1**, now more commonly known as vitamin B₂, exists essentially in nature as two different cofactors found in all flavoproteins: flavin adenine dinucleotide **2** (FAD) and flavin mononucleotide **3** (FMN) (Figure 2). Both were discovered in similar fashion. First, Theorell discovered FMN **3** in 1935.⁹ Then, Warburg and Christian identified FAD **2**, in 1938,¹⁰ thanks to the work of Krebs who identified the existence of a different flavoprotein than that studied by Theorell.¹¹ Flavoproteins have attracted a lot of interest to date, this is primarily due to the very particular properties of the flavin component itself.

Chapter I: General Introduction

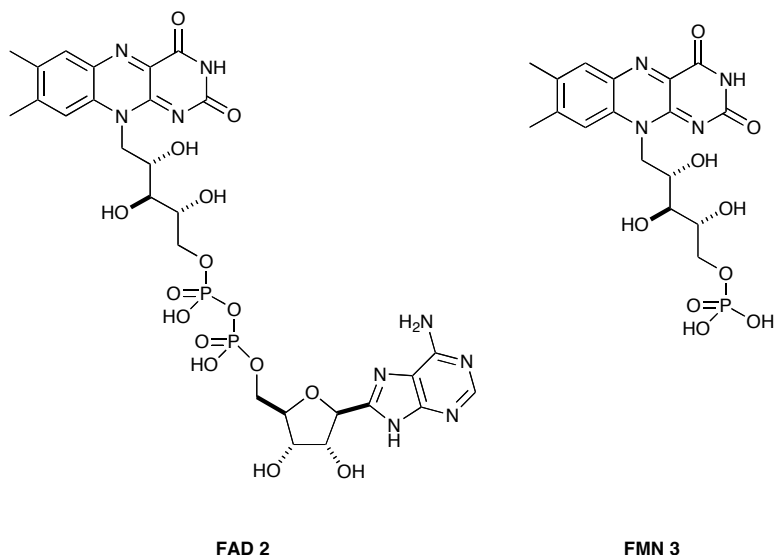


Fig. 2: Structure of FAD 2 and FMN 3 riboflavin cofactors.

2.2. Properties:

Flavins are a family of compounds derived from riboflavin. They are tricyclic heteronuclear aromatic compounds built around a pteridine 4 backbone. Flavins can also be referred to as isoalloxazine 5, the latter refers to the method used to synthesise flavins using alloxan condensation (Figure 3). These highly aromatic, electron rich systems have very interesting electronic, optical and physical properties.

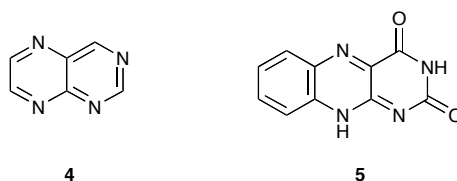


Fig. 3: General structure of pteridine 4 and isoalloxazine 5.

Flavins have the ability to participate in one and two electron transfer processes. They can therefore exist in three different redox states: fully oxidised, one electron reduced (semiquinone) and two electron (fully) reduced flavins. In 1982 Heelis proposed that unbounded flavins in free solution can exist in as many as nine different pH dependant

Chapter I: General Introduction

states (Figure 4).¹² This particular property makes flavoproteins a ubiquitous part of many redox processes in respiratory biological functions.¹⁰

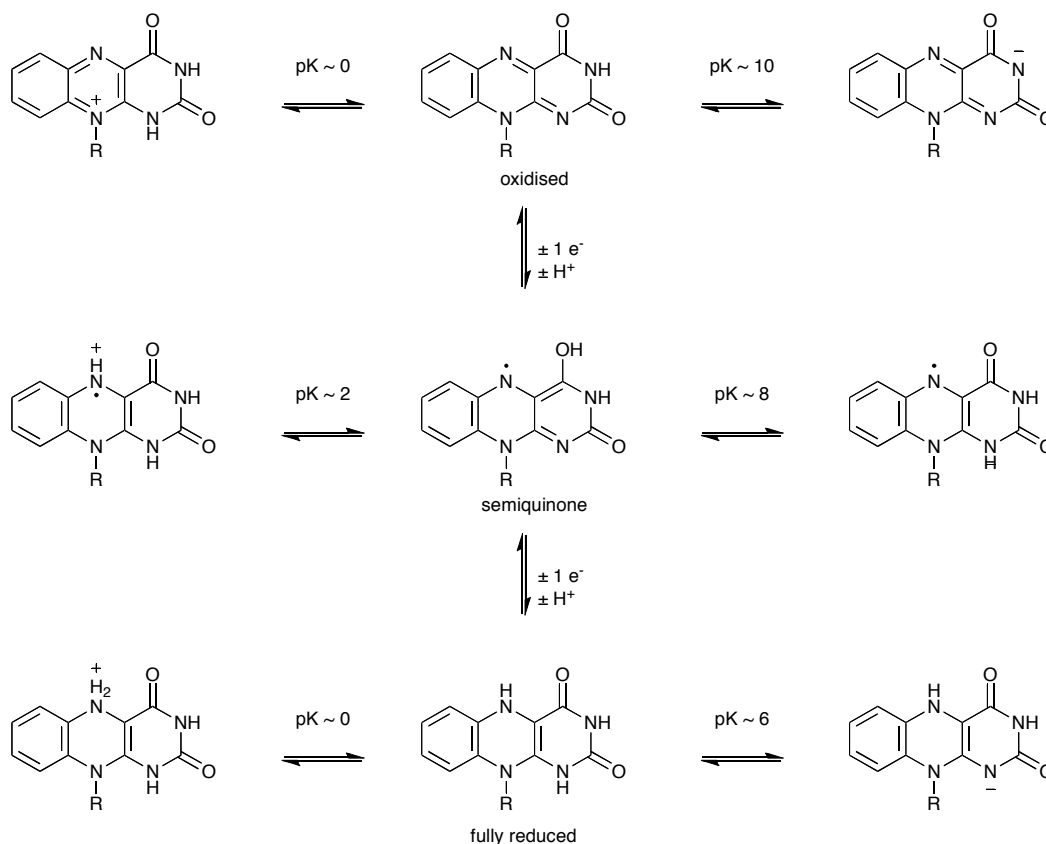


Fig. 4: Structures of the nine redox states of flavins.

The redox potential of riboflavin is known to be around -200 mV.^{13,14} However, this potential can be greatly influenced either by intermolecular interactions,^{14,15} often due to protein environment in biological systems, or by performing substitutions on the riboflavin core, examples of which will be seen shortly.¹⁶

Flavins are also very well known for the yellow-greenish fluorescence they emit upon excitation. This has meant that flavoproteins have been one of the most studied biological systems to date¹⁷. In 1962, Tether and Turnbull noted that the singlet and triplet states of flavins could be affected by structural changes¹⁸, therefore the

Chapter I: General Introduction

fluorescence would be affected as a result. Since then, many have studied the effects of structural and environmental changes to the optical properties of flavins.¹⁹

Over the last two decades, the collaboration between Cooke and Rotello has looked in depth into the modulation of flavin properties.²⁰ Their work has been focused on trying to synthesise model systems to understand flavoenzymes. This has enabled a much deeper understanding of the influences of substitutions and enzymatic environment on the redox potential, optical characteristics and supramolecular interactions.

In 2003, one study focused on redox potential and H-bonding binding affinity of flavins substituted at the C(7) and C(8) positions (Figure 5). From the published results two major conclusions can be drawn. The first, upon binding to a diaminopyridine (DAP) partner the redox potential of each flavin, regardless of substitutions, is shifted on average by + 80-90 mV (this has also been shown to be true in the case of intramolecular H-bonding)^{20c}. This suggests that in an enzymatic system the reduced flavin radical anion is stabilised by intermolecular interactions. The second, substitution at C(7) and C(8) modulate the redox potential of the flavin by about + 400 mV and an increase of the H-bonding affinity with DAP by 618 M⁻¹. Furthermore, Cooke, Rotello and co-workers showed in this publication that these properties could be correlated to linear free energy relationships. These correlations showed that, in an aprotic solvent, the redox properties of the flavin were affected by substitutions at the C(7) position whereas the binding of the oxidised flavin was influenced to a greater extent by substitutions at the C(8) position.^{20a} This conclusion was further sustained in a similar study of flavins with substituents only at the C(7) position.^{20f}

Chapter I: General Introduction

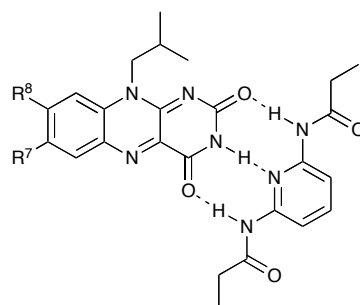


Fig. 5: Structures of flavins showing substitution sites at C(7) and C(8) and the three-way H-bonding interaction with DAP.

In 2004, Cooke, Rotello and co-workers investigated another environmental factor that is present in flavoenzymes.^{20b} They investigated the influence of π -stacking on H-bonding affinity and found that π -stacking interactions with flavin increase the binding constant by 14 times with increasing π -system in the oxidised form and by 2.5 times in the reduced form (Figure 6).

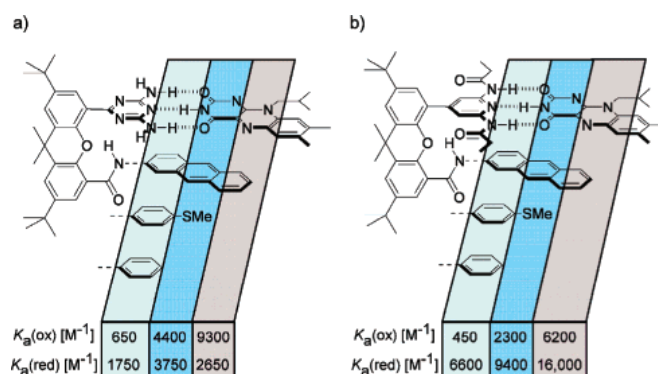


Fig. 6: Structures showing the influence of π -stacking on the binding constant of the three-way H-bonding interaction of flavins.^{20b}

In 2005, similar studies of a flavin derivative coupled to fullerene C₆₀ showed that the presence of C₆₀ quenched the fluorescence of the flavin unit and shifted the redox potential of the system by + 10-30 mV. This again shows that the reduced form of flavins (semiquinone radical cation) is stabilised by the π -interactions between the

Chapter I: General Introduction

flavin and C₆₀ units.^{20d} The same conclusions were also reached by investigating an intramolecular system **6** which provided elements of π -stacking and a DAP unit for binding (Figure 7).^{20e}

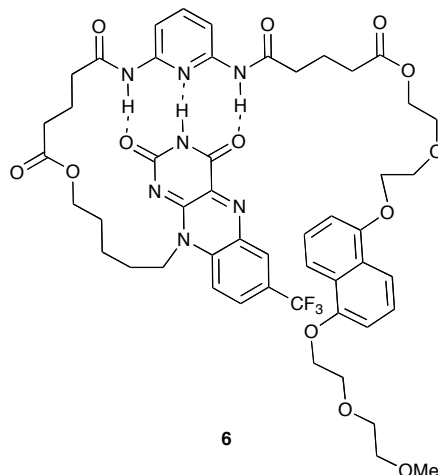


Fig. 7: Structure of a flavin system with intramolecular H-Bonding and π -stacking interactions.^{20e}

In summary, the properties of flavins can be easily modified/tuned by performing a range of substitutions around the isoalloxazine tricyclic system which offers many diversification loci (Figure 8) and/or by inter/intramolecular interactions such as hydrogen bonding (Figure 5) or π -stacking. This makes flavins a very interesting target for the synthesis of fine tuned organic compounds for a range of applications.

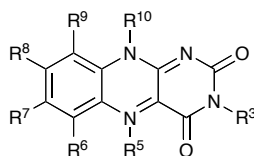


Fig. 8: Structures of isoalloxazines showing possible substitution sites.

2.3. Applications:

In this section, selected publications are presented, from research groups that have sought to utilise the properties of flavins outside of their original biological applications

Chapter I: General Introduction

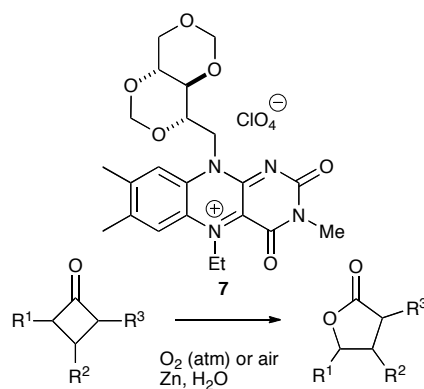
and in synthesis, in the fabrication of molecular devices and more recently the interest generated around the need for new fuels.

2.3.1. Flavins in synthesis and catalysis:

Due to the ubiquitous nature of flavins in biological enzymes that catalyse many redox processes, much research has been focused on using synthetic flavins as biomimetic catalysts. In the last few years, flavins have been used as organo-catalysts to catalyse reduction and oxidation reactions, particularly under aerobic conditions.

Notably, in 2005 Imada and co-workers reported the first aerobic Baeyer-Villiger reaction catalysed with an organocatalyst.²¹ Using the knowledge that flavin-peroxides can be formed in the presence of molecular oxygen, they devised a new method to perform a nucleophilic Bayer-Villiger reaction chemoselectively. In their publication they report the transformation of cyclobutanones to γ -butyrolactones using a riboflavin derivative **7**. Under the conditions described in scheme **1** the flavin is oxidised in a biomimetic fashion by elemental oxygen to form peroxide “carrier” **7b** (Figure 9) which operates the nucleophilic oxidation. Chemoselectivity comes from the absence of competing electrophilic epoxidation reactions which often occur in standard Bayer-Villiger conditions. This is due to the nature of the oxidants used in the standard reaction. Here only the nucleophilic Bayer-Villiger reaction is observed even in the presence of moieties liable to epoxidation.

Chapter I: General Introduction



Scheme 1: Aerobic organocatalytic Baeyer-Villiger reaction.

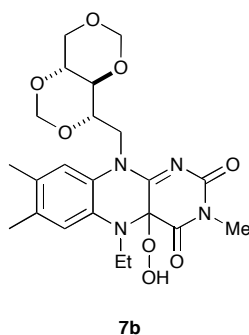


Fig. 9: Flavin peroxide **7b**.

This research has helped to develop several other flavin catalysts to perform other types of oxidative reactions, such as, the Dakin oxidation (Figure 10),²² the oxidation of aldehydes to carboxylic acids.²³ The oxidative power of flavins has even been used in the reduction of olefins. Flavin has been used to perform the catalytic oxidation of hydrazine to generate diimide (a known reducing agent).²⁴

Chapter I: General Introduction

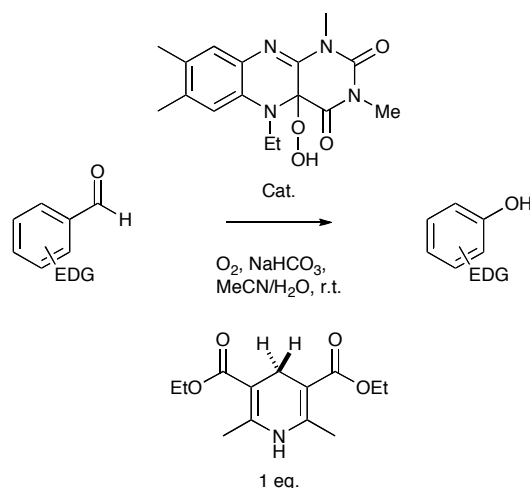


Fig. 10: Example of the Dakin oxidation using a flavin peroxide catalyst.

In August 2012, Glusac and co-workers published their work which uses the oxidative power of the *N*(5)-ethylflavinium ion **8** (Figure 11) to induce the catalytic reduction of water.²⁵ Their work describes the bulk electrolysis of an aqueous solution of *N*(5)-ethylflavinium ion which promotes the evolution of oxygen gas. This was the first example of a fully organic catalyst capable to perform the oxidation of water.

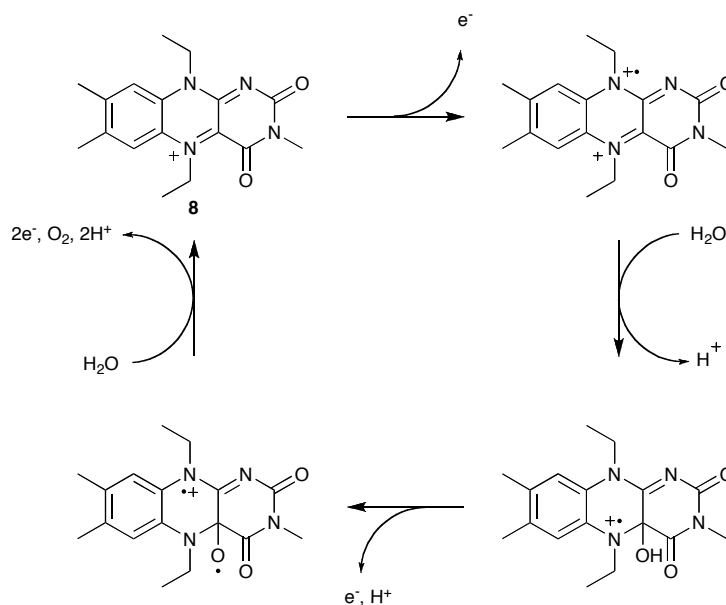


Fig. 11: Catalytic cycle of the oxidation of water by *N*(5)-ethylflavinium ion **8**.

Chapter I: General Introduction

2.3.2. Flavins as molecular devices:

The ability of flavins to participate in molecular recognition through H-bonding and π -stacking, their distinctive optical properties and their reversible redox properties makes them very interesting targets in the synthesis of organic devices.

-Optical probes:

In 2008, Ju and Papadimitrakopoulos reported the synthesis of a flavin functionalised single-walled carbon nanotube (SWNT) (Figure 12).²⁶ They reported that due to very strong π -stacking interactions between FMN and the SWNT the fluorescence of the flavin is quenched. They also report that this phenomenon can be reversible. Reduction of the FMN moiety to FMNH₂ by sodium dithionite disrupts the ability of FMN to interact with the SWNT thereby restoring the fluorescence. Subsequent oxidation in the presence of oxygen restored FMN to its fully oxidised form and promoted fluorescence quenching. Fluorescence was also restored upon addition of surfactants. These cover the surface of the nanotubes rendering π -stacking interactions impossible. This work is an example of a switchable luminescent device, which could see applications in biosensing.

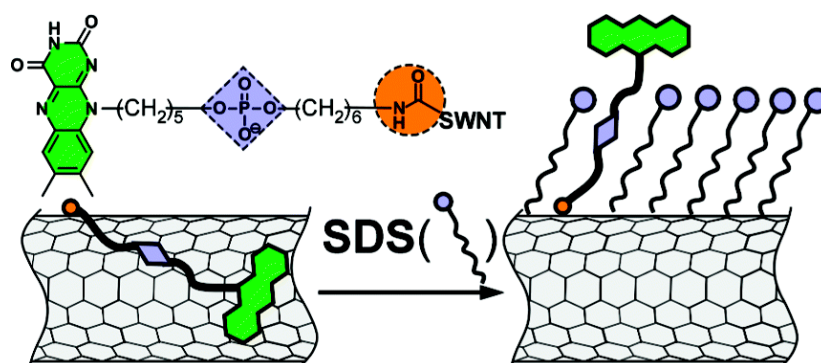


Fig. 12: Cartoon depicting the “on” and “off” positions of the flavin luminescence affected by π -stacking interactions with SWNT.²⁶

Chapter I: General Introduction

In 1999, Rotello and co-workers presented the use of FMN and *N*(10)-isobutyl flavin **9** (Figure 13) as polarity probes in both static and dynamic silica based systems.²⁷ Both flavins exhibit solvatochromic properties, for example compound **9** shows a λ_{max} of 374nm in polar aqueous solvents and a λ_{max} of 349nm in non-polar chloroform. They used this polarity induced bathochromic shift to assess different batches of silica. For instance in mesoporous silica prior to calcination the absorbance of compound **9** was 374 nm whereas in MCM-41 grade silica the absorbance was 349nm confirming the absence of polar sites. Similar effects were observed using FMN in sol-gel silicates.

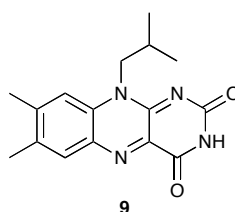
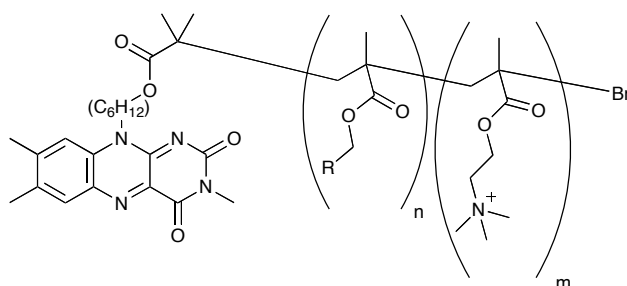


Fig. 13: *N*(10)-Isobutylflavin **9**.

Cooke and Rotello recently published work where the optical properties of flavins were used to monitor stimuli-responsive gels.²⁸ These gels are being studied extensively for their potential applications which ranges from drug delivery, to materials. Here, flavin is present as a probe to monitor the gelation process. The flavin containing polymers **10** (Figure 14) are shown to successfully promote gelation of deionised water at low concentration (1 wt%). Upon sonification the gel structure is disrupted and reverts to a more liquid-like form. UV-vis studies show a significant increase and bathochromic shift in absorbance at 337 nm when the gel is sonicated, this is believed to result from a solvatochromic effect characteristic of flavins. In gel form, the flavin is held in a non-polar environment, but when the gel is disrupted the flavin is exposed to the polar

Chapter I: General Introduction

aqueous environment. The flavin functionality embedded in polymer acts as a UV-vis probe to monitor the gelation process.



10 R= H / benzyl / naphthyl

Fig. 14: Structure of stimuli responsive polymers **10** containing a flavin probe.

Cooke, Rotello and co-workers showed that 8-[[*p*-[*bis*(ethyl)amino]phenyl]azo] isobutylflavin (ABFL) **11** (Figure 15) exhibits an absorbance shift that can be controlled by the extent of H-bonding with a DAP recognition probe.²⁹ They observed a shift of the intramolecular charge transfer band that could be tuned by increasing the amount of DAP complexed with the molecule. However, the methylated flavin MABFL **12** (Figure 15) showed no change in absorbance as it does not participate in H-bonding with DAP. The reversible aspect of this effect (due to H-bonding temperature dependence) means that such molecules could be used as optical probes using H-bonding recognition.

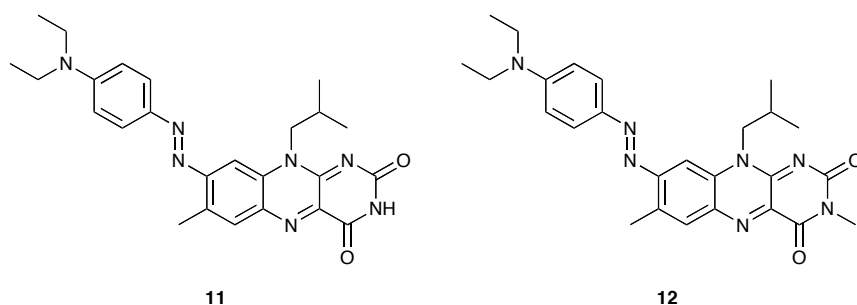


Fig. 15: Structure of ABFL **11** and MABFL **12**.

Chapter I: General Introduction

-Molecular machines:

Molecular machines are intrinsically part of nature's processes. Synthesising these molecules not only offers insight into the inner workings of our natural environment but also opens an avenue towards molecular devices such as switches. Molecular machines rely on inducing motion through controlled conditions, such as change in oxidation state and competing hydrogen-bonding. Cooke, Rotello and co-workers successfully synthesised a flavin based rotaxane **13**³⁰ and a catenane **14**³¹ (Figure 16).

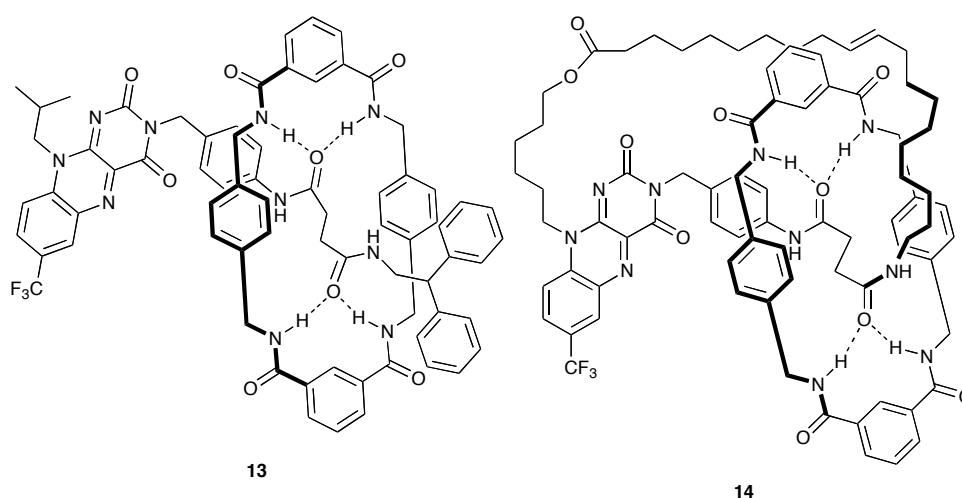


Fig. 16: Flavin based rotaxane **13** (left) and catenane **14** (right).

Analysis of both molecules showed that in the resting state the hydrogen bonding interaction lied over the succinamide group. However, voltammetry studies show that, in both cases, the redox potential of the flavin is shifted showing a stabilisation of the flavin radical anion. As previously characterised by Cooke and Rotello, such stabilisation is due to a great increase in hydrogen-bonding binding. Therefore, one can assume that in the reduced state, the macrocycle is displaced to rest over the flavin moiety. This redox induced motion could see applications in redox molecular switches.

Chapter I: General Introduction

-Molecular electronic devices:

In recent years, materials research has been focusing on developing organic electronic devices to replace expensive and less practical inorganic semi-conducting materials. The development of such organic electronic devices relies on the ability to conduct electrons efficiently between donor and acceptor organic molecules. The ability of flavins to accept one or two electrons and their ability to form macromolecular assemblies through molecular recognition has made them a target molecule in this burgeoning field.

An area of interest is focusing on self-assembly, the ability of small molecules to self-assemble into defined structures using non-covalent interactions. Cooke, Rotello and co-workers have published extensively on the ability of the flavin moiety to interact via hydrogen bonding and π -stacking. In 2008, they report a flavin derivative that has the ability to self-assemble into nanowires or platelets by regulating hydrogen-bonding affinity.³² ABFL **11** and MABFL **12** (cf Figure 15 p.32) are flavin derivatives with a large dipole moment induced by a “push-pull” donor- π -acceptor motif. The dipole-dipole interaction between the molecules is then responsible for the formation of nanostructures. Cooke and Rotello observed that the hydrogen-bonding ABFL forms nanowires whereas the non hydrogen bonding MABFL forms hexagonal platelets. They also observe that the morphology of the nanostructures can be modulated depending on the ratio of ABFL to MABFL (Figure 17).

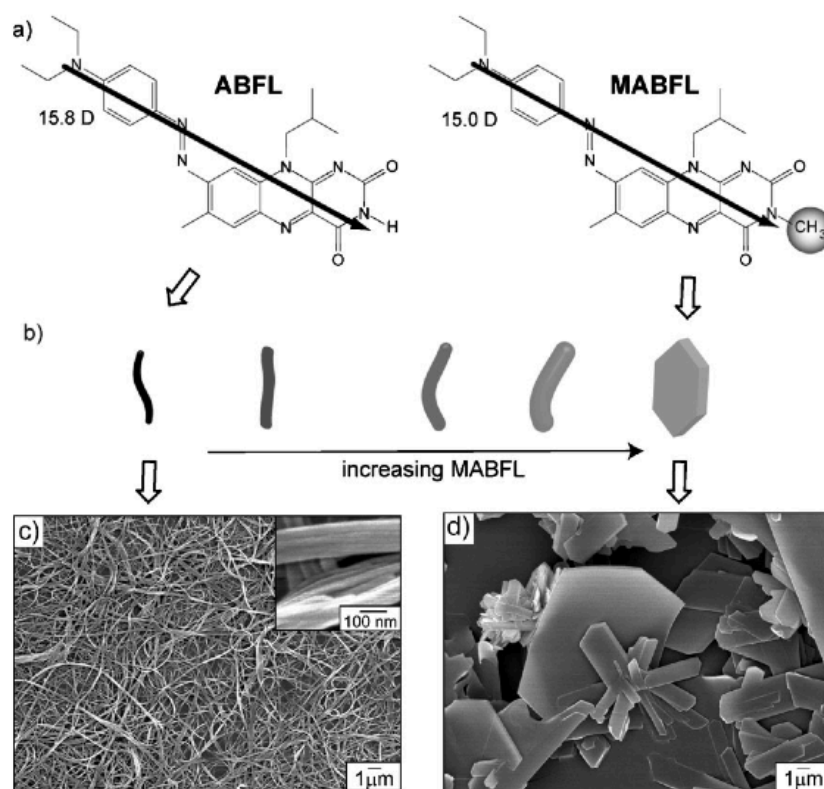


Fig. 17: Scanning electron microscopy micrographs of assemblies formed with c) ABFL and d) MABFL.

The ability to produce materials with defined nanostructures is important but flavins play a more important role in the search for organic electronic materials due to their ability to effect efficient electron transfer. In 2004, Isoda and co-workers showed that electron transfer occurred between a photo-excited flavin derivative **15** and porphyrin **16** in a Langmuir-Blodgett heterojunction film (Figure 18).³³ This work was following from several years of observing the photo induced electron transport in films containing FMN, cytochrome C and EDTA.³⁴ They showed in their research that flavin readily interacts with other compounds in heterojunctions and is able to effect efficient electron transfer.

Chapter I: General Introduction

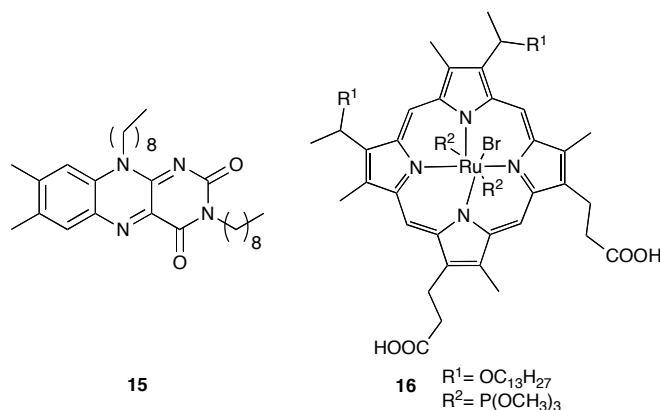


Fig. 18: Structure of flavin **15** and porphyrin **16**.

In 2011, Cooke and Rotello reported the synthesis of polymer-quantum dots self-assemblies with defined morphologies.³⁵ Polymers equipped with diaminotriazine (DAT) unit interacted *via* three point hydrogen bonding with thiamine functionalised CdSe/ZnS Quantum-Dots (QD) (Figure 19). The interaction between the polymer and the QD resulted in the formation of distinct, tuneable morphologies that were dependant on the ratio of polymer to QD. A year later, they report further investigation on the interaction between a Zn-Se quantum dot and flavin functionalised polymer.³⁶ Thymine functionalised quantum dots self assembled by three-point hydrogen-bonding with a DAP functional group on a polymer containing a flavin unit (Figure 20). This brought the quantum dot and the flavin in relative proximity, and enables the observation of Förster resonance energy transfer (FRET) in the solid state as well as in solution. This type of highly structured self-assembled QD incorporating photoactive molecules could find application as optoelectronic materials.

Chapter I: General Introduction

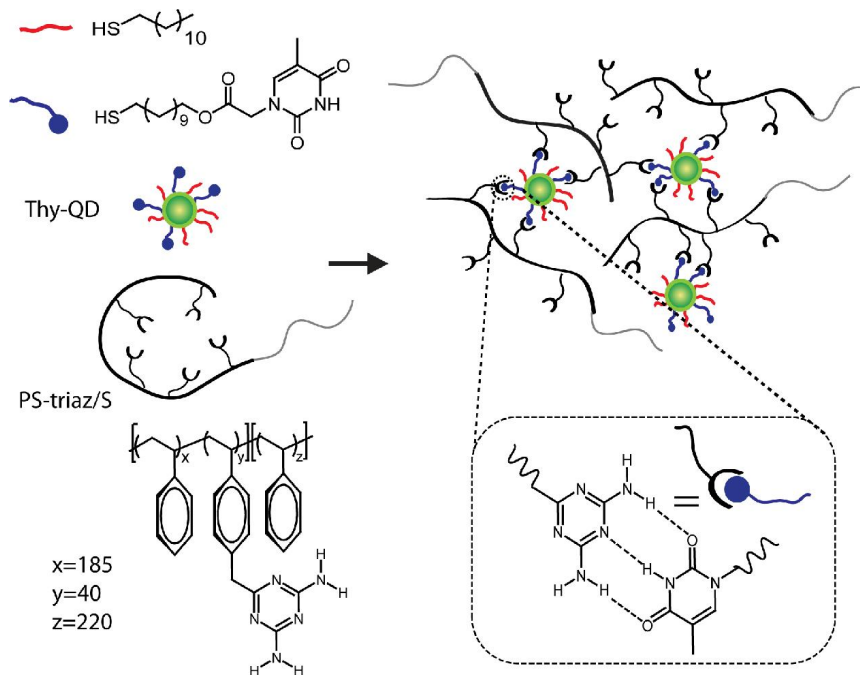


Fig. 19: Schematic of the QD-polymer assembly between Thy-QD and DAT-polymer promoted by H-bonding recognition.³⁵

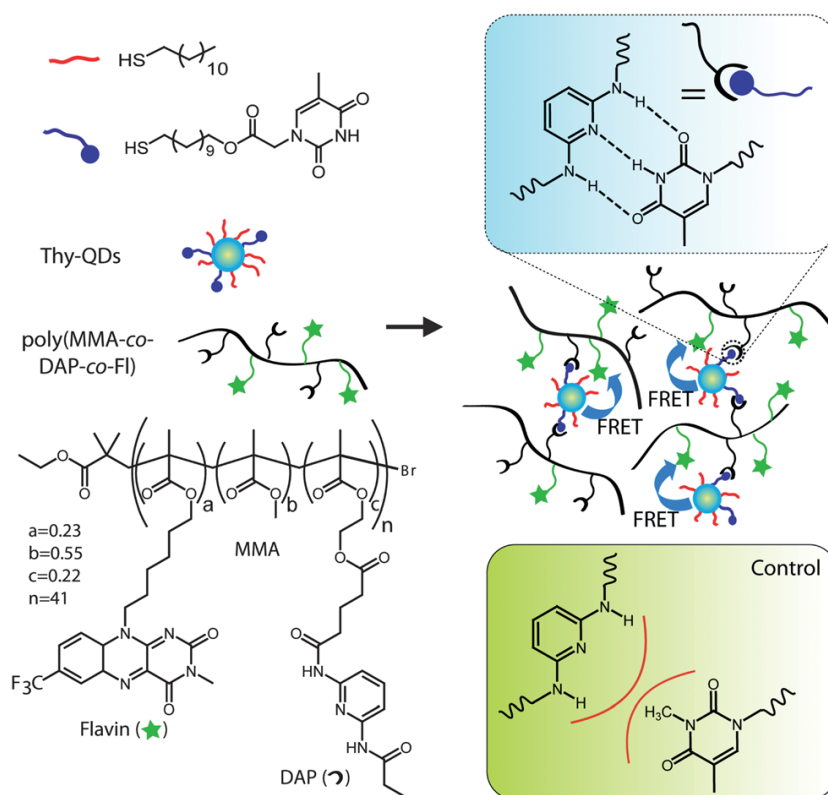


Fig. 20: Schematic of the QD-polymer assembly between Thy-QD and DAP-Flavin-polymer.³⁶

Chapter I: General Introduction

2. Ferrocene

2.1. History of ferrocene:

Ferrocene **17** is an organometallic compound that was serendipitously discovered in 1951 by Pauson and Kealy by reacting cyclopentadienyl magnesium bromide with ferric chloride (Scheme 2).³⁷ The structure of the organometallic compound was subject to much debate, but was correctly assigned a year later by Wilkinson and co-workers and Fischer and co-workers.³⁸



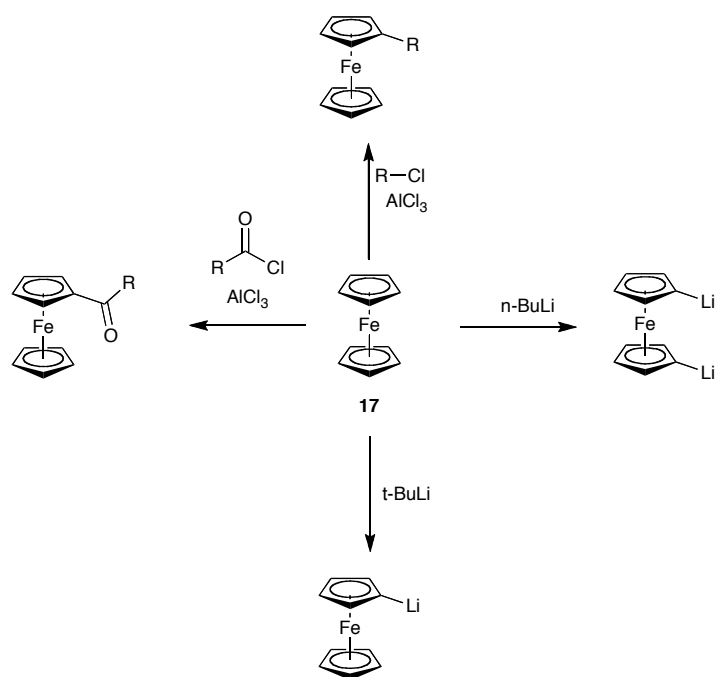
Scheme 2: Preparation of ferrocene **17**.

Both Fischer and Wilkinson were awarded a Nobel Prize in chemistry in 1973, “*for their pioneering work, performed independently, on the chemistry of the organometallic, so called sandwich compounds*”.³⁹ The elucidation of “sandwich” structure of ferrocene was a revolution in terms of understanding bonding in organometallic compounds. The organometallic compound is now considered to be an 18 electron compound with the iron centre having an oxidation of +2. The cyclopentadienyl rings each contribute 5 electrons to the complex, this is labeled as η^5 binding since the binding is not covalent in nature. The cyclopentadienyl rings donate π electrons to the metal centre from its delocalised π system, this why it adopts the sandwich structure. Since its discovery, ferrocene **17** has been at the heart of organometallic chemistry and its chemistry has been widely investigated.

Chapter I: General Introduction

2.2. Reactions of ferrocene:

Reactions of ferrocene **17** are many, and only a very small overview is presented to outline the types of reactions usually associated with ferrocene **17**. The chemistry of ferrocene **17** is very similar to that of aromatic compounds and due to its high electron density, it reacts readily with electrophiles. Friedel-Crafts alkylations and acylations are the most common methods used to functionalise ferrocene,⁴⁰ lithiation of ferrocene is also used to add functionality (Scheme 3).⁴¹



Scheme 3: Functionalisation of ferrocene **17**.

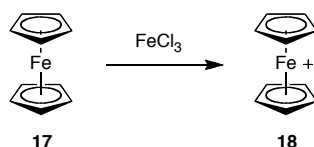
2.3. Properties:

2.3.1. Electrochemistry:

One of the major interests of ferrocene **17** has been in electrochemistry. Ferrocene **17** is known for its redox properties, it is readily oxidised to ferrocenium **18** (Scheme 4) at a relatively low potential (+ 0.4V vs. SCE, in acetonitrile and 0.1M $[NBu_4][PF_6]$)⁴². Most importantly the one electron oxidation of ferrocene **17** is fully reversible, therefore, it is

Chapter I: General Introduction

often used as a standard in cyclic voltammetry to characterise the redox potential of other organic compounds.⁴³



Scheme 4: Chemical oxidation of ferrocene **17** to ferrocenium **18**.

2.3.2. Electron richness:

As previously described, ferrocene is a sandwich compound made of two aromatic cyclopentadienyl rings. This makes ferrocene an extremely electron rich molecule. For instance, Alfrey-Price calculations (which offer “semi-empirical measure of electron richness”)⁴⁴ of vinylferrocene **19** give an e factor of -2.1 as compared to other recognised electron rich substituents (Figure 21).⁴⁴

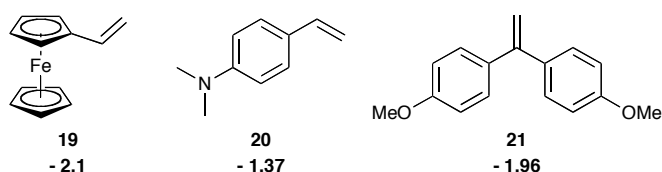


Fig. 21: Alfrey-Price e values of vinylferrocene **19**, *p*-*N,N*-dimethylaminostyrene **20** and 1,1'-dianisylethylene **21**.

2.4. Applications:

Ferrocene is one of the most common organometallic molecules in fields ranging from application in catalysis, medicinal chemistry and materials. In this section, a few recent examples of the uses of ferrocene in the afore mentioned fields are presented to outline the versatility of ferrocene which makes the molecule an interesting target in synthetic chemistry.

Chapter I: General Introduction

2.4.1. Ferrocene as a catalyst:

Catalysis research is driven by the search for powerful, robust and versatile ligands. The stability of the ferrocene moiety as well as the ability to tune its electronic properties by substitutions has made it a key target for the development of powerful ligands for organometallic catalysts. Ferrocenes are widely used in industry for homogeneous achiral and chiral catalysis.

1,1'-*bis*(Diphenylphosphino)ferrocene **22** (dppf) (Figure 22) is one of the most common ligands used in achiral palladium catalysis. A recent review describes the application of dppf as a ligand in many palladium-catalyzed cross-coupling reactions such as the Heck, Suzuki–Miyaura, Sonogashira, Negishi, Stille and Hiyama reactions.⁴⁵

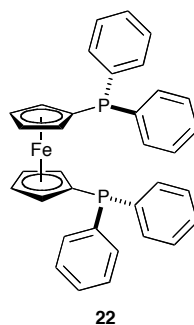


Fig. 22: Structure of dppf **22**.

Ferrocenyl ligands have also been used in chiral catalysis. Since ferrocene offers the possibility to desymmetrise by introducing both planar and/or central chirality. Planar chirality in 1,1'- adducts is only understood when bound as ligand and the two substituents are locked in position. Many 1,1'- and 1,2- type ligands (Figure 23) have been developed and used in synthesis as well as industry.⁴⁶

Chapter I: General Introduction

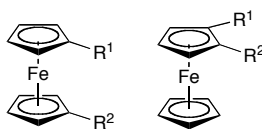
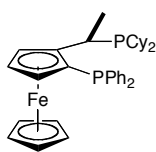


Fig. 23: 1,1'-type (left) and 1,2-type (right) ferrocenyl ligands.

In particular, Josiphos **23** (Figure 24) and its derivatives are of the most used ferrocenylphosphine achiral ligands. First discovered by Togni in 1996,⁴⁷ it has now been successfully used in the industrial synthesis of the pesticide Metolachlor and Biotin.⁴⁸

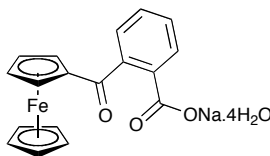


23

Fig. 24: Structure of Josiphos **23**.

2.4.2. Application in medicinal chemistry:

The versatility of the ferrocene moiety is quite extensive, as well as being used in catalysis it is used in medicinal chemistry. For example, Ferrocerone **24** (Figure 25) was marketed in the USSR as treatment for anaemia.⁴⁹



24

Fig. 25: Structure of Ferrocerone **24**.

Ferroquine **25** (Figure 26) was designed as part of an initiative to develop an alternative to the FDA approved antimalarial drug Chloroquine **26** (Figure 26).⁵⁰ Ferroquine has, as of 2011, successfully been through Phase II clinical trials.⁴⁹

Chapter I: General Introduction

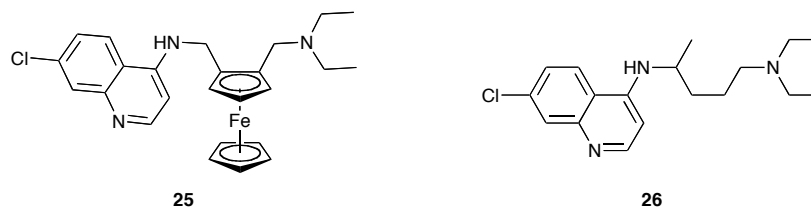


Fig. 26: Structures of Ferroquine **25** and Chloroquine **26**.

Another very promising ferrocene based drug target is Ferrocifen **27** (Figure 27). Like Ferroquine, Ferrocifen is a derivative of the FDA approved drug Tamoxifen **28** (used for treatment of breast cancer (Figure 27) and is one of many metallocenes showing promise for cancer treatment.⁴⁹

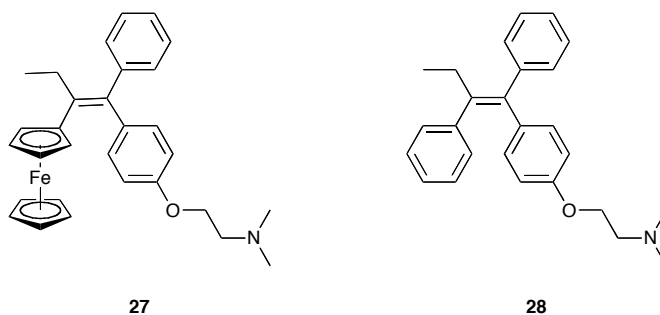


Fig. 27: Structure of Ferrocifen **27** and Tamoxifen **28**.

2.4.3. Materials:

Finally, ferrocene **17** has also seen many applications in materials chemistry. Mesogens (liquid crystals) are extremely interesting molecules with a range of applications. Metallomesogens are mesogenic polymers containing metal centers, such polymers attract a great deal of interest due to the possibility of combining the properties of the metal center and the processability of the polymer.⁵¹ Ferrocene **17** has successfully been incorporated to mesogenic polymers. The review by Gao and Shreeve outlines many different examples of ferrocene containing liquid crystals and identified the work of

Chapter I: General Introduction

Deschenaux and co-workers on ferrocene-[60]fullerenes **29** (Figure 28)⁵² as well as ferrocene-phosphorus polymers **30** (Figures 30) as the most promising materials.

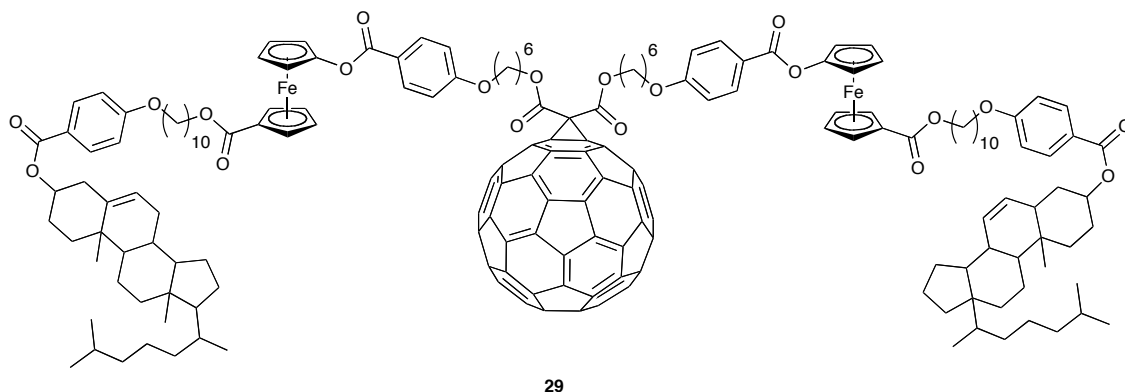


Fig. 28: Structure of a ferrocene-[60]fullerene **29**.⁵²

The combination of fullerene and ferrocene for instance could have application in the field of optoelectronics and other ferrocene-fullerene dyads have been synthesised and investigated to that purpose.⁵³ Prato and co-workers developed several ferrocene-C₆₀ dyads,⁵⁴ however the effects on the electrochemistry of C₆₀ was negligible.

However, in 2002, Prato and co-workers did report ferrocene-C₆₀ dyads (Figure 29) that not only exhibited efficient photoinduced electron transfer and favourable charge separation and charge recombination rates.⁵⁵ More importantly, dyad **31** also exhibited nanowire self-assembly on layer-by-layer thin films which facilitated charge transport and greatly improved photocurrent efficiency as compared with **32**. This goes to show that the organisation of donor and acceptors in organic electronic materials plays an important role and greatly affect efficiency of the electron transport processes.

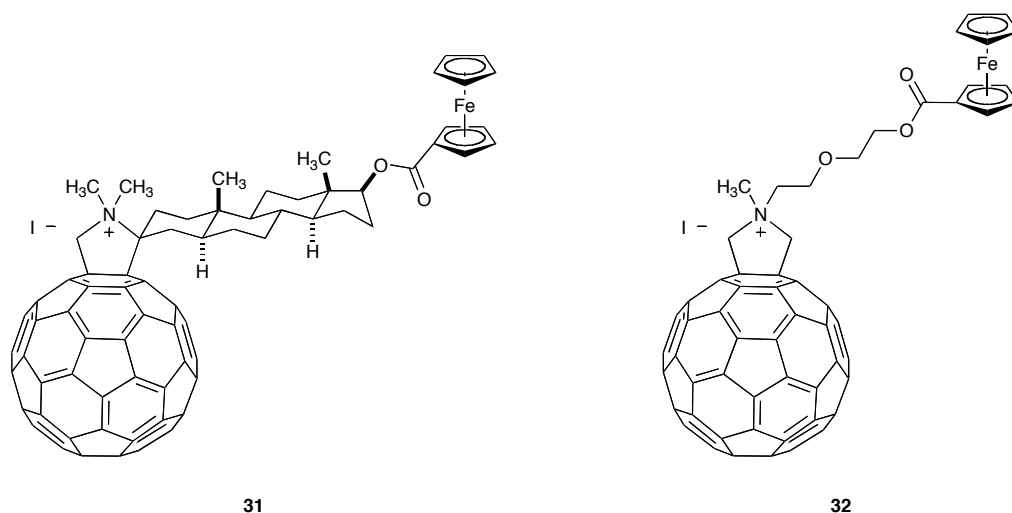


Fig. 29: Structure of a ferrocene-[60]fullerene dyads **31** and **32**.⁵⁵

Other applications of ferrocene containing polymers included the work of Kannan and co-workers, who reported the synthesis of ferrocene-phosphorus mesogenic polymers and indicate that the combination produced materials with noteworthy fire-retardant properties.⁵⁶ Ferrocene has also been incorporated to materials as a fuel additive for rocket fuel⁵⁷ or as an electrolyte in solar cells.⁵⁸

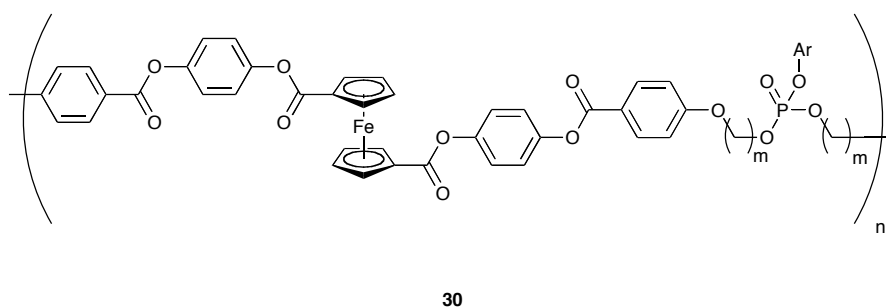


Fig. 30: Structure of a ferrocene-phosphorus **30**.^{56a}

As has been shown, the versatility of flavins and ferrocene makes both molecules very interesting targets for various applications. The following chapters will describe the work carried out with flavins as electron acceptors for the preparation of donor-acceptor systems for use in optoelectronic materials such as organic photovoltaics, as well as, the

Chapter I: General Introduction

combination of flavin and ferrocene in the development of a novel organic super-acceptor molecules and finally the development of new umpolung methodology using the redox properties of ferrocene.

CHAPTER II: SYNTHESIS AND CHARACTERISATION OF 8-ETHYL-6,7-BISTHIOPHENE-THIOPTERIDINE-2,4-(3H,8H)-DIONE AND ITS DERIVATIVES AS MATERIALS FOR OPTOELECTRONIC APPLICATIONS.

1. Introduction

Optoelectronics is a field of materials science which is concerned with devices that use electrical energy to produce an optical effect or use optical energy to produce electrical energy. These devices are primarily semiconductors and therefore were, until recently, solely based on inorganic materials such as silicon. However, organic small molecules and semiconducting polymers are progressively being used for such applications. Organic light emitting diode (OLED) displays are found in household televisions and displays while current research aims to commercialise indoors OLED lighting solutions to replace conventional bulbs. One field of organic optoelectronics which is thriving is the development of small molecules and conjugated polymers for photovoltaic devices. The photovoltaic effect was first observed by Edmond Becquerel in 1839⁵⁹ and consists of converting the energy of light into electricity. Considering the current need for clean renewable energy, research and development of photovoltaic devices is a vibrant area of scientific research. To date, industrial photovoltaic devices are mainly manufactured using inorganic semiconductors. However, a great deal of effort is being put in the research and development of organic semiconducting materials for use in photovoltaic devices.

1.1. The photovoltaic (PV) effect:

The photovoltaic effect as described by the Collins English Dictionary is “the effect observed when electromagnetic radiation, especially visible light from the sun, falls on a thin film of one solid deposited on the surface of a dissimilar solid producing a

Chapter II: Synthesis of 8-Ethyl-6,7-Bis-Thiopteridine-2,4-(3H,8H)-Dione

difference in potential between the two materials.”⁶⁰ In the current search for renewable energies as imposed by the depletion of fossil fuel resources, solar energy is at the forefront of scientific research to find new and better ways to harvest the electromagnetic energy of the sun (Figure 31).

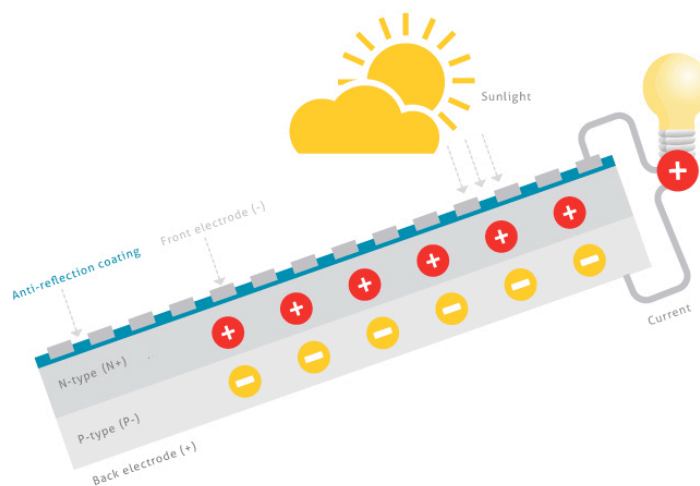


Fig. 31: Typical silicon PV cell cartoon representation.⁶¹

When designing a PV device it is important to try and capture as much of the energy as possible. Although only the visible part of the electromagnetic spectrum can be perceived by the naked eye, solar radiation includes ultraviolet and infrared radiations. It is important to notice that most of the energy in solar radiation is actually found in the infrared region of the spectrum (Figure 32).⁶² Although, the strongest energy output is in the visible region, the area under the curve from near-infrared to infrared region is much greater.

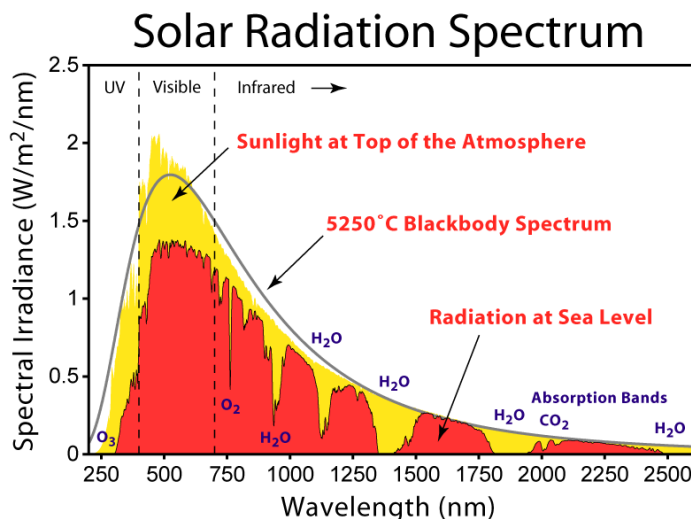


Fig. 32: Representation of solar radiation power against wavelength.⁶²

1.2. Overview of PV in the global market:

Modern photovoltaic devices are made up of a semiconducting material trapped between two electrodes. Several types of materials can be used the fabrication of PV devices, some of the more common ones are silicon, cadmium-telluride or copper indium gallium(di)selenide semiconductors.

To date, all commercial photovoltaic devices are made from inorganic materials.⁶³ These remain rather expensive, according to the Energy Saving Trust: “The average domestic solar PV system is 3.5 to 4kWp and costs around £7,000 (including VAT at 5%), with the typical cost ranging from £5,500 to £9,500.”⁶⁴ Efficiencies of commercial devices vary from 6% for a silicon thin-film to 29% for concentrated multijunction devices (Table 1).⁶⁵

TABLE 3.2 2010 COMMERCIAL MODULE EFFICIENCIES	
Technology	Commercial Module Efficiency
Monocrystalline silicon ^b	14%
Multicrystalline silicon ^b	14%
CdTe ^c	11%
a-Si ^d	6%
CIGS ^e	11%
Low-concentration CPV with 20%-efficient silicon cells	15%
High-concentration CPV with 38%-efficient III-V multi-junction cells	29%

^b The efficiency represents average production characteristics. Non-standard monocrystalline technologies—such as SunPower's rear-point-contact cell (19.3% efficiency) and Sanyo's HIT-cell-based module (17.1% efficiency)—are commercially available.

^c First Solar 2010a

^d Uni-Solar 2010. Based on a flexible laminate a-Si module.

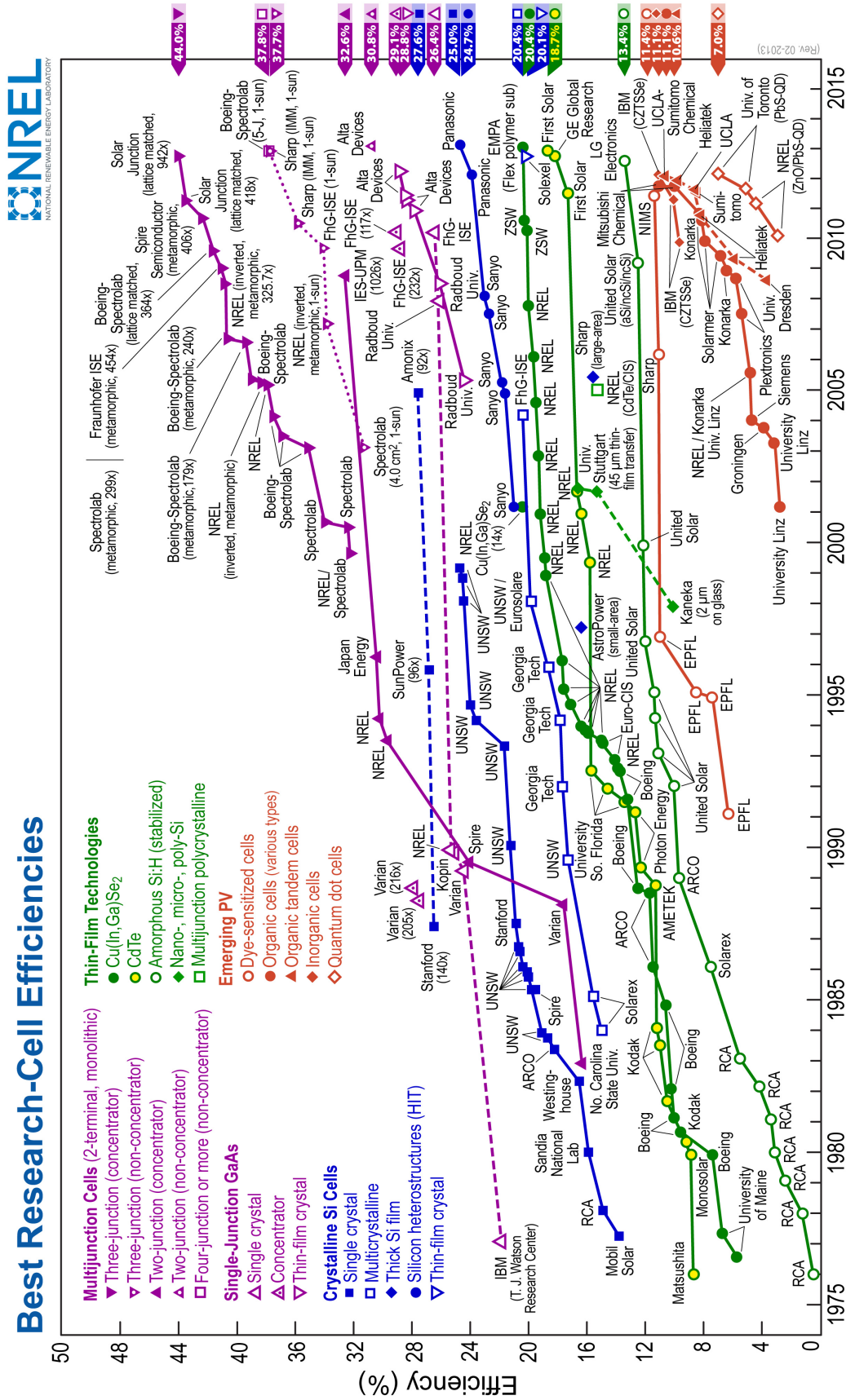
^e Mehta and Bradford 2009

Table 1: Table of commercial PV module efficiencies.⁶⁵

Mono and Multicrystalline silicon PV modules remain the largest part of the market representing 37% and 48% annual PV cell and module shipments respectively.⁶⁵ Despite major sale price reduction over the last 10 years, primarily due to the market growth, the cost of manufacture of inorganic PV remains high. For this reason, although the research for more efficient inorganic PV devices continues, a lot of effort is being spent in the development of organic materials that would be cheaper to manufacture and offer more practicality of use.

1.3. Emerging organic photovoltaics:

As can be seen from graph 1, research in emerging organic photovoltaics began ca. 1990 and has now has seen much growth particularly in the last decade. The research can be divided in three categories, dye-sensitised solar cells, quantum dot solar cells or conjugated organic small molecules and polymers.



Graph 1: Graph representing the best research in PV technology by efficiency over time.⁶⁵

Chapter II: Synthesis of 8-Ethyl-6,7-Bis-Thiopteridine-2,4-(3H,8H)-Dione

1.3.1. Dye-sensitised solar cells (DSSC):

A dye-sensitised solar cell is a thin-film solar cell where an organic dye is applied onto a mesoporous working electrode (TiO_2) separated from a counter electrode (Pt) by electrolytes.⁶⁶ As sunlight strikes the surface of the working electrode a photon with enough energy may oxidise the dye to an excited state that will provide an electron to the working electrode. This electron will then diffuse to the counter electrode through the electric circuit, at the same time the sensitizer is reduced by the electrolyte (I^-/I_3^- or $\text{Co}^{II}/\text{Co}^{III}$) and the oxidised electrolyte is itself regenerated at the counter electrode to close the circuit (Figure 33). The key factor for this type of device relies in the choice of dyes that will absorb photons to provide the electron to the conduction band of the working electrode. DSSCs function in very similar fashion to photosynthesis and many of the most efficient dyes are based around a chlorophyll porphyrin-like ring.

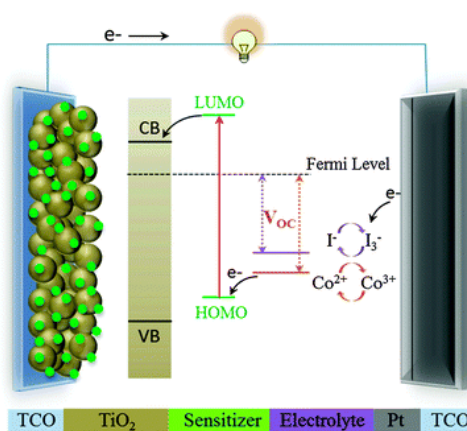


Fig. 33: Schematic representation of the composition and the operating principle of a DSSC.⁶⁶

Grätzel and O'Regan are regarded as the inventors of DSSCs. In 1991, they reported the first high efficiency DSSC device.⁶⁷ They managed to achieve 7.9% power conversion efficiency in artificial light. They introduced the use of TiO_2 as working electrode and the use ruthenium based dyes. Ruthenium dyes, notably "black dye" **33** (Figure 34) are amongst the best and have been reported to give some of the highest efficiency to date.

Chapter II: Synthesis of 8-Ethyl-6,7-Bis-Thiopteridine-2,4-(3H,8H)-Dione

Black dye **33**, for instance, was reported to achieve efficiency of 11.1% by Chiba and co-workers in 2006.⁶⁸ However, because ruthenium is an expensive material, recent efforts have been focusing on developing cheaper suitable dyes, particularly using porphyrins.

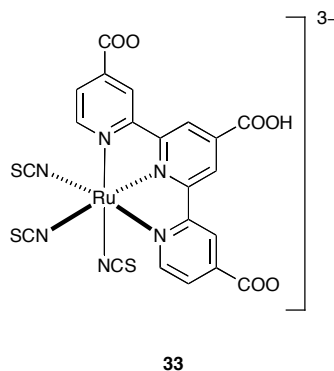


Fig. 34: Structure of “black dye” **33**.

To date, the highest recorded efficiencies are in excess of 12% for DSSC under AM 1.5 light.⁶⁹ Gratzel and co-workers developed a DSSC using a porphyrin dye and a cobalt couple as the electrolyte. They managed to achieve a power conversion efficiency of 12.3% using dye YD2-o-C8 **34** with co-sensitiser Y123 **35** (Figure 35).

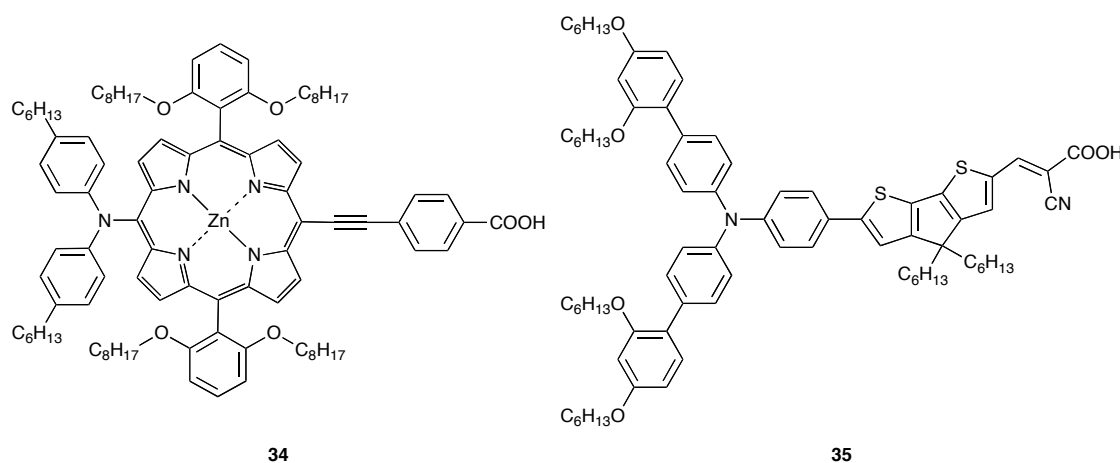


Fig. 35: Structure of YD2-o-C8 **34** and Y123 **35**.

Chapter II: Synthesis of 8-Ethyl-6,7-Bis-Thiopteridine-2,4-(3H,8H)-Dione

1.3.2. Quantum dot solar cells (QDSC):

In 1990, Barnham and Duggan first introduced the idea of using quantum dots as solar cell materials.⁷⁰ They noted that, since single material (single band gap) solar cells can only absorb a limited energy range of incident photons, the use of multi-band gap solar cells offered an effective way to extend the absorption range of devices. This had already been achieved with multi-junction devices, where two to three layers of semiconductors with different band gaps absorb photons of different energy as they go through the device.

However, the manufacture of such devices is complicated and costly. Barnham and Duggan present calculations which suggest that greater conversion efficiencies can be achieved by using quantum dots. Quantum dots are nanocrystalline semiconductors; the important feature of quantum dots is that their properties can be easily tuned simply by changing their size. Also, quantum dots have access to different quantum states and can produce more than one electron-hole pair if excited with a high energy photon.⁷¹ Therefore, a multi-band gap solar cell could be devised from a single quantum dot material. Unlike DSSCs quantum dot solar cells do not follow a single type of device architecture. QDSC can be found in the form of bulk heterojunctions, sensitisers or even polymer hybrid solar cells.⁷²

In 2012, Ip and co-workers reported a QDSC device, using halide passivated PbS quantum dots, that achieved a record efficiency in excess of 7.0%.⁷³ The addition of halide atoms and mercaptopropionic acid (MPA) to the quantum dot were instrumental in minimising “trap state” areas. These area are fundamentally responsible for the low power conversion of quantum dot devices because they promote charge recombination.

Chapter II: Synthesis of 8-Ethyl-6,7-Bis-Thiopteridine-2,4-(3H,8H)-Dione

Later the same year, Kim and co-worker reported a solid-state quantum dot sensitised solar cell.⁷⁴ Here PbI perovskites were deposited on as a heterojunction with TiO₂ doped with a hole transport medium. This particular cell achieved efficiency of 9.7% under AM 1.5 light.

In practice, quantum dot solar cells have been prepared using a range of different materials but have yet to achieve high efficiencies. However, QDSC research is still in its infancy and the potential for low-cost high efficiency devices remains.

1.3.3. Organic/polymer solar cells (OPV):

OPVs have been part of the emerging PV market for the last decade in an attempt to solve the shortcomings of traditional silicon PV systems. OPVs are either made with thin film polymers or small molecules. The main advantages are cost effective manufacturing processes (spin coating, printing...), low cost materials and applications to flexible substrates. Although OPVs are reckoned not to be able to exceed the power efficiencies of their inorganic counterparts, they could make up for it in value for money.

-Device architecture:

There are two main architecture types for OPVs, bi-layer and bulk heterojunction (BHJ). Bi-layer devices will, as the name suggests, be made of two layers sandwiched between two electrodes, very much like a crystalline silicon PV cell. One layer consists of an electron donor material, the other of an electron acceptor. On the other hand, bulk heterojunction devices consist of a blend of donor and acceptor molecules.

Apart from the active layer(s), the rest of the device architecture is the same in most cases. Most devices consist of a transparent substrate (glass, polymer, ...) coated with a

Chapter II: Synthesis of 8-Ethyl-6,7-Bis-Thiopteridine-2,4-(3H,8H)-Dione

transparent conductive oxide such as indium tin oxide (ITO) which is the anode. Then a layer of poly(3,4-ethylenedioxythiophene):poly(styrenesulfonate) (PEDOT:PSS) is often found (particularly in BHJ) as a protective layer and a hole transport layer (HTL). The HTL is particularly necessary in BHJ devices since both the donor and acceptor are in contact with both electrodes. The active layer is then applied and the device is then completed with the cathode, generally aluminium (Figure 36).

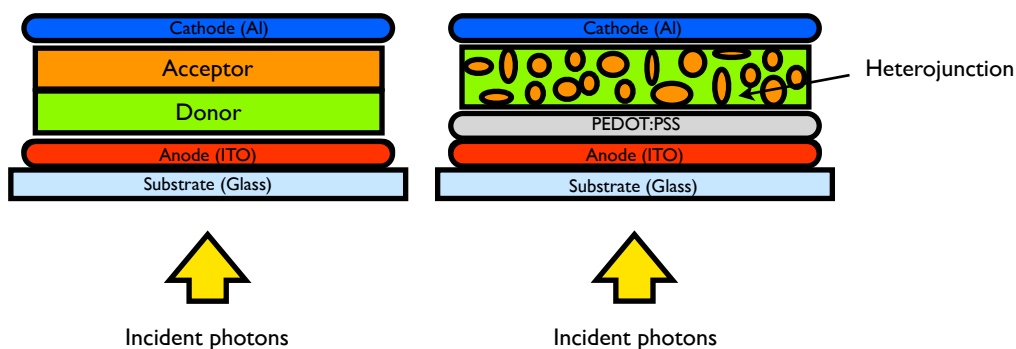


Fig. 36: Representation of device architectures, bilayer (left) and bulk heterojunction (right).

Since OPVs are still relatively new there is a lot of research around the materials used in their fabrication. For example, carbon nanotubes are being investigated as materials for the cathode, as well as acceptor materials.^{75, 76}

-Mode of action:

As a photon of light goes through the anode, it is absorbed by the donor material to produce an exciton (electron-hole pair). The exciton can then diffuse to the donor-acceptor interface and dissociate or it can recombine. The dissociated charges then travel toward their complementary electrodes, the electron travels to the cathode and then goes through the circuit back to the anode to generate current. The electron then recombines with a free hole and the process is repeated (Figure 37).⁷⁷

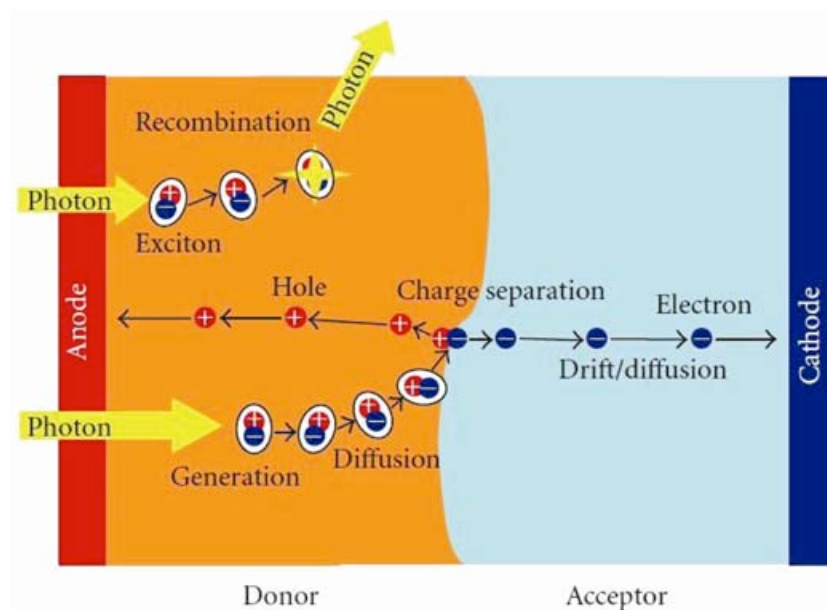


Fig. 37: Charge transfer process in a bi-layer device.⁷⁷

-Active layer materials:

As previously explained, OPVs consist of an active layer of donor and acceptor materials. Here a selected number of organic donor and acceptor materials and their key features are highlighted.

High power conversion efficiency depends on several factors, but non so important as charge transfer. As a photon of light is absorbed by the donor materials the exciton is formed by promotion of an electron from the highest occupied molecular orbital (HOMO) of the donor to its lowest unoccupied molecular orbital (LUMO). The key of charge transfer is to quickly transfer the electron from the LUMO of the donor to the LUMO of the acceptor before the charge recombines. Also if the HOMO of the donor is lower in energy than that of the acceptor then the whole exciton can transfer from the donor to the acceptor (Figure 38). The charge cannot be separated and there is no generation of current. Therefore, one key feature of OPVs is well matched donor/acceptor HOMO/LUMO levels.

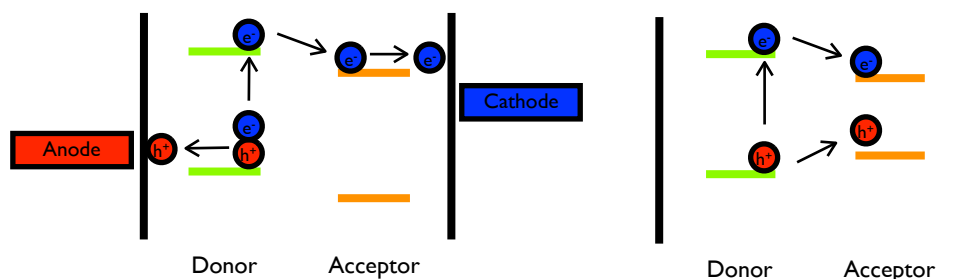


Fig. 38: Charge transfer process at the molecular orbital level, favourable staggered orbitals (right), disfavoured non staggered orbitals (left).

OPV materials are classed in two categories, small molecules and polymers. Since many review articles have already been produced on the progress of OPV active materials only a small number of important examples are highlighted here.^{77, 78}

For a long time the bench mark of small molecule OPVs were copper phthalocyanine **36** (CuPc) and fullerene C₆₀ **37**, as donor and acceptor respectively (Figure 39). The combination of both molecules represented the bench mark of small molecule OPV efficiency for a long time, achieving a maximum of 5% efficiency in a mixed-HJ device.⁷⁹

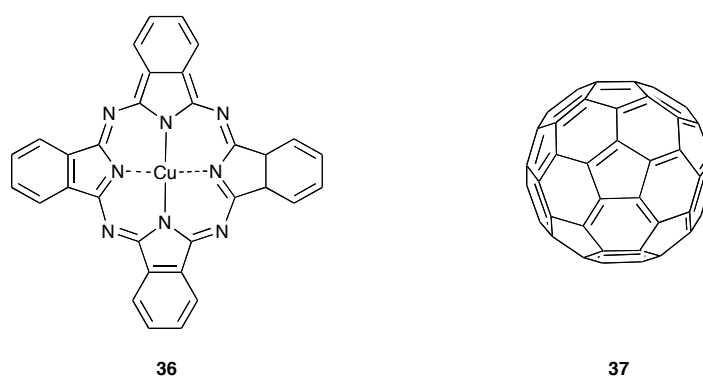


Fig. 39: Structures of CuPc **36** and C₆₀ **37**.

Chapter II: Synthesis of 8-Ethyl-6,7-Bis-Thiopteridine-2,4-(3H,8H)-Dione

In the years that followed, much work was done to find better donor molecules. Whereas, fullerene based acceptors have remained the acceptor molecule of choice, particularly phenyl-C₆₁-butyric acid methyl ester (PC₆₁BM) and its derivatives. New types of donor small molecules include squaraines (**38**)⁸⁰ and oligothiophenes (**39 & 40**)⁸¹ (Figure 40). All of which have been incorporated to devices with fullerene acceptors and achieving efficiencies above the 5% bench mark set by CuPc **36**.

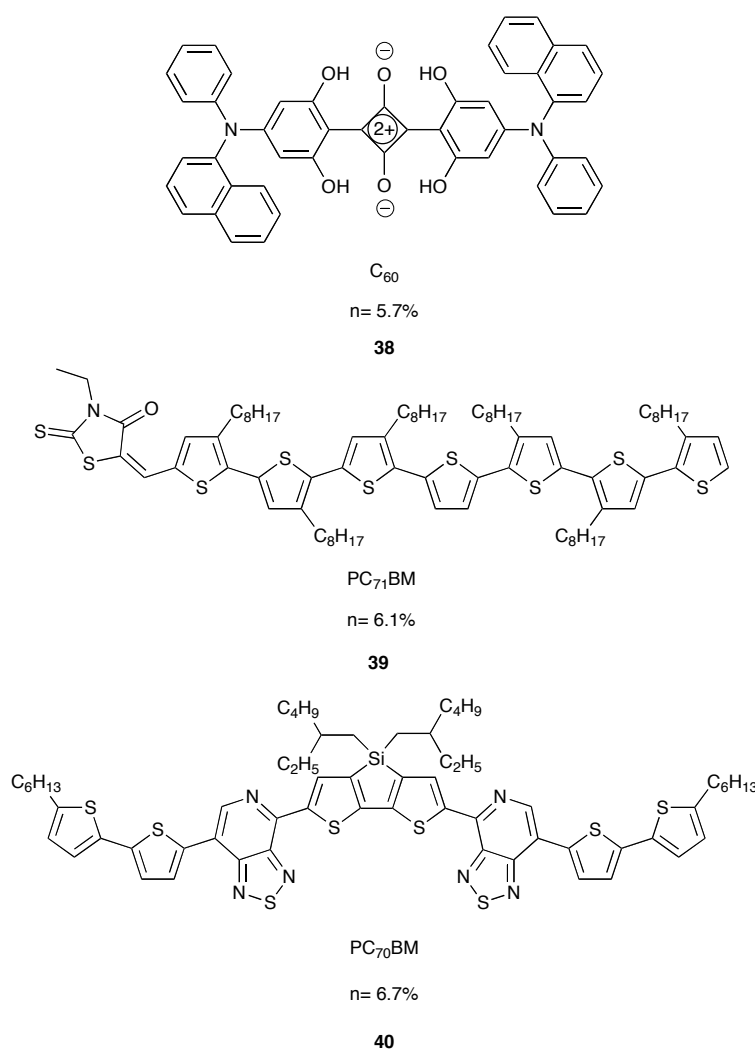
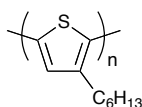


Fig. 40: Structures of alternative donor materials with acceptor partner and recorded efficiency.

Chapter II: Synthesis of 8-Ethyl-6,7-Bis-Thiopteridine-2,4-(3H,8H)-Dione

Polymers are also being used as OPV materials, the most note worthy is poly(3-hexylthiophene) **41** (P3HT, Figure 41). Regioregular alkyl-polythiophenes are recognised as “the best class of balanced high-performance materials used as p-type semiconductors”.⁸² P3HT **41** is the most used donor in high efficiency OPV devices and was recently combined with a fullerene acceptor and a thiophene additive to achieved 6.69% power conversion efficiency.⁸³



32

Fig. 41: Structure of P3HT **41**.

In 2012, Dou and co-workers achieved the highest efficiency for a polymer based OPV device (8.62%).⁸⁴ This was achieved using a tandem solar cell (multijunction). The first active layer consisted of a blend of P3HT **41** and IC₆₀BA **42** and the second active layer was a blend of PBDTT-DPP **43** and PC₇₁BM **44** (Figure 42). This kind of tandem solar cell using bend of small molecules and polymers could be the future of OPVs.

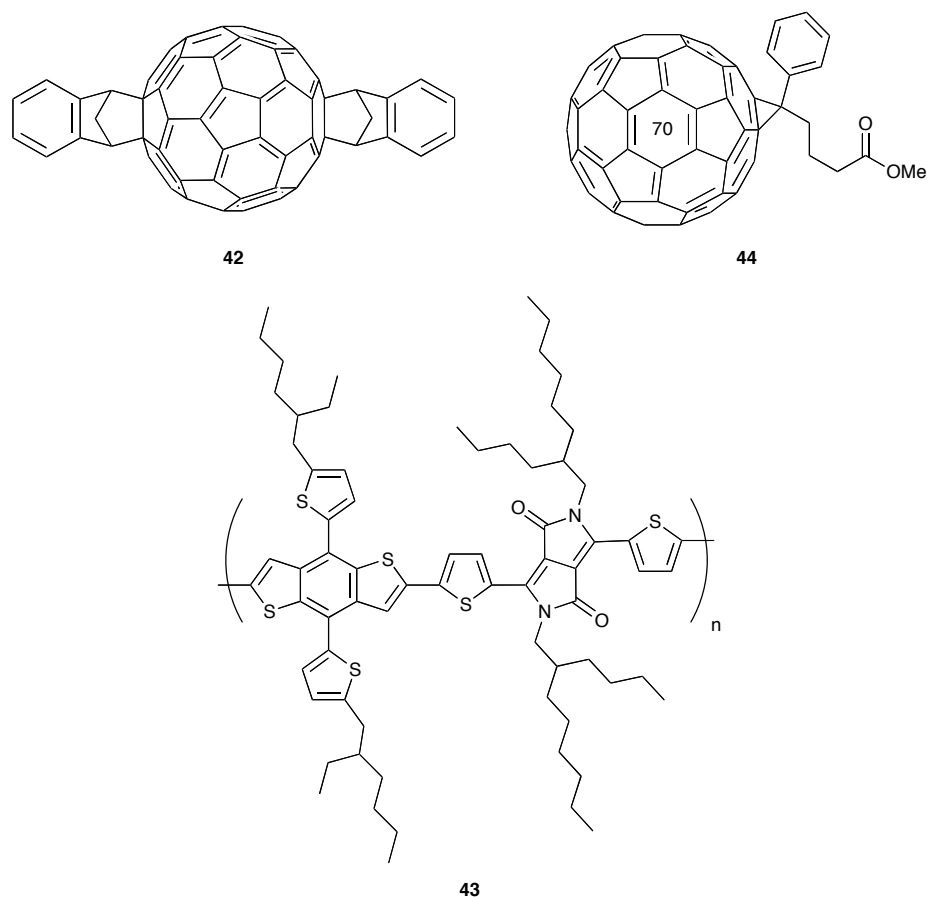


Fig. 42: Structures of IC₆₀BA **42**, PBDTT-DPP **43** and PC₇₁BM **44**.

However, there has been some interest in the development of “single material” OPVs where the donor and acceptor molecules are associated into one molecule/polymer.⁸⁵ Since charge transfer, charge mobility and charge separation is key to the efficacy of a PV device, it is thought that combining donor and acceptor moieties in single molecules might improve such factors. Also the combination of electron donating moieties to electron acceptor molecules is a very efficient way to tune electronic properties such as the HOMO-LUMO and absorption spectrum. So far, these dyads and triads have failed to rival efficiencies of blend devices,⁸⁶ however when used in conjunction with other OPV materials they show potential.⁸⁷

2. Aims

The aim of this project was to use recent findings by Cooke, Rotello and co-workers,⁸⁸ which suggest that flavins in a donor-acceptor dyad system have efficient energy and charge transfer properties. For this reason we used knowledge from general optoelectronic material and from current research being carried in the Cooke research group (unpublished results to date) to design a novel flavin based dyad.

10-Ethyl-6,9-bis-thiophene-benzopteridine-2,4-(3H,10H)-dione **45** (Figure 43) was previously prepared by the Cooke research group (unpublished). It was thought that adding thiophene donor at the C(6) and C(9) positions of a standard flavin would enhance electrochemical and optical properties of the flavin core. It would also make use of the three point hydrogen bonding ability of flavins for the potential formation of nanostructures. Investigation of the x-ray structure of **45** also provided knowledge that, in the solid state, only one of the thiophene rings was in conjugation with the flavin core. This is likely due to a combination of electronic effects and sterics from the ethyl side chain. After addition of an heptyl chain at the N(3) position to render the compound more soluble, selective bromination of the thiophene ring that is in conjugation with the flavin core was achieved to give flavin **46** (Figure 44). This gives a platform for further functionalisation and the formation of regioregular compounds with potential optoelectronic applications (dimersisation).

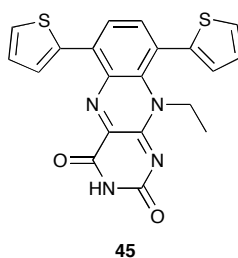


Fig. 43: Structure of compound **45**.

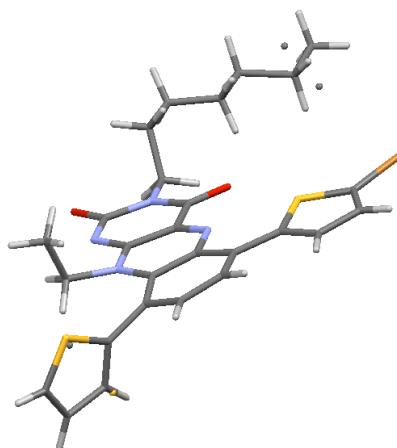


Fig. 44: X-ray structure of flavin **46**.

With that knowledge in hand 8-ethyl-6,7-*bis*-thiophene-thiophenepteridine-2,4-(3*H*, 8*H*)-dione **47** (Figure 45) was designed to be an effective donor-acceptor dyad for use in optoelectronic materials. Replacing the phenyl ring in the core flavin with thiophene and assuming that selective bromination would also happen with compound **47** in the same way as with compound **45**, could lead to the formation of flavin based olygothiophenes (Figure 46).

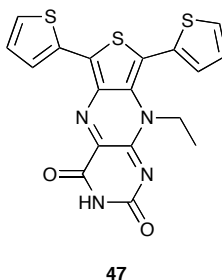


Fig. 45: Structure of compound **47**.

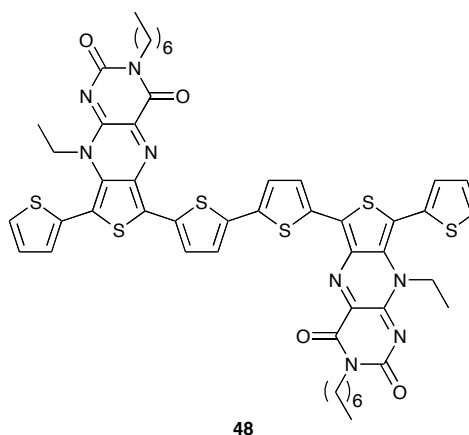
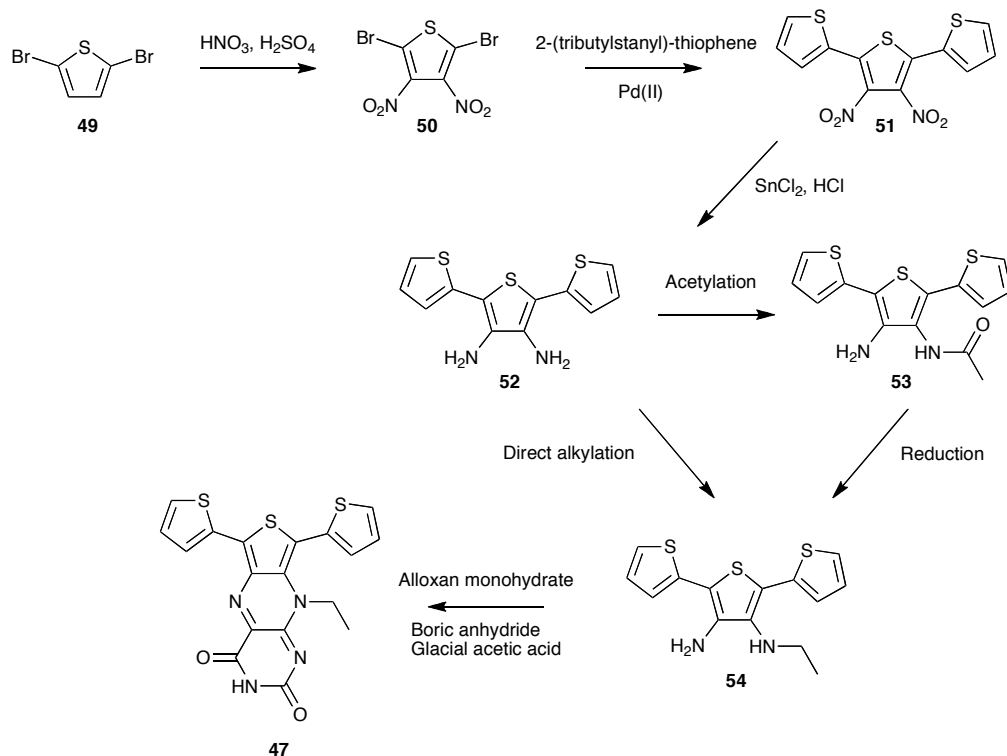


Fig. 46: Structure of sexi-thiophene target **48**.

The proposed synthesis of compound **47** follows a straightforward synthesis of the flavin from standard chemical transformations using relatively cheap starting materials. The first step would be the di-nitration of readily available 2,5-dibromothiophene **49** using standard conditions followed by a Stille type coupling using 2-(tributylstanyl)-thiophene and a palladium (II) catalyst to give the terthiophene 3',4'-dinitro-[2,2',5',2'']-terthiophene **51**. Then, reduction of the two nitro groups would give the diamino product **52** which would then undergo either mono *N*-alkylation or *N*-acylation and subsequent reduction to give *N*-ethyl-[2,2',5',2'']-terthiophene-3',4'-diamine **53**. Finally, **53** would undergo alloxan condensation under standard conditions to afford the target flavin **47** (Scheme 5).

Chapter II: Synthesis of 8-Ethyl-6,7-Bis-Thiopteridine-2,4-(3H,8H)-Dione



Scheme 5: Proposed strategy for the synthesis of **47**.

The next stage in the synthesis would see the functionalisation of flavin **47** to make a suitable material for photovoltaic applications. *N*-Alkylation of **47** to afford 3-heptyl-8-ethyl-6,7-bis-thiophene-thiophenepteridine-2,4-(3*H*,8*H*)-dione **55** (Figure 47) would first improve the solubility of the material.

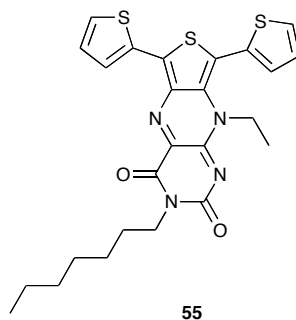
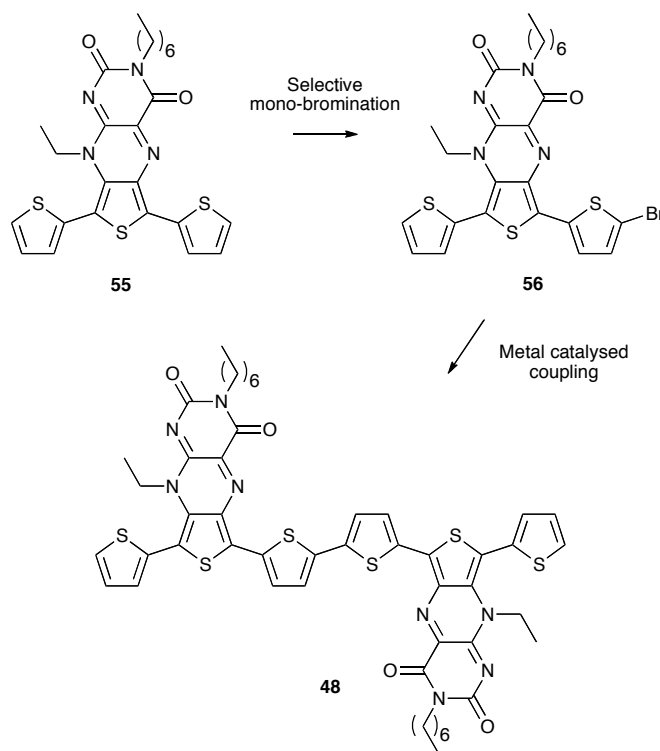


Fig. 47: Structure of compound **55**.

Chapter II: Synthesis of 8-Ethyl-6,7-Bis-Thiopteridine-2,4-(3H,8H)-Dione

Subsequent selective mono bromination would afford a platform to achieve the synthesis of the desired sexi-thiophene **48** via metal-catalysed coupling conditions (Scheme 6). Finally, these materials would be fully characterised and their potential for the fabrication of a photovoltaic device assessed.

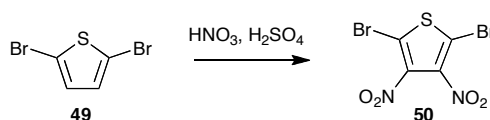


Scheme 6: Synthetic strategy toward sexi-thiophene dimer **48**.

3. Results and discussion

3.1. Synthesis of 8-ethyl-6,7-bisthiophene-thiopteridine-2,4-(3H,8H)-dione **47**:

3.1.1. Synthesis of 3,4-dinitro-2,5-dibromothiophene **50**:

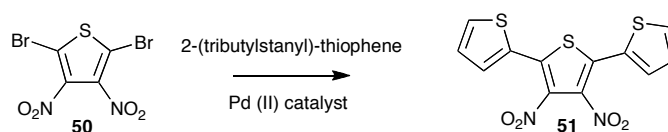


The first attempts to perform the nitration of 2,5-dibromothiophene **49** were done under standard conditions using a 3:2 mixture of concentrated sulfuric acid and concentrated nitric acid. This reaction was done on different scales ranging from a few milligrams to

Chapter II: Synthesis of 8-Ethyl-6,7-Bis-Thiopteridine-2,4-(3H,8H)-Dione

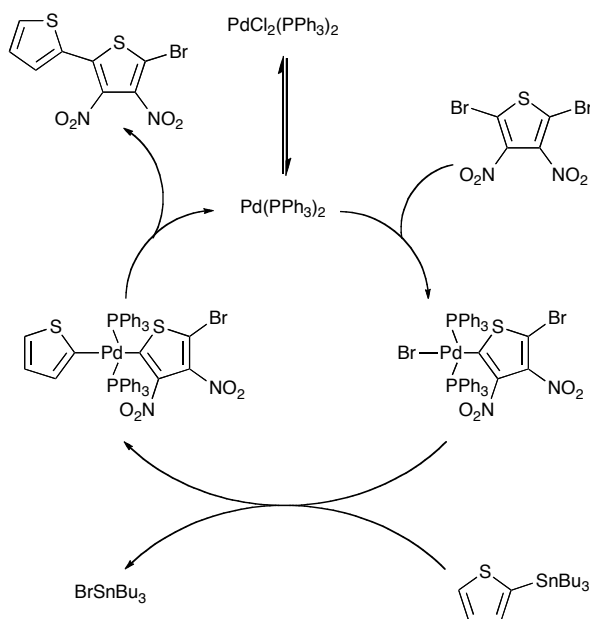
several grams and showed a peak efficiency on a ten gram scale and diminishing yields when further increasing the scale. Though very reproducible, this reaction was very low yielding averaging around 25%. This was not an issue since both reagents and the starting material are reasonably inexpensive. However, after looking further in the literature, it was noticed that by changing concentrated acids to fuming acids the yield of this reaction could be greatly improved.⁸⁹ Rasmussen *et. al.* reported a 47% yield by using mixtures of both concentrated and fuming acids. In an attempt to keep costs as low as possible whilst still improving the yield of this reaction, the use of fuming nitric acid with concentrated sulfuric acid proved to be a good compromise and achieved routinely a 53% yield on a multi-gram scale.

3.1.2. 3',4'-Dinitro-[2,2',5',2'']-terthiophene 51:



The Stille coupling reaction is one of many palladium mediated cross-coupling reactions. The Stille cross-coupling reaction was discovered by John K. Stille and David Milstein in the late 1970's and reported the palladium mediated coupling of sp^2 -hybridised organo-halide centers with organo-tin compounds.⁹⁰ The mechanism of the Stille reaction is now well understood and proceeds via activation of the palladium species from palladium(II) to palladium(0). Then, the organo-halide reagent undergoes oxidative addition and *cis/trans* isomerisation. Transmetalation with the organotin reagent gives an intermediate which can undergo reductive elimination thereby giving the desired product and regenerating the catalyst (Scheme 7).

Chapter II: Synthesis of 8-Ethyl-6,7-Bis-Thiopteridine-2,4-(3H,8H)-Dione



Scheme 7: Stille coupling catalytic cycle.

In this reaction the product of the first coupling reaction can react again through the same cycle with the catalyst and the stannane to give the desired terthiophene product. Product **51** was successfully and reproducibly synthesised in quantitative yields.

3.1.3. Reduction of nitro groups:

With the three thiophenes now in place, the nitro groups needed to be reduced to primary amines. This reaction proved a lot more troublesome than it first appeared.

The reduction of aromatic nitro groups can be achieved using many different methods, catalysed hydrogenation⁹¹ and metal reduction⁹² are amongst the most used. Several methods were used to perform this reaction and some are reported in table 2.

Chapter II: Synthesis of 8-Ethyl-6,7-Bis-Thiopteridine-2,4-(3H,8H)-Dione

Reagents	Conditions	Time	Yield
SnCl ₂ , EtOH, conc. HCl	N ₂ , 30 °C	18 h	27 - 63% varying purity
Sn, conc HCl	r.t.	18 h	no product
Fe, NH ₄ Cl, H ₂ O, MeOH	reflux	100 h	no product
SnCl ₂ , EtOH, conc. HCl, Toluene	90 °C	18 h	90-97%

Table 2: Optimisation of dinitro reduction.

After much trial and many unsuccessful reactions it was found that addition of toluene to the reaction mixture, using SnCl₂ as the reducing agent, improved the yield and reproducibility, achieving routinely yields between 90-97%. In the original SnCl₂ procedure, toluene was used as solvent to extract the product from the tin residue. However, that procedure proved to be inefficient and often unsuccessful as the tin residue can be hard to extract fully, particularly on multi-gram scales. Therefore, by adding toluene to the reaction, the product was directly extracted into the organic layer as it is being formed and thus, the work up only consisted of separating and washing the layers.

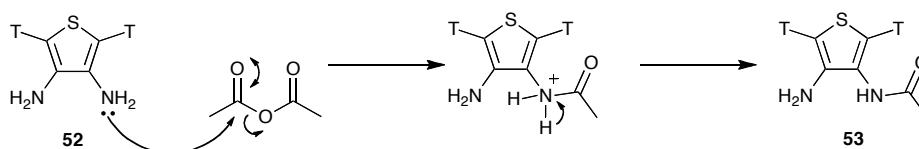
3.1.4. Synthesis of *N*-Ethyl-[2,2',5',2'']-terthiophene-3',4'-diamine **54**:

The next step in the synthesis was to prepare of *N*-ethyl-[2,2',5',2'']-terthiophene-3',4'-diamine **54**. This could be done in one of two ways, either by direct alkylation or by *N*-acylation and subsequent reduction.

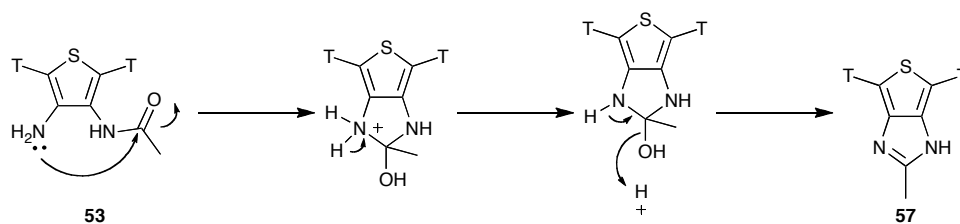
Chapter II: Synthesis of 8-Ethyl-6,7-Bis-Thiopteridine-2,4-(3H,8H)-Dione

-Acylation and reduction:

The acylation was performed under standard conditions using acetic anhydride in pyridine (mechanism, Scheme 8). The reaction was successful but yielded only 49% of the mono-amide **53** after flash column chromatography on neutral alumina, as the amide product is susceptible to ring closure (Scheme 9).⁹³



Scheme 8: Acylation mechanism (T=thiophene).



Scheme 9: Intramolecular *N*-cyclisation mechanism (T=thiophene).⁹³

Following the acylation reaction, the product was reduced under standard conditions using lithium aluminium hydride. This should give the *N*-alkylated amine **54** which, being also unstable, was transferred to the alloxan condensation step without purification. However, only a very small amount of the desired flavin **47** was isolated. Upon closer investigation of the NMR data of the two presumed precursors **53** and **54**, the integration of the peaks was found to be incompatible with the synthesis of the mono adducts, but could correspond to a mixture of the *bis* and *mono*-adducts of the acylated and reduced products **58** and **59** (Figure 48).

Chapter II: Synthesis of 8-Ethyl-6,7-Bis-Thiopteridine-2,4-(3H,8H)-Dione

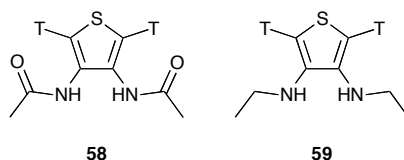


Fig. 48: Di-acylated **58** and di-alkylated **59** terthiophene products (T=thiophene).

-Direct alkylation:

It is well known that the direct alkylation of primary amines usually leads to over-alkylated products. This is due to the greater reactivity of the secondary amine towards alkylation. In this case the presence of the large aromatic system renders the amines even more reactive. Nevertheless, the mono-alkylation of diamine **52** was attempted.

In the first attempt, ethyl bromide was used in the presence of potassium carbonate.⁹⁴ The reaction was first attempted at room temperature without success, the temperature was then increased to 40 °C but without any formation of the desired product. A third attempt saw the addition of sodium iodide to promote halide exchange between bromine and iodine.⁹⁵ This, however, did not make any difference and still no product was found upon work-up.

After some research in the literature it was found that the *N*-alkylation of phenyldiamines was achieved in high yield by reacting a dialkylcarbonate in the presence of a NaY zeolite catalyst.⁹⁶ Unfortunately, this method did not work for this system and returned unreacted starting materials and unidentified side products. This is probably due to the fact that the cavity of the zeolite is not big enough to accommodate the terthiophene substrates.

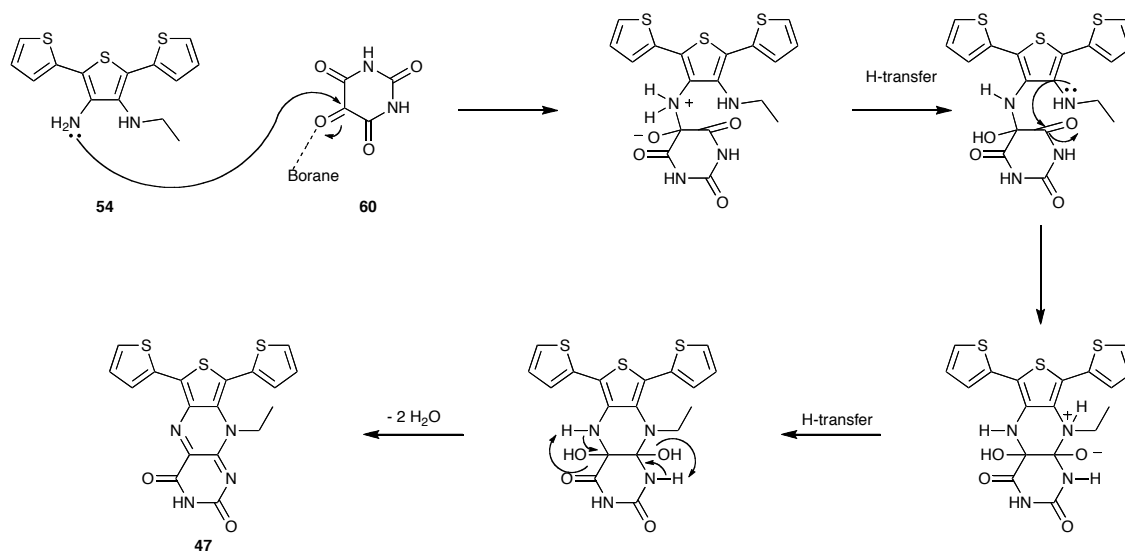
In a last attempt to perform the direct alkylation of the diamine substrate, the activation of the alkylating agent towards S_N2 substitution was again reconsidered and the use of an alkyl triflate reagent was investigated. This proved to be the method of choice,

Chapter II: Synthesis of 8-Ethyl-6,7-Bis-Thiopteridine-2,4-(3H,8H)-Dione

though the alkylated diamine was not isolated, the ^1H NMR spectrum of the crude material showed almost quantitative conversion to the desired product which was then used without purification in the next step of the synthesis.

3.1.5. Alloxan condensation:

Alloxan condensation has been the reaction used by many for the synthesis of isoalloxazines. The general procedure involves the activation of alloxan **60** by a borane reagent (here boric anhydride although boric acid is more commonly used) which promotes the first intermolecular condensation and then the second intramolecular condensation takes place to give the final product (Scheme 10).



Scheme 10: Proposed mechanism of alloxan condensation.

This final step afforded the desired flavin **47** in 53% yield over 2 steps which proved the relative success of the alkylation reaction.

Chapter II: Synthesis of 8-Ethyl-6,7-Bis-Thiopteridine-2,4-(3H,8H)-Dione

3.2. Analysis and characterisation of 47:

Compound **47** was compared to its analogue 10-ethyl-6,9-bisthiophenebenzopteridine-2,4-(3H,10H)-dione **44** that had been previously synthesised in the group. As previously observed in compound **44**, X-ray crystallography of **47** (Figure 48) shows that the thiophene ring on the same side of the ethyl side chain is orthogonal to the flavin core resulting in only one thiophene ring being truly in conjugation with the flavin core (Figure 50). This is likely due to a combination of steric hindrance of the ethyl chain and an electronic bias toward the other thiophene ring. This interesting feature of both flavin derivatives is what lead us to believe that mono bromination of **35** would be regiospecific as previously observed with flavin **46**.

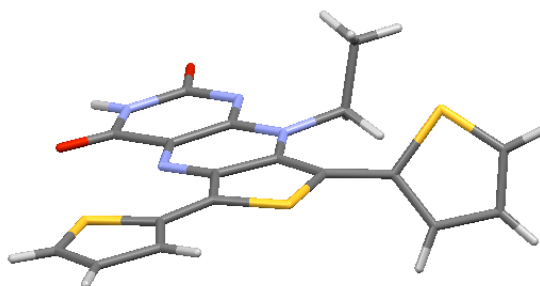


Fig. 49: X-ray structure of compound **47**.

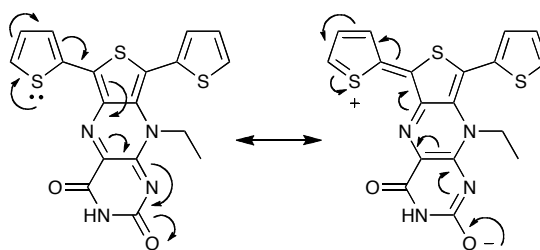


Fig. 50: Resonance structures of **47** showing conjugation of the “in-plane” thiophene.

Chapter II: Synthesis of 8-Ethyl-6,7-Bis-Thiopteridine-2,4-(3H,8H)-Dione

Secondly, the UV-visible spectrum of **47** was compared to that of **44**. At the same concentration, compound **44** shows stronger absorption between 250 nm and 300 nm. Relatively similar absorption is shown between 400 nm and 500 nm showing the typical flavin three peak absorption. However, **47** shows a slight increase in absorption toward the near infrared region with a peak at $\lambda_{\max} = 551\text{ nm}$ and an onset at $\lambda_{\text{onset}} = 671\text{ nm}$ (Figure 51).

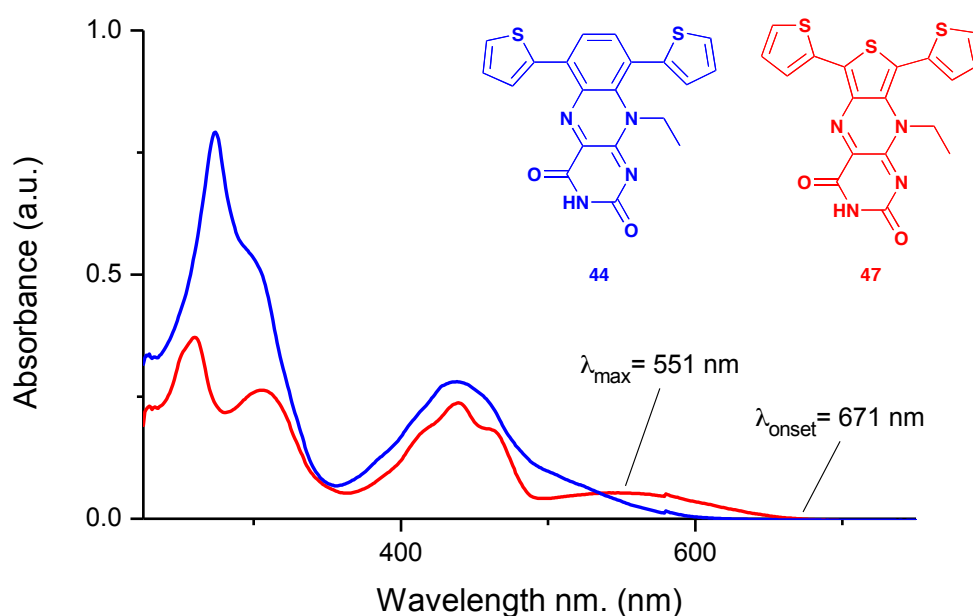
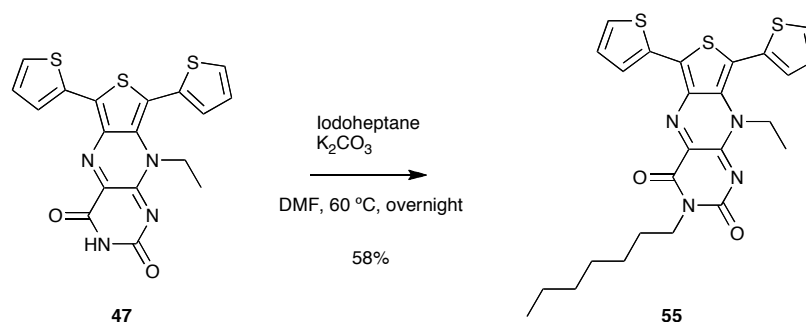


Fig. 51: Comparison of absorption spectra of **47** and **44** (5×10^{-5} M, in DCM).

3.3. Synthesis and characterisation of flavin dyads for optoelectronic applications:

After having successfully synthesised compound **47**, it was necessary to try improving the solubility of this compound for its application in the manufacture of a thin-film organic photovoltaic device. Therefore, a long alkyl chain was added at the N(3) terminus of the molecule to synthesise 3-heptyl-8-ethyl-6,7-bis-thiophene-thiophene pteridine-2,4-(3H,8H)-dione **55**. Compound **55** was successfully synthesised in one step in 58% yield from **47** using standard *N*-alkylation conditions. (Scheme 11).

Chapter II: Synthesis of 8-Ethyl-6,7-Bis-Thiopteridine-2,4-(3H,8H)-Dione



Scheme 11: Alkylation of the *N*(3) terminus of **47**.

As previously mentioned, the thiophene ring on the same side as the ethyl side chain is orthogonal to the aromatic system. For this reason regiospecific bromination of **55** should take place on the ring which is part of the conjugated system preferentially, as it should be more reactive. This reaction was first developed by Dr Brian Fitzpatrick, within the Cooke group, who worked on the synthesis of the benzene flavin analogue 10-ethyl-6,9-*bis*-thiophene-benzopteridine-2,4-(3*H*,10*H*)-dione **44**. After some trial and error, the mono bromination of **55** was successfully performed. This reaction needs to be carried out in the absence of light as it otherwise promotes the formation of the dibrominated species **61** (Figure 52).

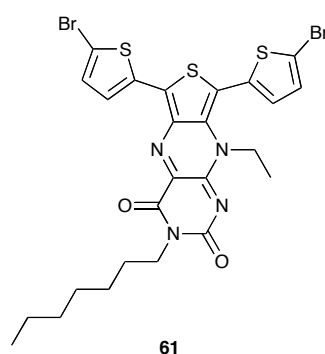


Fig. 52: Structure of compound **61**.

After purification, the desired mono-brominated flavin was obtained in 81% yield with the dibrominated-flavin being isolated as 6% yield. X-ray crystallography of the

Chapter II: Synthesis of 8-Ethyl-6,7-Bis-Thiopteridine-2,4-(3H,8H)-Dione

monobrominated species shows very clearly that, in both compounds **46** and **56**, the bromine atom is added regioselectively (Figure 53). This then opens the platform for the synthesis of regioselective oligothiophene dimers.



Fig. 53: X-ray crystals of monobrominated flavins **46** and **56**.

Because of the time constraints of this project, the remainder of the synthesis was carried out by Dr Brian Fitzpatrick (for synthesis, see appendices 1-5). Who successfully obtained the sexi-thiophene dimer **48** and we also managed to extend the conjugation by adding thiophene spacer units to give oligothiophene dimers **62** and **63** (Figure 54). Compounds **48**, **62** and **63** were obtained in 43%, 55% and 63% yield respectively.

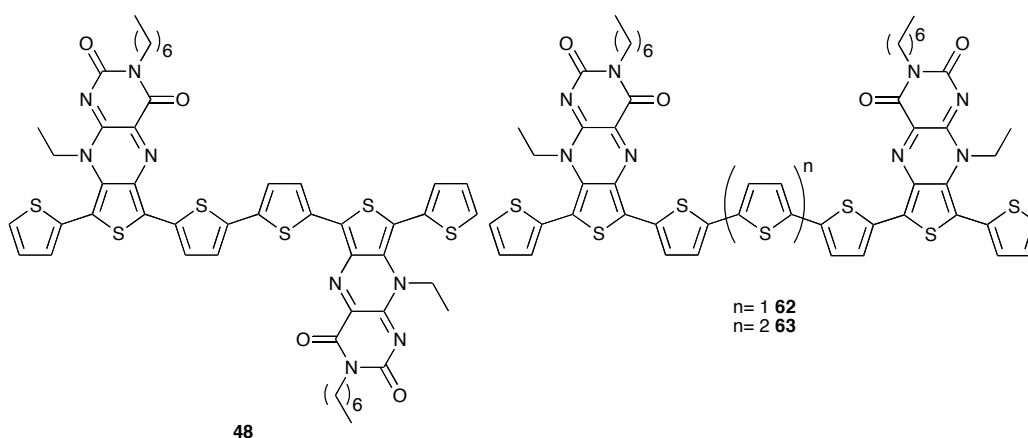


Fig. 54: Structures of the oligothiophene dimers **48**, **62** and **63**.

Chapter II: Synthesis of 8-Ethyl-6,7-Bis-Thiopteridine-2,4-(3H,8H)-Dione

3.4. Analysis and characterisation:

UV-vis and cyclic voltammetry studies of the target compounds were carried out, in order to assess their potential as materials for optoelectronic applications.

-UV-vis spectroscopy (Figure 55):

As previously shown the parent flavin molecule **47** showed some absorbance in the near IR with λ_{\max} of 551 nm and an onset of absorbance at 671 nm. The absorption spectra of the oligothiophene dimers **48**, **62** and **63** were therefore compared with that of **47**. As can be observed from graph 3, the absorption spectra of the oligothiophene dimers shows a bathochromic red-shift of the absorption peak of the parent molecule ($\lambda_{\max} = 551$ nm) and greater absorbance with increasing number of thiophene units. This increase in absorption toward the near IR region of the electromagnetic spectrum is evidence of efficient intramolecular charge transfer within the dyads.

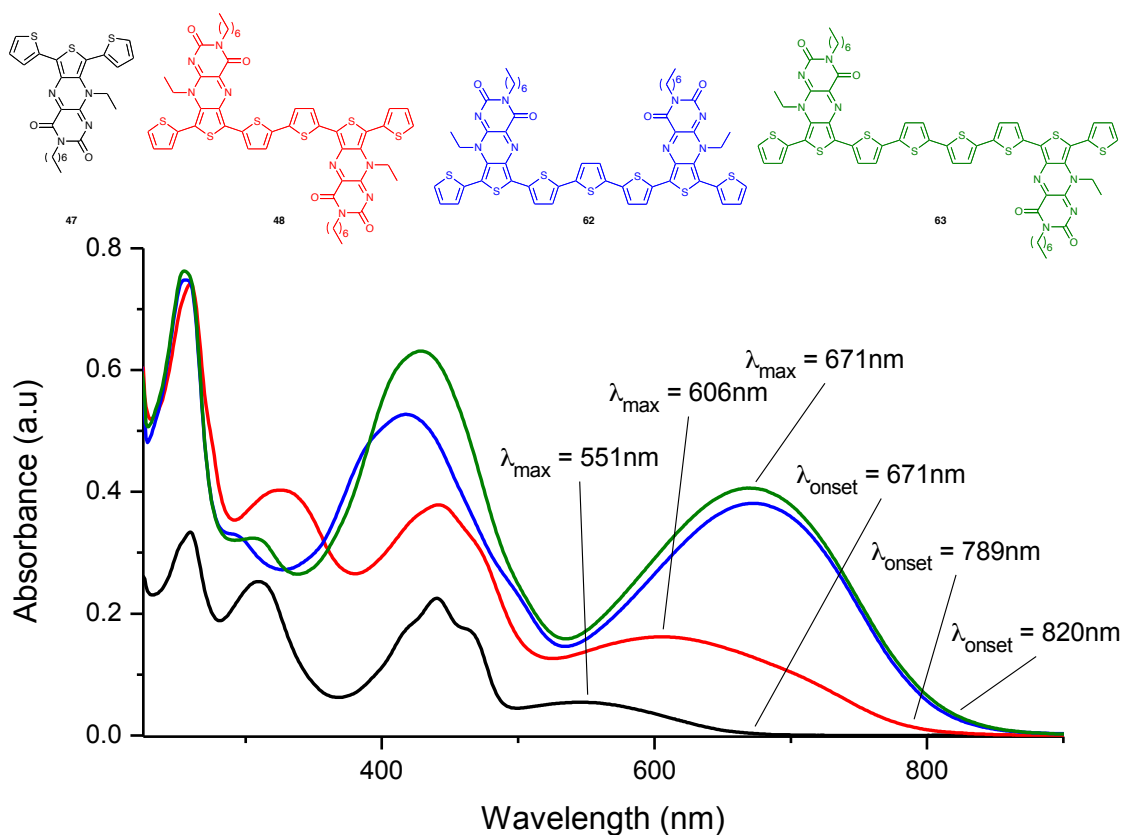


Fig. 55: Comparison of absorption spectra of **47**, **48**, **62** and **63** (1×10^{-5} M, in DCM).

-Voltammetry studies:

Cyclic and square wave voltammetry studies were carried out on compounds **47**, **48**, **62** and **63**. Derivation of $E_{1/2}$ (oxidation) and $E_{1/2}$ (reduction) was obtained using cyclic voltammetry at 1×10^{-5} M concentrations in DCM using TBA.PF₆ as the electrolyte with a 1.6 mm diameter platinum working electrode, a platinum wire counter electrode and a silver wire reference electrode calibrated versus the ferrocene/ferrocenium (Fc/Fc⁺) redox couple (Figure 56). Derivation of E_{diff} (oxidation) and E_{diff} (reduction) was obtained using square wave voltammetry at 1×10^{-5} M concentrations in DCM. Direction of sweep from -2.0 V to +1.1 V vs Fc/Fc⁺. Cell conditions were identical to that of cyclic voltammetry described above and the anodic current is depicted as positive (Figure 57).

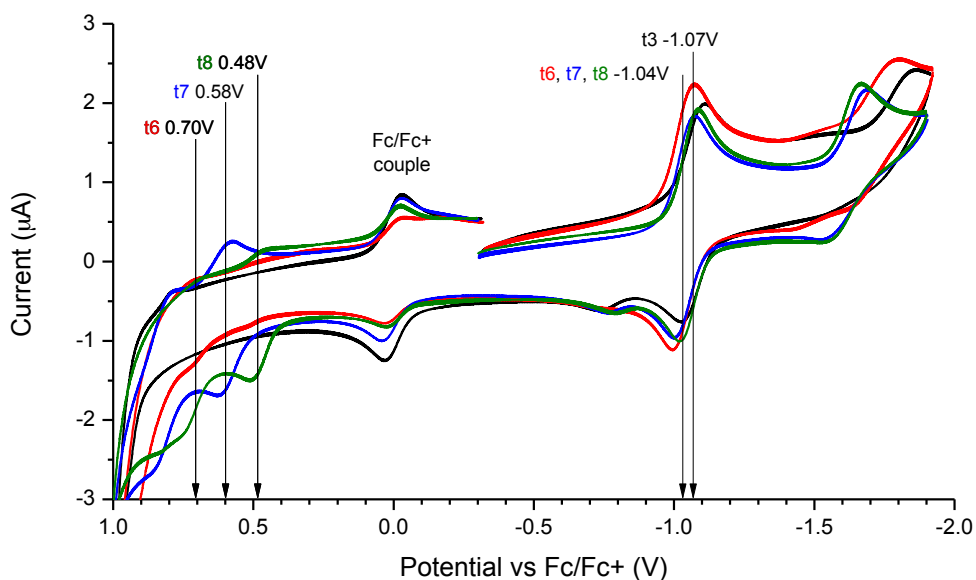


Fig. 56: CV traces of **47** (t3, black), **48** (t6, red), **62** (t7, blue) and **63** (t8, green) with corresponding $E_{1/2}$ values (1×10^{-5} M, in Acetonitrile).

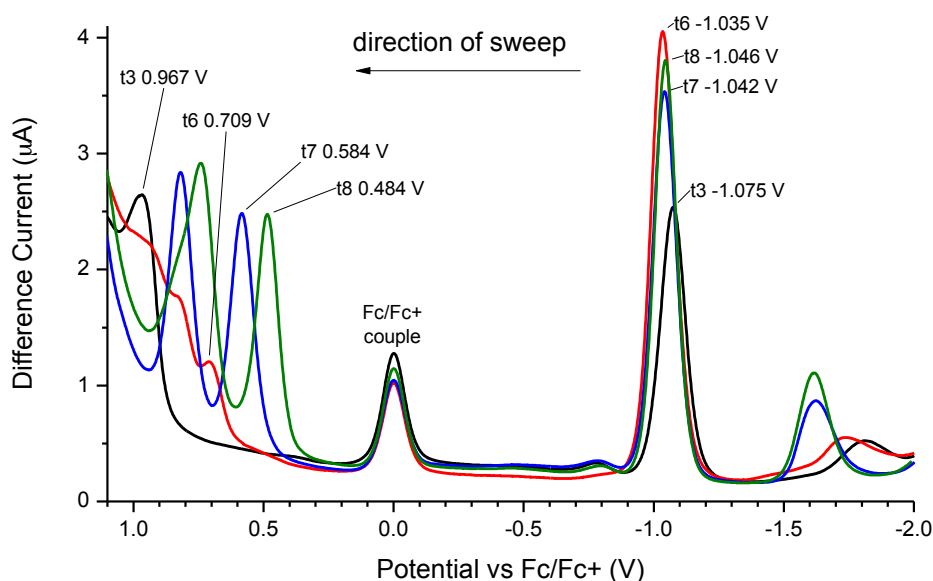


Fig. 57: Square wave voltammetry traces of **47** (t3, black), **48** (t6, red), **62** (t7, blue) and **63** (t8, green) with corresponding E_{diff} values (1×10^{-5} M, in Acetonitrile).

These analyses show that the reduction potential of the oligothiophene dimer **48**, **62** and **63** is only affected by a small amount (0.03-0.04 V). However, the oxidation potentials are significantly shifted by -0.26 V, -0.38V and -0.48 V for compounds **48**, **62** and **63** respectively. This means that the band gap of each molecule is significantly narrowed with increasing number of thiophene rings.

-Optoelectronic data:

HOMO and LUMO levels as well as band gap can be determined from both the UV-vis and voltammetry data using the following equations:

$$(1) E_{HOMO} = - (4.8 + E_{\frac{1}{2}}(\text{oxidation})) = - (4.8 + E_{diff}(\text{oxidation})) \quad (\text{in eV})$$

$$(2) E_{LUMO} = - (4.8 + E_{\frac{1}{2}}(\text{reduction})) = - (4.8 + E_{diff}(\text{reduction})) \quad (\text{in eV})$$

$$(3) E_{gap} = | E_{LUMO} - E_{HOMO} | \quad (\text{in eV})$$

$$(4) E_{gap} = hc / \lambda_{onset} = 1240 / \lambda_{onset} \quad (\text{in eV})$$

h = Plank's constant (4.135×10^{-15} eV.s); c = speed of light (3×10^8 m.s⁻¹).

Chapter II: Synthesis of 8-Ethyl-6,7-Bis-Thiopteridine-2,4-(3H,8H)-Dione

Equations (1) and (2) are used to calculate the experimental value of the HOMO and LUMO energy levels from the voltammetry data.⁹⁷ These levels correspond to the absolute potentials of oxidation and reduction and are therefore calculated with respect to the reference used. In this case HOMO and LUMO levels are calculated with respect to the absolute potential of the Fc/Fc⁺ couple (-4.8 eV).⁹⁸ This enables us to calculate the electrochemical band gap using equation (3). On the other hand, the UV-vis data can be used to calculate the optical band gap, using equation (4).⁹⁹ A summary of the data obtained and the result of the calculations is found in table 3.

Flavin	Electrochemical properties								Optical properties		
	Cyclic Voltammetry			Square wave voltammetry					UV-Vis		
	E _{1/2} (ox) (V)	E _{1/2} (red) (V)	E _{gap} (eV)	E _{diff} (ox) (V)	E _{diff} (red) (V)	E _{HOMO} (eV)	E _{LUMO} (eV)	E _{gap} (eV)	λ _{max} (nm)	λ _{onset} (nm)	E _{gap} (eV)
47	x	-1.07	x	0.97	-1.08	-5.77	-3.73	2.04	547	652	1.90
48	0.70	-1.04	1.74	0.71	-1.04	-5.51	-3.77	1.74	606	789	1.57
62	0.58	-1.04	1.62	0.58	-1.04	-5.38	-3.76	1.63	671	820	1.51
63	0.48	-1.04	1.52	0.48	-1.05	-5.28	-3.75	1.53	673	820	1.51

Table 3: Summary of electrochemical and optical data. (x: data unavailable)

The table shows that the energies derived from cyclic voltammetry and square wave voltammetry are in good agreement with each other. It also confirms the conclusions made from observation of the voltammetry traces, that the band gap is significantly narrowed from 2.04 eV for the parent flavin **47** to 1.53 eV for the octathiophene compound **63**. This is primarily due to the HOMO level being raised as the LUMO levels for each compound remains effectively unchanged.

Density Functional Theory (DFT) calculations of the heptathiophene dimer **62** show some disparity between the theoretical and experimental LUMO levels. However, there

Chapter II: Synthesis of 8-Ethyl-6,7-Bis-Thiopteridine-2,4-(3H,8H)-Dione

is reasonable correlation between the predicted and experimental energy level of the HOMO, and that the HOMO is predicted to lie primarily on the conjugated thiophene backbone (Figure 58). This confirms experimental observations that the band gap is narrowed with increasing number of conjugated thiophenes.

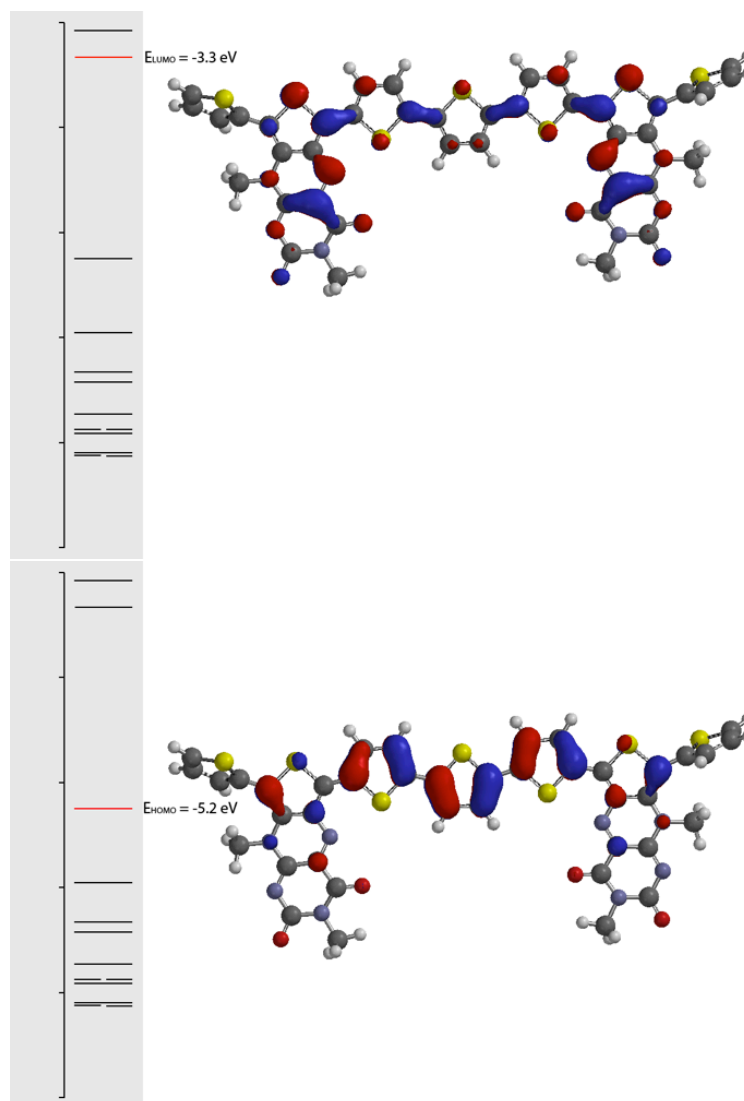


Fig. 58: DFT calculations of HOMO/LUMO levels for heptathiophene dimer **62**.

Calculations performed on Spartan '08, B3LYP exchange-correlation function with Basis Set 6-31G*

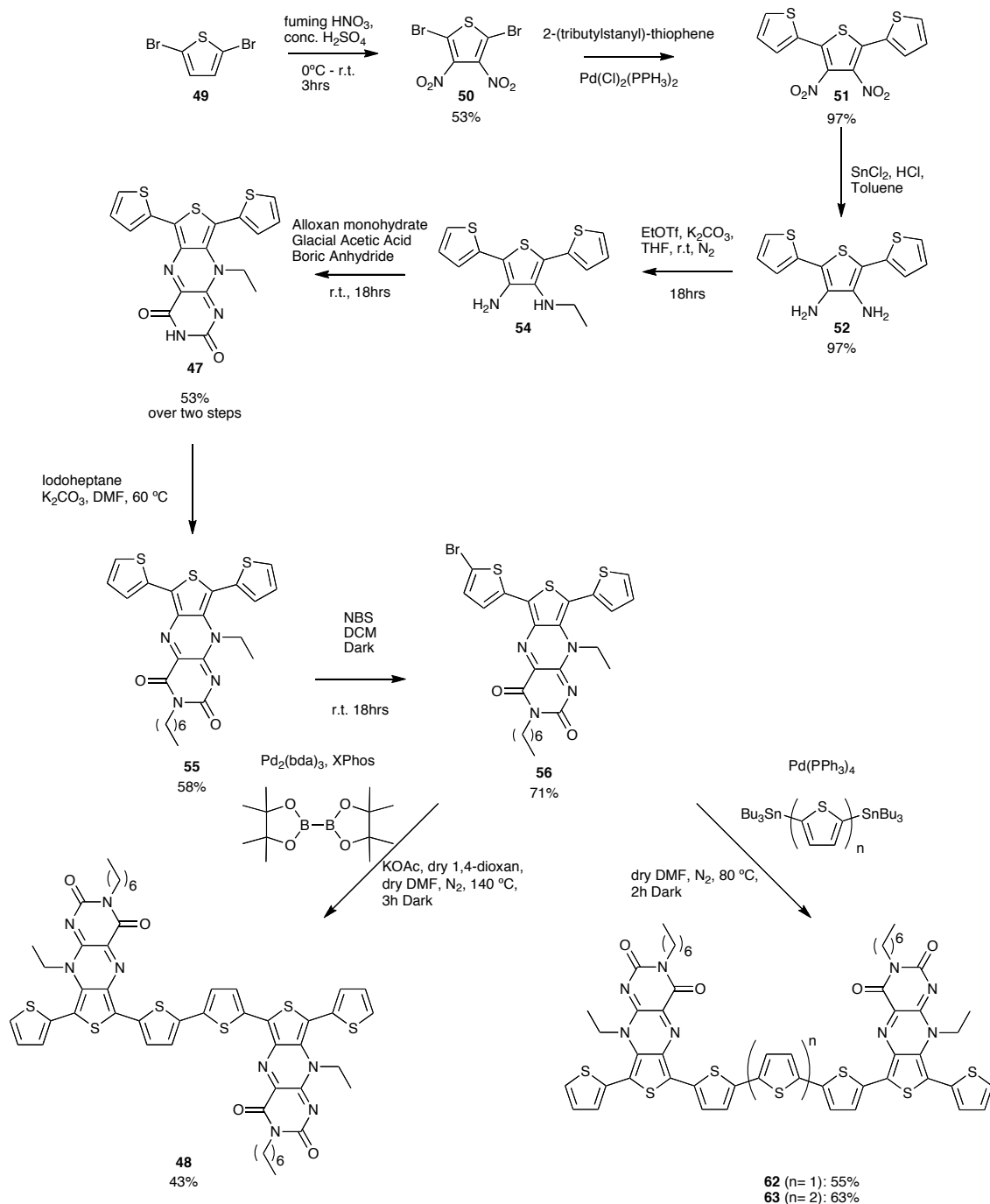
Finally, the HOMO level of the octathiophene compound **63** is very close to that of the P3HT **41** donor (-5.10 eV), **63** (-5.28 eV) and that the LUMO level is close to that of the IC₆₀BA **42** acceptor (-3.7 eV), **63** (-3.75 eV).

Chapter II: Synthesis of 8-Ethyl-6,7-Bis-Thiopteridine-2,4-(3H,8H)-Dione

4. Conclusions

The synthesis of a flavin based donor-acceptor dyad **47** was successfully completed and

47 was used to synthesise three oligothiophene dimers **48**, **62** and **63** (Scheme 16).



Scheme 12: Summary of the synthesis of targets **47**, **48**, **62**, **63**.

Chapter II: Synthesis of 8-Ethyl-6,7-Bis-Thiopteridine-2,4-(3H,8H)-Dione

These molecules were assessed for their potential optoelectronic application. All four molecules exhibit absorption spectra with absorbance in the near IR region of the electromagnetic spectrum. Also, the absorbance in this region increased significantly from the parent molecule **47** with increasing number of thiophene rings. Voltammetry studies provided characterisation of the HOMO/LUMO band gap of these molecules and showed that the band gap decreased with increasing number of thiophene rings also. This change is attributed to the change in the HOMO levels of the target molecules. Finally, the HOMO and LUMO levels of compound **63** (narrowest band gap) corresponded adequately to that of P3HT **41**, a recognised donor, and IC₆₀BA **42** a recognised acceptor used in photovoltaic cells.

The aim of this project was to synthesise a new family of organic donor-acceptor dyads for use in optoelectronic devices. These target compounds show properties desirable in both donor and acceptor compounds (high HOMO level, low LUMO level and narrow band gap) and could prove to be good donor-acceptor molecules.

5. Future work

In the first instance, the oligothiophene dimers will be sent to Professor Ifor Samuel at the University of St Andrews. There, they will be used to produce photovoltaic devices and will be assessed for their power conversion efficiency. From the observations made in this project, these devices should be tested as BHJ devices as well as single molecule devices. The BHJ devices could be made from either a blend of the compounds with P3HT **41** or with an acceptor or even with all three compounds blended together.

Since the number of conjugated thiophenes plays an important role in manipulating the HOMO levels, future work could include the synthesis of more derivatives with

Chapter II: Synthesis of 8-Ethyl-6,7-Bis-Thiopteridine-2,4-(3H,8H)-Dione

increasing number of conjugated thiophenes (Figure 59). This may help to reach an optimum band gap and might increase absorbance as well. Other targets could include dimers with extended thiophene side chains to ascertain the role of the non-conjugated thiophene ring (Figure 60).

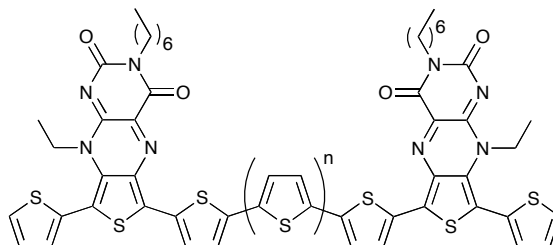


Fig. 59: Structure of future oligothiophene dimers with $n \leq 3$.

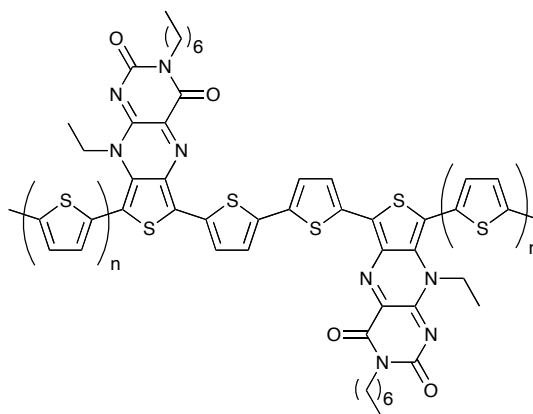


Fig. 60: Structure of future dimers with extended non conjugated thiophene side chains, with $n \leq 2$.

CHAPTER III: SYNTHESIS AND CHARACTERISATION OF 8-(3'-FERROCENE-1',1',4',4'-TETRACIANO BUTADIENE)-10-ISOBUTYL FLAVIN AS AN ORGANIC ELECTRON SUPER-ACCEPTOR.

1. Introduction

As previously described in chapters I and II, flavins are interesting targets for optoelectronic materials. This chapter describes the synthesis of an electron “super-acceptor” molecule featuring a flavin unit. The term “super-acceptor” was coined by Diederich and co-workers¹⁰⁰ and describes a class of organic acceptor molecules. These molecules were designed around known potent cyanocarbon acceptors tetracyanoethene **64** (TCNE) and 7,7,8,8-tetracyanoquinodimethane **65** (TCNQ) (Figure 61).

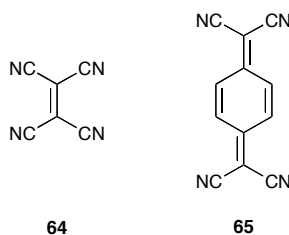


Fig. 61: Structures of TCNE **64** and TCNQ **65** (TCNQ).

TCNE **64** and TCNQ **65** are part of the family of chemical compounds known as cyanocarbons. These are molecules bearing highly electron withdrawing nitrile groups. Cyanocarbons contain a sufficient amount of nitrile groups to alter the electronic properties of the molecule.¹⁰¹ In view of the interesting properties of cyanocarbons, Diederich and co-workers set out to synthesise new cyanocarbon materials for electronic and non-linear optics applications.¹⁰²

Chapter III: Synthesis of Ferrocene-Flavin Super-acceptors

Following from their seminal work, they investigated a range of cyanoethene compounds (Figure 62), their synthesis and optical properties. The research focused particularly on donor substituted cyanoethynylethene diads,¹⁰³ but soon took to a new class of cyanocarbons. In 2005, Diederich and co-workers introduced tetracyano-butadienes (Figure 63, TCBD) as a new class of non-linear optical materials.¹⁰⁴



Fig. 62: Structure of generic cyanoethene.

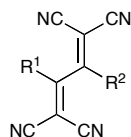
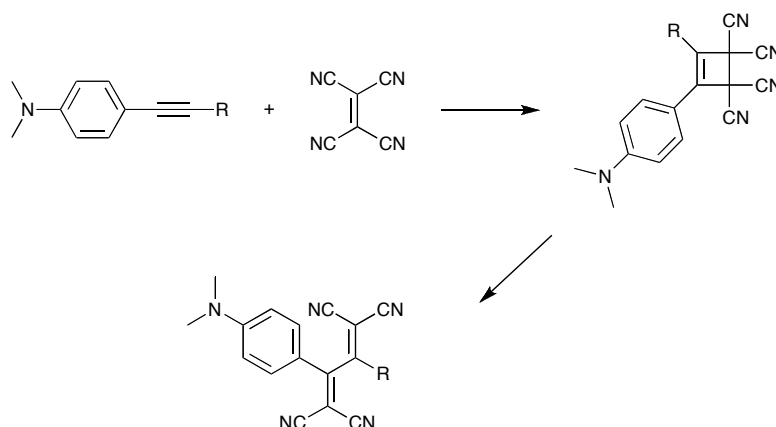


Fig. 63: Structure of generic tetracyano-butadiene.

These molecules result from the very high yielding reaction of TCNE **56** with dimethylaminophenyl-ethylenes. The reaction follows a [2+2] cycloaddition step followed by electrocyclic ring opening of the resulting cyclobutene to give the desired TCBD compound (Scheme 13).



Scheme 13: Formation of TCBD via cyclobutene intermediate.

Chapter III: Synthesis of Ferrocene-Flavin Super-acceptors

Diederich and co-workers have since produced a substantial amount of publications relating to the formation of TCBD molecules and investigations toward optoelectronic applications. Their research primarily focused on the use of such molecules for non-linear optic applications due to efficient charge transfer that can be observed between the donor moiety and the TCBD component of such molecules. This relationship is even more interesting due to the fact that these molecules exhibit extensive conjugation through a non-planar system (Figure 64).^{104,105}

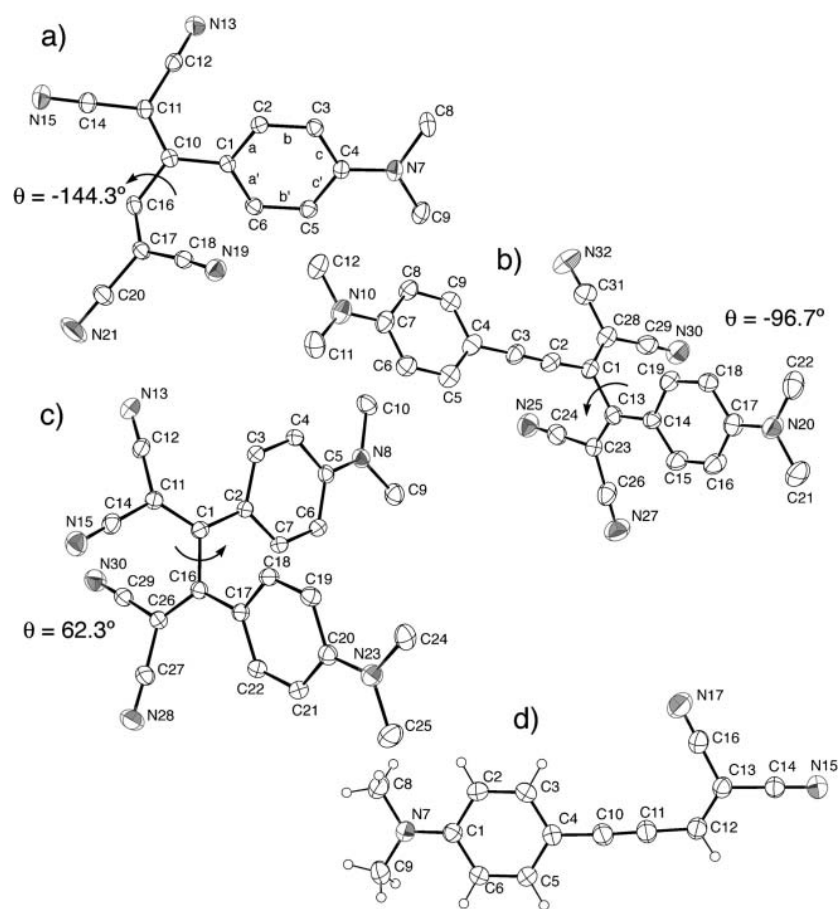
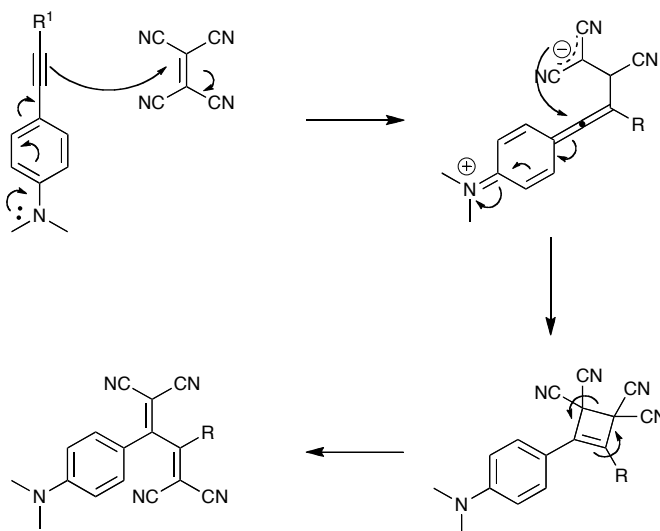


Fig. 64: X-ray structure of push-pull TCBD compounds showing non-planarity.¹⁰⁵

Chapter III: Synthesis of Ferrocene-Flavin Super-acceptors

Diederich and co-workers also published mechanistic studies of the cycloaddition of TCNE **64** to 4-(*N,N*-dimethylamino)phenylacetylenes (DMA). They observed and concluded that the reaction most likely proceeded via a zwitterionic intermediate with the anionic charge highly stabilised between the two nitrile groups (Scheme 14).¹⁰⁶



Scheme 14: Proposed reaction mechanism for the formation of TCBDs.

Nitrile groups are often incorporated in strong electron acceptor molecules for varied electronics and optoelectronic applications. For example, 2,3-dicyano-5,6-di-(4-(2,3,4,5-tetraphenylphenyl)phenyl)pyrazine **66** (Figure 65) was used as a blue-light emitting compound in the fabrication of a blue organic light-emitting diode (OLED).¹⁰⁷ The authors reported that addition of the highly electron withdrawing nitrile groups increased “injection and transfer of electrons”.

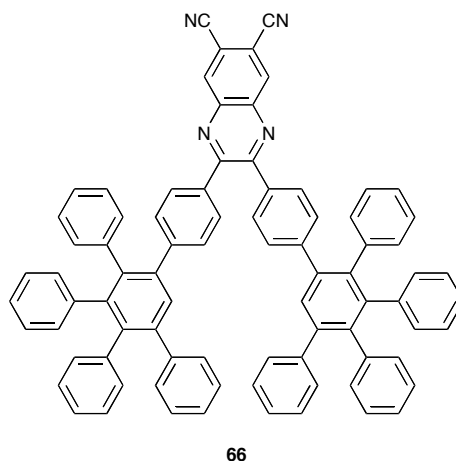


Fig. 65: Structure of compound **66**.

Cyanocarbons are known in particular for the high stability of their radical anion form and their ability to form charge transfer salts.¹⁰⁸ As discussed previously, one of the key features of optoelectronic materials is to have good charge transfer properties. Recently many groups have been investigating the use of cyanocarbons in solar cells. Agarwal and co-worker published the synthesis and characterisation of several cyanocarbazole derivatives **67** (Figure 66) and showed that their band gaps were similar to that of PC₆₁BM and well matched to common donors P3HT **41** and CuPc **36**.¹⁰⁹ They also showed that most derivatives exhibited efficient charge transfer with P3HT **41**.

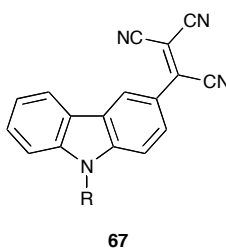


Fig. 66: Structure of cyanocarbazole organic acceptors **67**.

Roncalli and co-workers also used TCBDs in the synthesis of donor-acceptor-donor triad as donor material **68** for OPV (Figure 67).¹¹⁰ A few other groups have also been investigating TCBDs as optoelectronic materials.¹¹¹

Chapter III: Synthesis of Ferrocene-Flavin Super-acceptors

addition of TCNE to the polymer resulted in a net increase in the decomposition temperature of the polymer from 291 °C to 409 °C and a slight increase in the glass transition temperature. In the same, it was found that upon reaction with TCNE the TCBD functionalised polymer showed an increase in a charge transfer band at 470 nm.

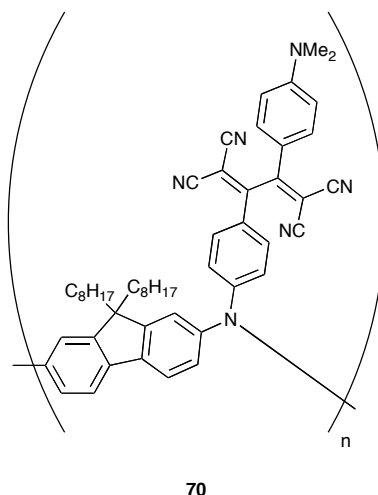
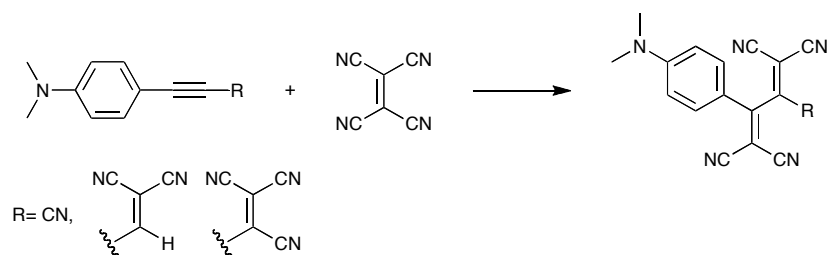


Fig. 69: Structure of TCBD functionalised conjugated polymer **70**.

As part of the research for the development of TCBDs as optoelectronic materials, Diederich and co-workers introduced the previously mentioned super-acceptors.¹⁰⁰ These super-acceptor molecules are designed to be “push-pull” electronic systems. They include an alkyne spacer which, upon reaction with TCNE **64** or TCNQ **65**, inserts the very strong TCBD donor moiety in the molecules (Scheme 15). In effect, super-acceptors are fully conjugated donor-acceptor-acceptor triads. The result of having such an electronic configuration produces small molecules with a very large dipole.

Chapter III: Synthesis of Ferrocene-Flavin Super-acceptors



Scheme 15: Synthetic pathway of super-acceptors.

Diederich and co-workers showed that despite not being planar this new class of molecules exhibited efficient intramolecular charge transfer well into the near infrared region. They also noted that these molecules had highly reversible redox properties and that their calculated electron affinities were in some cases higher than TCNE **64**, TCNQ **65**. This indicates that these super-acceptors are good targets for optoelectronic applications.

2. Aims

Following the work of Diederich and co-workers, 8-(3'-ferrocene-1',1',4',4'-tetracyanobutadiene)-10-isobutyl flavin **71** (Figure 70) was designed to be an electron super-acceptor molecule. As previously mentioned TCBD compounds have interesting electronic and optical properties with potential applications in non-linear-optics. The core of the push-pull system works through an extensive conjugation system built around a TCBD moiety with a flavin electron acceptor and a ferrocene donor. Compound **71** could be obtained from the flavin precursor 8-ethynylferrocene-10-isobutyl-benzopteridine-2,4(3*H*,10*H*)dione **72** (Figure 70) using the TCNE reaction described by Diederich and co-workers.

Precursor **72** was designed as a strong “push-pull” system, following the observations of Cooke and Rotello (Ch. I section 2.2) that substitutions at the C(7) and C(8) positions

Chapter III: Synthesis of Ferrocene-Flavin Super-acceptors

can affect the electronics of flavins to a great extent. For the design of this molecule functionalisation was made at the C(8) position in the same way that the already reported strong push-pull ABFL flavin **11**. Although the C(7) position offers significant influence of the electronics of flavins,^{20a} the C(8) position provides a resonance structure that goes from the ferrocene to the carbonyl group of the flavin. This provides delocalisation showing a standard Switerionic structure with the positive charge stabilised over the ferrocene moiety (Figure 71). Also, nature seems to favours electron donating groups at the C(8) position for the functionalisation of flavins (roseoflavin **73**, Figure 72).¹¹²

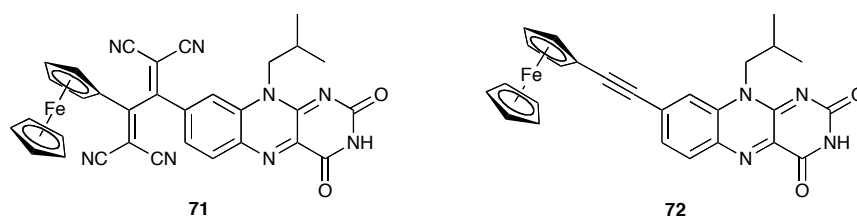


Fig. 70: Structure of TCBD-flavin **71** and it's precursor ferrocene-flavin **72**.

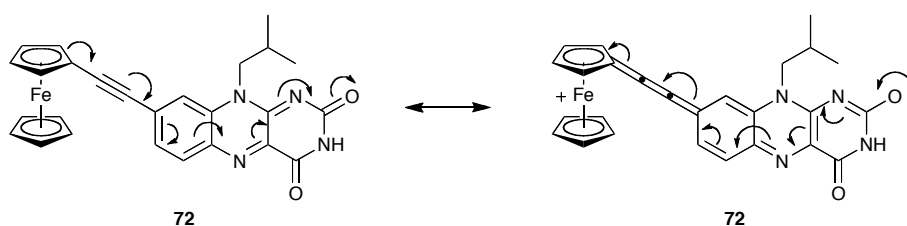


Fig. 71: Resonance structure of compound **72**.

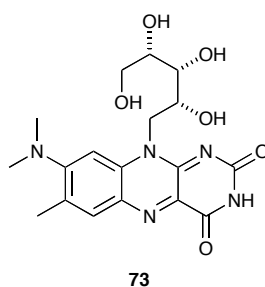
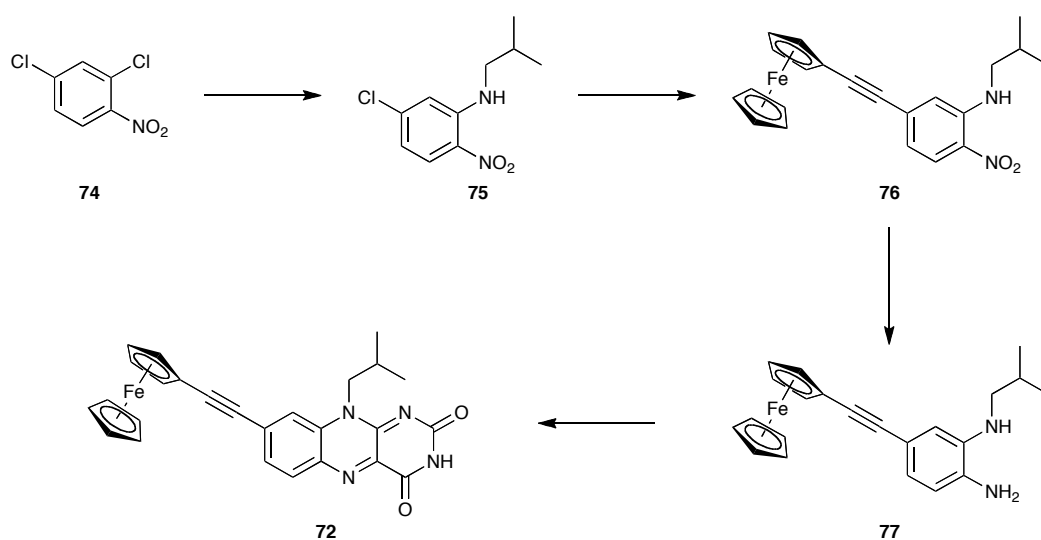


Fig. 72: Structure of roseoflavin **73**.

Chapter III: Synthesis of Ferrocene-Flavin Super-acceptors

The flavin precursor **72** could be synthesised from inexpensive starting material 2,4-dichloronitrobenzene **74**. In the first instance, **74** would be converted into mono-amine **75** by nucleophilic aromatic substitution. Sonogashira coupling would then be used to incorporate the ethynylferrocene moiety to give **76**. Diamine **76** would be obtained by the reduction of the aromatic nitro group. **76** would then undergo condensation with alloxan to give the target flavin **77**. (Scheme 16). The target super-acceptor molecule would then be synthesised using the conditions described by Diederich and co-workers.



Scheme 16: Proposed synthetic approach towards **72**.

3. Results and discussion

3.1. First approach:

Unfortunately the approach described in scheme 3 proved to be inadequate as it was impossible to separate *N*-isobutyl-2-nitro-5-chloro-aniline **75** from its regional isomer *N*-isobutyl-3-chloro-4-nitro-aniline **78** (Figure 73).

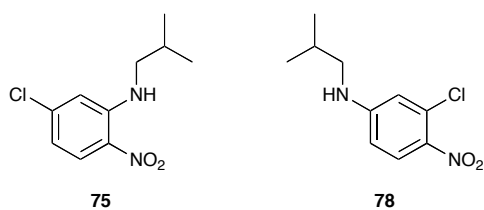
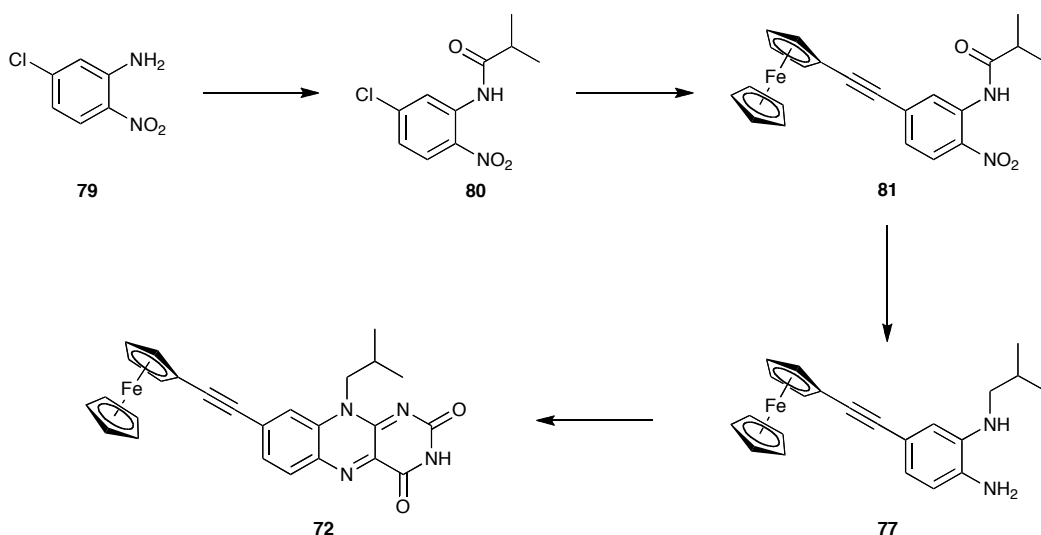


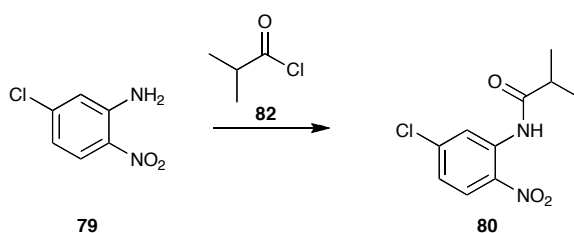
Fig. 73: Structures of two regioisomers **75** and **78**.

Therefore, the strategy was changed to use 5-chloro-2-nitro-aniline **79** as starting material. Compound **79** would be converted to isobutyramide **80**, which would then undergo Sonogashira coupling to give compound **81**. Reduction of the aromatic amine and of the amide would give di-amine **77** and after alloxan condensation, would give the target flavin **72** (Scheme 21).



Scheme 17: Alternative synthetic route to **72**.

3.2. Synthesis of *N*-(5-chloro-2-nitro-phenyl)isobutyramide **80**:



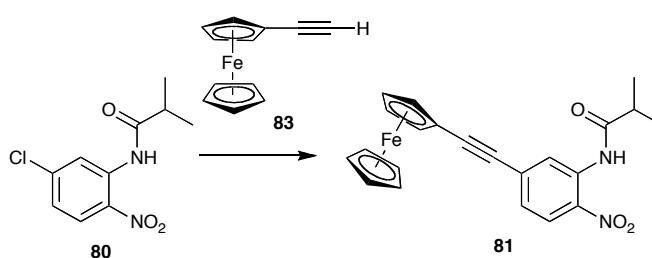
Chapter III: Synthesis of Ferrocene-Flavin Super-acceptors

The first attempt to convert compound **79** into **80** was done under standard amide formation conditions using isobutyrylchloride **82** in triethyl amine at room temperature. However, this was unsuccessful as primarily unreacted starting material was recovered. The next attempt was done under the same conditions but at reflux temperature and gave **80** in 63% yield. In a final attempt to increase the yield, a catalytic amount of *N,N*-dimethyl-4-aminopyridine (DMAP) was used and compound **80** was successfully isolated in 94% yield (table 1).

Reagents	Conditions	Time	Yield
Isobutyrylchloride, Et ₃ N, THF	r.t.	18 h	starting material
Isobutyrylchloride, Et ₃ N, THF	reflux	18 h	63%
Isobutyrylchloride, Et ₃ N, DMAP, THF	reflux	18 h	94%

Table 4: Optimisation of amide formation.

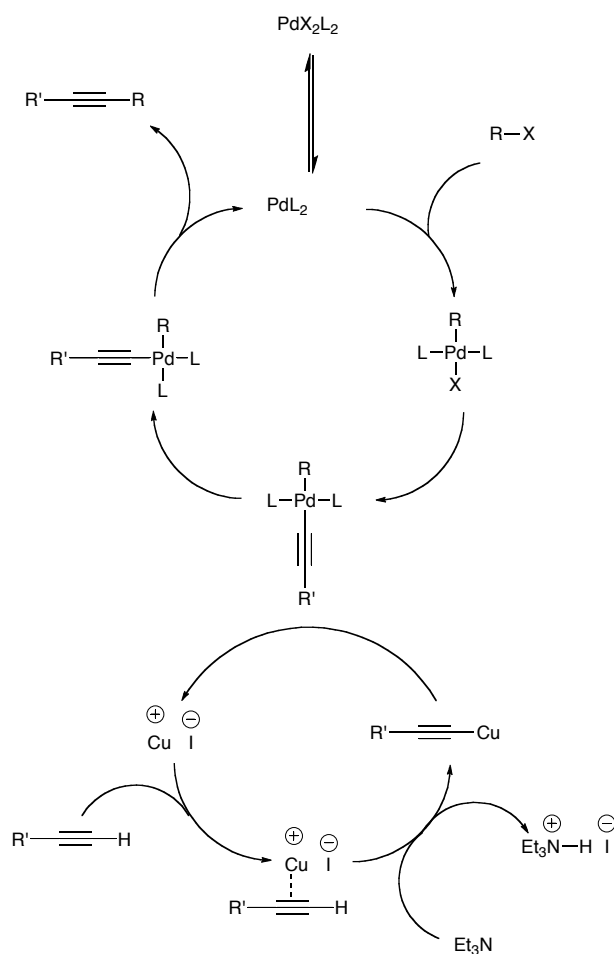
3.3. Synthesis of *N*-(2-nitro-4-ethynylferrocene-phenyl)isobutyramide **81**:



The next step in the synthesis of **72** is the Sonogashira cross-coupling of **80** with ethynylferrocene **83**. The Sonogashira cross-coupling reaction was first introduced by Sonogashira and co-workers in 1975.¹¹³ It is used to couple alkynes together with aryl halides in the presence of a palladium catalyst. While the acetylene is activated in a parallel copper mediated cycle, the aryl halide is activated by the palladium catalyst.

Chapter III: Synthesis of Ferrocene-Flavin Super-acceptors

The two cycles meet with transmetalation liguand exchange, and after isomerisation the desired species is obtained by reductive elimination (Scheme 22).



Scheme 18: Proposed catalytic cycle of Sonogashira cross-coupling.
(R= aryl; R'= alkyl, aryl...;X= halide)

This transformation was first attempted using standard conditions but this proved to be unsuccessful. This was thought to be due to general low reactivity of arylchlorides. However, copper-free conditions reported to improve yields particularly with arylchlorides were used,¹¹⁴ and after some optimisation, **81** was synthesised in 62% yield (Table 5).

Chapter III: Synthesis of Ferrocene-Flavin Super-acceptors

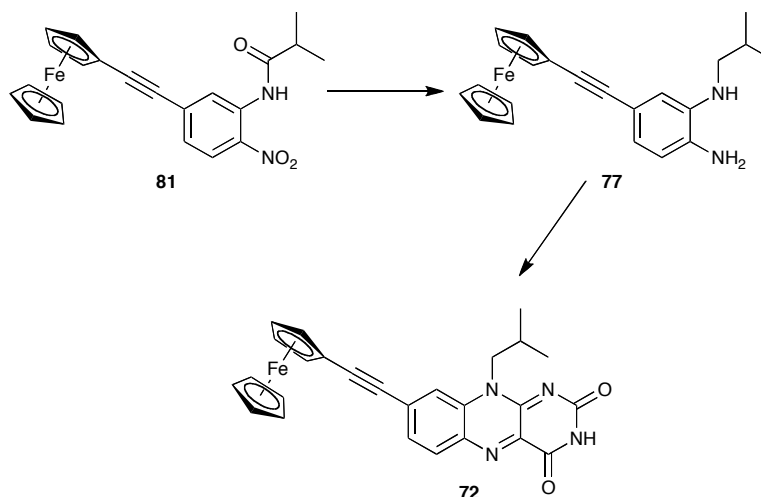
Reagents	Catalyst loading	Ligand loading	Conditions	Time	Yield
Ethynylferrocene, PdCl ₂ (PPH ₃) ₂ / CuI, Et ₃ N	2.5% / 5%	N/A	r.t., N ₂	24 h	3%
Ethynylferrocene, PdCl ₂ (PPH ₃) ₂ / CuI, Et ₃ N	2.5% / 5%	N/A	reflux, N ₂	24 h	7%
Ethynylferrocene, XPhos, Pd/C (10% w/w), K ₂ CO ₃ , DMA	5%	5%	110 °C, Ar	18 h	17%
Ethynylferrocene, XPhos, Pd/C (10% w/w), K ₂ CO ₃ , DMA	5%	5%	110 °C, N ₂	24 h	0%
Ethynylferrocene, SPhos, Pd/C (10% w/w), K ₂ CO ₃ , DMA	5%	5%	110 °C, Ar	2h	40%
Ethynylferrocene, SPhos, Pd/C (10% w/w), K ₂ CO ₃ , DMA	5%	5%	110 °C, N ₂	2h	62%

Table 5: Optimisation of Sonogashira cross-coupling conditions.

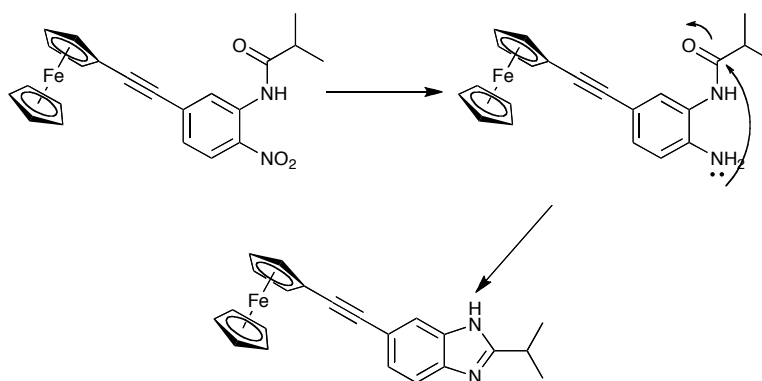
3.4. Synthesis of 8-ethynylferrocene-10-isobutyl-benzopteridine-2,4(3*H*,10*H*) dione 72:

In the next step both the nitro and amide moieties needed to be reduced to perform the alloxan condensation step (Scheme 19). After consideration about which should be reduced first to avoid potential intramolecular reactions from happening (Scheme 20), reduction of the amide was attempted first.

Chapter III: Synthesis of Ferrocene-Flavin Super-acceptors



Scheme 19: Final strategy towards synthesis of **72**.

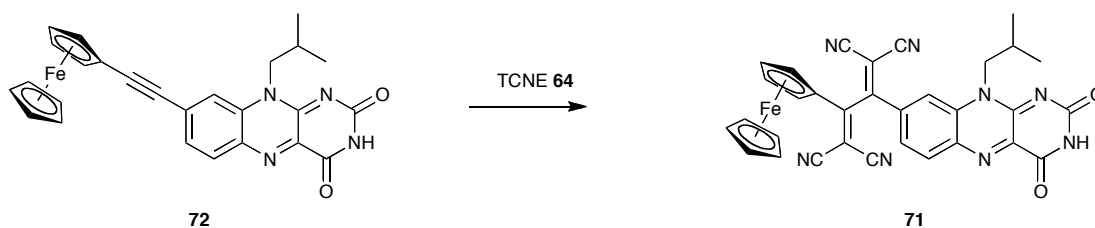


Scheme 20: Possible side products if nitro group is reduced before the amide group.

However, when performing the hydride reduction of the isobutyramide, the crude product showed the reduction of both the amide and the nitro units in the one step. The crude product was therefore taken forward without further purification to the alloxan condensation step, as the diamine product was not very stable on silica. 8-Ethynylferrocene-10-isobutyl-benzopteridine-2,4(3*H*,10*H*)dione **72** was thereby isolated as a green solid in 34% yield over the two steps.

Chapter III: Synthesis of Ferrocene-Flavin Super-acceptors

3.5. Synthesis of 2-(ferrocene)-3-[8-(10-isobutyl-benzopteridine-2,4(3H,10H)dione)]-1,4-buta diene-1,1,5,5-tetracarbonitrile **71**:



Having successfully synthesised the flavin push-pull system, the synthesis of the flavin based super-acceptor **71** was attempted using the conditions described by Diederich and co-workers. The first attempt at the TCNE **64** reaction yielded the desired product in 44% yield. For the second attempt, the reaction was left to stir for a longer time but yielded mostly decomposition products. Finally, the reaction was attempted in the dark for 72 hours where the target TCBD product **71** was isolated in 74% yield (Table 6).

Reagents	Solvent	Conditions	Time	Yield
60 , TCNE	THF	reflux, N ₂	24 h	44%
60 , TCNE (excess)	THF	reflux, N ₂	72 h	Decomposition
60 , TCNE	THF	reflux, N ₂ , dark	72 h	74%

Table 6: Optimisation of TCNE reaction.

3.6. Analysis and Characterisation:

UV-vis and cyclic voltammetry studies of the target compounds **72** and **71** were carried out. The super-acceptor characteristics of **71** were assessed as well as its potential as an optoelectronic material.

Chapter III: Synthesis of Ferrocene-Flavin Super-acceptors

-UV-vis spectroscopy:

In the first instance, the absorption spectrum of **72** was recorded in solvents of different polarities to show evidence of solvatochromism, a feature of molecules with large dipole moments and can indicate NLO properties (Figure 74). It is interesting to note that the molecule shows a significant increase in absorption in the near IR region when recorded in DMSO with $\lambda_{\text{max}} = 750$ nm and an onset at 1024 nm.

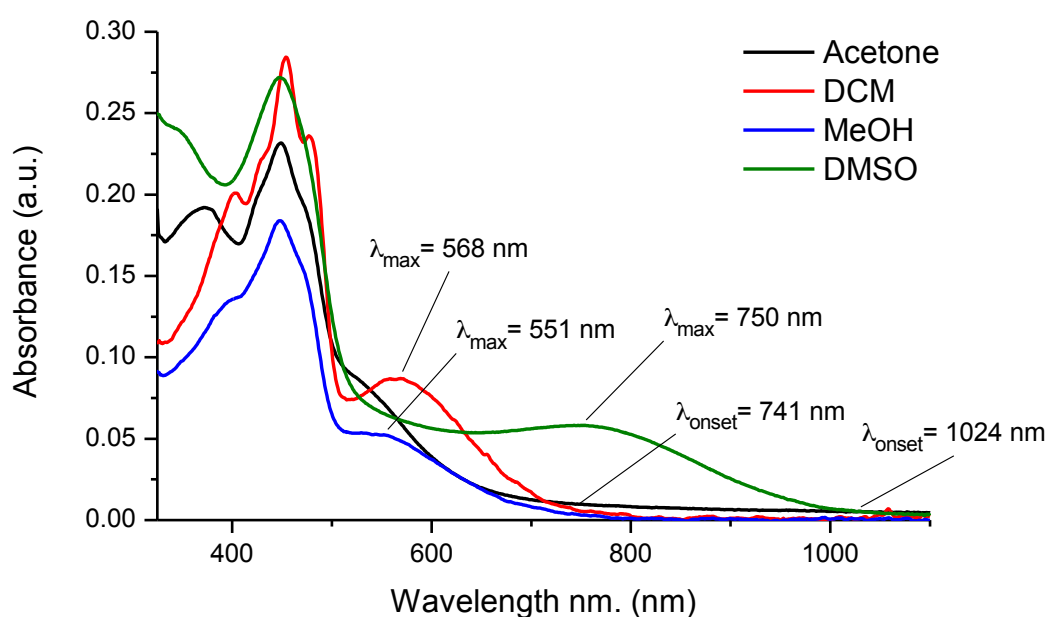


Fig. 74: Absorption spectra of **72** in different polarity solvents (all samples were recorded at 1×10^{-5} M).

The absorption spectra of **72** and **71** were then overlaid for comparison (Figure 75). Although absorbance is lesser for the TCBD compound, a relative redshift of the absorbance is seen. This increase in absorption toward the near IR region of the electromagnetic spectrum gives evidence of intramolecular charge transfer.

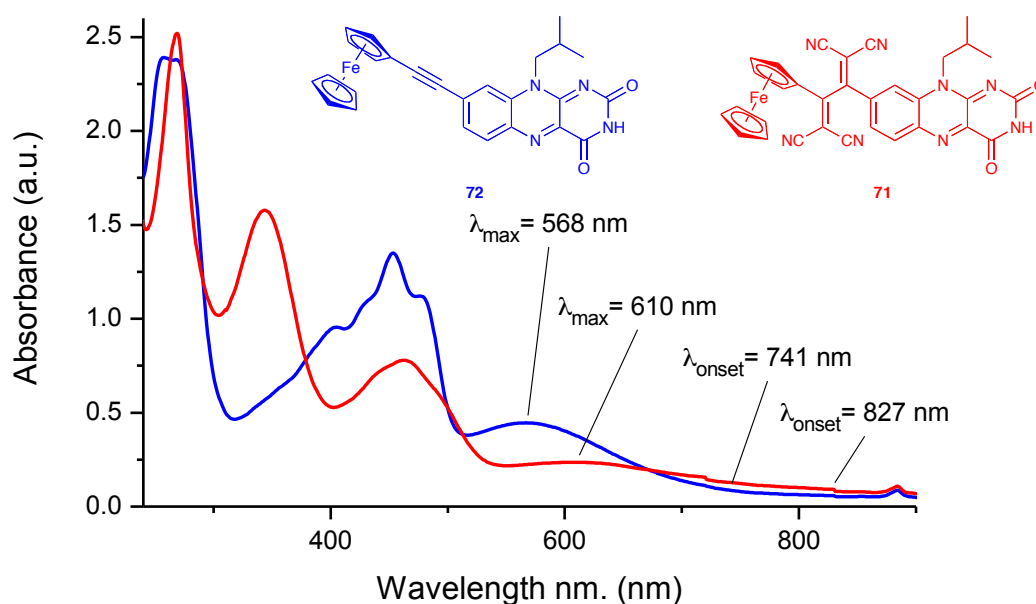


Fig. 75: Absorption spectra of **72** and **71** (1×10^{-5} M in DCM).

-Cyclic voltammetry studies:

In order to characterise the electronic properties of the TCBD compound cyclic voltammetry studies were carried out (Figure 76). Derivation of $E_{1/2}$ (oxidation) and $E_{1/2}$ (reduction) was obtained using cyclic voltammetry at 1×10^{-5} M concentration in acetonitrile using TBA.PF₆ as the electrolyte with a 1.6 mm diameter platinum working electrode, a platinum wire counter electrode and a silver wire reference electrode calibrated versus the ferrocene/ferrocenium (Fc/Fc⁺) redox couple.

The cyclic voltammetry traces show that both the oxidation and reduction potentials of the TCBD compound **71** are significantly more positively shifted compared with the flavin parent molecules **72**. In contrast with the one electron reduction wave of flavin **72**, compound **71** shows four distinct reversible one electron reduction waves. The first two reduction waves of **71** are likely to be the result of a one electron reduction at each of the TCNE derived moieties, the third is likely to be the flavin reduction.

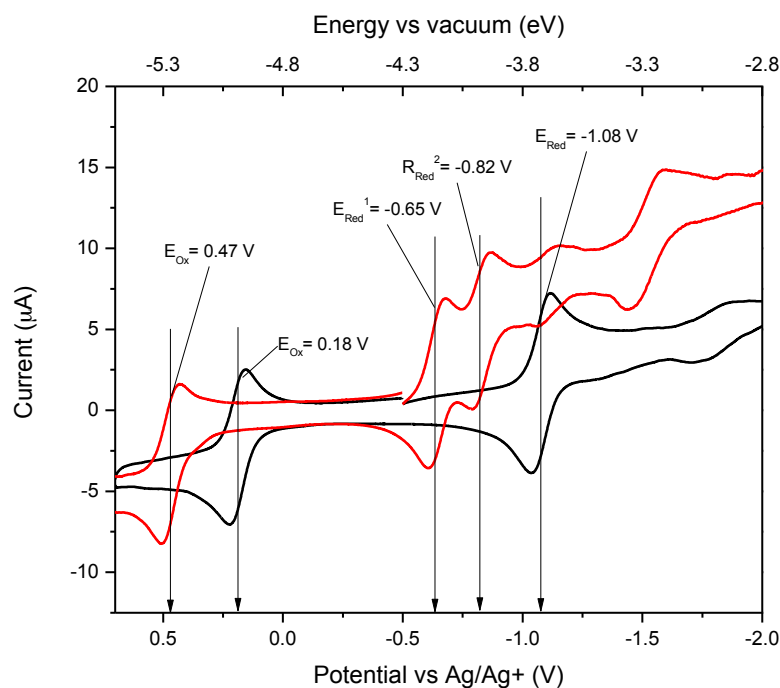


Fig. 76: CV traces of **72** (black), **71** (red) with corresponding $E_{1/2}$ values (1×10^{-5} M, in Acetonitrile).

-Optical and electronic data:

As previously shown in chapter II, the HOMO and LUMO energy levels as well as the band gap can be calculated from for the spectroscopic and voltammetry data. The results of these calculations are shown in table 7.

	Electrochemical properties					Optical properties		
	Cyclic Voltammetry					UV-Vis		
	$E_{1/2}$ (ox) (V)	$E_{1/2}$ (red) (V)	E_{HOMO} (eV)	E_{LUMO} (eV)	E_{gap} (eV)	λ_{max} (nm)	λ_{onset} (nm)	E_{gap} (eV)
Flavin								
72	0.18	-1.08	-4.98	-3.72	1.26	568	741	1.67
71	0.47	-0.65	-5.27	-4.15	1.12	610	827	1.50

Table 7: Summary of electrochemical and optical data.

The table shows that the electrochemical band gap of compound **72** is already “narrow” (1.26 eV) and transformation to the TCBD adduct **71** narrows the band gap even further (1.12 eV). These values are within the scale of Diederich’s super-acceptor

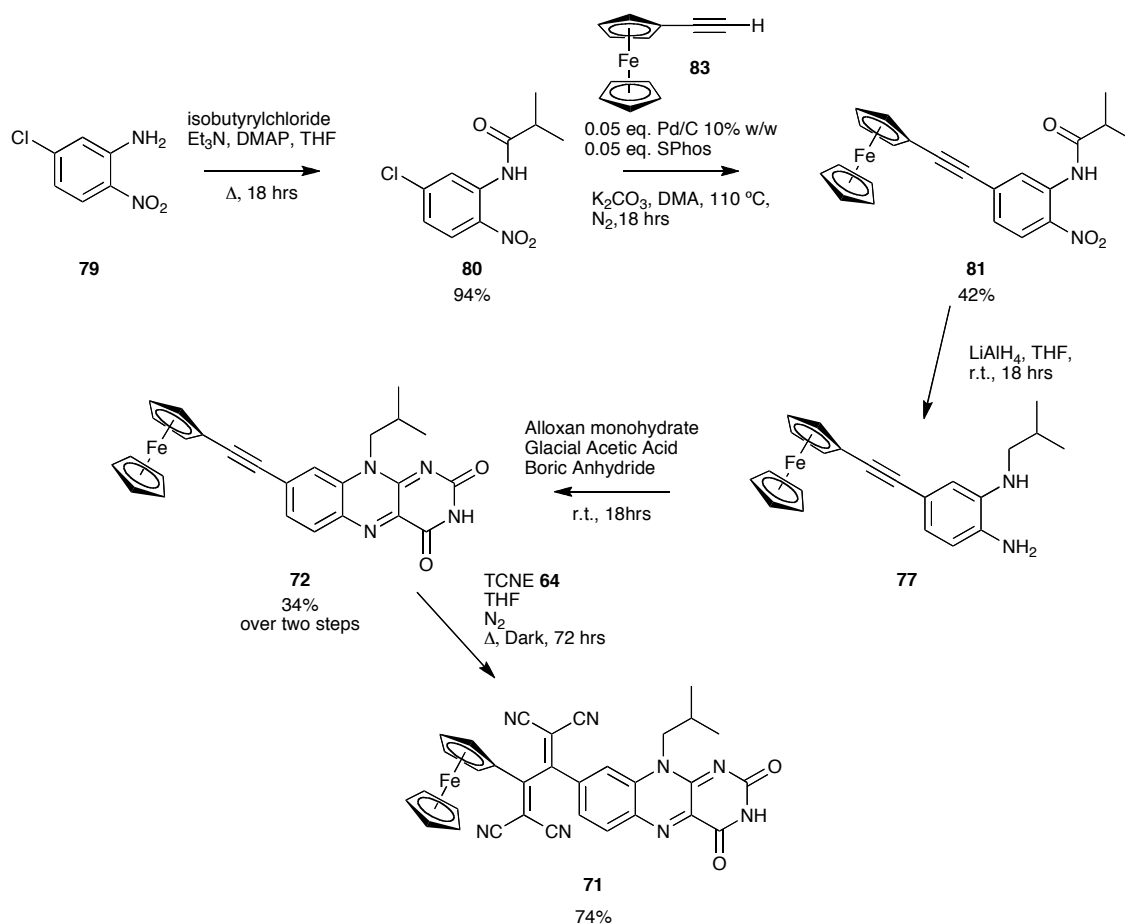
Chapter III: Synthesis of Ferrocene-Flavin Super-acceptors

molecules ($0.48 \leq \Delta \leq 1.55$ eV). However, the energy level of the first reduction wave of the TCBD compound **72** (-4.15 eV) remains higher than that of Diederich's super-acceptors ($-4.50 \leq E_{1/2(\text{red})}^1 \leq -4.96$ eV). The optical properties of the TCBD adduct show absorbance in the near infrared region of the electromagnetic spectrum. These values are good but remain in the lower end of the scale compared with Diederich's super-acceptors ($820 \leq \lambda_{\text{onset}} \leq 1640$ nm). However, as compared with strong acceptor IC₆₀BA, the LUMO level of **72** remains considerably lower (-3.7 eV and -4.15 eV respectively).

4. Conclusions

A push-pull ferrocene-flavin acetylene compound was successfully synthesised and the conditions described by Diederich and co-workers were used to perform a thermal [2+2] cycloaddition and retrocyclisation of TCNE **64** with compound **72**. This provided a novel TCBD compound **71** as a potential super-acceptor molecule (Scheme 21). The final compound was characterised by UV-vis spectroscopy and cyclic voltammetry to estimate its electron accepting properties. Although the band gap of **71** is very narrow (1.12 eV) and optical properties show increased absorbance in the near infrared ($\lambda_{\text{onset}}=827$ nm), cyclic voltammetry shows that the first reduction potential did not match that of other super-acceptor molecules described by Diederich and co-workers. However, as compared to standard electron acceptor molecules used in optoelectronic devices the TCBD compound **71** could still be considered as a super-acceptor molecule.

Chapter III: Synthesis of Ferrocene-Flavin Super-acceptors



Scheme 21: Summary of the synthesis of targets **72** and **71**.

5. Future work

In the first instance, compounds **72** and **71** should be sent to our collaborator, Professor Ifor Samuel, in St Andrews University to be assessed for their use in photovoltaic devices. Due to their narrow band gap and good match to the energy levels of ITO and aluminium, these compounds could be used in unimolecular photovoltaic devices. On the other hand, since the energy levels of both compounds are very complimentary (Figure 77) they could be used to fabricate bulk heterojunction devices.

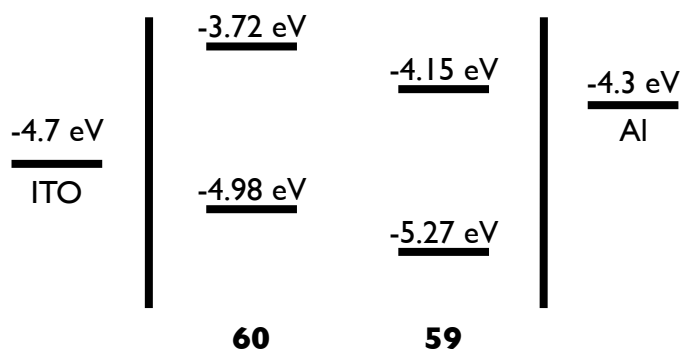


Fig. 77: HOMO and LUMO level representation of **72** and **71** with respect to ITO and aluminium.

An important continuation from this work would be the synthesis of the C(7) substituted analogue of **71** (Figure 78). The synthetic strategy used for **71** should be applied, using 4-chloro-2-nitroaniline as a starting material. Comparison of the electronic and optical data of both compounds would bring new insights into the electronic behaviour of flavins and the effect of substituents at the C(7) or C(8) position.

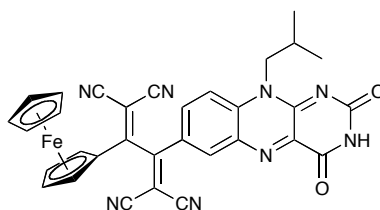


Fig. 78: Structure of the C(7) substituted TCBD flavin **84**.

Future synthesis of flavin based TCBD compounds could include the [2+2] cycloaddition of TCNQ **65** and F₄-TCNQ **85** with **72** (Figure 79). The ferrocene moiety could also be substituted with *N,N*-dimethylaniline. Furthermore, the introduction of thiophene spacers may improve the absorbance properties of these compounds toward the near infrared region (Figure 80), this should also have an important influence on the electrochemical properties of these compounds.

Chapter III: Synthesis of Ferrocene-Flavin Super-acceptors

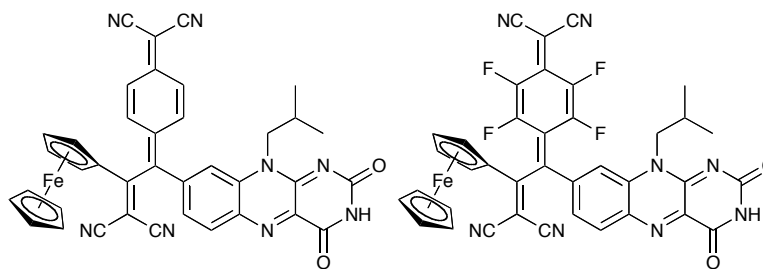


Fig. 79: Structure of products of TCNQ **65** and F₄-TCNQ **85** addition to **72**.

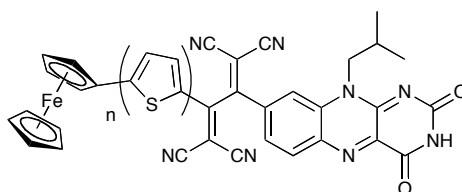


Fig. 80: Structure of potential extended conjugation flavin-ferrocene TCBD compound ($1 \leq n \leq 3$).

Also, in the same way as described in the future work section of chapter II, the interaction of **72** and **71** with complementary hydrogen-bonding partners should be investigated and the consequences on electronic properties assessed. Finally, as described by Diederich and co-workers, other applications could be investigated such as non-linear optics, OLEDs and other optoelectronic materials.

CHAPTER IV: NEW REDOX UMPOLUNG MEDIATED REACTIONS OF VINYLFERROCENE.

1. Introduction

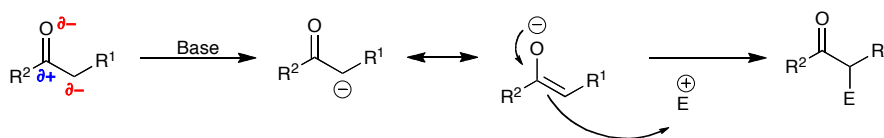
1.1. Umpolung chemistry: concept and history

The reactivity of organic molecules is largely governed by the patterns imposed by functional groups. In the same way, carbon-carbon bond forming reactions depend on the reactivity of such functional group. Carbonyl groups for instance are known to have a polar character imposed by the difference in electronegativity between carbon and oxygen (Figure 81).



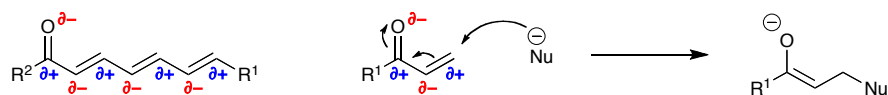
Fig. 81: Reactivity of a carbonyl group.

This reactivity also affects adjacent atoms in a way that enables reactions such as the Aldol condensation via the formation of an enolate (Scheme 22). In fact, this alternate reactivity pattern can be repeated infinitely through conjugated systems. This pattern is used for instance to promote reactions such as the Michael addition (Scheme 23).



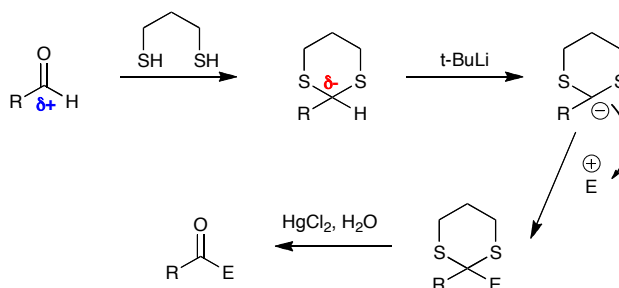
Scheme 22: Formation of enolate governed by reactivity of carbonyl groups (E= electrophile).

Chapter IV: New Redox Umpolung Mediated Reactions Of Vinylferrocene



Scheme 23: Conjugated reactivity and Michael addition (Nu= nucleophile).

The concept of umpolung (reversed polarity) controlled reactions was first introduced by Seebach and Corey in 1975.¹¹⁵ Umpolung is a German term that effectively means inversion of polarity. They realised that the reaction of a carbonyl with a dithiol produced a new species (dithiane) that reacted with opposite affinity to the original carbonyl group. Furthermore, the dithiane functional group could be hydrolysed back to a carbonyl moiety. Effectively, the “masking” of a carbonyl with a 1,3-dithiane moiety inverts the polarity of the carbon centre so that the previously electrophilic carbon of the carbonyl could now be considered as nucleophilic (Scheme 24).



Scheme 24: Use of thioacetals to change the reactivity of carbonyls towards electrophiles (E= electrophile).

1.2. Synthetic examples of umpolung chemistry:

The use of dithianes forms a big part of modern organic synthesis. Not only are they used as per the original umpolung chemistry described by Seebach and Corey, but also as carbonyl protecting groups, which arguably is a form of umpolung chemistry. Nowadays, umpolung chemistry is not only carbonyl and dithiane chemistry. The

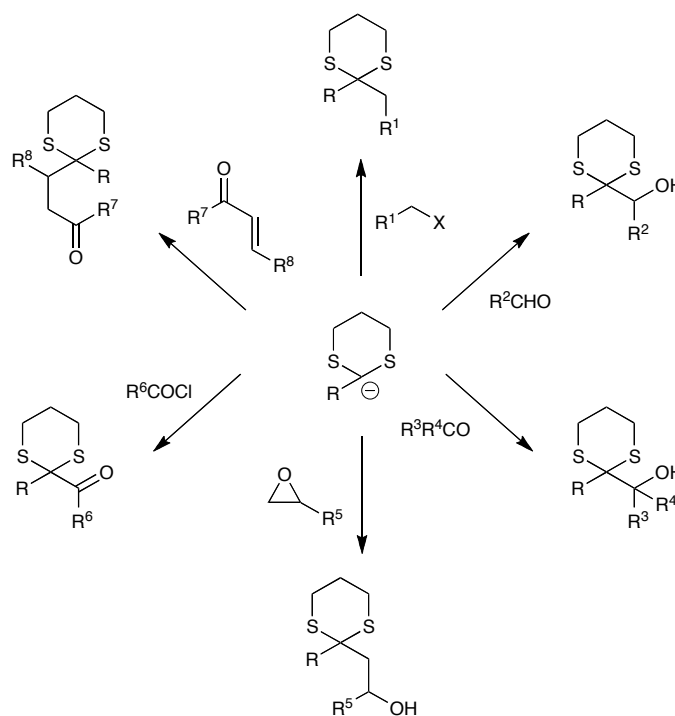
Chapter IV: New Redox Umpolung Mediated Reactions Of Vinylferrocene

umpolung concept has been used in the context of organocatalysis using *N*-heterocyclic carbenes (NHC) and into the area of materials where umpolung is used not to govern reactivity but physical properties. Umpolung methodology is undoubtedly a powerful synthetic tool and has been used as a key strategic tool in many syntheses. The applications of this method have been clearly seen in synthesis through chemical changes of functional groups in order to promote or prevent reaction.

1.2.1. Examples of umpolung by chemical conversion:

-Chemistry of dithianes:

Dithianes have played a key part in the synthesis of many natural products. The versatility of reactions that can be performed with carbonyl functional groups is greatly increased by using dithianes. In particular, the ability to access 1,2 and 1,4-diketones and α -hydroxyketones (Scheme 25).



Scheme 25: Key reactions of dithianes.

Chapter IV: New Redox Umpolung Mediated Reactions Of Vinylferrocene

One recent example of the use of dithianes as a strategic synthetic tool can be seen in the total synthesis of Spirastrellolide A Methyl Ester **86** (Figure 82).¹¹⁶ Here, a dithiane was used in a key step to join fragments of the macrocycle and the dithiane moiety was later hydrolysed to a ketone (Scheme 26).

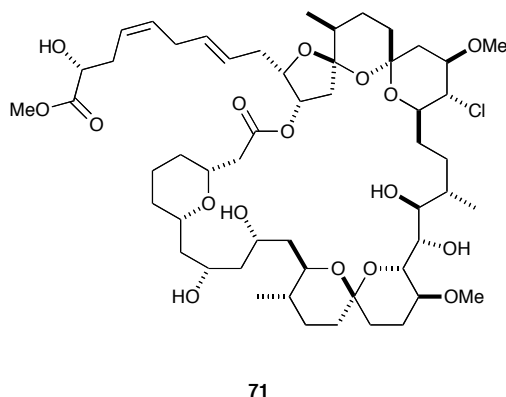
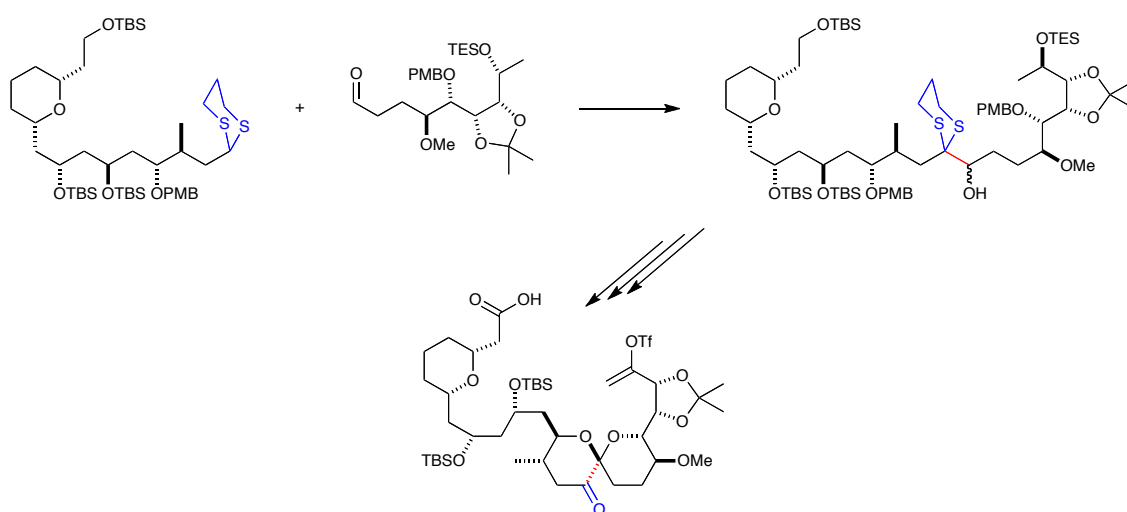


Fig. 82: Structure of Spirastrellolide A Methyl Ester **86**.

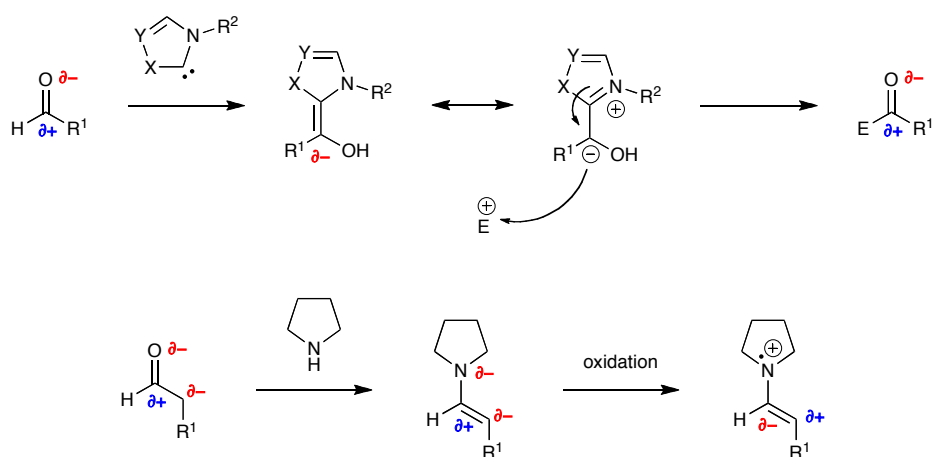


-N-Heterocyclic carbenes and organocatalysis:

Organocatalysis is one of the most active research fields of organic chemistry. NHCs, phosphines and enamine-iminium catalysts are at the heart of this research. The interest in the field lies principally in an attempt to move away from expensive and rare

Chapter IV: New Redox Umpolung Mediated Reactions Of Vinylferrocene

transition-metal catalysts that have a limited availability. The use of such organocatalysts encompasses numerous types of transformations. However, one interest lies in the ability to use NHCs and other organocatalysts as umpolung activators (Scheme 27).¹¹⁷ The interest generated by the research in umpolung methodology has moved us to investigate whether the redox chemistry of the ferrocene moiety (as described in Chapter I) could be used as an umpolung activator.



Scheme 27: Generic schemes of NHC and enamine-iminium umpolung catalytic processes.

1.3. Redox umpolung (Ferrocene):

Although chemical conversion is the standard understanding of the umpolung concept introduced by Corey and Seebach, the very notion of umpolung relies on the principle of polarity inversion. In that respect, redox processes could be seen as umpolung processes, if the oxidation change operates a radical change in polarity and this change is used to switch on or off the properties or reactivity of the reagents involved. A successful redox umpolung method has many advantages, they are versatile processes that can be chemically or electrochemically controlled. Redox processes are ubiquitous to nature and many core transformations that the scientific world is trying to emulate in the search for new materials, drug candidates and energy materials. Redox chemistry is

Chapter IV: New Redox Umpolung Mediated Reactions Of Vinylferrocene

often seen as a greener type of chemistry, particularly when coupled with electrochemistry which offers scaling up at lower cost, as well as synthesis that doesn't use harsh and toxic oxidising reagents. Ferrocene's well known and characterised redox properties, along with the known polarity inversion which comes with switching from ferrocene to ferrocenium makes it an excellent target for redox umpolung processes.

In 2005, Plenio and co-workers incorporated the ferrocene moiety to the NHC ligand of the Hoveyda-Grubbs 2nd generation (H-G II) catalyst **87** (Figure 83).¹¹⁸ In their work, they found that oxidation and reduction of ferrocene could be used to dictate the solubility properties of the catalyst. This, in turn, was used to switch the activity of the catalyst on and off. It also gives a new and efficient way to separate the catalyst from the products. Plenio later published an article where ferrocene was again used as a means to ease purification of Mitsunobu reactions (Figure 84).¹¹⁹ This process, labeled as a "phase-tag" by the authors, is an example of umpolung property control using the ferrocene moiety.

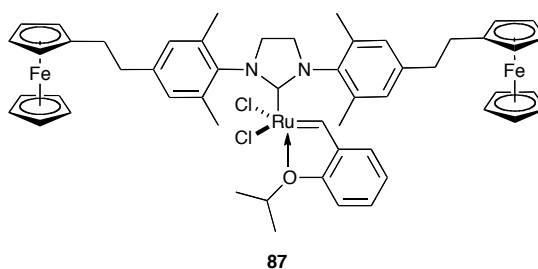


Fig. 83: Structure of ferrocene modified H-G II catalyst **87**.

Chapter IV: New Redox Umpolung Mediated Reactions Of Vinylferrocene

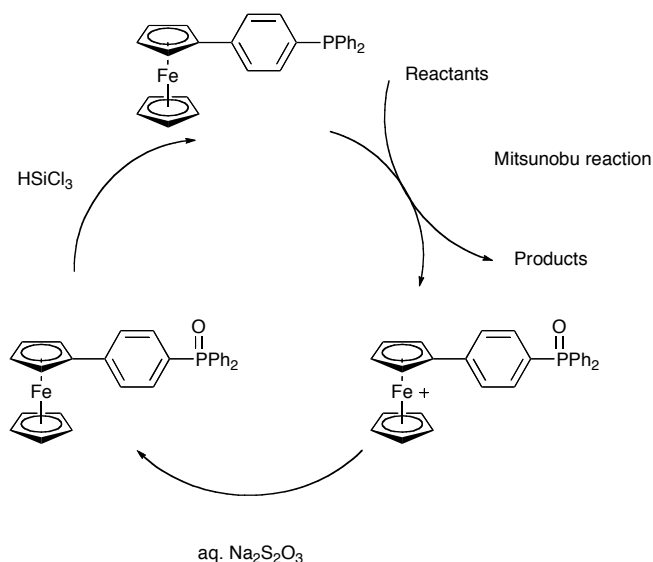


Fig. 84: Recycling cycle of ferrocene-phosphine unit.

In 2008, Fang and co-workers reported the synthesis of ferrocene appended cholesterol compound **88** as low molecular mass organic gelator (Figure 85).¹²⁰ They found that compound **88** was an excellent super-gelator (requiring only 0.09 wt % concentration) in the preparation of sol-gels in both cyclohexane and tetrachloromethane at room temperature and successfully prepared the gel into a flexible film. One of the key goals of sol-gel research is to be able to switch from solution to gel upon application of a stimulus. They found that the gels containing compound **88** were responsive to the typical stimuli of heating and sonicating/shaking, however Fang and co-workers used the ability to easily switch the oxidation of ferrocene to be an effective switch from solution to gel. Upon chemical oxidation with $(\text{NH}_4)_2\text{Ce}(\text{NO}_3)_6$ they found the gels would turn, gradually, from an orange gel to a green suspension. In the same way, addition of hydrazine and reduction of the ferrocene gradually turned the solution back to orange and gelation occurred within seconds.

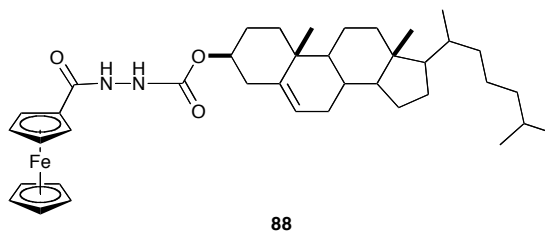


Fig. 85: Structure of ferrocene appended cholesterol “super-gelator” **88**.

Similarly, Vancso and co-workers presented their work on the development of redox-responsive poly(ferrocenylsilane) gelators.¹²¹ They present a number of polymeric materials with extremely interesting properties and show that umpolung activation of ferrocene is used as a stimulus to control the morphology of the gels (swelling/de-swelling). Their research shows real application of this redox response of gel morphology in colour displays or artificial muscles.

Although the applications of umpolung methodology show great promise for the development of smart reactions and smart materials, from our search of the literature very few examples exist of ferrocene being used for umpolung reactivity control (i.e. selective promotion of reaction). Nevertheless, a good example of how ferrocene can be used for reaction control using umpolung methodology was presented by White and co-workers.¹²² They modified a *bis*(iminophenoxide) ligand used in polymerisation catalysis, and functionalised it to contain ferrocene units (Figure 86). In the first instance, they devised a method to chemically oxidise and reduce the ferrocene moieties. They used silver triflate as an oxidant and decamethylferrocene a reducing agent and both the reduced and oxidised forms of the catalyst **89** (**89** and **89*** respectively) could be successfully isolated. They then proceeded to check that umpolung effected a switch in the activity of the polymerisation catalyst.

Chapter IV: New Redox Umpolung Mediated Reactions Of Vinylferrocene

Polymerisation of *rac*-lactide was attempted with both **89** and **89***. They found that the polymerisation of *rac*-lactide was of the order of thirty times faster using **89**. This showed that by switching the polarity of the ferrocenyl units, the reactivity of the catalyst was greatly affected. They also showed that *in situ* oxidation and reduction of the catalyst during the polymerisation process effectively turned the catalyst into an *on/off* switchable catalytic initiator.

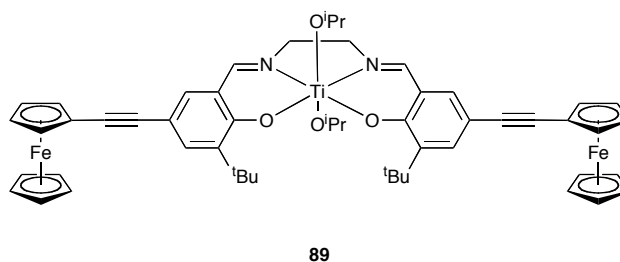
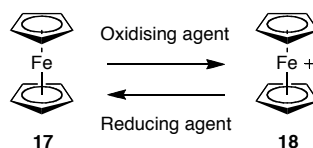


Fig. 86: Structure of ferrocene appended cholesterol “super-gelator” **89**.

2. Aims

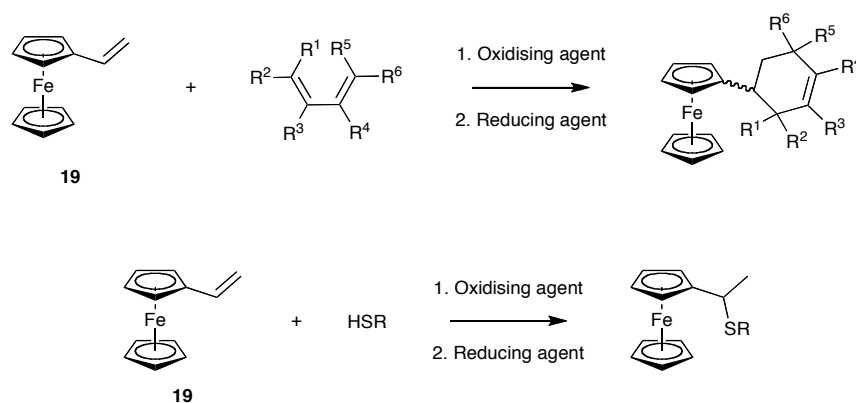
In order for ferrocene to be used successfully in umpolung controlled reactions, it is important for the inversion of polarity to be fully reversible. Therefore, it was important to develop a reliable and reproducible method for the chemical oxidation and reduction of ferrocene **17** (Scheme 28).



Scheme 28: Chemical oxidation and reduction of ferrocene **17**.

The goal was to investigate umpolung controlled reactions of vinylferrocene **19**, cycloadditions and nucleophilic additions (Scheme 29). These reactions were chosen because of their high dependence on the electronic configuration of the reagents.

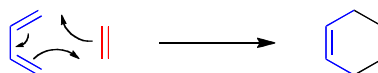
Chapter IV: New Redox Umpolung Mediated Reactions Of Vinylferrocene



Scheme 29: Redox umpolung controlled reactions of vinylferrocene **19**.

2.1. Cycloadditions:

The most popular cycloaddition reaction has to be the Nobel prize reaction developed by and bearing the name of Otto Diels and Kurt Alder.¹²³ The Diels-Alder reaction is a [4+2] cycloaddition reaction, where a diene reacts with a dienophile to form a cyclic alkene species (Scheme 30).



Scheme 30: Standard [4+2] Diels-Alder cycloaddition.

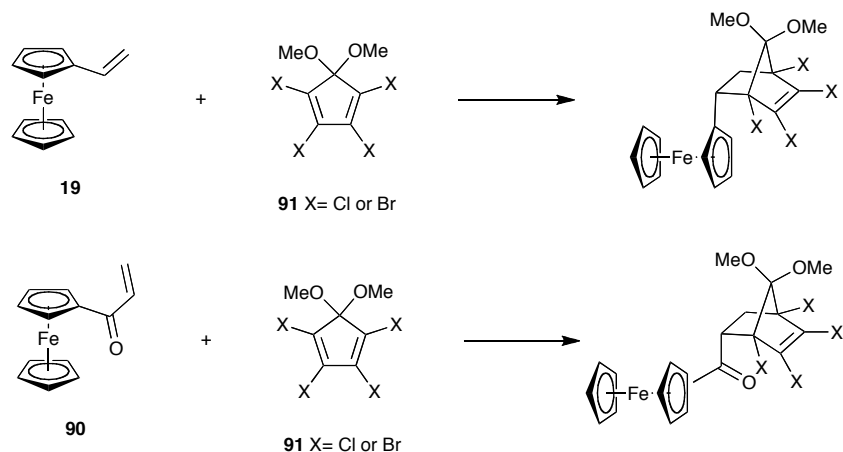
The Diels-Alder reaction has a number of requirements but it proceeds best when two conditions are met. The diene needs to be electron rich and able to exist in a *cis*-configuration (preferentially locked in a *cis* position), on the other hand the alkene or dienophile reacts more readily if it is electron deficient. The reverse demand cycloaddition is also possible using reciprocal inverse electronic configuration of the diene and dienophile (Scheme 31).

Chapter IV: New Redox Umpolung Mediated Reactions Of Vinylferrocene



Scheme 31: Ideal Diels-Alder configuration and reverse demand configuration.

A reverse demand Diels-Alder reaction of vinylferrocene has already been reported in the literature.¹²⁴ Khan and Upadhyay reported the reaction of vinylferrocene **19** and acryloylferrocene **90** with 1,2,3,4-tetrahalo-5,5-dimethoxycyclopentadienes **91** (Scheme 32). The electron rich vinyl groups reacted readily with the electron deficient dieneophiles and gave *endo* products exclusively in high yields. They also report that the range of norbornyl derivatives they synthesised had varying values of half-wave potential depending on the nature of the substituents on the norbornyl moiety.



Scheme 32: Reverse demand Diels-Alder cycloaddition of vinylferrocene **19** and acryloylferrocene **90** with 1,2,3,4-tetrahalo-5,5-dimethoxycyclopentadienes **91**.

For this reason, vinylferrocene should not be a good target for normal demand Diels-Alder reactions as the ferrocene renders the alkene electron rich, however, by

Chapter IV: New Redox Umpolung Mediated Reactions Of Vinylferrocene

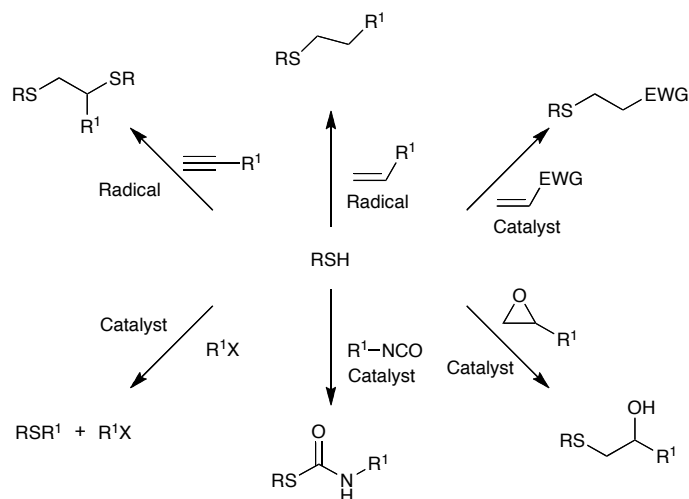
converting the ferrocene substituent to ferrocenium the polarity of the system would be inverted (umpolung) and should render the alkene electron deficient and more reactive.

This newly developed method of oxidation and reduction of ferrocene will therefore be used to activate vinylferrocene **19** towards Diels-Alder reaction with *cis*-dienes.

2.2. Umpolung nucleophilic additions:

Thiols and thioethers are amongst the most common functional groups in natural products, such as proteins and enzymes. Cysteine, biotin, lipoic acid and thiamine are amongst the most common sulfur containing biological compounds.¹²⁵ Many biologically active compounds rely on the formation of carbon-sulfur bonds. Therefore, much effort has been spent in developing synthetic robust methods to make carbon-sulfur bonds,¹²⁶ and in particular the development of thiol-click reactions (Scheme 33).¹²⁷ Thiol-click reactions include: radical thiol-ene and thiol-yne reactions, thiol-epoxy, thiol-isocyanate, thiol-halogen and thiol-Michael reactions. Although thiol-click reactions do not wholly encompass the “click” chemistry requirements, it is used to describe controlled reactions of thiols. Thiols are inherently very reactive and are prone to “over-react” and reactions of thiols can have many outcomes. One of the core principles of “click” chemistry for a reaction to be simple and yielding only one product. It is developing controlled reactions of thiols, that afford one selective product, that earns the classification of thiol-click.

Chapter IV: New Redox Umpolung Mediated Reactions Of Vinylferrocene

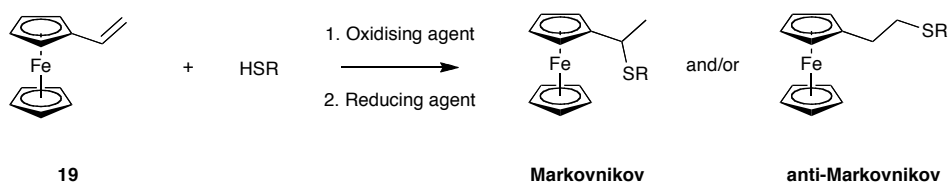


Scheme 33: Scope of thiol-click reactions.

As well as its application in the synthesis of pharmaceutical candidates, sulfur compounds are found increasingly in ligands, chiral auxiliaries and materials. Thiols are increasingly being used to functionalise reactive surfaces such as nano-particles.¹²⁸ As a result thiol-click reactions are being increasingly used to afford functionalised nanostructures.

Nucleophilic additions of thiols to electron deficient olefins (including styrene) are well known reactions that are either acid catalysed (protic and lewis acids)¹²⁹ or occur through a free-radical process (thiol-ene reaction).¹³⁰ However, as discussed previously, the vinyl group of vinylferrocene **19** is electron rich. Therefore, the method developed for the activation of vinylferrocene **19** toward cycloaddition could be used to promote the nucleophilic addition of thiols. Nucleophilic additions of thiols to electron deficient olefins can produce either or both the Markovnikov or anti-Markovnikov products (Scheme 34).

Chapter IV: New Redox Umpolung Mediated Reactions Of Vinylferrocene

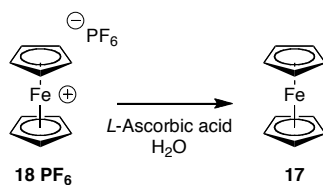


Scheme 34: Potential outcome of umpolung activated nucleophilic addition.

If the method for the activation of vinylferrocene proves successful the activation of vinylferrocene toward nucleophilic addition will also be investigated. This new method may prove to be a new type of thiol-click reaction promoted by umpolung activation. If successful it would pave the way for the functionalisation of thiol containing compounds with a ferrocene redox tag with applications that could reach from medicinal chemistry to materials.

3. Results and discussion

3.1. Reduction of ferrocium hexafluorophosphate **18 PF₆**:



L-Ascorbic acid was the reducing agent of choice for the reduction of **18 PF₆**. Ascorbic acid, otherwise known as vitamin C, is a known antioxidant found in many biological processes. It is also a relatively cheap very powerful reducing agent. One of the reasons why ascorbic acid was chosen to reduce the ferrocenium species is that it is very soluble in water just like ferrocenium, whereas ferrocene species are not. This means that the work-up of the reduction step would be straightforward and the organic ferrocene species would be easily extracted from aqueous solutions.

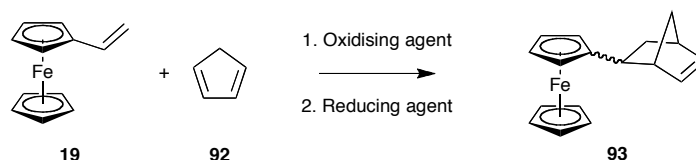
Chapter IV: New Redox Umpolung Mediated Reactions Of Vinylferrocene

In this methodology, ferrocenium hexafluorophosphate **18** PF₆ was dissolved in THF and an aqueous solution of *L*-ascorbic acid was added. THF was chosen as the solvent of choice since it is a versatile organic solvent and is miscible with water. The green ferrocenium solution turned orange within seconds of the addition of *L*-ascorbic acid showing the change from iron(III) to iron(II). After extraction with DCM, ferrocene **17** was recovered in quantitative yield proving the suitability of the reducing agent. The same procedure was repeated starting with ferrocene **17**. FeCl₃ was added to a solution of ferrocene **17** in THF, the solution turned from orange to green instantly attesting to the oxidation of ferrocene **17** to ferrocenium **18**. Subsequently, aqueous *L*-ascorbic acid was added and the solution reverted to orange, after extraction, ferrocene **17** was recovered in quantitative yield. With a viable chemical oxidation and reduction procedure in hand, the same method was used for the promotion of cycloadditions.

3.2. Umpolung controled cycloaddition of vinylferrocene 19:

In the first instance, it was necessary to find out whether umpolung activation of vinylferrocene **19** would promote Diels-Alder reactions with cyclopentadiene and to develop a reliable, reproducible procedure for this transformation. This method would then be used for the umpolung reactions of vinylferrocene **19**, by keeping the same conditions it would ensure direct comparison between reactions and would enable the use of the method for “blank reactions” (reactions necessary to prove that the reaction is umpolung activated). The reaction of vinylferrocene **19** with cyclopentadiene **92** was chosen as a template reaction (Scheme 35).

Chapter IV: New Redox Umpolung Mediated Reactions Of Vinylferrocene



Scheme 35: The template reaction for method development, cycloaddition with cyclopentadiene **92**.

3.2.1. Cycloadditions with cyclopentadiene **92**:

-Control reaction without oxidising agent:

In order to prove that the cycloaddition of vinylferrocene and cyclopentadiene is umpolung controlled. The first attempts at the Diels-Alder reaction without oxidation of ferrocene were carried out under various conditions (Table 8). As predicted, no reaction was observed even with prolonged reaction times and higher temperatures.

Entry	Conditions	Time	Observation
1	Acetone, N ₂ , r.t	72 hrs	SM
2	Acetone, N ₂ , reflux	72 hrs	SM
3	THF, N ₂ , 50 °C	24 hrs	SM
4	THF, N ₂ , reflux	72 hrs	SM

Table 8: Various conditions for the blank reaction of vinylferrocene **19** and cyclopentadiene **92**.

-Optimisation of conditions:

In order to optimise the reaction of vinylferrocene **19** with cyclopentadiene **92** a wide range of conditions were used around the general oxidation and reduction procedure developed with ferrocene (Table 9). The first attempts showed straight away that under the umpolung conditions a Diels-Alder product was synthesised, although in low yield. However, the difference of outcome from entry 1 to entry 2 already showed that the reaction was very susceptible to condition changes. A change of solvent from acetone and water to neat acetone gave two very different products, one of which remains

Chapter IV: New Redox Umpolung Mediated Reactions Of Vinylferrocene

uncharacterised. Also, addition of FeCl₃ was quite vigorous and from that point forward the addition of FeCl₃ was done at subzero temperatures. This resulted in a direct improvement in yield of the desired product (comparison between entry 8 and entries 7, 10 and 11). Entries 7, 10 and 11 also show that a peak of efficiency of 60% was reached when the reaction was warmed up to temperatures nearing or equal to the boiling point of THF (45 - 66 °C). In entry 13, the reaction temperature was raised to 110 °C using toluene as a solvent in an effort to maximise yields. However, only decomposition products were obtained.

One of the major side products of this reaction was the formation of dicyclopentadiene **94** (Figure 87), which is the product of the dimerisation of cyclopentadiene via Diels-Alder cycloaddition. Therefore, the number of equivalents of cyclopentadiene was increased to overcome this competitive side reaction. Equivalents of cyclopentadiene were increased from 5, to 10, to 20 and showed progressive increase in yield. Finally, an acceptable and reproducible yield of 88% was achieved by using 50 equivalents of cyclopentadiene (entry 14). Although 50 equivalents of cyclopentadiene may seem excessive, it remains acceptable due to the effective cost of cyclopentadiene.

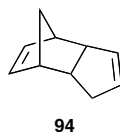


Fig. 87: Structure of dicyclopentadiene **94**.

Chapter IV: New Redox Umpolung Mediated Reactions Of Vinylferrocene

Entry	Oxidising agent	Cp equivalents	Conditions	Reducing agent	Time	Observation
1	FeCl ₃	15	Acetone/H ₂ O, r. t.	L-Ascorbic Acid	18 hrs	40% (endo)
2	FeCl ₃	15	Acetone, N ₂ , r.t	L-Ascorbic Acid	18 hrs	unknown product
3	FeCl ₃	5	Acetone, N ₂ , -10 °C	L-Ascorbic Acid	4 hrs	SM
4	FeCl ₃	5	DCM, N ₂ , 0 °C (load) warm to r.t.	L-Ascorbic Acid	1 h	40% (endo)
5	FeCl ₃	5	THF, N ₂ , -78 °C	L-Ascorbic Acid	18 hrs	SM
6	Ferrocenium PF ₆	5	DCM, N ₂ , -78 °C	Decamethyl ferrocene	18 hrs	SM
7	FeCl ₃	5	THF, N ₂ , -20 °C (load) warm to 50 °C	L-Ascorbic Acid	24 hrs	60% (endo)
8	FeCl ₃	5	THF, N ₂ , r.t (load), reflux	L-Ascorbic Acid	18 hrs	49% (endo)
9	FeCl ₃	5	THF, N ₂ , r.t. (load) reflux	Na ₂ S ₂ O ₃	18 hrs	34% (endo)
10	FeCl ₃	5	THF, N ₂ , -20 °C (load) warm to 45 °C	L-Ascorbic Acid	24 hrs	57% (endo)
11	FeCl ₃	5	THF, N ₂ , -20 °C (load), reflux	L-Ascorbic Acid	24 hrs	59% (endo)
12	FeCl ₃	5	THF/H ₂ O, N ₂ , -20 °C (load), r.t.	L-Ascorbic Acid	24 hrs	traces of endo
13	FeCl ₃	5	Toluene, N ₂ , -20 °C (load), reflux	L-Ascorbic Acid	24 hrs	decomposition
14	FeCl ₃	50	THF, N ₂ , -40 °C (load), warm to 55 °C	L-Ascorbic Acid	18 hrs	88% (endo)

Table 9: Optimisation of the reaction of **19** with cyclopentadiene **92** (Cp). Endo product was the major isomer in all cases generally 11:1 ratio. All reaction carried out several times and were performed on a 100 mg scale of vinylferrocene.

-Characterisation of products:

It is important to remember that, if one or both of the reagents in a Diels-Alder reaction have substituents, the outcome of the reaction will give rise to a number of different

Chapter IV: New Redox Umpolung Mediated Reactions Of Vinylferrocene

isomers categorised as *endo* or *exo*. In this case since the diene is symmetrical there can be two *exo* and two *endo* products. However, the *endo* product should be favoured because it is the kinetic product and because of potential secondary orbital overlap (SOO) with ferrocene (Figure 88). The aim was to maximise the formation of the *endo* product, having kept reaction times relatively low.

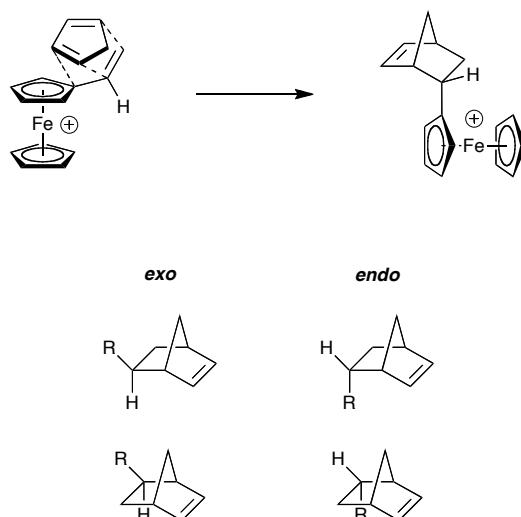


Fig. 88: *Endo* preference because of SOO and *endo/exo* products.

The two *exo* products are diastereoisomers of the two *endo* products and might therefore be separable from each other but would remain as two different mixtures of enantiomer. Unfortunately, the diastereoisomers of this reaction were not successfully separated even with high performance liquid chromatography (HPLC). Nonetheless, the *endo* product was characterised as the major isomer using NMR spectroscopy (Figure 89). In particular NOE (Nuclear Overhauser Effect) experiments were used to show the through space interaction between the hydrogen in the C(5) pseudo-axial position and the cyclopentadienyl hydrogens at C(9) and/or C(12). The NOE experiment reveals that the hydrogen in the pseudo axial (5(ax)) position interacts with hydrogens at positions 5(eq), 4, 6, 3 and only one of the hydrogens on the cyclopentadienyl ring, as well as a

Chapter IV: New Redox Umpolung Mediated Reactions Of Vinylferrocene

very small interaction with hydrogens at positions 13 to 17 (Figure 90). On the other hand the hydrogen at position 5(eq) shows no interaction with protons 9 to 12 (appendix 5). This is further proof that the major product of the reaction is the *endo* product. It also indicates that there may be a rotational lock (interaction of 5(ax) with only one of the ferrocene hydrogens 9 or 12) due to the disfavoured steric interaction of the norbornene and the ferrocene.

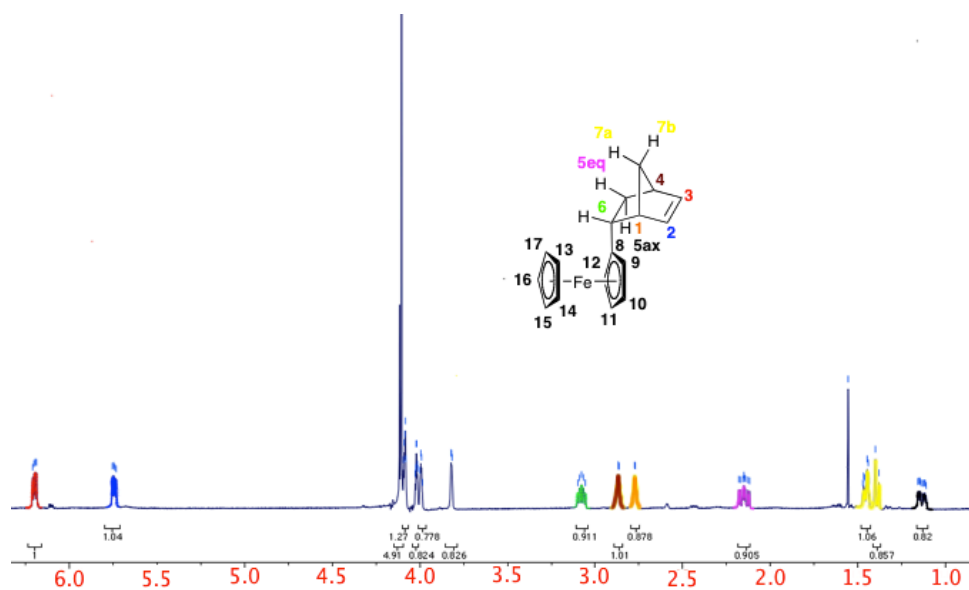


Fig. 89: NMR spectrum of compound 93.

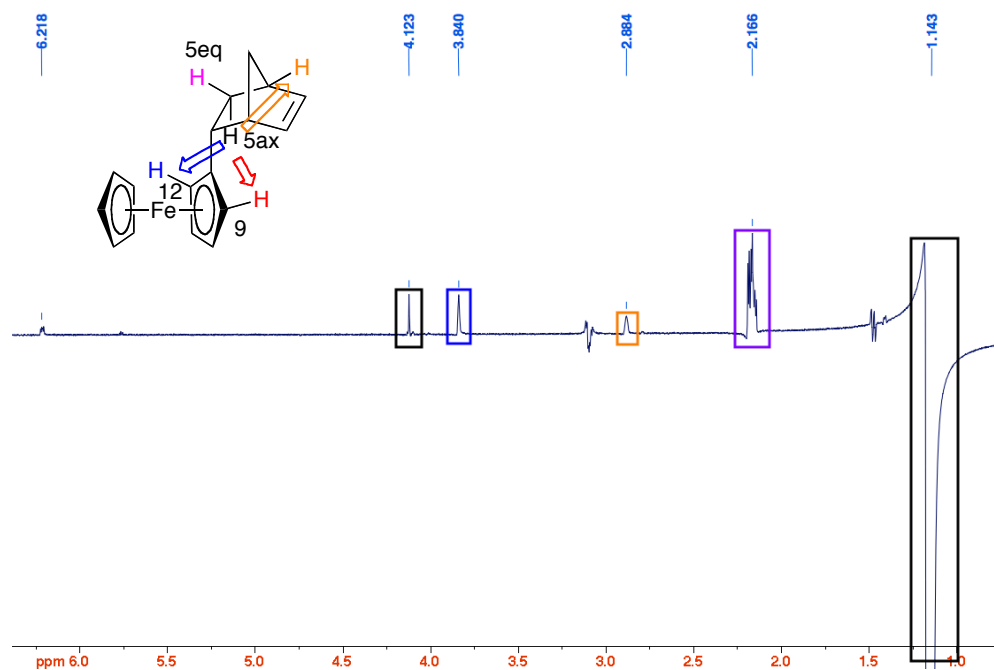


Fig. 90: NOE interaction in compound 93.

Chapter IV: New Redox Umpolung Mediated Reactions Of Vinylferrocene

Entry 2 remains the most challenging of compounds to identify. Although the mass spectrometry analysis gives a single molecular ion peak of 278 m/z (same as the desired product **93**), the NMR spectrum of the product suggests mixture of three isomers that do not resemble **93**. The major product shows some similarities to **93**, for instance, the two alkene peaks at 5.6 ppm and 6.25 ppm resemble closely those of **93** (Figure 91a) and the ferrocene peaks are somewhat similar too. However, a clear doublet at 0.95 ppm (major isomer) integrating to three hydrogens suggests the presence of a methyl group next to a single hydrogen. Also the signals corresponding to the bridge hydrogens have disappeared (Figure 91b).

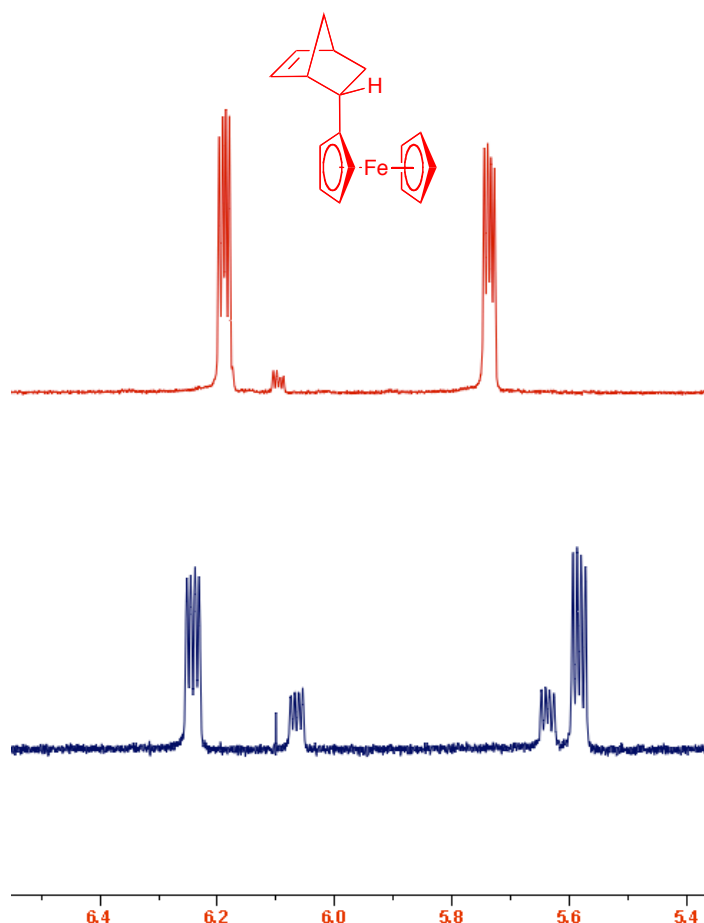
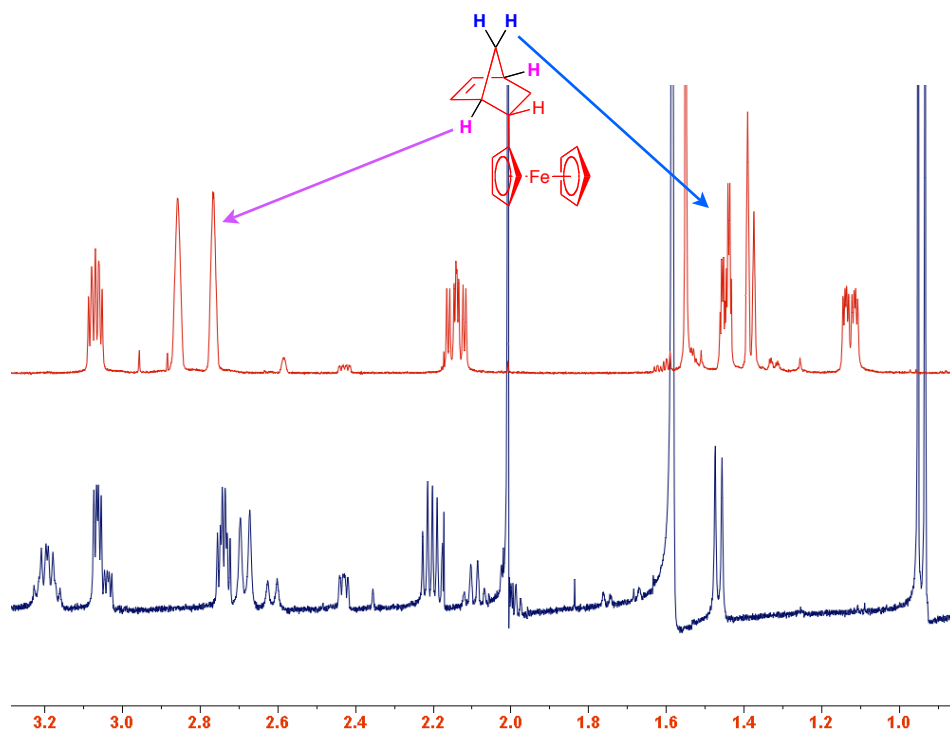
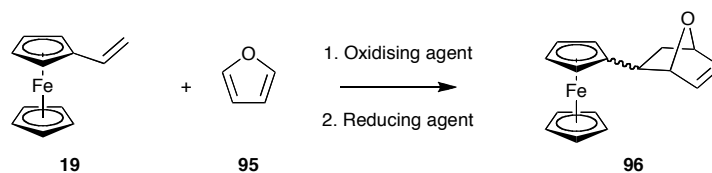
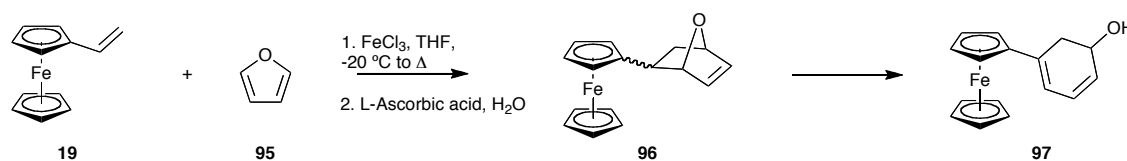


Fig. 91a: Comparison of the NMR of **93** (red) and the product of entry 2 (blue).

Fig. 91b: Comparison of the NMR of **93** (red) and the product of entry 2 (blue).3.2.2. Cycloadditions with furan **95**:

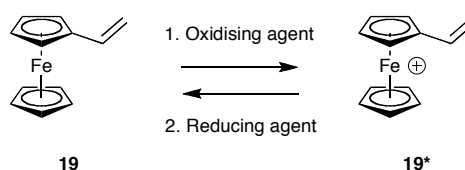
Having successfully developed a reliable procedure for the umpolung controlled Diels-Alder reaction of vinylferrocene **19** the same procedure was used with furan **95** as the diene. Furan **95** was reacted with vinylferrocene **19** in the hope to obtain the desired Diels-Alder product **96**. However, the Diels-Alder norbornene type product was not isolated as it undergoes β -elimination and ring opening to give **97** (isolated in 22% yield) (Scheme 36).

Scheme 36: Umpolung controlled Diels-Alder reaction of vinylferrocene **19** and furan **95**.

Chapter IV: New Redox Umpolung Mediated Reactions Of Vinylferrocene

Unlike the reaction with cyclopentadiene **92**, several side products were isolated. After characterisation, these side products were identified as products of the self reaction of vinylferrocene. These products were investigated further and are described in the following section.

3.2.3. Oxidation and reduction of vinylferrocene **19** in absence of a diene:



The oxidation (and reduction) of **19** in the absence of a diene was investigated. Therefore, the same conditions that we developed for the Diels-Alder reaction were used, although omitting the addition of the diene. The major product of this reaction was an unidentifiable polymer like product that was assumed to be the result of the chemical polymerisation of vinylferrocene **19**. However, out of several minor side products two in particular were successfully identified.

The first identifiable side product of this reaction was isolated after flash column chromatography. Electron ionisation mass spectrometry gave a single molecular ion peak at 424.0 m/z , which corresponds to twice the mass of vinylferrocene (212 $\text{g}\cdot\text{mol}^{-1}$). It's NMR spectrum shows the typical ferrocene peaks corresponding to eighteen hydrogens, two vinyl hydrogen peaks, one single hydrogen peak and a doublet corresponding to three hydrogens (Figure 92). After 2D NMR analysis (COSY and HSQC and DEPT) the product was identified as 1,3-*bis*-ferrocene-but-1-ene **98** (Figure 93). This product is believed to result from a [2+2] addition of vinylferrocene with itself followed by a 1,3-sigmatropic rearrangement (Scheme 37).

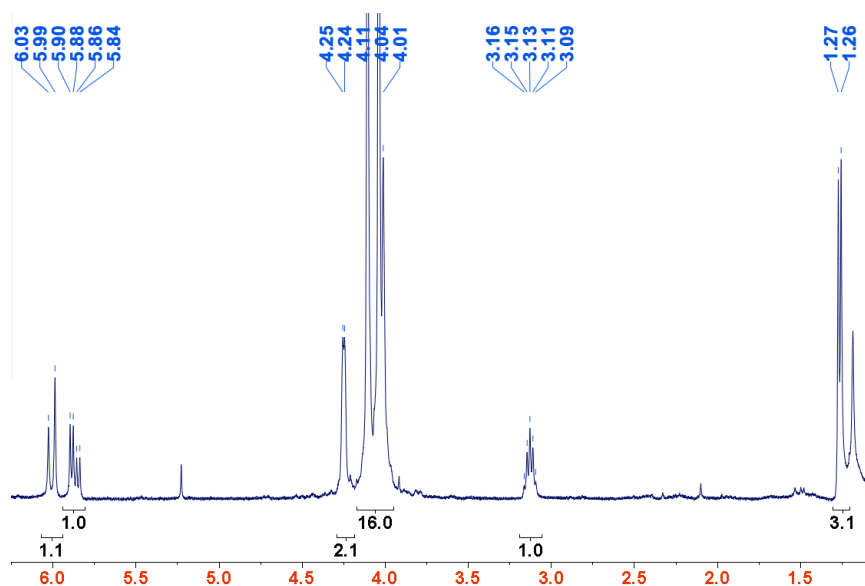
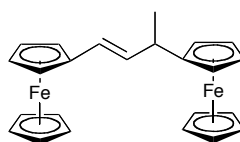
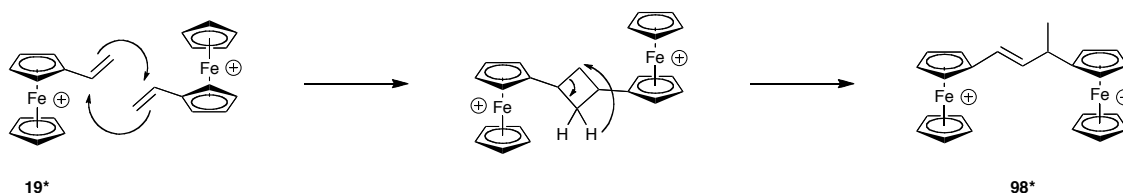


Fig. 92: NMR of compound **98**.



98

Fig. 93: Structure of compound **98**.



Scheme 37: Proposed mechanism for the formation of compound **98**.

The second product which was identified is 1,3-*bis*-ferrocene-butan-1-one **99** (Figure 94). 1,3-*bis*-Ferrocene-butan-1-one **99** provides another indication toward the [2+2] cycloaddition of vinylferrocene with itself. The formation of this side product is intriguing as the reaction was carried out under strict oxygen and water free conditions, the only potential source of oxygen is the extremely hydroscopic FeCl_3 . This was

Chapter IV: New Redox Umpolung Mediated Reactions Of Vinylferrocene

confirmed as no trace of **99** was found when the reaction was done using silver tetrafluoroborate as the oxidant, however 1,3-*bis*-ferrocene-but-1-ene **98** was isolated when using those conditions.

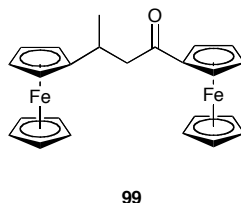
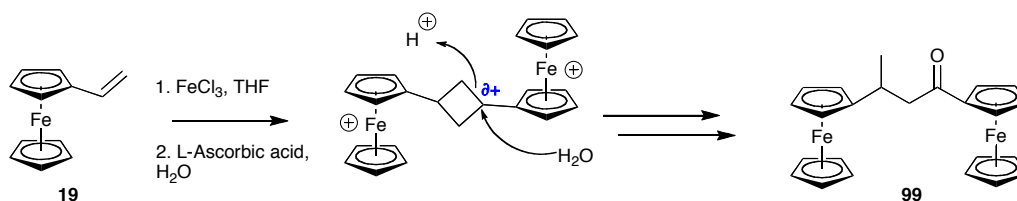


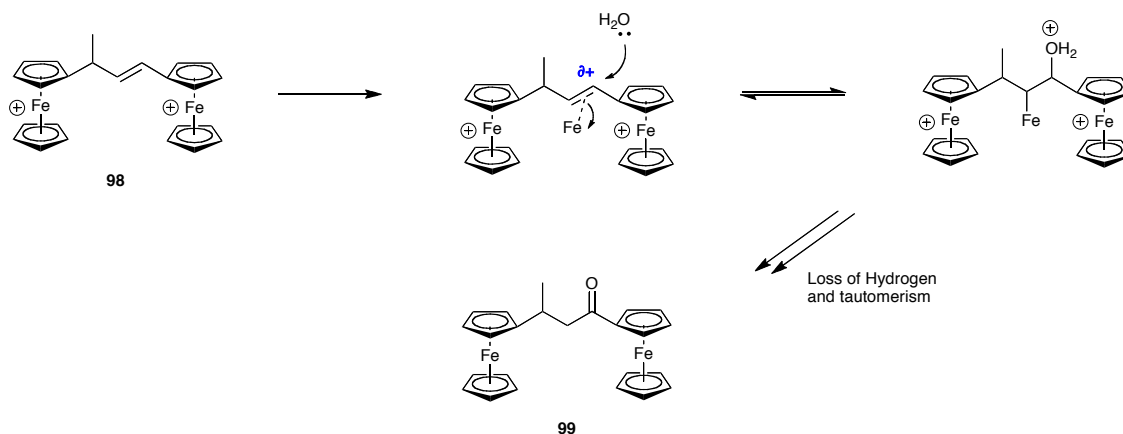
Fig. 94: Structure of compound **99**.

The formation of 1,3-*bis*-ferrocene-butan-1-one **99** can be rationalised in one of two ways. Oxygen (likely in the form of H₂O) could be introduced to the cyclobutane dimer of vinylferrocene **19** and be oxidised in the generally oxidising condition of the reaction (Scheme 38a), or it could be the result of an oxidation of 1,3-*bis*-ferrocene-but-1-ene **98** mediated by FeCl₃ (Scheme 38b). The electron withdrawing ability of the oxidised ferrocenium species is likely to facilitate this transformation by rendering the carbon alpha to the ferrocene electrophilic.



Scheme 38a: First proposed mechanism for the formation of compound **99**.

Chapter IV: New Redox Umpolung Mediated Reactions Of Vinylferrocene



Scheme 38b: Second proposed mechanism for the formation of compound **99**.

The remainder of side products remains too complex to characterise but generally resembles the two products described above with some characteristic peaks distinguishable by NMR. Regardless, the formation of such products is another indication that the oxidation of ferrocene is responsible for the promotion of such reactions.

3.3. Reactions of 6-ferrocene-bicyclo[2.2.1]hept-2-ene **93**:

Having successfully developed a reliable umpolung controlled synthesis of 6-ferrocene-bicyclo[2.2.1]hept-2-ene **93**, several transformations were attempted on the substrate in order to scope-out some applications of this new method.

3.3.1. Ferrocene as a redox auxiliary:

The concept of chemical auxiliaries was first introduced by Corey in 1978,¹³¹ after having synthesised a chiral prostaglandin intermediate using 8-phenylmenthol as a chiral “director” for a Diels-Alder reaction.¹³² The use of chiral auxiliaries has been made more popular by the work of Evans and co-workers with oxazolidinones in chiral aldol transformations.¹³³

Chapter IV: New Redox Umpolung Mediated Reactions Of Vinylferrocene

Chiral auxiliaries are chemical compounds which impart chiral direction to the substrates they are attached to. Once the desired transformation is complete they are removed to reveal only the desired products. There was a sure value in assessing if ferrocene could be seen as an auxiliary in the Diels-Alder reaction that I developed. However, ferrocene is known to be extremely stable, both chemically and thermally. Nevertheless, it has been shown that ferrocene can be reduced to cyclopentanes by catalytic hydrogenation.^{134,135}

First, Van Bekkum and co-workers described the catalytic hydrogenation of ferrocene using palladium on charcoal (10% w/w) in acid medium.¹³⁴ The two major observations were that the rate of hydrogenation was greatly increased when using strongly acidic media (trichloroacetic acid and perchloric acid) and that substituted ferrocenes were less reactive. Nevertheless, the hydrogenation could be done under relatively mild conditions and offers a route to substituted cyclopentanes.

A few years later Sokolov and co-workers used this method as a way to access disubstituted and chiral cyclopentanes.¹³⁵ Substituted cyclopentanes are of particular interest as they can form a good platform towards the synthesis of prostaglandins or more generally prostanoids (Figure 95).

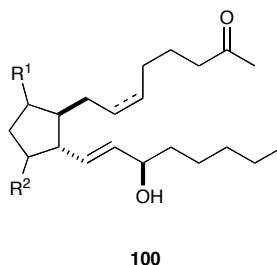
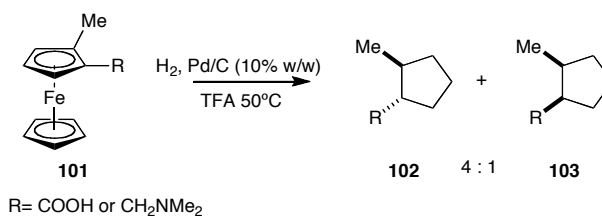


Fig. 95: General structure of prostaglandins **100** R¹= H, O, OH, R²= H, O, OH.

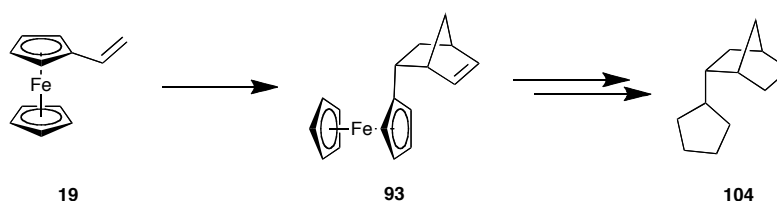
Chapter IV: New Redox Umpolung Mediated Reactions Of Vinylferrocene

Sokolov managed to show that the hydrogenation of ferrocenes had a 4:1 bias in favour of the *trans* product which is the right stereo chemistry for prostanoids (Scheme 39).



Scheme 39: Stereospecific hydrogenation of ferrocene.

In view of this precedent, the reduction of the ferrocene moiety in the Diels-Alder product would be attempted to afford a functionalised cyclopentane. Ferrocene would not only be responsible for the activation of the diene towards cycloadditions but could also be responsible for stereospecific hydrogenation as per Sokolov's observations (for multisubstituted ferrocenes). Finally, the ferrocene moiety would effectively be removed after the key transformations had taken place making it a kind of redox auxiliary (Scheme 40).

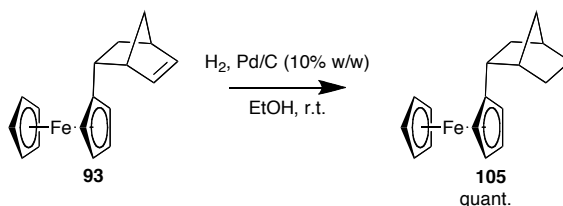


Scheme 40: Redox auxiliary synthetic strategy.

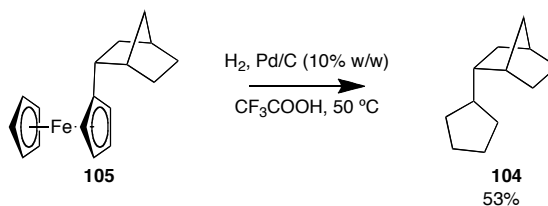
-Synthesis of 1-cyclopentane-bicyclo[2.2.1]heptane **104**:

In the first instance, 6-ferrocene-bicyclo[2.2.1]hept-2-ene **93** was reduced using standard hydrogenation procedures (Scheme 41). 1-ferrocene-bicyclo[2.2.1]heptane **105** was obtained in quantitative yield reproducibly and was then subjected to the hydrogenation conditions described by Sokolov (Scheme 42).

Chapter IV: New Redox Umpolung Mediated Reactions Of Vinylferrocene

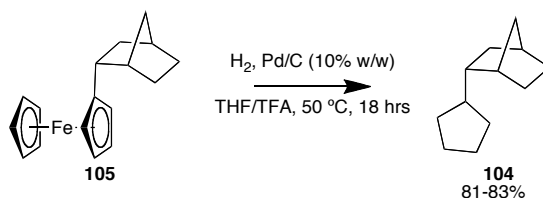


Scheme 41: Hydrogenation of **93** to **105**.



Scheme 42: Hydrogenation of **105** to **104**.

The first observation was that during the reaction, addition of the trifluoroacetic acid (TFA) turned the solution dark green, suggesting oxidation of ferrocene to ferrocenium. Also, the solid in the reaction mixture did not seem to dissolve readily in TFA and this was assumed to be the reason for very low initial yields. Therefore, the reaction was attempted again using a mixture of THF and TFA. In the first instance, the reaction was carried out at room temperature for four hours and yielded 52% of the desired product. Finally, the reaction was carried out at 50°C for eighteen hours and obtained routinely 81-83% of the desired product (Scheme 43).



Scheme 43: Hydrogenation conditions of **105** to **104**.

Chapter IV: New Redox Umpolung Mediated Reactions Of Vinylferrocene

Although neither Sokolov and Van Bekkum tried to explain why the reductive hydrogenation of ferrocene was made possible under those conditions, these observations lead to suggest that the strong acidic conditions generate a ferrocenium species (typical ferrocene/ferrocenium colour change from orange to green was observed). It could be that this “less stable” ferrocenium species is activated toward hydrogenation in an umpolung fashion.

Identification and characterisation of the product could only be done by gas chromatography-mass spectrometry as it has no distinctive functional groups and is only composed of aliphatic cycles. It is therefore not suitable for IR spectroscopy or NMR as it only appears as a series of complicated overlapping multiplets (Figure 96).

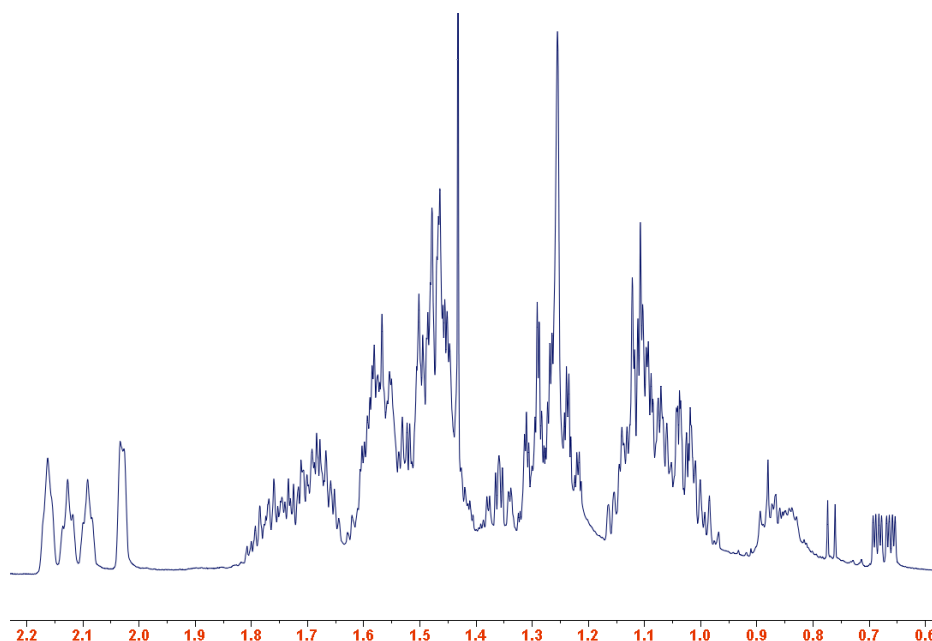


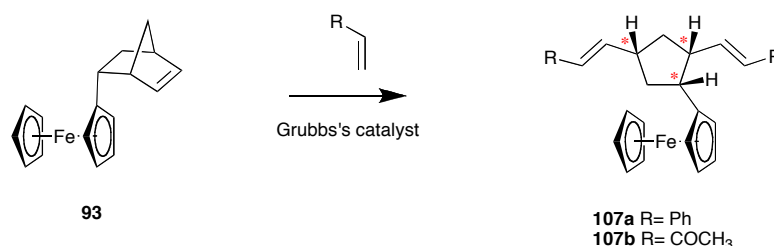
Fig. 96: NMR spectrum of compound **104**.

3.3.2. Ring opening metathesis-cross metathesis (ROM-CM):

In a view to investigate further reaction of 6-ferrocene-bicyclo[2.2.1]hept-2-ene **93** and ferrocene reduction, the decision was made to functionalise the Diels-Alder product using ROM-CM reactions (Scheme 44). In the first attempt at the ROM-CM reaction,

Chapter IV: New Redox Umpolung Mediated Reactions Of Vinylferrocene

styrene **106** was used as the cross metathesis partner (Table 10). The desired ROM-CM product 1-[(±)ferrocene]-2*R*,4*S*-[bis-(styrene)]-cyclopentane **107a** was isolated only in 8% yield, this was attributed to the formation of *E*-stilbene **108** and the ring opening metathesis polymerisation product of 6-ferrocene-bicyclo[2.2.1]hept-2-ene **93**, 1-ferrocene-polynorbornene **109** (Figure 97).



Scheme 44: ROM-CM of 6-ferrocene-bicyclo[2.2.1]hept-2-ene **93**.

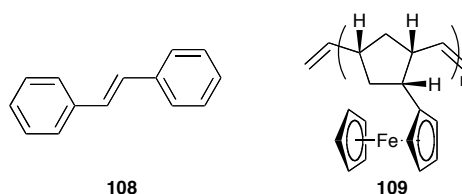
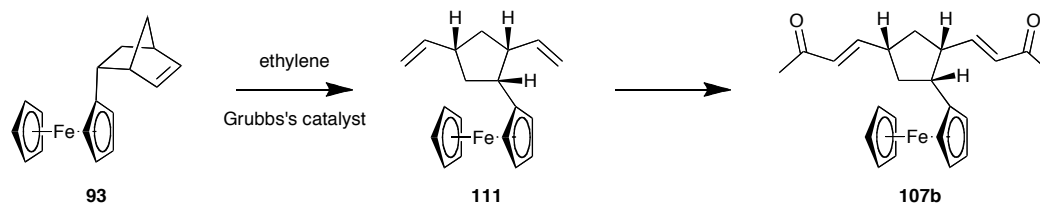


Fig. 97: Structures of *E*-stilbene **108** and 1-ferrocene-polynorbornene **109**.

E-Stilbene **108** is the known product of the homodimerisation of styrene **106**. In Grubbs' "categorisation of selectivity in olefin cross metathesis", it is categorised as a type I olefin, meaning it undergoes fast homodimerisation with Grubbs 2nd generation catalyst.¹³⁶ Therefore methyl vinyl ketone **110** was chosen as the cross metathesis partner since it falls under type II category (slow homodimerisation). In addition, norbornenes are known to readily undergo ring opening metathesis polymerisation (ROMP) using Grubbs catalyst. Therefore, the reaction was carried out using a higher concentration of methyl vinyl ketone to norbornene (maximise cross metathesis) and in overall more dilute conditions to minimise the formation of the ROMP product **109**.

Chapter IV: New Redox Umpolung Mediated Reactions Of Vinylferrocene

As seen in entry 2 (Table 10) hardly any product was recovered. The reaction was therefore attempted at higher temperatures, under an atmosphere of ethylene to maximise the lifetime of the ring-opened intermediate **111** (Scheme 45) and to add the catalyst in portions,¹³⁷ which gave **107b** in 17% (entry 3).



Scheme 45: ROM-CM reaction with ethylene to maximise intermediate **111** lifetime.

Finally, the reaction was attempted using a different catalyst (Hoveyda-Grubbs II) and gave the desired product in 34% yield in the first instance. After optimisation of the conditions and reaction procedure, compound **107b** was reproducibly isolated in acceptable 65% yield (entry 5). Subsequently, 1-[(±)ferrocene]-2*R*,4*S*-[bis-(buten-3-one)]-cyclopentane **107b** was successfully reduced, under standard hydrogenation conditions, to 1-[(±)ferrocene]-2*R*,4*S*-[bis-(butan-3-one)]-cyclopentane **112** in quantitative yield (Figure 98).

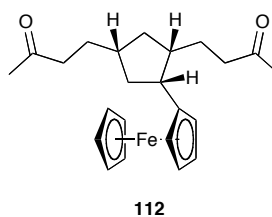


Fig. 98: Structure of compound **112**.

Chapter IV: New Redox Umpolung Mediated Reactions Of Vinylferrocene

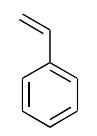
Entry	CM partner	Catalyst	Conditions	Time	Product
1	 106 5eq.	Grubbs II 1 mol%.	DCM, N ₂ , r.t.	18 hrs	107a 8% ^a
2	 87 10 eq.	Grubbs II 5 mol%	DCM, N ₂ , r.t.	18 hrs	107b less than 1% ^a
3	 87 10 eq.	Grubbs II 5 mol%	Toluene, 110 °C, ethylene 1 atm	24 hrs	107b 17% ^b
4	 87 30 eq.	Hoveyda-Grubbs II 1 mol%	Toluene, 110 °C, ethylene 1 atm	24 hrs	107b 34% ^b
5	 87 30 eq.	Hoveyda-Grubbs II 1 mol%	Toluene, 110 °C, N ₂	3 hrs	107b 65% ^c

Table 10: Optimisation of ROM-CM conditions. a: catalyst added in one portion; b: catalyst dissolved in toluene and added in two portions, 1 hour apart; c: catalyst and **93** dissolved in toluene (0.01 and 0.1 mol.L⁻¹ respectively), added in six portions over 1 hour.

Although the hydrogenation of the ferrocene moiety was attempted the time constraints attached with my research program did not allow enough time to fully interpret the results of what transpired to be a very complicated reaction. The desired product **113** (Figure 99) was not observed at all.

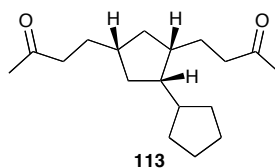
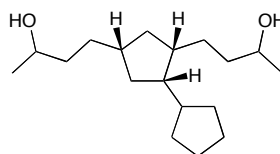


Fig. 99: Desired product for the hydrogenation of **112**.

However, it is possible that in such acidic conditions the ketone groups may have been reduced to give 1-[(±)cyclopentane]-2*R*,4*S*-[bis-(butan-3-ol)]-cyclopentane **114**

Chapter IV: New Redox Umpolung Mediated Reactions Of Vinylferrocene

(Figure 100). If that was the case, the product may have been extracted into the aqueous phase during work-up, explaining why no products were found in the organic phase.



114

Fig. 100: Potential product of the ferrocene hydrogenation of **112**.

3.3.3. Ring opening metathesis polymerisation (ROMP):

As previously mentioned norbornenes readily undergo ring opening metathesis polymerisation and we have previously observed that 6-ferrocene-bicyclo[2.2.1]hept-2-ene **93** underwent polymerisation, although the product was not characterised at the time. Polynorbornenes are an important class of polymers that attract a lot of interest. Polynorbornenes are attractive polymers due to their high regioregularity, they are known for their high transparency, chemical resistance and electric properties,¹³⁸ and are also known to form liquid crystalline polymers.¹³⁹

Polynorbornenes containing ferrocene have been synthesised with the ferrocene moiety attached in a side chain.¹⁴⁰ Masuda and co-workers, have reported ferrocene containing polymers with charge/discharge properties as targets for organometallic batteries,¹⁴¹ and norbornene polymers with pendant tetramethylpiperidine groups showing similar charge/discharge properties (Figure 101).¹⁴² Therefore, polynorbornene polymers with pendant ferrocene could have similar applications. 1-Ferrocene-polynorbornene **109** (Figure 102) was synthesised by ROMP using Grubbs II catalyst and was isolated as a glassy solid in 80% with an average molecular weight of 8499 g.mol⁻¹ and polydispersity index of 1.45.

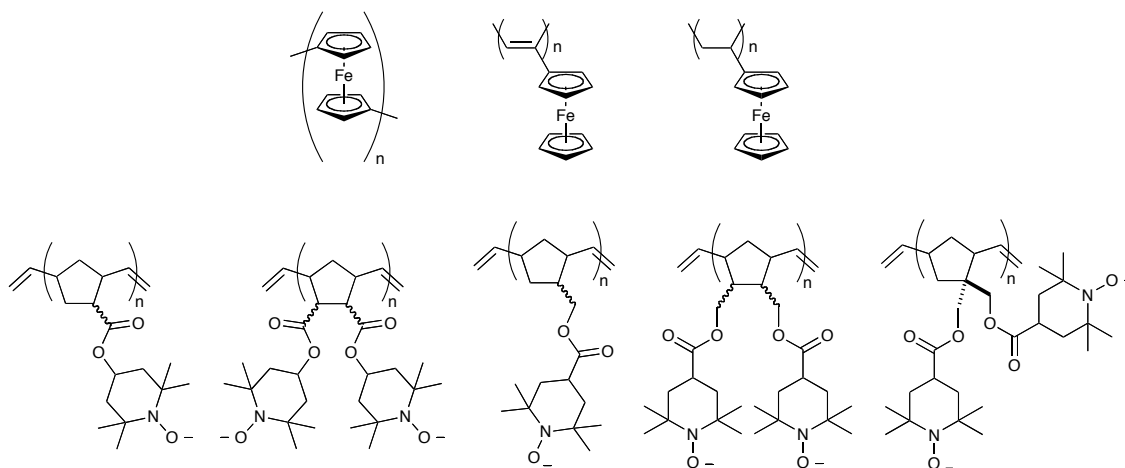


Fig. 101: Structures of the charge/discharge polymers developed by Masuda and co-workers.

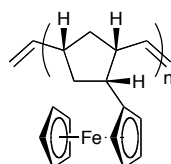


Fig. 102: Structure of 1-ferrocene-polynorbornene **109**.

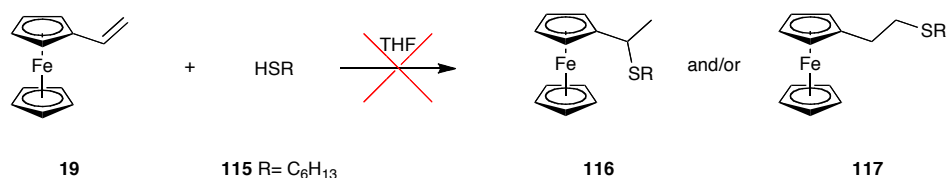
3.4. Umpolung controlled nucleophilic additions:

Having successfully developed a method for the umpolung activation of vinylferrocene **19** toward cycloadditions, the same method would be adapted to attempt reactions of umpolung activated vinylferrocene **19** with nucleophiles (thiols).

3.4.1. Control reaction with oxidising agent:

As per the development of the cycloaddition reactions, there is need to prove that the reaction of vinylferrocene **19** with thiols only proceeded with umpolung activation of vinylferrocene **19**. Therefore, the first attempt at the reaction was done in the absence of FeCl_3 . As expected, no reaction was observed between vinylferrocene **19** and hexane thiol **115** (Scheme 46) and only unreacted starting materials were recovered.

Chapter IV: New Redox Umpolung Mediated Reactions Of Vinylferrocene



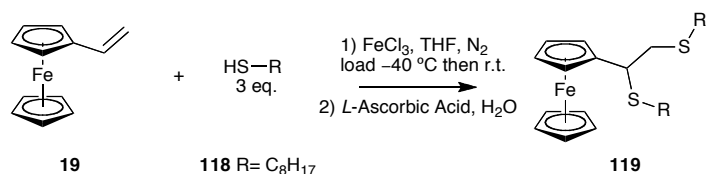
Scheme 46: Blank reaction of vinylferrocene **12** with hexanethiol **115**.

3.4.2. Umpolung activated reactions of vinylferrocene **19** with thiols:

Having proved that no reaction occurred between vinylferrocene **19** and hexanethiol **115**, the reaction of vinylferrocene **19** with thiols using the FeCl₃/*L*-ascorbic acid redox activation method was attempted under several conditions (Table 11, p. 147).

-Entry 1: First attempt

As a first attempt the reaction was carried out at room temperature before trying higher temperatures (entries 1 & 2). Two equivalents of hexanethiol were mixed with vinylferrocene and cooled to -40 °C, FeCl₃ was added to the reaction mixture, which was then allowed to warm to room temperature (Scheme 47). Mostly unreacted vinylferrocene **19**, octanethiol **118** (or disulfide) and an unidentifiable polymer like compound were recovered from this reaction. However, a product of thiol addition was identified as 1,2-*bis*-octanesulfide-ethylferrocene **119**.



Scheme 47: Reaction of vinylferrocene **19** and octanethiol **118** entry 1.

This double addition product can be explained by the use of an excess of thiol reagent in the reaction. Also, as was found in later reactions both 1-ethyl-1'-alkylsulfide-ferrocene

Chapter IV: New Redox Umpolung Mediated Reactions Of Vinylferrocene

116 and *E*-1-ferrocene-2-alkylsulfide-ethene **120** products were isolated from this type of transformation (Figure 103).

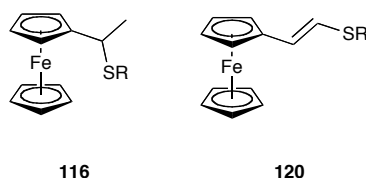
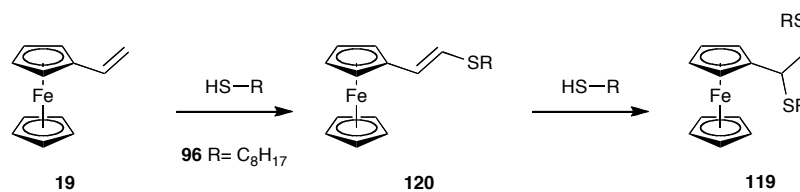


Fig. 103: Structures of compound **116** and compound **120**.

One possible explanation for the formation of 1,2-*bis*-octanesulfide-ethylferrocene **119** would be primary formation of the *E*-alkene with the first thiol addition and secondary Markovnikov thiol addition to the *E*-alkene (Scheme 49).



Scheme 48: Proposed reaction progression for the formation of 1,2-*bis*-octanesulfide-ethylferrocene **119**.

-Entries 2 to 5: Optimisation of conditions

Following the results given in entry 1 the temperature was raised to the boiling point of THF in an effort to increase the yield of the double addition product. However, increasing the temperature had a dramatic effect on the reaction and gave no thiol addition products. The major products were recovered thiol and an unidentifiable polymer-like compound. However, when the thiol was present from the start of the reaction trace amounts of 1,3-*bis*-ferrocene-but-1-ene **98** were isolated and small amounts of a compound consistent with 1-hexanesulfide-1-cyclopentadiene-3-ferrocene-butane **121** (8%) (Figure 104) and vice-versa when the thiol was added after the oxidant. 1-Hexanesulfide-1-cyclopentadiene-3-ferrocene-butane **121** is a suggested

Chapter IV: New Redox Umpolung Mediated Reactions Of Vinylferrocene

product from the NMR data available, full characterisation was not achieved but the evidence provided remains strong in favour of this interpretation (appendix 4).

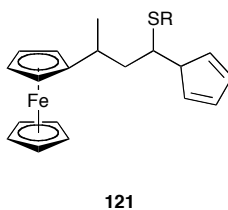
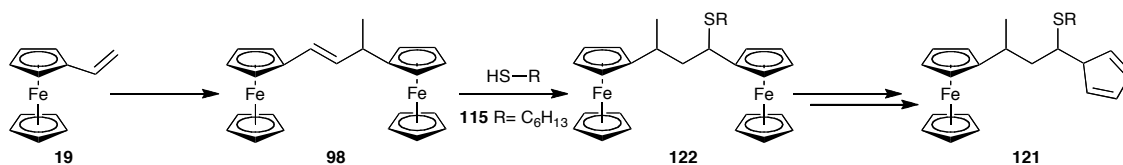


Fig. 104: Structure of compound **121** (R= C₆H₁₃).

1-Hexanesulfide-1-cyclopentadiene-3-ferrocene-butane **121** is likely to be the product of the Markovnikov thiol addition of hexane thiol to 1,3-*bis*-ferrocene-but-1-ene **98** and of the subsequent decomposition of the ferrocene at C(1) to cyclopentadiene (Scheme 49).

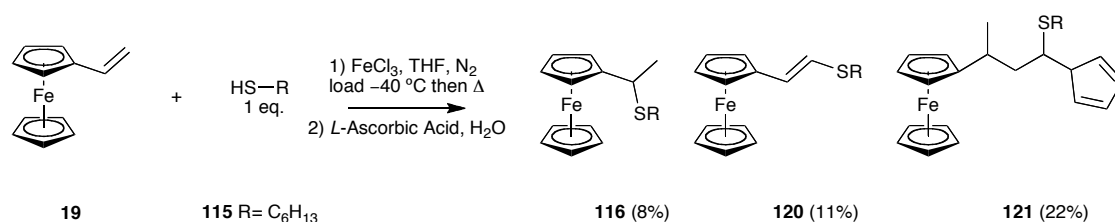


Scheme 49: Proposed reaction progression for the formation of compound **121**.

It was previously inferred that decomposition of ferrocene occurred under strongly acidic conditions which likely generated a less stable ferrocenium species that could be decomposed through catalytic hydrogenation. The observation that ferrocene decomposes under these conditions strengthens this hypothesis as it is probably made possible from the fact that the reaction is carried out under redox conditions (generation of ferrocenium) and acidic conditions that may be the result of the generation of HCl from the reaction of FeCl₃ with hexanethiol **115**.

Chapter IV: New Redox Umpolung Mediated Reactions Of Vinylferrocene

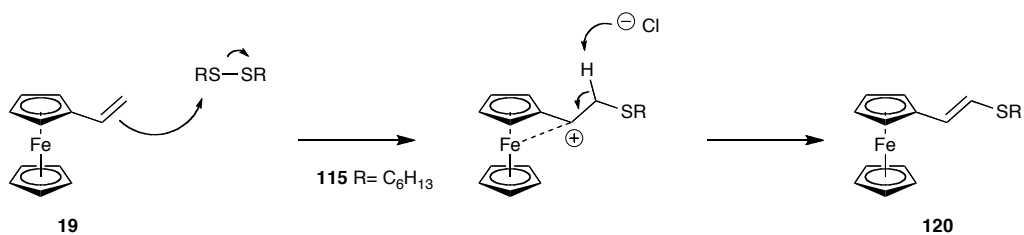
Having tried umpolung-activated thiol additions with an excess of thiol, it is possible that the excess thiol had a detrimental effect on the reaction and promoted further reactions of the desired products (Markovnikov or anti-Markovnikov) (entries 3, 4 & 5). Therefore, the reaction was attempted again at reflux temperature, with one equivalent of thiol added both before and after the oxidant. When the thiol was added after the oxidant only trace amounts of compound **121** were isolated with mainly unidentifiable polymeric by-products. When the thiol was added before FeCl₃ the major product again was unidentifiable, however, three minor identifiable products were isolated in low yields (Scheme 50). These products were identified as 1-hexanesulfide-1-cyclopentadiene-3-ferrocene-butane **121** (22%), *E*-1-ferrocene-2-hexanesulfide-ethene **120** (11%) and the desired Markovnikov product 1-ethyl-1'-hexanesulfide-ferrocene **116** (8%).



Scheme 50: Reaction of vinylferrocene **19** and hexanethiol **115** entry 3 (thiol added before FeCl₃).

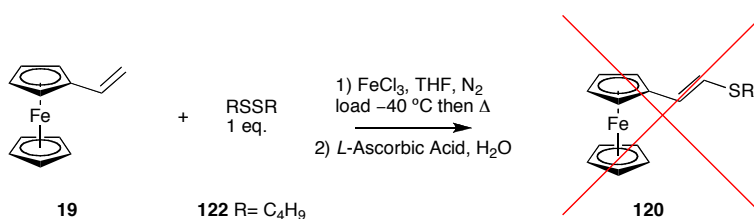
E-1-Ferrocene-2-hexanesulfide-ethene **120** is an unexpected product for this reaction and could result from a number of mechanisms. One potential mechanism could be seen to come from a nucleophilic attack of the alkene toward a disulfide which could be formed in solution in the presence of FeCl₃. The ferrocene iron centre could be seen to stabilise the carbocation intermediate, and elimination of hydrogen by chlorine present in solution would afford the alkene (Scheme 51).

Chapter IV: New Redox Umpolung Mediated Reactions Of Vinylferrocene



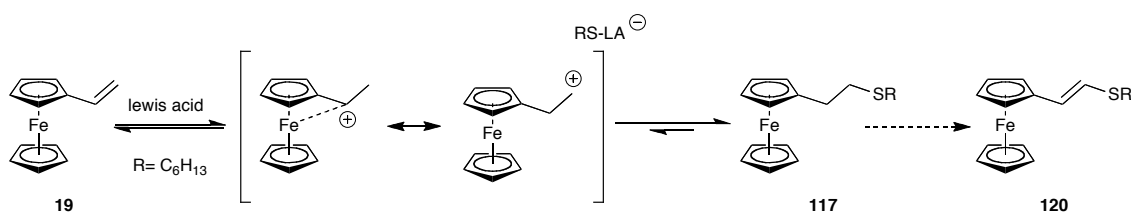
Scheme 51: Proposed mechanism for the formation of compound **120**.

This hypothesis was put to the test by reacting vinylferrocene **19** with butanedisulfide **122** under the same conditions (Scheme 52) but no evidence of the formation of the *E*-alkene product was found.



Scheme 52: Reaction of vinylferrocene **19** with butanedisulfide **122**.

The only other hypothesis is that *E*-1-ferrocene-2-hexanesulfide-ethene **120** may be the result of further reaction of the anti-Markovnikov product but this remains to be investigated further (Scheme 53).



Scheme 53: Proposed mechanism for the formation of compound **120**.

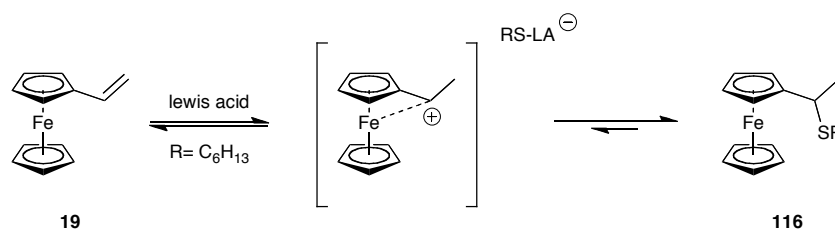
Since formation of polymers and potential oxidation of the thiol seemed to be the greatest obstacle to overcome, the same reaction was carried out at lower temperatures in an effort to promote the other reaction. When the thiol was added before FeCl₃, formation of compound **120** and 1-ethyl-1'-hexanesulfide-ferrocene **116** did not

Chapter IV: New Redox Umpolung Mediated Reactions Of Vinylferrocene

improve, giving yields of 10% and 13% respectively. However, formation of products resulting from the dimerisation of vinylferrocene **19** was significantly reduced. This was further proved when the reaction was tried at 0 °C and the yields of formation of compound **116** were unchanged but yields of dimerisation products were further reduced.

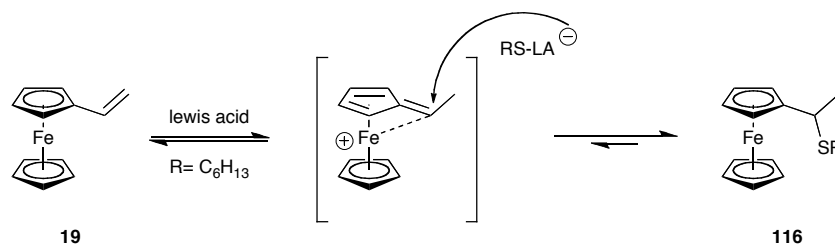
-Entry 4: Key result

Finally, the desired Markovnikov product was successfully isolated in 67% yield by adding the thiol after the oxidant. This reaction is analogous to that of styrene with thiols using lewis acid catalysts which also gives the Markovnikov product preferentially.¹¹⁶ In this case the Markovnikov carbocation intermediate could be further stabilised by the neighbouring iron center (Scheme 54). Another interpretation for the promotion of this reaction could see the formation of a ferrocene fulvalene intermediate that would promote addition at the Markovnikov position in a Michael like addition (Scheme 55). Both interpretations could be valid but extensive analysis would be required to truly understand the mechanism of this reaction.



Scheme 54: Proposed reaction mechanism for the Markovnikov thiol addition.

Chapter IV: New Redox Umpolung Mediated Reactions Of Vinylferrocene



Scheme 55: Proposed reaction mechanism for the Michael-like Markovnikov thiol addition.

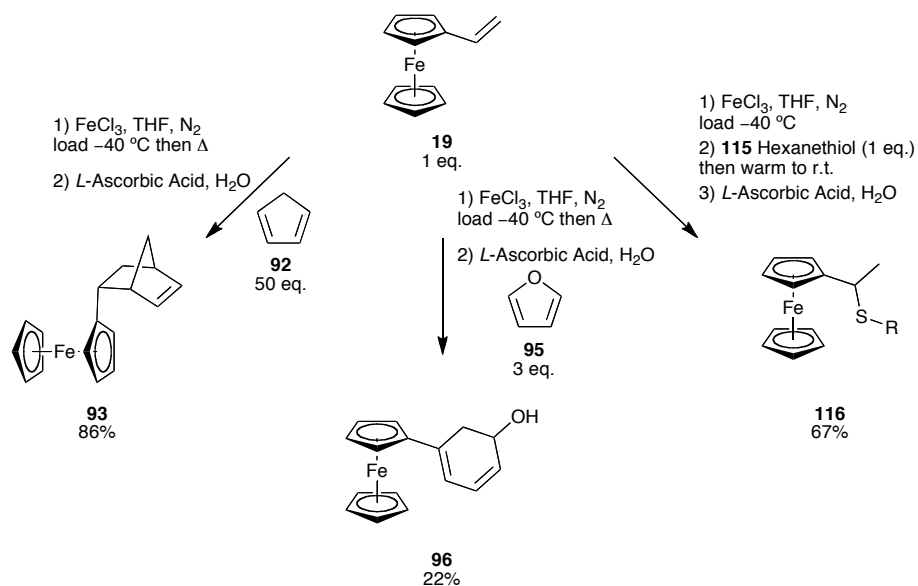
Entry	RSH	Conditions	Products	
			RSH added before FeCl ₃	RSH added after FeCl ₃
1	3 eq.	1) FeCl ₃ , THF, N ₂ , -40 °C (load), warm to r.t., 18 hrs 2) L-Ascorbic acid, H ₂ O	119 (27%)	
2	3 eq.	1) FeCl ₃ , THF, N ₂ , -40 °C (load), warm to reflux, 18 hrs 2) L-Ascorbic acid, H ₂ O	121 (8%) 98 (traces)	121 (traces) 98 (8%)
3	1 eq.	1) FeCl ₃ , THF, N ₂ , -40 °C (load), warm to reflux, 18 hrs 2) L-Ascorbic acid, H ₂ O	116 (8%) 120 (11%) 121 (22%)	121 (traces)
4	1 eq.	1) FeCl ₃ , THF, N ₂ , -40 °C (load), warm to r.t., 18 hrs 2) L-Ascorbic acid, H ₂ O	116 (10%) 120 (13%) 121 (9%) 99 (8%)	116 (67%) 121 (9%)
5	1 eq.	1) FeCl ₃ , THF, N ₂ , -40 °C (load), warm to 0 °C, 18 hrs 2) L-Ascorbic acid, H ₂ O	116 (9%) 99 (3%)	

Table 11: Optimisation of the reaction of vinylferrocene **19** with thiols (RSH). All reaction performed on a 50 mg scale of vinylferrocene.

Unlike the cycloaddition reactions this reaction produced a wide array of products and side products. Nevertheless, a reliable and reproducible result was obtained whereby umpolung activation of vinylferrocene toward nucleophilic attack gave the Markovnikov product in high yields.

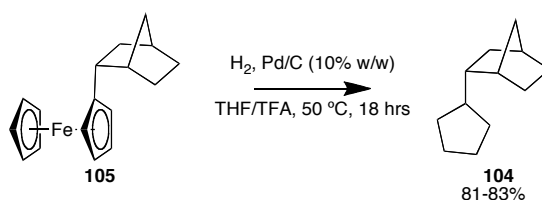
4. Conclusions

A new method was successfully developed for the promotion of Diels-Alder cycloaddition of vinylferrocene **19** with cyclopentadiene **92** via umpolung activation. The same method was also implemented successfully to the promotion of nucleophilic addition of thiols to vinylferrocene (Scheme 56).



Scheme 56: Umpolung activated reactions of vinylferrocene **19**.

The reductive hydrogenation of ferrocene after promotion of the Diels-Alder reactions was also investigated, so as to consider ferrocene as a redox umpolung auxiliary (scheme 57). This method gives access to novel ferrocene and cyclopentane derivatives with potential materials and biological applications.



Scheme 57: Reductive hydrogenation of ferrocene.

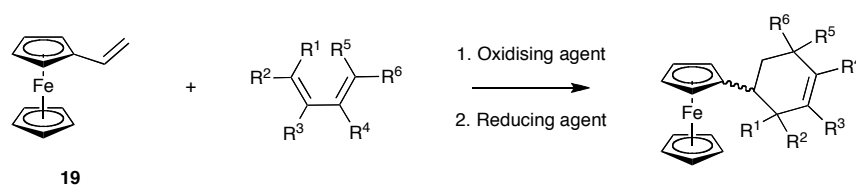
Chapter IV: New Redox Umpolung Mediated Reactions Of Vinylferrocene

Much work remains to be carried out to investigate other transformations and understanding mechanisms of those described above. However, I believe that sufficient progress has been made to support further research interest in this redox umpolung method.

5. Future work

As part of a general approach, further optimisation of this method could be pursued. Particularly investigations into different oxidising and reducing methods. One may find that milder oxidising agents could be used and that these could be more compatible with other substrates. Also, in an interest to scale up such reactions and to develop greener synthetic protocols, the redox umpolung method could be adapted to an electrochemical set-up.

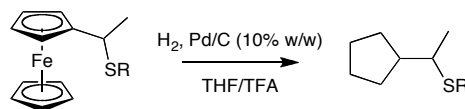
Future work for the umpolung activated cycloadditions of vinylferrocene **19** should include a wide array of cycloadditions to investigate the scope of compatibility of this method with other dienes (Scheme 58). Also since the observations made in this project showed that vinylferrocene readily undergoes homo-ene reactions, reactions of vinylferrocene in other [2+2] cycloadditions as well as other pericyclic reactions could be investigated. Similarly, in the case of nucleophilic additions, an array of thiols and other nucleophiles should be tested against this method to assess its robustness and versatility.



Scheme 58: Umpolung activated cycloadditions of vinylferrocene **19**.

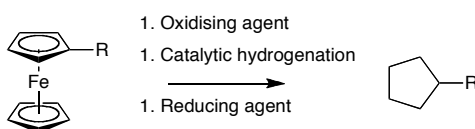
Chapter IV: New Redox Umpolung Mediated Reactions Of Vinylferrocene

Seminal work has been carried out with regard to developing this umpolung methodology into an umpolung auxiliary method. Further investigations into the decomposition of ferrocene need to be carried out. In the first instance, reduction of the ferrocene moiety in the thiol additions substrates should be carried out (Scheme 59).



Scheme 59: Reductive hydrogenation of the thiol addition products.

Also, in light of the decomposition product that has been isolated as part of the umpolung thiol reactions (1-hexanesulfide-1-cyclopentadiene-3-ferrocene-butane **121**), the hypothesis that the decomposition of ferrocene is also an umpolung driven process should be tested to try and understand that process better. Hydrogenation of ferrocene could be attempted under redox conditions in the absence of a strong acid (Scheme 60).



Scheme 60: Umpolung activated reductive hydrogenation of ferrocene.

As mentioned in the introduction to this chapter, the reaction of vinylferrocene with thiols could be used to introduce the vinylferrocene as a redox tag to proteins and biological systems as well as to the surfaces of nanoparticles. Nucleophilic addition of natural thiols such glutathione to vinylferrocene could be investigated as well as the reaction of vinylferrocene with nanoparticles functionalised with pendant thiols.

CHAPTER V: EXPERIMENTAL

Experimental terms and methods:

Flash Column Chromatography: Using silica gel (Sigma-Aldrich) 40-63 μm 60 \AA and solvent system is specified in each experimental.

TLC: Were performed using 5x4 cm SiO_2 coated aluminium plates

Dry solvents: Innovative Technology *inc.* Pure Solv 400-5-MD solvent purification system (activated alumina columns)

Reaction temperatures: Room temperature refers to 20-25 $^\circ\text{C}$ other temperatures were obtained using ice-water bath for 0 $^\circ\text{C}$ and acetone-dry ice bath for -78 $^\circ\text{C}$.

Analytical methods:

HPLC: Analytical and preparative HPLC were performed using a P680 Dionex HPLC pump system. Analytical HPLC: Supelco® reverse phase column (HS C18, 250 x 4.6mm, 5 μm). Preparative HPLC: Phenomenex® reverse phase semi-preparative column (C8, 250 x 10mm, 5 μm).

IR: Was recorded on a Perkin Elmer FT-IR instrument, absorption (ν_{max}) is given in wavenumbers (cm^{-1}) and peak intensities are qualified as strong (str), medium (m), weak (w) or broad (br).

MS: Mass spectrometry was performed by Jim Tweedie mass spectrometry technician at the University of Glasgow.

M.p.: Recorded on a SMP-10 Stuart Scientific melting point machine. Melting points are uncorrected.

Chapter V: Experimental

NMR: Performed on either Bruker Avance 500, Bruker Avance 400. All spectra were characterised from ^1H , ^{13}C , HMQC methods, and were analysed using the Mestrelab research iNMR© package (for MacOS X®).

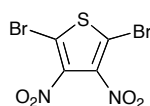
GPC: Performed using Polymer Lab GPC-50, on 2 Resipore columns (300 x 7.5 mm). The instrument was calibrated using MMA polymer standards.

CV: Performed using a CH Instrument Electrochemical Workstation (CHI 440a), Austin, TX, USA. Samples were analysed at 10^{-4} M concentrations using 0.1M TBA.PF₆ as the electrolyte

UV: Performed using a PerkinElmer Lambda 25 spectrometer

CHAPTER II:

2,5-Dibromo-3,4-dinitrothiophene **50**:

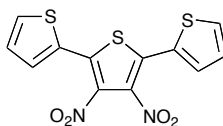


2,5-Dibromothiophene **49** (3.5 mL, 31.0 mmol) was added dropwise to a mixture of fuming nitric acid (11 mL) and concentrated sulphuric acid (33 mL) at 0 °C. The reaction mixture was then allowed to warm to room temperature and was stirred over 3 hours, after this time the reaction was quenched by pouring slowly onto ice. The resulting precipitate was then filtered off and then recrystallised from hot methanol to give title compound **50** as a yellow solid (5.5 g; 53%); m.p. 132–134 °C (lit. 135.8–136.7 °C)¹; $\nu_{\text{max}}/\text{cm}^{-1}$ (neat) 1534 (NO₂ *anti*), 1315 (NO₂ *symm*); δ_{C} (125 MHz, CDCl₃) 113.5 (C), 140.7 (C); m/z (EI +) 331.7930 [M]⁺ (C₄⁷⁹Br⁸¹BrN₂O₄S requires 331.7925).

¹ L. Wen, S. C. Rasmussen; *J. Chem. Crystal.*, **2007**, 37, 387-398

Chapter V: Experimental

3',4'-Dinitro-[2,2',5',2'']-terthiophene **51**:

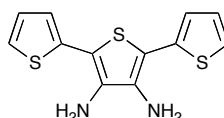


2,5-Dibromo-3,4-dinitrothiophene **50** (5.00 g, 15.06 mmol), 2(tributylstanyl)-thiophene (14.4 mL, 45.18 mmol) and dichloro-*bis*(triphenyl phosphino)-palladium II (1.12 g, 1.50 mmol) were dissolved in dry THF (50 mL). The reaction was heated under reflux overnight under N₂ atmosphere and the solvent was then removed under reduced pressure. The residue was then washed with hexane (4 × 100 mL) and purified by flash column chromatography (DCM:Petroleum ether; 4:1) to yield title compound **51** as an orange solid (5.09 g; 99%); m.p. 138–140 °C (lit. 147–149 °C)²; $\nu_{\max}/\text{cm}^{-1}$ (solid state) 3075 (C-H aromatic), 1537 (NO₂ *anti*), 1381 (NO₂ *symm*); δ_{H} (500 MHz, CDCl₃) 7.18 (2H, dd, *J* 5.1, 3.8, C(4, 4'')H), 7.55 (2H, dd, *J* 3.8, 1.1, C(3, 3'' or 5, 5'')H), 7.61 (2H, dd, *J* 5.1, 1.1, C(3, 3'' or 5, 5'')H); δ_{C} (125 MHz, CDCl₃) 128.1 (C), 128.5 (CH), 131.2 (CH), 131.3 (CH), 133.9 (C); *m/z* (EI⁺) 337.9492 [M]⁺ (C₁₂H₆N₂O₄S₃ requires 337.9490).

² Xia, Yangjun; *Macromolecular Chemistry and Physics*, **2006**, 207, 511-520

Chapter V: Experimental

[2,2',5',2'']-Terthiophene-3',4'-diamine **52**:

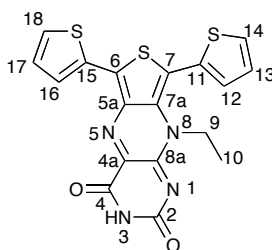


3',4'-Dinitro-[2,2',5',2'']-terthiophene **51** (3.00 g, 8.8 mmol) was dissolved in EtOH (70 mL) and concentrated HCl (70 mL) a solution of SnCl₂ (16.68 g, 88.0 mmol) in EtOH (70 mL) and toluene (140 mL) was then added and the reaction was left to stir at 90 °C overnight under a N₂ atmosphere. The crude product was then extracted with more toluene (3 × 100mL) and washed with brine (4 × 20 mL), then water (2 × 20 mL) and dried over MgSO₄. The drying agent was filtered off and the solvents were removed under vacuum. The resulting oil was then triturated with petroleum ether (40-60 °C) and the product was then filtered off and dried under vacuum to yield **52** as a green solid (2.37 g, 97%); m.p. 83-85 °C (lit. 96-98 °C)³; $\nu_{\max}/\text{cm}^{-1}$ (solid state) 3365 (NH₂) 3107-3065 (C-H aromatic); δ_{H} (500 MHz, CDCl₃) 3.65 (4H, broad s, 2 × NH₂), 6.98-7.02 (4H, m, C(3,5,3'',5'')H), 7.18 (2H, dd, *J* 4.9, 1.4, C(4,4'')H); δ_{C} (125 MHz, CDCl₃) 110.1 (C), 123.9 (CH), 124.0 (CH), 127.8 (CH), 133.6 (C), 136.0 (C); *m/z* (EI +) 278.0003 [M]⁺ (C₁₂H₁₀N₂S₃ requires 278.0006).

³ Xia, Yangjun; *Macromolecular Chemistry and Physics*, **2006**, 207, 511-520

Chapter V: Experimental

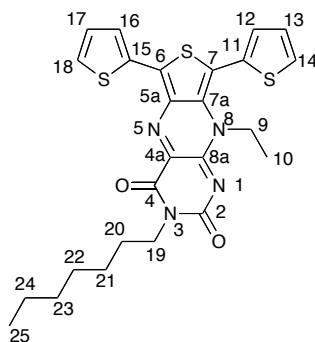
8-Ethyl-6,7-bis-thiophene-thiophenepteridine-2,4-(3*H*,8*H*)-dione **47**:



[2,2',5',2'']-Terthiophene-3',4'-diamine **52** (0.8 g, 2.9 mmol) and K_2CO_3 (0.48 g, 3.5 mmol) were dissolved in dry THF (5 mL) under N_2 atmosphere. Ethyltriflate (0.39 mL, 3.0 mmol) was then added slowly and the reaction was left to stir overnight under N_2 . The crude product was extracted into DCM (2 x 20 mL) and dried over $MgSO_4$. The drying agent was then removed by filtration and the solvents were removed under vacuum to yield 3'-amino-4'-*N*-ethyl-[2,2',5',2'']-terthiophene **54** as a dark brown solid. This was used without further purification and dissolved into glacial acetic acid (50 mL) with boric anhydride (0.47 g, 6.8 mmol) and alloxan monohydrate (0.56 g, 3.5 mmol). The reaction mixture was left to stir at room temperature overnight and the solvents were then removed under reduced pressure. The crude product was then purified by flash column chromatography (THF:Hexane; 1:3) to yield the title compound **47** as a red-greenish solid (0.63 g, 53%); m.p. decomposed; ν_{max}/cm^{-1} (solid state) 3159 (amide N-H), 1673 (amide C=O); δ_H (500 MHz, $CDCl_3$) 1.22 (3H, t, J 7.0, CH_3), 4.43 (2H, q, J 7.0, CH_2), 7.17-7.20 (2H, m, C(13&17) \underline{H}), 7.34 (1H, dd, J 3.5, 1.2, C(12 or 16) \underline{H}), 7.60 (1H, dd, J 5.3, 1.2, C(14 or 18) \underline{H}), 7.63 (1H, dd, J 5.1, 1.0, C(14 or 18) \underline{H}), 7.83 (1H, dd, J 3.8, 1.0, C(12 or 16) \underline{H}), 8.48 (1H, s, NH); δ_C (125 MHz, $CDCl_3$) 12.7 (\underline{C} (10) H_3), 41.4 (\underline{C} (9) H_2), 106.1 (\underline{C}), 107.4 (\underline{C}), 127.4 (\underline{C}), 127.5 (\underline{C} (13 or 17) H), 128.17 (\underline{C} (13 or 17) H), 129.0 (\underline{C} (12 or 16) H), 129.8 (\underline{C} (14 or 18) H), 130.6 (\underline{C}), 131.6 (\underline{C} (14 or 18) H), 132.1 (\underline{C}), 132.6 (\underline{C} (12 or 16) H), 133.9 (\underline{C}), 135.1 (\underline{C}), 142.3 ($\underline{C}=\underline{O}$), 150.3 ($\underline{C}=\underline{O}$); m/z (FAB⁺) 413.0202 [$M+H$]⁺ ($C_{18}H_{13}N_4O_2S_3$ requires 413.0201).

Chapter V: Experimental

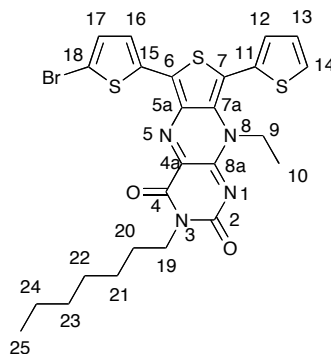
3-Heptyl-8-ethyl-6,7-bis-thiophene-thiophenepteridine-2,4-(3*H*,8*H*)-dione **55**:



Iodoheptane (0.16 mL, 1.0 mmol) was added to a solution of 12-ethyl-8,10-bis-thiophene-thiopteridine-2,4(3*H*,12*H*)-dione **47** (0.15 g, 0.36 mmol) and potassium carbonate (0.19 g, 1.4 mmol) in acetone (20 mL). The reaction was stirred under reflux overnight. The solvent was then evaporated and the reaction quenched with water (20 mL). The crude product was extracted with chloroform (3 × 15 mL), washed with water (2 × 25 mL) and brine (2 × 25 mL). The combined organics were then dried over MgSO₄, filtered and the solvent was removed under reduced pressure. The crude product was then purified by flash column chromatography (hexane / ethyl acetate; 3:1) to yield the title compound **55** as a red solid (106 mg, 58%); m.p. 189-191 °C; $\nu_{\text{max}}/\text{cm}^{-1}$ (solid state) 2951-2855 (C-H aliphatic), 1659, 1585, 1558, 1524, 1435; δ_{H} (500 MHz, CDCl₃) 0.87 (3H, t, *J* 6.8, C(25)H₃), 1.18 (3H, t, *J* 7.0, C(10)H₃), 1.25-1.42 (8H, m, C(21-24)H₂), 1.72 (2H, dt, *J* 14.9, 7.5, C(20)H₂), 4.06 (2H, t, *J* 7.5, C(19)H₂), 4.37 (2H, q, *J* 7.0, C(9)H₂), 7.14 (2H, ddd, *J* 5.1, 3.7, 1.1, C(13 & 17)H), 7.31 (1H, dd, *J* 3.7, 1.1, C(12)H), 7.56 (2H, ddd, *J* 5.1, 3.7, 1.1, C(14 & 18)H), 7.78 (1H, dd, *J* 3.7, 1.1, C(16)H); δ_{C} (125 MHz, CDCl₃) 12.9 (C(25)H₃), 14.2 (C(10)H₃), 22.7 (C(24)H₂), 27.1 (C(21)H₂), 28.0 (C(20)H₂), 29.2 (C(22)H₂), 31.9 (C(23)H₂), 40.9 (C(9)H₂), 42.3 (C(19)H₂), 107.0 (C), 127.5 (C(13 or 17)H), 127.6 (C), 128.1 (C(13 or 17)H), 128.8 (C(16)H), 129.7 (C(14 or 18)H), 131.0 (C), 131.3 (C(14 or 18)H), 132.4 (C), 132.6 (C(12)H), 133.8 (C), 135.2 (C), 141.6 (C), 148.9 (C), 155.9 (C=O), 159.6 (C=O); *m/z* (FAB +) 511.1295 [M + H]⁺ (C₂₅H₂₇N₄O₂S₃ requires 511.1296).

Chapter V: Experimental

3-Heptyl-8-ethyl-6-(5'-bromothiophene)-7-thiophene-thiophenepteridine-2,4-(3*H*,8*H*)-dione **56**:

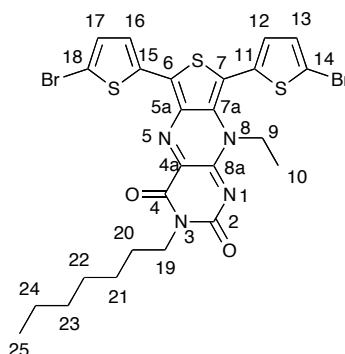


3-Heptyl-8-ethyl-6,7-*bis*-thiophene-thiophenepteridine-2,4-(3*H*,8*H*)-dione **55** (170 mg, 0.32 mmol) was dissolved into DCM (10 mL) and the flask was covered with aluminium foil to ensure “dark” conditions. *N*-Bromosuccinamide (64 mg, 0.36 mmol) was then added and the reaction mixture was left to stir overnight. The reaction was then quenched with water (100 mL) and the crude product extracted into DCM (3 x 50 mL). The combined organics were then dried over MgSO₄, filtered and the solvent was removed under reduced pressure. The crude product was then purified by flash column chromatography (DCM 100%) to yield the title compound **56** as a green solid (158 mg, 81%); m.p. 242–244 °C; δ_{H} (500 MHz, CDCl₃) 0.88 (3H, t, *J* 6.9, C(25)H₃), 1.18 (3H, t, *J* 7.0, C(10)H₃), 1.26-1.43 (8H, m, C(21-24)H₂), 1.69-1.75 (2H, m, C(20)H₂), 4.06 (2H, t, *J* 7.7, C(19)H₂), 4.37 (2H, q, *J* 7.0, C(9)H₂), 7.10 (1H, d, *J* 4.0, C(17)H), 7.15 (1H, dd, *J* 5.3, 3.5, C(13)H), 7.31 (1H, dd, *J* 3.5, 1.2, C(12)H), 7.43 (1H, d, *J* 4.0, C(16)H), 7.57 (1H, dd, *J* 5.3, 1.2, C(14)H); δ_{C} (125 MHz, CDCl₃) 12.9 (C(10)H₃), 14.3 (C(25)H₃), 22.8 (CH₂), 27.2 (CH₂), 28.0 (C(20)H₂), 29.2 (CH₂), 31.9 (CH₂), 40.9 (C(9)H₂), 42.4 (C(19)H₂), 107.3 (C), 120.3 (C(18)Br), 127.5 (C), 127.6 (C(13)H), 128.2 (C(16)H), 129.9 (C(14)H), 130.6 (C(17)H), 130.8 (C), 132.7 (C(12)H), 133.8 (C), 133.9 (C), 135.3 (C), 140.4 (C), 149.0 (C) 155.8 (C=O), 159.5 (C=O); *m/z* (ES⁺) 611.0196 [M + Na]⁺ (C₂₅H₂₅⁷⁹BrN₄NaO₂S₃ requires 611.0215).

Chapter V: Experimental

3-Heptyl-8-ethyl-6,7-(5',5''-bromothiophene)-thiophenepteridine-2,4-(3*H*,8*H*)-dione

61:

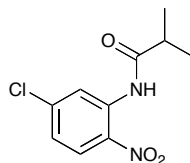


Synthesis: see 3-Heptyl-8-ethyl-6-(5'-bromothiophene)-7-thiophene-thiophenepteridine-2,4-(3*H*,8*H*)-dione **56**, compound **61** was isolated as a brown powder (13 mg, 6%); $\nu_{\max}/\text{cm}^{-1}$ (evaporated film) 2958, 2929, 2858, 1708, 1658, 1587, 1561, 1529, 1505; δ_{H} (500 MHz, CDCl_3) 0.88 (3H, t, J 4.7, C(25)H₃), 1.22 (2H, t, J 7.0 Hz, C(10)H₃), 1.44 – 1.20 (8H, m, C(21-24)H₂), 1.71 (2H, quin, J 7.1, C(20)H₂), 4.05 (1H, t, J 7.6, C(19)H₂), 4.40 (1H, quin, J 7.2, C(9)H₂), 7.07 (1H, d, J 3.9, C(13)H), 7.10 (1H, d, J 4.0, C(17)H), 7.12 (1H, d, J 3.9, C(12)H), 7.42 (1H, d, J 4.0, C(16)H); δ_{C} (125 MHz, CDCl_3) 12.9 (C(10)H₃), 14.2 (C(25)H₃), 22.8 (CH₂), 27.2 (CH₂), 28.0 (CH₂), 29.2 (CH₂), 31.9 (CH₂), 41.0 (CH₂), 42.4 (CH₂), 105.8 (C), 116.4 (C), 120.8 (C), 127.9 (C), 128.4 (CH), 130.5 (CH), 130.7 (CH), 132.3 (C), 133.1 (CH), 133.6 (C), 134.0 (C), 135.1 (C), 140.9 (C=N), 149.0 (C=N), 155.7 (C=O), 159.4 (C=O); m/z (EI⁺) 668.9481 [$\text{M}+\text{H}$]⁺ ($\text{C}_{25}\text{H}_{25}^{79}\text{Br}_2\text{N}_4\text{O}_2\text{S}_3$ requires 668.9481).

Chapter V: Experimental

CHAPTER III:

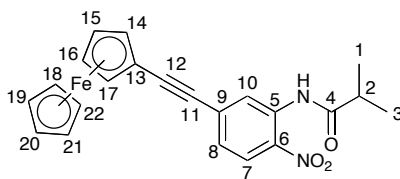
N-(5-Chloro-2-nitro-phenyl)isobutyramide **80**:



Isobutyryl chloride **82** (1.84 mL, 17.40 mmol) and triethylamine (2.43 mL, 17.40 mmol) were added drop-wise to a solution of 5-chloro-2-nitroaniline **79** (2.00 g, 11.60 mmol) in THF (100 mL). The reaction was stirred at reflux overnight and the solvents were then evaporated under reduced pressure. The crude product was then purified by flash column chromatography (petroleum ether / ethyl acetate; 5:95) and then recrystallised from hot ethanol to yield title compound **80** as yellow needles (2.66 g, 94%); m.p. 92-93 °C; $\nu_{\text{max}}/\text{cm}^{-1}$ (solid state) 3358 (N-H, amide), 3119, 2972-2876 (C-H aliphatic), 1710, 1605, 1578, 1489; δ_{H} (500 MHz, CDCl₃) 1.31 (6H, d, J 6.9, 2 x CH₃), 2.66 (1H, sept, J 6.9, CH isobutyl), 7.13 (1H, dd, J 9.0, 2.2 C(4)H), 8.19 (1H, d, J 9.0 C(3)H), 8.98 (1H, d, J 2.2, C(6)H), 10.6 (1H, br. s, NH); δ_{C} (125 MHz, CDCl₃) 19.5 (2 x CH₃), 37.8 (CH isobutyl), 121.9 (C(6)H), 123.5 (C(4)H), 127.2 (C(3)H), 134.5 (C(1 or 2)), 136.3 (C(1 or 2)), 143.1 (C(5)), 176.4 (C=O); m/z (EI⁺) 242.0455 [M]⁺ (C₁₀H₁₁N₂O₃³⁵Cl requires 242.0458).

Chapter V: Experimental

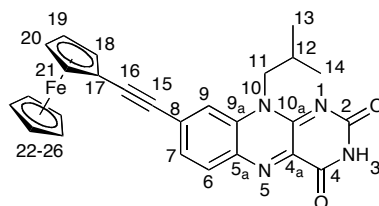
N-(2-Nitro-4-ethynylferrocene-phenyl)isobutyramide **81**:



N-(5-chloro-2-nitro-phenyl)isobutyramide **80** (2.00 g, 8.2 mmol), ethynylferrocene **83** (2.60 mg, 12.4 mmol), 10% Pd/C (0.44 g, 0.4 mmol), SPhos (0.17 g, 0.4 mmol), K₂CO₃ (1.71 g, 12.4 mmol) and DMA (10 mL) were stirred at 110 °C under an atmosphere of N₂. After 2 hours the charcoal residue was filtered off and washed with water (500 mL) and Et₂O (2 x 500 mL). The crude product was extracted with Et₂O (2 x 500 mL), the organics were then dried over MgSO₄ and the solvent was removed under reduced pressure. The product was purified by flash column chromatography (toluene) and isolated as a red solid (2.12 g, 62%); m.p. 129-131 °C (decomposition); RF: 0.38 (toluene); $\nu_{\max}/\text{cm}^{-1}$ (solid state) 3333 (*w.* N-H) 2973-2872 (*w.* C-H aliphatic), 2196 (*m.* C≡C), 1705 (*m.* C=O), 1603 (*m.*), 1569 (*str.*), 1546 (*w.*); δ_{H} (500 MHz, CDCl₃) 1.33 (6H, d, *J* 6.9, C(1 & 3)H₃), 2.68 (1H, sept, *J* 6.9, C(2)H), 4.26 (5H, s, C(18 - 22)H), 4.32 (2H, t, *J* 1.9, C(14 & 17)H or C(15 & 16)H), 4.55 (2H, t, *J* 1.9, C(14 & 17)H or C(15 & 16)H), 7.20 (1H, dd, *J* 8.8, 1.8, C(8)H), 8.19 (1H, d, *J* 8.8, C(7)H), 8.97 (1H, d, *J* 1.8, C(10)H), 10.60 (1H, s, NH); δ_{C} (125 MHz, CDCl₃) 19.7 (C(1 & 3)H₃), 37.9 (C(2)H), 63.7 (C(13)), 69.9 (C(14 & 17)H or C(15 & 16)H), 70.4 (C(18 - 22)H), 72.2 (C(14 & 17)H or C(15 & 16)H), 85.2 (C(11 or 12)), 96.4 (C(11 or 12)), 124.2 (C(10)H), 125.6 (C(8)H), 126.2 (C(7)H), 132.9 (C(5, 6 or 9)), 134.5 (C(5, 6 or 9)), 135.6 (C(5, 6 or 9)), 176.5 (C=O); *m/z* (EI⁺) 416.0822 [M+H]⁺ (C₂₂H₂₀FeN₂O₃ requires 416.0824).

Chapter V: Experimental

8-Ethynylferrocene-10-isobutyl-benzopteridine-2,4(3*H*,10*H*)dione **72**:

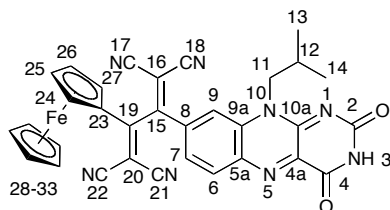


LiAlH₄ (626.2 mg, 16.50 mmol) was added portion-wise to a solution of *N*-(2-nitro-4-ethynylferrocene-phenyl)isobutyramide **81** (685.0 mg, 1.65 mmol) in THF (120 mL). The reaction mixture was stirred overnight at room temperature under an atmosphere of N₂. The reaction was then quenched by the addition of water (120 mL) and further addition of 10% NaOH (100 mL). The resulting precipitate was then filtered off and washed with Et₂O (5 × 40 mL). The organic phase was then separated and dried over MgSO₄ and filtered. The solvent was then removed under reduced pressure to give *N*-(2-amino-4-ethynylferrocene-phenyl)isobutyl **77** as a crude product which was used without further purification.

The crude *N*-(2-amino-4-ethynylferrocene-phenyl)isobutyl **77**, alloxan monohydrate (317.0 mg, 1.98 mmol) and boric anhydride (203.0 mg, 2.9 mmol) were dissolved in glacial acetic acid (50 mL) and stirred at room temperature overnight. The solvents were then removed under reduced pressure and the crude product was then purified by flash column chromatography (Et₂O:EtOAc; 4:1) to yield the title compound **72** as a green solid (268.4 mg, 34%); $\nu_{\max}/\text{cm}^{-1}$ (solid state) 3012 (*br. w.* N-H), 2834 (*w.* C-H aliphatic), 1711 (*m.*), 1653 (*m.*), 1561 (*m.*), 1529 (*str.*); δ_{H} (500 MHz, CDCl₃) 1.12 (6H, d, *J* 6.9, C(13 & 14)H₃), 2.51 (1H, tt, *J* 14.0, 6.9, C(11)H), 4.32 (5H, s, C(22-26)H), 4.43 (2H, t, *J* 1.8, C(18&21 or 19&20)H), 4.65 (2H, t, *J* 1.8, C(18&21 or 19&20)H), 7.64 (1H, d, *J* 1.3, C(9)H), 7.63 (1H, dd, *J* 8.5, 1.6, C(7)H), 8.25 (1H, d, *J* 8.5, C(6)H), 8.43 (1H, s, N(3)H); δ_{C} (125 MHz, CDCl₃) 20.1 (C(13&14)H₃), 27.5 (C(12)H), 51.4 (C(15 or 16)), 62.9 (C(15 or 16)), 70.2 (C(18&21 or 19&20 or 22-26)H), 70.3 (C(18&21 or 19&20 or 22-26)H), 72.2 (C(18&21 or 19&20)H), 117.3 (C(9)H), 129.8 (C(7)H), 132.5 (C), 133.3 (C(6)H), 133.5 (C), 135.1 (C), 151.3 (C=O), 154.8 (C=O); *m/z* (FAB⁺) 479.1176 [M+H]⁺ (C₂₆H₂₃N₄⁵⁶FeO₂ requires 479.1171).

Chapter V: Experimental

2-(Ferrocene)-3-[8-(10-isobutyl-benzopteridine-2,4(3H,10H)dione)]-1,3-butadiene-1,1,4,4-tetracarbonitrile **71**:

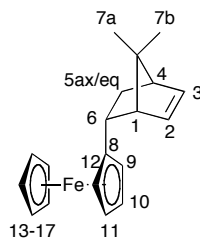


Tetracyanoethylene **64** (12.8 mg, 0.1 mmol) and 8-ethynylferrocene-10-isobutylbenzopteridine-2,4(3H,10H)dione **77** (50.0 mg, 0.1 mmol) were dissolved in dry THF (10 mL) in a flask covered with tin foil to keep out light. The reaction was left to stir at reflux temperature for 72 hours. The solvent was then removed under reduced pressure and the crude product was purified by flash column chromatography (EtOAc 100%). The product was then dissolved into DCM (2 mL) and was precipitated into petroleum ether (300 mL) and filtered to furnish the title compound **71** as a green solid (45.1 mg, 74%); $\nu_{\max}/\text{cm}^{-1}$ (solid state) 3205 (*br. w.* N-H), 2917 (*w.* C-H aliphatic), 2363, 2224, 1719 (*m.*), 1676 (*m.*), 1583 (*m.*), 1551 (*str.*), 1518 (*m.*), 1443 (*w.*), 1399 (*w.*), 1295 (*w.*), 1245 (*w.*); δ_{H} (500 MHz, CDCl_3) 1.03 (6H, d, *J* 6.9, C(13 & 14) $\underline{\text{H}}_3$), 2.31 (1H, tt, *J* 14.0, 6.9, C(12) $\underline{\text{H}}$), 4.44 (1H, m, C(24 or 27) $\underline{\text{H}}$), 4.55 (5H, s, C(28-33) $\underline{\text{H}}$), 4.99 (1H, td, *J* 2.7, 1.1, C(25 or 26) $\underline{\text{H}}$), 5.19 (1H, td, *J* 2.7, 1.2, C(25 or 26) $\underline{\text{H}}$), 5.68 (1H, m, C(24 or 27) $\underline{\text{H}}$), 7.53 (1H, dd, *J* 8.6, 1.8, C(7) $\underline{\text{H}}$), 7.77 (1H, d, *J* 1.8, C(9) $\underline{\text{H}}$), 8.34 (1H, d, *J* 8.6, C(6) $\underline{\text{H}}$), 8.65 (1H, s, N(3) $\underline{\text{H}}$); δ_{C} (125 MHz, CDCl_3) 20.3 ($\underline{\text{C}}$ (13 or 14) $\underline{\text{H}}_3$), 20.4 ($\underline{\text{C}}$ (13 or 14) $\underline{\text{H}}_3$), 28.2 ($\underline{\text{C}}$ (12) $\underline{\text{H}}$), 52.2 ($\underline{\text{C}}$ (11) $\underline{\text{H}}_2$), 71.0 ($\underline{\text{C}}$ (24 or 27) $\underline{\text{H}}$), 73.7 ($\underline{\text{C}}$ (24 or 27) $\underline{\text{H}}$), 73.8 ($\underline{\text{C}}$ (28-33) $\underline{\text{H}}$), 74.8 ($\underline{\text{C}}$), 75.8 ($\underline{\text{C}}$ (25 or 26) $\underline{\text{H}}$), 78.0 ($\underline{\text{C}}$ (25 or 26) $\underline{\text{H}}$), 79.2 ($\underline{\text{C}}$ (16 or 20), 89.7 ($\underline{\text{C}}$ (16 or 20), 111.2 ($\underline{\text{C}}$ (17 or 18 or 21 or 22)), 111.2 ($\underline{\text{C}}$ (17 or 18 or 21 or 22)), 113.2 ($\underline{\text{C}}$ (17 or 18 or 21 or 22)), 113.4 ($\underline{\text{C}}$ (17 or 18 or 21 or 22)), 116.8 ($\underline{\text{C}}$ (9) $\underline{\text{H}}$), 125.6 ($\underline{\text{C}}$ (7) $\underline{\text{H}}$), 133.6 ($\underline{\text{C}}$), 135.0 ($\underline{\text{C}}$ (6) $\underline{\text{H}}$), 136.9 ($\underline{\text{C}}$), 137.5 ($\underline{\text{C}}$), 140.6 ($\underline{\text{C}}$), 151.5 ($\underline{\text{C}}$), 154.6 ($\underline{\text{C}}$), 158.5 ($\underline{\text{C}}$), 164.4 ($\underline{\text{C}}=\text{O}$), 171.8 ($\underline{\text{C}}=\text{O}$); *m/z* (FAB+) 629.1088 [$\text{M}+\text{Na}$]⁺ ($\text{C}_{32}\text{H}_{22}\text{N}_8^{56}\text{FeO}_2\text{Na}$ requires 629.1107).

Chapter V: Experimental

CHAPTER IV:

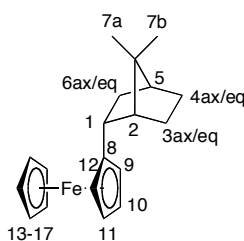
6-Ferrocene-bicyclo[2.2.1]hept-2-ene **93**:



Cyclopentadiene **95** (0.18 mL, 2.40 mmol) was added to a solution of vinylferrocene **19** (100.0 mg, 0.47 mmol) in anhydrous THF (10 mL). The mixture was stirred under nitrogen and cooled to $-40\text{ }^{\circ}\text{C}$, FeCl_3 (80.4 mg, 0.50 mmol) was then added to the reaction mixture which was stirred at $-40\text{ }^{\circ}\text{C}$ for a further 30 minutes. The reaction mixture was then allowed to warm up to room temperature before being left to stir at reflux for 24 hours under nitrogen. After this time the reaction mixture was allowed to cool to room temperature before adding a solution of L-ascorbic acid (250.0 mg, 1.40 mmol) in water (10 mL). The solvent was removed under reduced pressure and the product extracted into DCM (3 x 20 mL) and dried over MgSO_4 and filtered. The solvent was then removed under reduced pressure. The crude product was then purified by flash column chromatography (100% petroleum ether) to yield the title compound **93** as a yellow oil (115.7 mg, 59%) as an inseparable mixture of diastereomers (7:1, *endo:exo*); *endo*-6-ferrocene-bicyclo[2.2.1]hept-2-ene: $\nu_{\text{max}}/\text{cm}^{-1}$ (solid state) 2961-2867 (*w*, C-H aliphatic), 1449 (*w*), 1337 (*w*); δ_{H} (500 MHz, CDCl_3) 1.13 (1H, ddd, J 11.6, 4.5, 2.6, C(5eq)H), 1.38 (1H, m, C(7a or b)H), 1.45 (1H, tdd, J 5.1, 2.9, 2.1, C(7a or b)H), 2.14 (1H, ddd, J 11.6, 9.1, 3.7, C(5ax)H), 2.77 (1H, d, J 1.1, C(1)H), 2.86 (1H, d, J 1.1, C(4)H), 3.07 (1H, dt, J 9.1, 4.5, C(6)H), 3.81 (1H, s, C(9)H), 3.98 (1H, s, C(10 or 11)H), 4.01 (1H, s, C(10 or 11)H), 4.08 (1H, s, C(12)H), 4.10 (5H, s, C(13-17)H), 5.74 (1H, dd, J 5.7, 3.0, C(2)H), 6.19 (1H, dd, J 5.7, 2.9, C(3)H); δ_{C} (125 MHz, CDCl_3) 33.8 (C(5)H₂), 38.5 (C(6)H), 42.9 (C(4)H), 49.1 (C(1)H), 50.3 (C(7)H₂), 66.8 (C(9, 10, 11 or 12)H), 66.9 (C(9, 10, 11 or 12)H), 67.0 (C(9, 10, 11 or 12)H), 68.2 (C(13-17)H), 68.5 (C(8)), 92.2 (C(9, 10, 11 or 12)H), 133.3 (C(2)H), 136.7 (C(3)H); m/z (EI⁺) 278.0757 [M]⁺ (C₁₇H₁₈⁵⁶Fe requires 278.0758).

Chapter V: Experimental

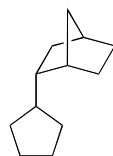
1-Ferrocene-bicyclo[2.2.1]heptane **105**:



A solution of 6-ferrocene-bicyclo[2.2.1]hept-2-ene **93** (129.4 mg, 0.47 mmol) in ethanol (5 mL) was added to a flask containing palladium on charcoal (10% w/w, 20 mg) under a hydrogen atmosphere. The reaction mixture was left to stir at room temperature for 4 hours, after this time the flask was carefully flushed with nitrogen and then restored to a normal atmosphere. The palladium residue was filtered off and washed with DCM (3 x 10 mL), the solvent was then removed under reduced pressure. The crude product was then purified by flash column chromatography (petroleum ether 100%) to afford the title compound **105** as a yellow oil (130.2 mg, quantitative) as an inseparable mixture of diastereomers; 1R-Ferrocene-bicyclo[2.2.1]heptane **105**: $\nu_{\text{max}}/\text{cm}^{-1}$ (solid state) 2947-2868 (w. C-H aliphatic), 1456 (w.); δ_{H} (500 MHz, CDCl_3) 1.17 (1H, ddd, J 9.5, 4.0, 1.9, C(4ax)H₂), 1.22 (1H, td, J 4.6, 2.1, C(3ax)H₂), 1.24-1.26 (1H, m, C(6ax)H₂), 1.27-1.32 (1H, m, C(4eq)H₂), 1.36 (1H, dq, J 9.3, 2.0, C(7b)H₂), 1.48 (1H, dt, J 3.5, 1.8, C(7a)H₂), 1.50 (1H, dt, J 3.5, 1.9, C(3eq)H₂), 1.92-2.00 (1H, m, C(6eq)H₂), 2.04 (1H, br. t, J 4.0, C(2)H), 2.24 (1H, br. t, J 4.5, C(5)H), 2.93 (1H, dddd, J 11.7, 5.7, 4.0, 1.8, C(1eq)H), 4.02-4.04 (1H, m, C(9 or 10 or 11 or 12)H), 4.06-4.09 (3H, m, C(9 or 10 or 11 or 12)H), 4.10 (5H, s, C(13-17)H); δ_{C} (125 MHz, CDCl_3) 23.4 (C(4)H₂), 30.2 (C(3)H₂), 36.0 (C(6)H₂), 37.5 (C(5)H), 40.7 (C(7)H₂), 41.4 (C(1)H), 43.7 (C(2)H), 66.8 (C(9, 10, 11 or 12)H), 67.2 (C(9, 10, 11 or 12)H), 67.6 (C(9, 10, 11 or 12)H), 68.4 (C(13-17)H), 69.2 (C(9, 10, 11 or 12)H), 77.7 (C(8)); m/z (EI⁺) 440.0523 [M]⁺ (280.0916 C₁₇H₂₀⁵⁶Fe requires 280.0915).

Chapter V: Experimental

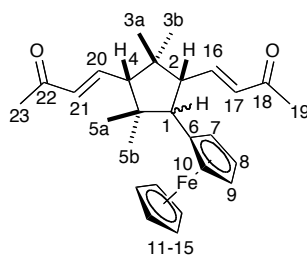
1-Cyclopentane-bicyclo[2.2.1]heptane **106**:



A solution of 1-ferrocene-bicyclo[2.2.1]heptane **105** (108.0 mg, 0.39 mmol) in THF (5 mL) was added to a flask containing palladium on charcoal (10% w/w, 110 mg) that had been previously flushed to a hydrogen atmosphere. Trifluoroacetic acid (5 mL) was then added and the reaction mixture was left to stir at 50 °C for 18 hours, after this time the flask was carefully flushed with nitrogen and then restored to a normal atmosphere. The palladium residue was filtered off and washed with DCM (3 × 10 mL), the solvent was then reduced almost to dryness under reduced pressure. The residue was then triturated with aqueous KOH (5%) and the product was extracted with Et₂O (3 × 20 mL) and washed with brine (20 mL). The combined organics were then dried over MgSO₄, filtered and the solvent was removed under reduced pressure to afford the title compound **106** as a colourless oil (51.2 mg, 81%); GC-MS (column temperature programme: 50 °C, 3 min; 10 °C/min; 250 °C, 30 min): retention time 13.08 min, MS (EI) – m/z (%): 164 (M⁺, **106**, 69%), 220 (2,6-bis-(1,1-dimethylethyl)-4-methylphenol, 31%)

Chapter V: Experimental

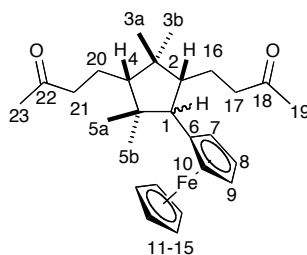
1-[(±)Ferrocene]-2*R*,4*S*-[bis-(buten-3-one)]-cyclopentane **107b**:



Buten-3-one (0.8 mL, 9.60 mmol) was dissolved in dry toluene (8 mL) and left to stir at reflux temperature under N₂ atmosphere. *endo*-6-Ferrocene-bicyclo[2.2.1]hept-2-ene **93** (88 mg, 0.32 mmol) was dissolved into dry toluene (3 mL) and in a separate flask Hoveyda-Grubb's catalyst (2nd generation) (19 mg, 0.03 mmol) was dissolved in dry toluene (3 mL). Both *endo*-6-ferrocene-bicyclo[2.2.1]hept-2-ene **93** and Hoveyda-Grubb's II catalyst were added to the reaction mixture in 6 equal (0.5 mL) portions at half hour intervals. After the last addition the reaction was left to stir at reflux temperature for 4 hours. After this time the catalyst was filtered off and washed with petrol (3 x 10 mL), the combined organics were reduced by evaporation under reduced pressure. The crude product was purified by flash column chromatography (SiO₂, petroleum ether 100%) to yield the title compound **107b** as a mixture of diastereoisomers (6:1) as a yellow oil (81.8 mg, 65%); 1*R*-(Ferrocene)-2*R*,4*S*-[bis-(buten-3-one)]-cyclopentane **107b**: $\nu_{\max}/\text{cm}^{-1}$ (solid state) 2955-2854 (*w*. C-H aliphatic), 1722 (*w*.), 1695 (*w*.), 1672 (*str*. C=O), 1622 (*w*.); δ_{H} (500 MHz, CDCl₃) 1.53 (1H, ddd, *J* 12.7, 10.6, 9.9, C(3b)H), 1.85 (1H, ddd, *J* 13.2, 10.4, 8.6, C(5b)H), 1.99 (3H, s, C(19)H₃), 2.01-2.07 (1H, m, C(3a)H), 2.30 (3H, s, C(23)H₃), 2.48 (1H, dtd, *J* 13.2, 7.7, 1.1, C(5a)H), 2.80-2.92 (2H, m, C(2 and 4)H), 3.30 (1H, dd, *J* 16.6, 8.6, C(1)H), 3.93-3.94 (2H, m, C(7 and 10)H), 4.09-4.10 (2H, m, C(8 and 9)H), 4.11 (5H, s, C(11-15)H), 5.81 (1H, dd, *J* 16.0, 1.0, C(17)H), 6.17 (1H, dd, *J* 15.9, 1.2, C(21)H), 6.25 (1H, dd, *J* 16.0, 8.6, C(16)H), 6.86 (1H, dd, *J* 15.9, 7.4, C(20)H); δ_{C} (125 MHz, CDCl₃) 26.4 (C(19)H₃), 27.4 (C(23)H₃), 37.8 (C(3)H₂), 38.4 (C(5)H₂), 42.3 (C(4)H), 44.1 (C(1)H), 47.4 (C(2)H), 66.5 (C(7 or 10)H), 67.9 (C(8 or 9)H), 68.0 (C(8 or 9)H), 68.7 (C(11-15)H), 69.3 (C(7 or 10)H), 89.1 (C(6)), 130.3 (C(21)H), 130.9 (C(17)H), 150.0 (C(16)H), 150.1 (C(20)H), 198.3 (C(18 or 22)=O), 198.4 (C(18 or 22)=O); *m/z* (EI⁺) 390.1280 [M]⁺ (C₂₃H₂₆⁵⁶FeO₂ requires 390.1282).

Chapter V: Experimental

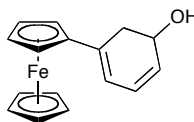
1-[(±)Ferrocene]-2*R*,4*S*-[bis-(butan-3-one)]-cyclopentane **112**:



A solution of 1-[(±)ferrocene]-2*R*,4*S*-bis-(buten-3-one)-cyclopentane **107b** (23.0 mg, 0.059 mmol) in DCM (2 mL) was added to a flask containing palladium on charcoal (10% w/w, 2 mg) that had been previously flushed to a hydrogen atmosphere. The reaction mixture was left to stir at room temperature for 4 hours, after this time the flask was carefully flushed with nitrogen and then restored to a normal atmosphere. The palladium residue was filtered off and washed with DCM (3 x 10 mL), the solvent was then removed under reduced pressure. The crude product was then purified by flash column chromatography (petroleum ether 100%) to afford the title compound **112** as a yellow oil (23.2 mg, quantitative) as an inseparable mixture of diastereomers (6:1): 1*R*-(Ferrocene)-2*R*,4*S*-[bis-(buten-3-one)]-cyclopentane **112**: $\nu_{\max}/\text{cm}^{-1}$ (solid state) 2932-2856 (w. C-H aliphatic), 1713 (*str.* C=O), 1411 (w.), 1357 (*m.*); δ_{H} (500 MHz, CDCl₃) 0.74-0.78 (1H, m, C(3b)H), 0.84-0.92 (1H, m, C(16a or 16b)H), 1.20-1.24 (1H, m, C(16a or 16b)H), 1.41 (1H, dt, *J* 13.0, 9.0, C(5b)H), 1.61 (1H, m, C(20a or 20b)H), 1.66 (1H, m, C(20a or 20b)H), 1.72-1.82 (3H, m, C(2, 3b and 4)H), 1.93 (3H, m, C(19 or 23)H₃), 2.11 (3H, s, C(19 or 23)H), 2.13 (2H, t, *J* 7.8, C(17)H₂), 2.23 (1H, dt, *J* 12.6, 7.8, C(5a)H), 2.43 (2H, t, *J* 7.7, C(21)H₂), 2.91 (1H, q, *J* 8.1, C(1)H), 3.85 (1H, m, C(7 or 10)H), 3.93-3.94 (1H, m, C(8 or 9)H), 3.99-4.00 (1H, m, C(7 or 10)H), 4.01-4.02 (1H, m, C(8 or 9)H), 4.03 (5H, s, C(11-15)H); δ_{C} (125 MHz, CDCl₃) 26.6 (C(16)H₂), 29.8 (C(19 or 23)H₃), 30.0 (C(19 or 23)H₃), 30.4 (C(20)H₂), 38.6 (C(4)H), 38.6 (C(3 or 5)H₂), 38.9 (C(3 or 5)H₂), 42.4 (C(1)H), 43.0 (C(17 or 21)H₂), 43.2 (C(17 or 21)H₂), 43.2 (C(2)H), 67.9 (C(7 or 8 or 9 or 10)H), 68.1 (C(7 or 8 or 9 or 10)H), 68.2 (C(7 or 8 or 9 or 10)H), 69.4 (C(11-15)H), 70.1 (C(7 or 8 or 9 or 10)H), 77.7 (C(6)H), 208.9 (C(18 or 22)=O), 209.1 (C(18 or 22)=O); *m/z* (EI⁺) 394.1586 [M]⁺ (C₂₃H₃₀⁵⁶FeO₂ requires 394.1595).

Chapter V: Experimental

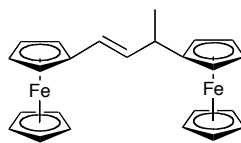
1-Ferrocene-cyclohexan-1,3-diene-5-ol **97**:



Furan **95** (0.10 mL, 1.40 mmol) was added to a solution of vinylferrocene **19** (100.0 mg, 0.47 mmol) in anhydrous THF (10 mL). The mixture was stirred under nitrogen and cooled to $-20\text{ }^{\circ}\text{C}$, FeCl_3 (81.0 mg, 0.50 mmol) was then added to the reaction mixture which was stirred at $-20\text{ }^{\circ}\text{C}$ for a further 30 minutes. The reaction mixture was then allowed to warm up to room temperature before being left to stir under reflux for 24 hours under nitrogen. After this time the reaction mixture was allowed to cool down to room temperature before adding a solution of L-ascorbic acid (250.0 mg, 1.40 mmol) in water (10 mL). The solvent was reduced under reduced pressure and the product extracted into DCM (3 x 20 mL) and dried over MgSO_4 and filtered. The solvent was then removed under reduced pressure. The crude product was then purified by flash column chromatography (100% petroleum ether) to yield the title compound **97** as a yellow oil (29.0 mg, 22%); $\nu_{\text{max}}/\text{cm}^{-1}$ (solid state) 2961-2867 (*w.* C-H aliphatic), 1449 (*w.*), 1337 (*w.*); δ_{H} (500 MHz, CDCl_3) 1.56 (2H, d, J 7.2, C(6)H₂), 3.86 (1H, q, J 7.2, C(5)H), 4.08-4.12 (9H, m, C(ferrocene)H), 5.95 (1H, dt, J 3.2, 0.8, C(4)H), 6.28 (1H, dd, J 3.2, 1.8, C(3)H), 7.32 (1H, dd, J 1.8, 0.8, C(2)H); δ_{C} (125 MHz, CDCl_3) 20.0 (C(6)H₂), 33.0 (C(5)H), 66.5, 67.1, 67.3, 67.5, 68.6 (C(ferrocene)H), 103.9 (C(4)H), 109.9 (C(3)H), 140.6 (C(2)H), 159.6 (C(1)); m/z (EI⁺) 440.0523 [M]⁺ ($\text{C}_{24}\text{H}_{24}^{56}\text{Fe}_2\text{O}$ requires 440.0527).

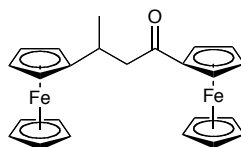
Chapter V: Experimental

1,3-*bis*-Ferrocene-but-1-ene **98**:



$\nu_{\max}/\text{cm}^{-1}$ (solid state) 3094(*w.*) 2926-2852 (*w.* C-H aliphatic); δ_{H} (500 MHz, CDCl_3) 1.34 (3H, d, J 6.8, C(4)H₃), 3.20 (1H, *pseudo*-quintet, J 7.0, C(3)H), 4.01-4.22 (16H, m, C(Ferrocene)H), 4.33 (2H, m, C(Ferrocene)H), 5.94 (1H, dd, J 15.8, 7.6, C(2)H), 6.08 (1H, d, J 15.8, C(1)H); m/z (EI⁺) 424.0577 [M]⁺ ($\text{C}_{24}\text{H}_{24}^{56}\text{Fe}_2$ requires 424.0574).

1,3-*bis*-Ferrocene-butan-1-one **99**:

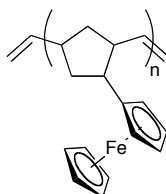


FeCl_3 (0.4 g, 2.50 mmol) was then added to a cooled solution of vinylferrocene **19** (0.5 g, 2.40 mmol) in anhydrous THF (25 mL) at $-20\text{ }^\circ\text{C}$. The mixture was stirred under nitrogen at $-20\text{ }^\circ\text{C}$ for 30 minutes and was then allowed to warm up to room temperature before being left to stir at reflux temperature for 24 hours under nitrogen. After this time the reaction mixture was allowed to cool down to room temperature before adding a solution of L-ascorbic acid (1.25 g, 7.10 mmol) in water (25 mL). The solvent was reduced under reduced pressure and the product extracted into DCM (3 \times 30 mL) and dried over MgSO_4 . The solvent was then removed under reduced pressure. The crude product was then purified by flash column chromatography (100% DCM) to yield the title compound **99** as an orange solid (40.2 mg, 4%); $\nu_{\max}/\text{cm}^{-1}$ (solid state) 3094(*w.*) 2878-2832 (*w.* C-H aliphatic), 1667 (*m.* C=O), 1451 (*m.*), 1404 (*w.*); δ_{H} (500 MHz, CDCl_3) 1.33 (3H, d, J 6.8, C(4)H₃), 2.75 (1H, dd, J 16.2, 8.7, C(2)H_{a/b}), 2.91 (1H, dd, J 16.2, 5.1, C(2)H_{a/b}), 3.21-3.28 (1H, m, C(3)H), 4.08-4.10 (1H, m, C(3'Ferrocene)H), 4.11-4.12 (1H, m, C(3'Ferrocene)H), 4.13-4.14 (1H, m, C(3'Ferrocene)H), 4.15 (10H, 2 \times s, 2 \times C(1' & 3'cyclopentadienyl)H), 4.47-4.49 (2H,

Chapter V: Experimental

m, C(1'Ferrocene)H), 4.72-4.76 (2H, m, C(1'Ferrocene)H); m/z (EI⁺) 440.0523 [M]⁺ (C₂₄H₂₄⁵⁶Fe₂O requires 440.0527).

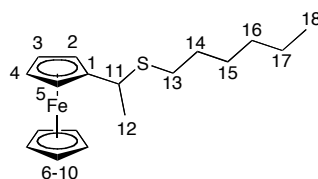
1-Ferrocene-polynorbornene **109**:



A solution of Grubb's 2nd generation catalyst (34 mg, 0.040 mmol) in DCM (1 mL) was added to a solution of 6-ferrocene-bicyclo[2.2.1]hept-2-ene **93** (113.0 mg, 0.41 mmol) in DCM (2 mL) under nitrogen atmosphere. The resulting mixture was left to stir at room temperature for 4 hours. After this time, the reaction was quenched with ethyl vinyl ether (0.02 mL, 0.20 mmol). The reaction mixture was then poured unto methanol (150 mL) to precipitate the desired polymer. The product was then filtered off to yield a glassy yellow solid (80 mg, 71%): GPC (THF, 1 mL/min, 30 °C) Mn: 8499 g.mol⁻¹, PDI: 1.45; δ H (400 MHz, CDCl₃) 1.70-3.13 (7H, broad multiplets, cyclopentane aliphatic), 4.06 (7H, broad singlet, ferrocene CH), 4.55 (1H, broad singlet, ferrocene CH), 4.84 (1H, broad singlet, ferrocene CH), 5.15-5.70 (2H, broad, vinyl CH).

Chapter V: Experimental

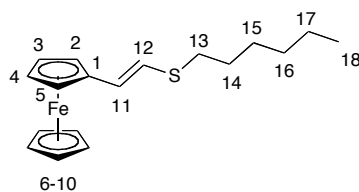
1-Ethyl-1'-hexanesulfide-ferrocene **116**:



Vinylferrocene **19** (50 mg, 0.24 mmol) was dissolved in dry THF (5 mL) and cooled to $-40\text{ }^{\circ}\text{C}$. FeCl_3 (42 mg, 0.26 mmol) was then added to the reaction mixture after 5 minutes hexanethiol (34 μL) was also added. The reaction mixture was allowed to warm to room temperature and was left to stir at room temperature overnight. After this time a mixture of L-ascorbic acid (127 mg, 0.72 mmol) in water (10 mL) was added to the reaction mixture. The crude product was then extracted with DCM (3 \times 20 mL) and washed with brine (30 mL). The combined organics were dried over MgSO_4 , filtered and the solvent was removed under reduced pressure. The product was then purified by flash column chromatography (DCM:Petrol; 5:95) to yield the title compound **116** as a brown oil (53.2 mg, 67%); $\nu_{\text{max}}/\text{cm}^{-1}$ (solid state) 3095 (*w*), 2956-2856 (*m*. C-H aliphatic), 1724 (*m*), 1411 (*w*), 1457 (*m*), 1369 (*m*), 1262 (*m*); δ_{H} (500 MHz, CDCl_3) 1.88 (3H, t, *J* 7.0, C(18)H₃), 1.25-1.37 (6H, m, C(15 and 16 and 17)H₂), 1.68-1.54 (2H, m, C(14)H₂), 1.65 (3H, d, *J* 6.9, C(12)H₃), 2.44 (2H, td, *J* 7.4, 2.1, C(13)H₂), 3.72 (1H, q, *J* 6.9, C(11)H), 4.11 (2H, t, *J* 1.9, C(2, 3, 4 or 5)H), 4.14 (6H, s, C(6-10 and 2, 3, 4 or 5)H), 4.17 (1H, q, *J* 1.7, C(2, 3, 4 or 5)H); δ_{C} (125 MHz, CDCl_3) 14.1 (C(18)H₃), 21.7 (C(12)H₃), 22.7 (C(16)H₂), 28.9 (C(15)H₂), 29.9 (C(14)H₂), 31.2 (C(13)H₂), 31.6 (C(17)H₂), 39.2 (C(11)H), 66.0 (C(2-10)H), 67.6 (C(2-10)H), 67.7 (C(2-10)H), 68.0 (C(2-10)H), 68.8 (C(2-10)H), 92.2 (C(1)); *m/z* (EI⁺) 330.1108 [M]⁺ ($\text{C}_{18}\text{H}_{26}^{56}\text{FeS}$ requires 330.1105).

Chapter V: Experimental

E-1-Ferrocene-2-hexylsulfide-ethene **120**:

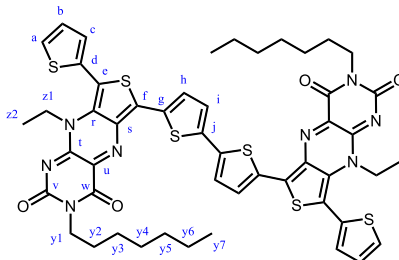


$\nu_{\max}/\text{cm}^{-1}$ (solid state) 3095 (*w.*), 2927-2849 (*m.* C-H aliphatic), 1635 (*m.*), 1457 (*w.*); δ_{H} (500 MHz, CDCl_3) 0.89 (3H, t, J 7.0, C(18)H₃), 1.30-1.34 (4H, m, C(15 and 16)H₂), 1.41-1.50 (2H, m, C(14)H₂), 1.73 (2H, td, J 8.2, 15.8, C(14)H₂), 2.74 (2H, t, J 7.6, C(13)H₂), 4.16 (5H, s, C(6-10)H), 4.36 (2H, m, C(2, 3, 4 or 5)H), 4.44 (2H, n, C(2, 3, 4 or 5)H), 6.39 (1H, d, J 15.3, C(11 or 12)H), 7.07 (1H, d, J 15.3, C(11 or 12)H); m/z (EI⁺) 328.0944 [M]⁺ ($\text{C}_{18}\text{H}_{24}^{56}\text{FeS}$ requires 328.0948).

APPENDICES:

Appendix 1: Experimental of **48**, **62** and **63**. Courtesy of Dr B. Fitzpatrick:

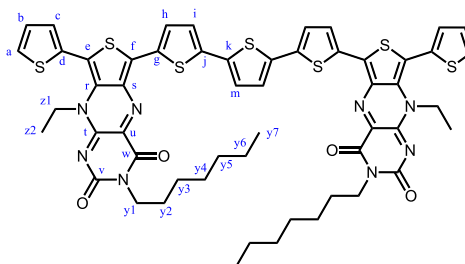
5'-bis-[3-Heptyl-8-ethyl-6,7-bis-thiophene-thiophenepteridine-2,4-(3*H*,8*H*)-dione] **48**



3-Heptyl-8-ethyl-6-(5'-bromothiophene)-7-thiophene-thiophenepteridine-2,4-(3*H*,8*H*)-dione **56** (120 mg, 0.2 mmol), tris(dibenzylideneacetone)dipalladium(0) (3.7 mg, 4.0 μmol), *bis*-(pinacolato)diboron (105mg, 0.4 mmol), K_2OAc (40mg, 0.4 mmol) and X-phos (40mg, 8.0 μmol) were added to a Schlenk tube, which was then evacuated and backfilled with N_2 gas three times. A solvent mixture of dry 1,4-dioxane (15 mL) and dry DMF (5 mL) was added under N_2 flow and the tube then sealed, protected from light and placed in an oil bath at 140°C where the reaction mixture was stirred and monitored by TLC every hour. The reaction was terminated after 3h by diluting with DCM (100 mL) and washed with water. The organic layer was dried over MgSO_4 , filtered and the solvent evaporated under vacuum. The product was purified by column chromatography (100% DCM) to afford the title compound **48** (45 mg, 43%); **48**; m.p. $295 - 297^\circ\text{C}$; $\nu_{\text{max}}/\text{cm}^{-1}$ (film) 2929, 2857, 1705, 1655, 1585, 1559, 1523, 1475; δ_{H} (500 MHz, CDCl_3) 7.64 (2H, d, J 4.0, C(h)H), 7.55 (2H, dd, J 5.3, 1.2, C(a)H), 7.28 (2H, dd, J 3.5, 1.2, C(c)H), 7.27 (2H, d, J 4.0, C(i)H), 7.13 (2H, dd, J 5.3, 3.6, C(b)H), 4.35 (4H, q, J 6.8, C(z1)H₂), 4.03 (4H, t, J 8.0, C(y1)H₂), 1.70 (4H, quint, J 7.5, C(y2)H₂), 1.41 – 1.21 (16H, m, C(y3-y6)H₂), 1.16 (6H, t, J 7.0, C(z2)H₃), 0.86 (6H, t, J 6.9, C(y7)H₃); δ_{C} (125 MHz, CDCl_3) 159.5 (C=O), 155.8 (C=O), 148.9 (C=N), 140.9 (C=N), 140.3 (C), 135.9 (C), 135.5 (C), 134.1 (C), 133.6 (CH), 132.6 (CH), 130.8 (C), 129.9 (CH), 129.0 (CH), 127.6 (C), 127.6 (CH), 107.8 (C), 42.4 (CH₂), 40.9 (CH₂), 31.9 (CH₂), 29.2 (CH₂), 28.0 (CH₂), 27.2 (CH₂), 22.8 (CH₂), 14.2 (CH₃), 12.9 (CH₃); m/z (EI^+) 1041.2123 [$\text{M}+\text{Na}$]⁺ ($\text{C}_{50}\text{H}_{50}\text{N}_8\text{O}_4\text{S}_6\text{Na}$ requires 1041.2171).

Redox active molecules with molecular electronics and synthetic applications

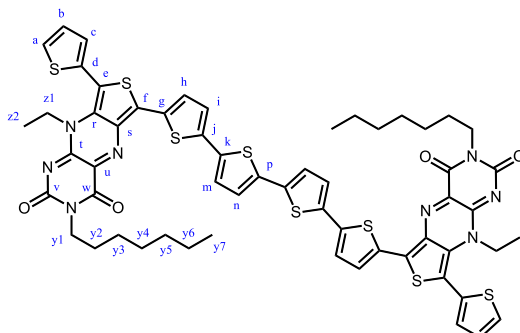
2,5-bis-[3-Heptyl-8-ethyl-6,7-bis-thiophene-thiophenepteridine-2,4-(3*H*,8*H*)-dione] thiophene **62**



Compound **56** (110 mg, 0.2 mmol), 2,5-bis-(tributylstannyl)thiophene (55 μ L, 0.1 mmol) and tetrakis(triphenylphosphine)palladium(0) (6 mg, 5.0 μ mol) were added, under N_2 gas, to a two neck flask containing dry DMF (2 mL). The flask was sealed under N_2 gas, protected from light and stirred at 80 $^{\circ}C$ for 2h. The reaction was terminated by diluting with DCM (75 mL) and then washed with water (75 mL x3), dried over $MgSO_4$ and filtered. The solvent was evaporated under vacuum and the product was purified by column chromatography (DCM 100%) to yield the title compound **62** (60 mg, 55%); m.p. 298 $^{\circ}C$; ν_{max}/cm^{-1} (film) 2929, 2857, 1704, 1653, 1584, 1557, 1510; δ_H (500 MHz, $CDCl_3$) 7.66 (2H, d, J 4.0, C(h)H), 7.54 (2H, dd, J 5.3, 0.9, C(a)H), 7.30 (2H, dd, J 3.4, 0.9, C(c)H), 7.23 (2H, s, C(m)H), 7.16 (2H, d, J 4.0, C(i)H), 7.13 (2H, dd, J 5.0, 3.5, C(b)H), 4.33 (4H, q, J 7.0, C(z1)H₂), 4.03 (4H, t, J 8.0, C(y1)H₂), 1.70 (4H, quint, J 7.3, C(y2)H₂), 1.42-1.19 (16H, m, C(y3-y6)H₂), 1.14 (6H, t, J 7.0, C(z2)H₃), 0.85 (6H, t, J 6.8, C(y7)H₃); δ_C (125 MHz, $CDCl_3$) 159.60 (C=O), 155.87 (C=O), 148.97 (C=N), 142.77 (C=N), 140.99 (C), 136.81 (C), 135.49 (C), 133.32 (C), 132.66 (CH), 131.55 (C), 130.94 (C), 129.89 (CH), 129.81 (CH), 127.61 (C), 127.57 (CH), 126.32 (CH), 124.85 (CH), 106.88 (C), 42.34 (CH₂), 40.87 (CH₂), 31.93 (CH₂), 29.23 (CH₂), 28.07 (CH₂), 27.18 (CH₂), 22.76 (CH₂), 14.25 (CH₃), 12.91 (CH₃); m/z (EI⁺) 1123.2049 [M+Na]⁺ (C₅₄H₅₂N₈O₄S₇ requires 1123.2049).

Redox active molecules with molecular electronics and synthetic applications

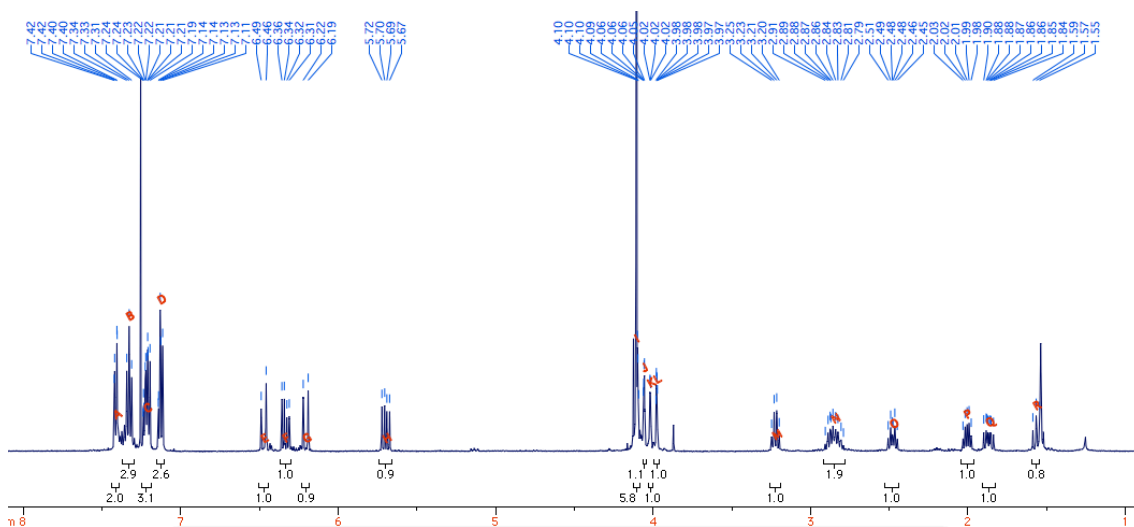
2,5'-bis-[3-Heptyl-8-ethyl-6,7-bis-thiophene-thiophenepteridine-2,4-(3*H*,8*H*)-dione]-5,2'-bis-thiophene **63**



Compound **56** (210 mg, 0.41 mmol), 5,5'-bis-(tributylstannyl)-2,2'-bithiophene (0.12 mL, 0.2 mmol) and tetrakis(triphenylphosphine)palladium(0) (12 mg, 0.01 mmol) were added, under N₂ gas, to a two neck flask containing dry DMF (4 mL). The flask was sealed under N₂ gas, protected from light and stirred at 80 °C for 2h. The reaction was terminated by diluting with DCM (100 mL) and then washed with distilled water (100 mL x 3), dried over MgSO₄ and filtered. The solvent was evaporated under vacuum and the product purified by column chromatography (DCM 100%) to afford compound **63** (150 mg, 63%); m.p. > 300 °C); $\nu_{\max}/\text{cm}^{-1}$ (film) 2923, 2853, 1704, 1651, 1582, 1556, 1530, 1509; δ_{H} (500 MHz, C₂D₂Cl₄) 7.73 (2H, d, *J* 4.0, C(h)H), 7.61 (2H, dd, *J* 5.3, 1.0, C(a)H), 7.34 (2H, dd, *J* 3.5, 1.0, C(c)H), 7.30 (2H, d, *J* 3.8, C(i)H), 7.22 (2H, d, *J* 3.9, C(m)H), 7.19 (2H, d, *J* 3.5, C(n)H), 7.17 (2H, t, *J* 4.1, C(b)H), 4.34 (4H, q, *J* 6.9, C(z1)H₂), 4.03 (4H, t, *J* 7.3, C(y1)H₂), 1.71 (4H, quint, *J* 6.5, C(y2)H₂), 1.46 – 1.24 (16H, m, C(y3-y6)H₂), 1.19 (6H, td, *J* 7.0, 3.2, C(y7)H₃), 0.91 (6H, t, *J* 6.8, C(z2)H₃); δ_{C} (125 MHz, C₂D₂Cl₄) 159.4 (C=O), 155.3 (C=O), 148.6 (C=N), 142.4 (C=N), 140.7 (C), 137.0 (C), 135.5 (C), 135.2 (C), 133.0 (C), 132.5 (CH), 131.0 (C), 130.3 (C), 130.0 (CH), 129.7 (CH), 127.4 (CH), 127.2 (C), 126.1 (CH), 125.1 (CH), 124.7 (CH), 106.9 (C), 41.9 (CH₂), 40.8 (CH₂), 31.7 (CH₂), 29.0 (CH₂), 27.9 (CH₂), 26.9 (CH₂), 22.6 (CH₂), 14.1 (CH₃), 12.6 (CH₃); *m/z* (EI⁺) 1205.1926 [M+Na]⁺ (C₅₈H₅₄N₈O₄S₈ requires 1205.1926).

Appendix 2:

1-[(±)Ferrocene]-2R,4S-[bis-(styrene)]-cyclopentane:



Appendix 3:

X-ray data for compound **47**

Identification code	aaw011
Empirical formula	C ₁₈ H ₁₂ N ₄ O ₂ S ₃
Formula weight	412.50
Temperature	150(2) K
Wavelength	0.71073 Å
Crystal system, space group	Monoclinic, P2(1)/c
Unit cell dimensions	a = 9.1742(4) Å alpha = 90 deg. b = 7.4390(3) Å beta = 90.260(5) deg. c = 25.1811(16) Å gamma = 90 deg.
Volume	1718.51(15) Å ³
Z, Calculated density	4, 1.594 Mg/m ³
Absorption coefficient	0.455 mm ⁻¹
F(000)	848
Crystal size	0.75 x 0.15 x 0.02 mm

Redox active molecules with molecular electronics and synthetic applications

Theta range for data collection 2.86 to 25.35 deg.
Limiting indices $-11 \leq h \leq 11$, $-8 \leq k \leq 8$, $-30 \leq l \leq 30$
Reflections collected / unique 13849 / 3134 [R(int) = 0.0994]
Completeness to theta = 25.35 99.8 %
Absorption correction Analytical
Max. and min. transmission 0.9910 and 0.7267
Refinement method Full-matrix least-squares on F^2
Data / restraints / parameters 3134 / 18 / 268
Goodness-of-fit on F^2 1.047
Final R indices [$I > 2\sigma(I)$] $R_1 = 0.0562$, $wR_2 = 0.1207$
R indices (all data) $R_1 = 0.1128$, $wR_2 = 0.1491$
Extinction coefficient none
Largest diff. peak and hole 0.49 and -0.41 e. \AA^{-3}

Table 2. Atomic coordinates ($\times 10^4$) and equivalent isotropic displacement parameters ($\text{\AA}^2 \times 10^3$) for aaw011.

U(eq) is defined as one third of the trace of the orthogonalized U_{ij} tensor.

	x	y	z	U(eq)
C(1)	1895(6)	7795(5)	6395(2)	45(1)
C(2)	3206(5)	7080(6)	6329(2)	52(1)
C(3)	3348(15)	6570(20)	5769(5)	46(7)
C(3')	1130(30)	7780(40)	5876(8)	130(20)
C(4)	2054(4)	6960(5)	5477(2)	30(1)
C(5)	1776(4)	6618(5)	4926(2)	30(1)
C(6)	537(4)	6974(5)	4623(2)	28(1)
C(7)	642(4)	6414(5)	4078(2)	29(1)
C(8)	1952(4)	5598(5)	3963(2)	31(1)
C(9)	2546(4)	4619(6)	3500(2)	34(1)
C(10)	2730(20)	2760(20)	3431(8)	56(9)
C(10')	3230(30)	5230(20)	3041(7)	36(7)
C(11)	3362(5)	2225(7)	2943(2)	50(1)
C(12)	3670(5)	3747(7)	2683(2)	50(1)
C(13)	-4158(5)	8536(5)	3833(2)	31(1)
C(14)	-3137(4)	8796(5)	4738(2)	32(1)
C(15)	-1793(4)	7957(5)	4515(2)	28(1)
C(16)	-1808(4)	7500(5)	3954(2)	28(1)
C(17)	-530(5)	6336(5)	3176(2)	34(1)
C(18)	-20(5)	7958(5)	2868(2)	44(1)
N(1)	-678(3)	7741(4)	4837(1)	29(1)

N(2)	-569(3)	6717(4)	3752(1)	30(1)
N(3)	-2899(4)	7782(4)	3631(1)	32(1)
N(4)	-4222(3)	8981(4)	4374(1)	32(1)
O(1)	-5223(3)	8837(4)	3552(1)	39(1)
O(2)	-3244(3)	9258(4)	5201(1)	37(1)
S(1)	853(4)	7915(4)	5893(1)	33(1)
S(1')	3655(7)	6418(8)	5768(2)	34(1)
S(2)	3032(1)	5583(1)	4531(1)	36(1)
S(3)	3249(4)	5621(6)	2941(2)	42(1)
S(3')	2564(8)	2344(10)	3503(3)	39(1)

Table 3. Bond lengths [Å] and angles [deg] for aaw011.

C(1)-C(2)	1.326(6)
C(1)-S(1)	1.584(6)
C(2)-C(3)	1.469(13)
C(3)-C(4)	1.423(12)
C(4)-C(5)	1.433(6)
C(4)-S(1)	1.681(5)
C(5)-C(6)	1.391(5)
C(5)-S(2)	1.710(4)
C(6)-N(1)	1.365(5)
C(6)-C(7)	1.437(6)
C(7)-C(8)	1.378(5)
C(7)-N(2)	1.396(5)
C(8)-C(9)	1.481(5)
C(8)-S(2)	1.735(4)
C(9)-C(10)	1.400(14)
C(9)-S(3)	1.721(6)
C(10)-C(11)	1.420(15)
C(11)-C(12)	1.339(6)
C(12)-S(3)	1.586(6)
C(13)-O(1)	1.225(5)
C(13)-N(3)	1.383(5)
C(13)-N(4)	1.404(5)
C(14)-O(2)	1.220(5)
C(14)-N(4)	1.358(5)
C(14)-C(15)	1.494(5)
C(15)-N(1)	1.312(5)
C(15)-C(16)	1.453(6)
C(16)-N(3)	1.304(5)
C(16)-N(2)	1.377(5)
C(17)-N(2)	1.479(5)
C(17)-C(18)	1.509(5)

Redox active molecules with molecular electronics and synthetic applications

C(2)-C(1)-S(1)	117.9(4)
C(1)-C(2)-C(3)	107.9(7)
C(4)-C(3)-C(2)	111.4(9)
C(3)-C(4)-C(5)	127.5(7)
C(3)-C(4)-S(1)	108.2(6)
C(5)-C(4)-S(1)	124.3(3)
C(6)-C(5)-C(4)	129.7(4)
C(6)-C(5)-S(2)	108.5(3)
C(4)-C(5)-S(2)	121.7(3)
N(1)-C(6)-C(5)	122.0(4)
N(1)-C(6)-C(7)	123.8(4)
C(5)-C(6)-C(7)	114.2(3)
C(8)-C(7)-N(2)	129.8(4)
C(8)-C(7)-C(6)	112.9(4)
N(2)-C(7)-C(6)	117.3(3)
C(7)-C(8)-C(9)	134.9(4)
C(7)-C(8)-S(2)	109.0(3)
C(9)-C(8)-S(2)	115.8(3)
C(10)-C(9)-C(8)	128.7(8)
C(10)-C(9)-S(3)	106.3(7)
C(8)-C(9)-S(3)	124.9(3)
C(9)-C(10)-C(11)	115.7(12)
C(12)-C(11)-C(10)	105.8(7)
C(11)-C(12)-S(3)	119.4(4)
O(1)-C(13)-N(3)	121.8(4)
O(1)-C(13)-N(4)	118.8(4)
N(3)-C(13)-N(4)	119.4(4)
O(2)-C(14)-N(4)	123.7(4)
O(2)-C(14)-C(15)	123.2(4)
N(4)-C(14)-C(15)	113.0(4)
N(1)-C(15)-C(16)	125.1(3)
N(1)-C(15)-C(14)	117.4(4)
C(16)-C(15)-C(14)	117.4(4)
N(3)-C(16)-N(2)	118.1(4)
N(3)-C(16)-C(15)	124.9(3)
N(2)-C(16)-C(15)	117.0(4)
N(2)-C(17)-C(18)	111.0(3)
C(15)-N(1)-C(6)	116.3(3)
C(16)-N(2)-C(7)	120.5(3)
C(16)-N(2)-C(17)	117.8(3)
C(7)-N(2)-C(17)	121.6(3)
C(16)-N(3)-C(13)	118.5(4)
C(14)-N(4)-C(13)	126.7(3)
C(1)-S(1)-C(4)	94.5(3)
C(5)-S(2)-C(8)	95.3(2)

C(12)-S(3)-C(9) 92.7(3)

Symmetry transformations used to generate equivalent atoms:

Table 4. Anisotropic displacement parameters ($\text{Å}^2 \times 10^3$) for aaw011.

The anisotropic displacement factor exponent takes the form:

$$-2 \pi^2 [h^2 a^{*2} U_{11} + \dots + 2 h k a^* b^* U_{12}]$$

	U11	U22	U33	U23	U13	U12
C(1)	55(3)	42(3)	37(3)	-5(2)	10(2)	-4(2)
C(2)	39(3)	62(3)	56(4)	17(3)	-16(3)	-11(2)
C(4)	18(2)	36(2)	37(3)	2(2)	3(2)	-3(2)
C(5)	19(2)	29(2)	41(3)	-1(2)	6(2)	0(2)
C(6)	19(2)	29(2)	37(3)	5(2)	5(2)	-1(2)
C(7)	21(2)	32(2)	34(3)	1(2)	1(2)	0(2)
C(8)	19(2)	35(2)	40(3)	-1(2)	8(2)	1(2)
C(9)	18(2)	41(3)	42(3)	-7(2)	9(2)	2(2)
C(10)	41(10)	75(15)	51(10)	30(8)	-3(7)	-10(7)
C(11)	30(3)	62(3)	59(4)	-18(3)	0(3)	11(2)
C(12)	20(2)	90(4)	40(3)	-1(3)	1(2)	6(2)
C(13)	22(2)	34(2)	37(3)	1(2)	5(2)	2(2)
C(14)	19(2)	39(2)	37(3)	7(2)	4(2)	3(2)
C(15)	19(2)	33(2)	33(3)	1(2)	6(2)	0(2)
C(16)	16(2)	30(2)	37(3)	-1(2)	3(2)	-1(2)
C(17)	26(2)	43(2)	34(3)	-5(2)	5(2)	8(2)
C(18)	42(3)	49(3)	40(3)	-1(2)	8(2)	5(2)
N(1)	17(2)	33(2)	37(2)	1(2)	7(2)	4(1)
N(2)	21(2)	34(2)	35(2)	0(2)	4(2)	2(1)
N(3)	19(2)	39(2)	37(2)	-1(2)	5(2)	4(2)
N(4)	18(2)	41(2)	36(2)	-2(2)	7(2)	8(1)
O(1)	25(2)	49(2)	44(2)	-2(1)	-4(2)	6(1)
O(2)	27(2)	51(2)	34(2)	-2(1)	6(1)	9(1)
S(1)	28(1)	35(1)	37(1)	0(1)	2(1)	-2(1)
S(1')	18(2)	39(2)	46(3)	0(1)	3(1)	9(2)
S(2)	18(1)	47(1)	44(1)	-2(1)	7(1)	4(1)
S(3)	27(2)	51(2)	46(2)	4(2)	12(1)	3(1)
S(3')	31(2)	42(2)	43(3)	-2(2)	17(2)	8(2)

X-ray data of compound **46**

Table 1. Crystal data and structure refinement for bftf.

Identification code	bftf
Empirical formula	C ₂₇ H ₂₇ Br N ₄ O ₂ S ₂
Formula weight	583.55
Temperature	150(2) K

Redox active molecules with molecular electronics and synthetic applications

Wavelength	0.71073 Å
Crystal system, space group	Monoclinic, P 21/c
Unit cell dimensions	a = 15.7775(19) Å alpha = 90 deg. b = 17.7289(19) Å beta = 100.785(6) deg. c = 9.3599(9) Å gamma = 90 deg.
Volume	2571.9(5) Å ³
Z, Calculated density	4, 1.507 Mg/m ³
Absorption coefficient	1.794 mm ⁻¹
F(000)	1200
Crystal size	0.200 x 0.050 x 0.010 mm
Theta range for data collection	2.495 to 25.390 deg.
Limiting indices	-15<=h<=19, -20<=k<=21, -10<=l<=11
Reflections collected / unique	16791 / 4646 [R(int) = 0.0631]
Completeness to theta = 25.242	98.7 %
Refinement method	Full-matrix least-squares on F ²
Data / restraints / parameters	4646 / 15 / 335
Goodness-of-fit on F ²	1.016
Final R indices [I>2sigma(I)]	R1 = 0.0584, wR2 = 0.1266
R indices (all data)	R1 = 0.1203, wR2 = 0.1530
Extinction coefficient	n/a
Largest diff. peak and hole	1.031 and -0.550 e.Å ⁻³

Table 2. Atomic coordinates (x 10⁴) and equivalent isotropic displacement parameters (Å² x 10³) for bftf.

U(eq) is defined as one third of the trace of the orthogonalized U_{ij} tensor.

	x	y	z	U(eq)
C(1)	3093(4)	758(3)	8115(5)	32(1)
C(2)	3578(4)	1226(3)	9101(5)	31(1)
C(3)	4459(4)	1078(3)	9202(5)	27(1)
C(4)	4640(4)	507(3)	8300(5)	24(1)
C(5)	5501(4)	251(3)	8197(5)	24(1)
C(6)	6223(4)	543(3)	9094(5)	28(1)
C(7)	7043(4)	374(3)	8894(5)	26(1)
C(8)	7223(4)	-120(3)	7847(5)	27(1)
C(9)	8121(4)	-104(3)	7554(5)	34(1)
C(10)	8428(9)	245(10)	6409(17)	42(7)
C(10')	8929(11)	-350(20)	8420(30)	29(10)
C(11)	9324(5)	210(4)	6497(9)	68(2)
C(12)	9651(5)	-154(4)	7730(8)	67(2)

C(13)	5668(3)	-304(2)	7160(4)	21(1)
C(14)	6508(3)	-517(3)	7040(5)	22(1)
C(15)	7407(4)	-1536(3)	6191(5)	31(1)
C(16)	7564(4)	-2018(3)	7532(6)	42(2)
C(17)	5875(3)	-1424(2)	5229(5)	21(1)
C(18)	5054(3)	-1111(2)	5347(4)	19(1)
C(19)	5267(4)	-2280(3)	3479(5)	24(1)
C(20)	4274(4)	-1418(3)	4401(5)	23(1)
C(21)	3700(4)	-2289(3)	2453(5)	27(1)
C(22)	3329(4)	-2993(3)	3011(5)	30(1)
C(23)	2477(4)	-3237(3)	2073(6)	34(1)
C(24)	1748(4)	-2711(4)	2139(8)	69(2)
C(25)	902(5)	-2967(5)	1237(8)	74(2)
C(26)	203(7)	-2345(8)	1213(16)	79(4)
C(27)	-637(7)	-2631(6)	424(12)	74(5)
C(26')	-4(14)	-2780(18)	1380(30)	96(12)
C(27')	-80(30)	-1990(19)	810(50)	155(19)
Br(1)	1894(1)	752(1)	7627(1)	50(1)
S(1)	3684(1)	147(1)	7296(1)	27(1)
S(2')	8321(5)	356(5)	6144(9)	39(2)
S(2)	8974(2)	-430(4)	8717(6)	57(2)
N(1)	4951(3)	-599(2)	6283(4)	21(1)
N(2)	6589(3)	-1117(2)	6091(4)	21(1)
N(3)	5975(3)	-1994(2)	4372(4)	25(1)
N(4)	4438(3)	-1983(2)	3475(4)	21(1)
O(1)	3553(2)	-1198(2)	4435(3)	28(1)
O(2)	5329(2)	-2809(2)	2661(4)	34(1)

Table 3. Bond lengths [Å] and angles [deg] for bftf.

C(1)-C(2)	1.363(7)
C(1)-S(1)	1.703(5)
C(1)-Br(1)	1.862(6)
C(2)-C(3)	1.401(8)
C(3)-C(4)	1.381(7)
C(4)-C(5)	1.452(7)
C(4)-S(1)	1.742(5)
C(5)-C(6)	1.382(7)
C(5)-C(13)	1.441(6)
C(6)-C(7)	1.375(7)
C(7)-C(8)	1.384(7)
C(8)-C(14)	1.421(7)
C(8)-C(9)	1.493(8)
C(9)-C(10)	1.400(13)

Redox active molecules with molecular electronics and synthetic applications

C(9)-S(2)	1.668(7)
C(10)-C(11)	1.402(14)
C(11)-C(12)	1.338(9)
C(12)-S(2)	1.614(8)
C(13)-N(1)	1.371(6)
C(13)-C(14)	1.403(7)
C(14)-N(2)	1.407(6)
C(15)-N(2)	1.477(6)
C(15)-C(16)	1.501(7)
C(17)-N(3)	1.318(6)
C(17)-N(2)	1.369(6)
C(17)-C(18)	1.432(7)
C(18)-N(1)	1.294(6)
C(18)-C(20)	1.479(7)
C(19)-O(2)	1.225(5)
C(19)-N(3)	1.362(6)
C(19)-N(4)	1.411(7)
C(20)-O(1)	1.208(6)
C(20)-N(4)	1.379(6)
C(21)-N(4)	1.465(6)
C(21)-C(22)	1.513(7)
C(22)-C(23)	1.524(7)
C(23)-C(24)	1.491(8)
C(24)-C(25)	1.510(9)
C(25)-C(26)	1.556(12)
C(26)-C(27)	1.480(13)
C(26')-C(27')	1.50(2)

C(2)-C(1)-S(1)	114.0(4)
C(2)-C(1)-Br(1)	125.8(4)
S(1)-C(1)-Br(1)	120.1(3)
C(1)-C(2)-C(3)	110.8(5)
C(4)-C(3)-C(2)	114.3(5)
C(3)-C(4)-C(5)	124.9(5)
C(3)-C(4)-S(1)	109.9(4)
C(5)-C(4)-S(1)	125.2(4)
C(6)-C(5)-C(13)	115.5(5)
C(6)-C(5)-C(4)	121.2(4)
C(13)-C(5)-C(4)	123.3(5)
C(7)-C(6)-C(5)	121.7(5)
C(6)-C(7)-C(8)	123.9(5)
C(7)-C(8)-C(14)	116.2(5)
C(7)-C(8)-C(9)	116.5(5)
C(14)-C(8)-C(9)	126.8(4)
C(10)-C(9)-C(8)	128.7(7)
C(10)-C(9)-S(2)	107.5(7)

Redox active molecules with molecular electronics and synthetic applications

C(8)-C(9)-S(2)	123.4(4)
C(9)-C(10)-C(11)	115.1(11)
C(12)-C(11)-C(10)	107.1(8)
C(11)-C(12)-S(2)	116.8(6)
N(1)-C(13)-C(14)	122.4(4)
N(1)-C(13)-C(5)	115.4(5)
C(14)-C(13)-C(5)	122.2(5)
C(13)-C(14)-N(2)	116.9(4)
C(13)-C(14)-C(8)	119.5(4)
N(2)-C(14)-C(8)	123.6(5)
N(2)-C(15)-C(16)	110.2(4)
N(3)-C(17)-N(2)	118.9(5)
N(3)-C(17)-C(18)	123.9(5)
N(2)-C(17)-C(18)	117.2(4)
N(1)-C(18)-C(17)	123.6(4)
N(1)-C(18)-C(20)	117.9(5)
C(17)-C(18)-C(20)	118.3(4)
O(2)-C(19)-N(3)	121.1(5)
O(2)-C(19)-N(4)	117.8(5)
N(3)-C(19)-N(4)	121.1(4)
O(1)-C(20)-N(4)	122.7(5)
O(1)-C(20)-C(18)	123.1(4)
N(4)-C(20)-C(18)	114.2(5)
N(4)-C(21)-C(22)	113.1(4)
C(21)-C(22)-C(23)	113.1(4)
C(24)-C(23)-C(22)	113.7(5)
C(23)-C(24)-C(25)	113.4(6)
C(24)-C(25)-C(26)	110.2(7)
C(27)-C(26)-C(25)	109.3(10)
C(1)-S(1)-C(4)	90.9(3)
C(12)-S(2)-C(9)	93.5(4)
C(18)-N(1)-C(13)	118.6(4)
C(17)-N(2)-C(14)	120.7(4)
C(17)-N(2)-C(15)	116.8(4)
C(14)-N(2)-C(15)	121.4(4)
C(17)-N(3)-C(19)	118.7(4)
C(20)-N(4)-C(19)	123.6(4)
C(20)-N(4)-C(21)	117.4(4)
C(19)-N(4)-C(21)	119.1(4)

Symmetry transformations used to generate equivalent atoms:

Table 4. Anisotropic displacement parameters ($\text{\AA}^2 \times 10^3$) for bftf.

The anisotropic displacement factor exponent takes the form:

$$-2 \pi^2 [h^2 a^{*2} U_{11} + \dots + 2 h k a^* b^* U_{12}]$$

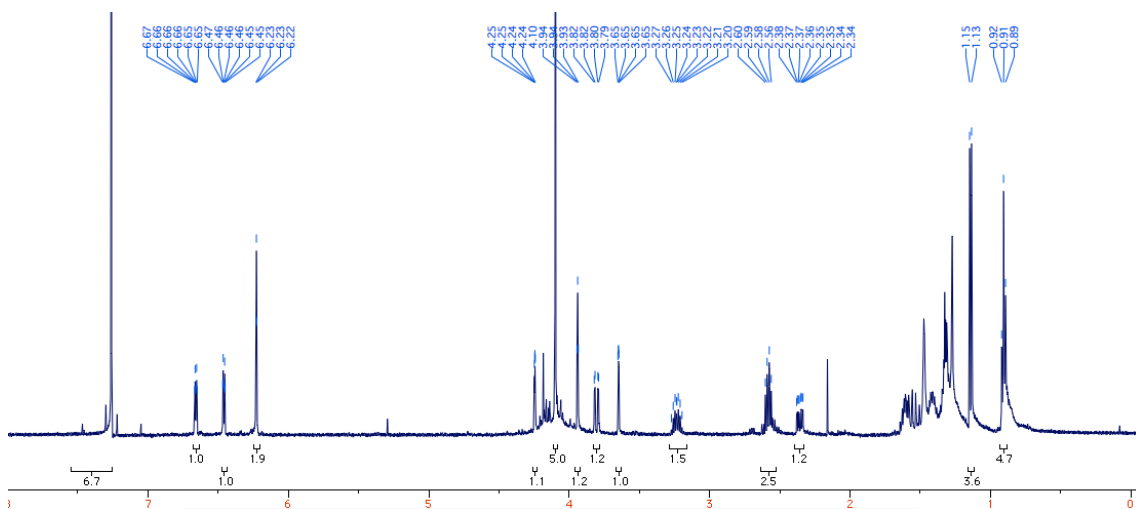
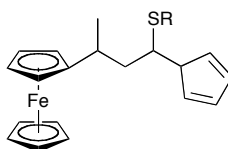
Redox active molecules with molecular electronics and synthetic applications

	U11	U22	U33	U23	U13	U12
C(1)	44(4)	26(3)	30(3)	8(2)	15(3)	4(3)
C(2)	51(4)	16(3)	29(3)	1(2)	14(3)	3(3)
C(3)	47(4)	19(3)	17(3)	-2(2)	10(2)	-2(3)
C(4)	45(4)	16(3)	13(2)	3(2)	11(2)	1(2)
C(5)	45(4)	15(3)	13(2)	3(2)	8(2)	-3(2)
C(6)	55(4)	16(3)	10(2)	-3(2)	2(2)	-2(3)
C(7)	40(4)	19(3)	18(3)	3(2)	-1(2)	-6(3)
C(8)	46(4)	19(3)	14(2)	2(2)	4(2)	-3(2)
C(9)	40(4)	28(3)	32(3)	-8(2)	7(3)	-9(3)
C(11)	80(6)	54(5)	83(6)	-8(4)	43(5)	-17(4)
C(12)	40(5)	68(5)	88(6)	-24(4)	1(4)	-4(4)
C(13)	42(4)	11(2)	9(2)	3(2)	6(2)	0(2)
C(14)	37(4)	17(3)	12(2)	4(2)	6(2)	6(2)
C(15)	36(4)	29(3)	29(3)	-8(2)	5(3)	1(3)
C(16)	43(4)	31(3)	51(4)	5(3)	6(3)	8(3)
C(17)	39(4)	11(2)	15(2)	4(2)	9(2)	3(2)
C(18)	39(3)	11(2)	10(2)	4(2)	7(2)	1(2)
C(19)	44(4)	15(3)	14(3)	1(2)	13(2)	0(2)
C(20)	39(4)	14(3)	16(2)	5(2)	8(2)	-1(2)
C(21)	43(4)	22(3)	15(3)	-2(2)	1(2)	0(3)
C(22)	46(4)	20(3)	22(3)	1(2)	3(2)	0(2)
C(23)	36(4)	33(3)	31(3)	-2(2)	6(3)	0(3)
C(24)	53(5)	76(5)	72(5)	-17(4)	1(4)	11(4)
C(25)	46(5)	107(7)	70(5)	12(5)	14(4)	14(5)
Br(1)	51(1)	46(1)	56(1)	-4(1)	17(1)	3(1)
S(1)	42(1)	19(1)	21(1)	-1(1)	10(1)	1(1)
S(2')	43(4)	42(4)	28(3)	14(3)	-1(2)	8(3)
S(2)	47(2)	77(3)	42(2)	2(2)	-4(1)	2(2)
N(1)	40(3)	13(2)	12(2)	4(2)	8(2)	0(2)
N(2)	32(3)	16(2)	17(2)	1(2)	10(2)	2(2)
N(3)	41(3)	18(2)	16(2)	-2(2)	9(2)	1(2)
N(4)	38(3)	12(2)	13(2)	-2(2)	3(2)	-1(2)
O(1)	35(2)	25(2)	23(2)	-4(2)	6(2)	1(2)
O(2)	52(3)	24(2)	28(2)	-12(2)	13(2)	-2(2)

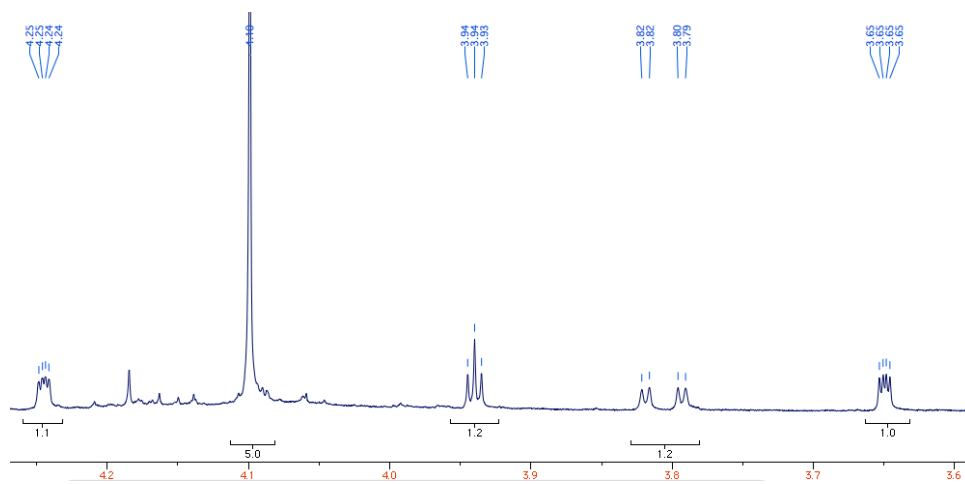
Appendix 4:

¹H NMR of 1-hexanesulfide-1-cyclopentadiene-3-ferrocene-butane **121**

Redox active molecules with molecular electronics and synthetic applications

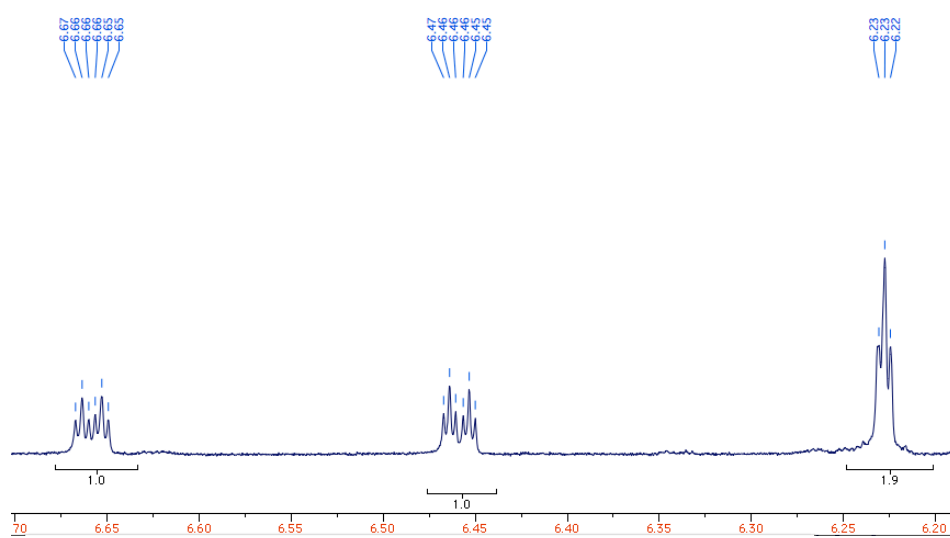


Full NMR spectrum: Noticeable large amount of aliphatic protons and several diastereotopic centres.



Zoom on 3.6 to 4.5 ppm showing only one ferrocene present

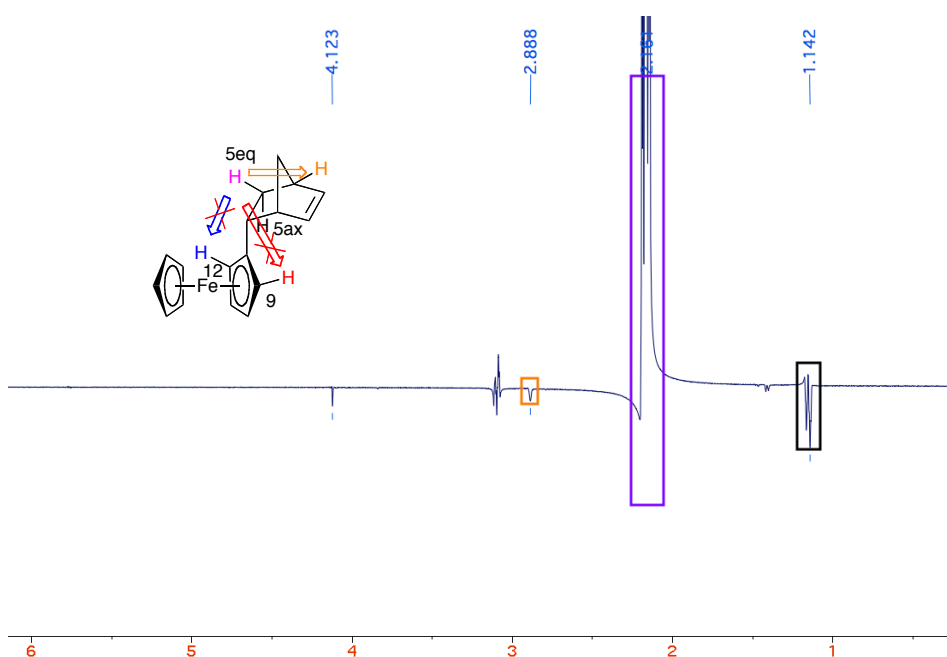
Redox active molecules with molecular electronics and synthetic applications



Zoom on 6.20 to 6.70 ppm: Showing evidence of a cyclopentadiene

Appendix 5:

NOE spectra of compound **93** irradiated at position C(5) pseudo-equatorial:



REFERENCES:

- 1) R. Kohen, A. Nyska; *Toxicologic Pathology*, **2002**, *6*, 620-650
- 2) R. Lonsdale, J. N. Harvey, A. J. Mulholland; *Chem. Soc. Rev.*, **2012**, *41*, 3025-3038
- 3) B. G. Davis, V. Boyer; *Nat. Prod. Rep.*, **2001**, *18*, 618-640
- 4) E. M. Gale, A. C. Simmonett, J. Telser, H. F. Schaefer, T. C. Harrop; *Inorg. Chem.*, **2011**, *50*, 9216-9218
- 5) A. W. Blyth; *J. Chem. Soc. Trans.*, **1879**, *35*, 530-538
- 6) V. Massey; *Biochem. Soc. Trans.*, **2000**, *28*, 283-296
- 7) R. Kuhn, K. Reinemund, F. Weygand; *Ber.*, **1934**, *67*, 1460-1463
- 8) P. Karrer, K. Schöpp, F. Benz; *Helv. Chim. Acta*, **1935**, *18*, 426-429
- 9) H. Theorell; *Biochem. J.*, **1935**, *275*, 344-346
- 10) O. Warburg, W. Christian; *Biochem. J.*, **1938**, *298*, 150-155
- 11) H. A. Krebs; *Biochem. J.*, **1935**, *29*, 1620-1644
- 12) P. F. Heelis; *Chem. Soc. Rev.*, **1982**, *11*, 15-39
- 13) O. S. Ksenzhek, S. A. Petrova; *Bioelectrochem. Bioenerg.*, **1983**, *11*, 105-127
- 14) S. Ghisla, V. Massey; *Eur. J. Biochem.*, **1989**, *181*, 1-17
- 15) M. Fraaije, R. H. H. van der Heuvel, W. J. H. van Berkel, A. Mattevi; *J. Bio. Chem.*, **1999**, *274*, 35514-35520
- 16) N. Choy, K. C. Russell, J. C. Alvarez, A. Fider; *Tett. Lett.*, **2000**, *41*, 1515-1518; J. J. Hasford, C. J. Rizzo; *J. Am. Chem. Soc.*, **1998**, *120*, 2251-2255
- 17) A. Bowd, P. Byrom, J. B. Hudson, J. H. Turnbull; *Photochem. Photobio.*, **1968**, *8*, 1-10
- 18) L. R. Tether, J. H. Turnbull; *J. Biochem.*, **1962**, *85*, 517-523
- 19) B. J. Fritz, S. Kasai, K. Matsui; *Photochem. Photobio.*, **1987**, *45*, 113-117; A. J. W. G. Visser, F. Muller; *Helv. Chim. Acta*, **1979**, *62*, 593-608; B. Attenberger, H. Schmaderer, B. König; *Synth.*, **2008**, *11*, 1767-1774
- 20) a) Y.-M. Legrand, M. Gray, G. Cooke, V. M. Rotello; *J. Am. Chem. Soc.*, **2003**, *125*, 15789-15795; b) M. Gray, A. J. Goodman, J. B. Carroll, K. Bardon, M. Markey, G. Cooke, V. M. Rotello; *Org. Lett.*, **2004**, *3*, 385-388; c) A. S. F. Boyd, J. B. Carroll, G. Cooke, J. F. Garety, B. J. Jordan, S. Mabruk, G. Rosair, V. M. Rotello; *Chem. Comm.*, **2005**, 2468-2470; d) J. B. Carroll, G. Cooke, J. F. Garety, B. J. Jordan, S. Mabruk, V. M. Rotello; *Chem. Comm.*, **2005**, 3838-3840; e) S. T. Caldwell, G. Cooke, S. G. Hewage, S. Mabruk, G. Rabani, V. Rotello, B. O. Smith, C. Subramani, P. Woisel; *Chem. Comm.*, **2008**, 4126-4128; f) S. T. Caldwell, L. J. Ferrugia, S. G. Hewage, N. Kryvokhyzha, V. M. Rotello, G. Cooke; *Chem. Comm.*, **2009**, 1350-1352; h) N. A. McDonald, C.

- Subramani, S. T. Caldwell, N. Y. Zainalabdeen, G. Cooke, V. M. Rotello; *Tet. Lett.*, **2011**, *52*, 2107-2110
- 21) Y. Imada, H. Iida, S-I. Murahashi, T. Naota; *Angew. Chem. Int. Ed.*, **2005**, *44*, 1704-1706
- 22) S. Chen, F. W. Foss Jr.; *Org. Lett.*, **2012**, *19*, 5150-5153
- 23) A. T. Murray, P. Matton, N. W. G. Fairhurst, M.P. John, D. R. Carbery; *Org. Lett.*, **2012**, *14*, 3656-3659
- 24) Y. Imada, H. Iida, T. Kitagawa, T. Naota; *Chem. Eur. J.*, **2011**, *17*, 5908-5920
- 25) E. Mirzakułova¹, R. Khatmullin¹, J. Walpita¹, T. Corrigan¹, N. M. Vargas-Barbosa, S. Vyas, S. Oottikkal, S. F. Manzer, C. M. Hadad, K. D. Glusac; *Nature Chem.*, **2012**, *4*, 794-801
- 26) S-Y. Ju, F. Papadimitrakopoulos; *J. Am. Chem. Soc.*, **2008**, *130*, 655-664
- 27) M. D. Greaves, R. Deans, T. H. Galow, V. M. Rotello; *Chem. Commun.*, **1999**, 785-786
- 28) B. Fitzpatrick, B. Creran, G. Cooke, V. M. Rotello; *Macromol. Chem. Phys.*, **2012**, *213*, 1758-1767
- 29) B. J. Jordan, M. A. Pollier, Y. Ofir, S. Joubanian, J. G. Mehtala, C. Sinkel, S. T. Caldwell, A. Kennedy, G. Rabani, G. Cooke, V. M. Rotello; *Chem. Commun.*, **2008**, 1653-1655
- 30) G. Cooke, J. F. Garety, B. Jordan, N. Kryvokhyzha, A. Parkin, G. Rabani, V. M. Rotello; *Org. Lett.*, **2006**, *11*, 2297-2300
- 31) S. T. Caldwell, G. Cooke, B. Fitzpatrick, D-L. Long, G. Rabani, V. M. Rotello; *Chem. Comm.*, **2008**, 5912-5914
- 32) B. J. Jordan, Y. Ofir, D. Patra, S. T. Caldwell, A. Kennedy, S. Joubanian, G. Rabani, G. Cooke, V. M. Rotello; *Small*, **2008**, *4*, 2074-2078
- 33) S. Isoda, K. Akiyama, S. Nishikawa, S. Ueyama, H. Miyasaka, T. Okada; *Thin Solid Films*, **2004**, *466*, 285-290
- 34) S. Isoda, M. Maeda, H. Miyasaka, N. Mataga; *Chem. Phys. Lett.*, **1991**, *182*, 379
- 35) V. Nandwana, C. Subramani, S. Eymur, Y-C. Yeh, G. Yesilbag Tonga, M. Tonga, Y. Jeong, B. Yang, M. D. Barnes, G. Cooke, V. M. Rotello; *Int. J. Mol. Sci.*, **2011**, *12*, 6357-6366
- 36) V. Nandwana, B. Fitzpatrick, Q. Liu, K. M. Solntsev, X. Yu, G. Yesilbag Tonga, S. Eymur, M. Tonga, G. Cooke, V. M. Rotello; *Polym. Chem.*, **2012**, *3*, 3072-3076
- 37) T. J. Kealy, P. L. Pauson; *Nature*, **1951**, *168*, 1039-1040
- 38) G. Wilkinson, M. Rosenblum, M. C. Whiting, R. B. Woodward; *J. Am. Chem. Soc.*, **1952**, *74*, 2125-2126; W. Pfab, E. O. Fischer; *Zeitschrift fur anorganische und allgemeine Chemie*, **1952**, *274*, 316-322

Redox active molecules with molecular electronics and synthetic applications

- 39) http://nobelprize.org/nobel_prizes/chemistry/laureates/1973/ accessed on 28/02/2013
- 40) Earliest Friedl-Crafts acylation: R. B. Woodward, M. Rosenblum, M. C. Whiting; *J. Am. Chem. Soc.*, **1952**, *74*, 3458 - 3459; alkylation: A. N. Nesmeyanov, N. S. Kochetkova; *Doklady Akademii Nauk SSSR*, **1957**, *112*, 583-585
- 41) Earliest functionalisation of ferrocene via lithiation: D. J. Booth, B. W. Rockett; *J. Chem. Soc. (C)*, **1971**, 3341-3344
- 42) N. G. Connelly, W. E. Geiger; *Chem. Rev.*, **1996**, *96*, 877-910
- 43) R. R. Gagne, C. A. Koval, G. C. Lisensky; *Inorg. Chem.*, **1980**, *19*, 2854-2855
- 44) *Seymour/Carraher's Polymer Chemistry*, 6th ed.; C. E. Carraher, R. B. Seymour, CRC Press, **2003**, Ch. 11 pp. 466
- 45) A. Fihri, P. Meunier, J-C. Hierso; *Coord. Chem. Rev.*, **2007**, *251*, 2017-2055
- 46) R. C. J. Atkinson, V. C. Gibson, N. J. Long; *Chem. Soc. Rev.*, **2004**, *33*, 313-328
- 47) A. Togni; *Chimia*, 1996, *50*, 86-93
- 48) H-U. Blaser, W. Brieden, B. Pugin, F. Spindler, M. Studer, A. Togni; *Topics in Catalysis*, **2002**, *19*, 3-16 (and references therein)
- 49) G. Gasser, I. Ott, N. Metzler-Nolte; *J. Med. Chem.*, **2011**, *54*, 3-25
- 50) D. Dive, C. Biot; *ChemMedChem*, **2008**, *3*, 383-391
- 51) Y. Gao, J. M. Shreeve; *J. Inorg. Organomet. Pol. Mat.*, **2007**, *1*, 19-36
- 52) R. Deschenaux, M. Evena, D. Guillon; *Chem. Comm.*, **1998**, 537-538
- 53) M. Prato; *J. Mater. Chem.*, **1997**, *7*, 1097-1109 and references therein
- 54) M. Prato, M. Maggini, C. Giacometti, G. Scorrano, G. Sandozh, G. Farnia; *Tetrahedron*, **1996**, *14*, 5221-5234
- 55) D. M. Guldi, C. Luo, D. Koktysh, N. A. Kotov, T. Da Ros, S. Bosi, M. Prato; *Nano Lett.*, **2002**, *7*, 775-780
- 56) a) S. Senthil, P. Kannan; *J. Appl. Polym. Sci.*, **2002**, *4*, 831-841; S. Senthil, P. Kannan; *J. Polym. Sci. Polym. Chem.*, **2001**, *39*, 2396
- 57) D. Saravanakumar, N. Sengottuvelan, V. Narayanan, M. Kandaswamy, T. L. Varghese; *J. Appl. Polym. Sci.*, **2011**, *5*, 2517-2524
- 58) S. Sönmezoğlu, C. Akyürek, S. Akin; *J. Phys. D: Appl. Phys.*, 2012, *45*, 425101
- 59) *Comptes rendus hebdomadaires des séances de l'Académie des sciences, tome neuvième*; E. Becquerel, Bachelier, **1839**, Tome 9 pp. 561-567 (accessed via: <http://gallica.bnf.fr> on 21/02/2013)
- 60) Photovoltaic effect: Dictionary.com; Collins English Dictionary - Complete & Unabridged 10th Edition, HarperCollins Publishers, (accessed via: [http://dictionary.reference.com/browse/photovoltaic effect](http://dictionary.reference.com/browse/photovoltaic%20effect) on 28/02/2013).

Redox active molecules with molecular electronics and synthetic applications

- 61) Picture downloaded from Stion PV manufacturer (accessed via: <http://www.stion.com/technology/photovoltaic-effect/> on 01/03/13)
- 62) Picture downloaded from wikipedia article “Sunlight” (accessed via: http://en.wikipedia.org/wiki/File:Solar_Spectrum.png on 01/03/2013)
- 63) Information from the National Renewable Energy Laboratory website. (accessed via: <http://www.nrel.gov> on 28/02/2013)
- 64) The energy savin trust. (accessed via: <http://www.energysavingtrust.org.uk/Generating-energy/Choosing-a-renewable-technology/Solar-panels-PV#3> on 28/02/2013)
- 65) NREL, 2010 Solar Technologies Market Report, US Department of Energy, November **2011** (accessed via: <http://www.nrel.gov> on 28/02/2013)
- 66) L-L. Li, E. W-G. Diau; *Chem. Soc. Rev.*, **2013**, *42*, 291-304. (with kind permission to use artwork from Prof. Diau)
- 67) B. O'Regan, M. Grätzel; *Nature*, **1991**, *353*, 737-740
- 68) Y. Chiba, A. Islam, Y. Watanabe, R. Komiya, N. Koide, L. Han; *Jpn. J. Appl. Phys.*, **2006**, *25*, L638-L640
- 69) A. Yella, H-W. Lee, H. N. Tsao, C. Yi, A. K. Chandiran, Md.K. Nazeeruddin, E. W-G. Diau, C-Y. Yeh, S. M. Zakeeruddin, M. Grätzel; *Nature*, **2011**, *334*, 629-634
- 70) K. W. J. Barnham, G. Duggan; *J. Appl. Phys.*, **1990**, *67*, 3490-3493
- 71) R. J. Ellingson, M. C. Beard, J. C. Johnson, P. Yu, O. I. Micic, A. J. Nozik, A. Shabaev, A. L. Efros; *Nano Lett.*, **2005**, *5*, 865-871
- 72) P. V. Kamat; *J. Phys. Chem. Lett.*, **2013**, Quantum Dot Solar Cells. The Next Big Thing in Photovoltaics, **Just Accepted Manuscript** (Downloaded from <http://pubs.acs.org> on 05/03/2013)
- 73) A. H. Ip, S. M. Thon, S. Hoogland, O. Voznyy, D. Zhitomirsky, R. Debnath, L. Levina, L. R. Rollny, G. H. Carey, A. Fischer, K. W. Kemp, I. J. Kramer, Z. Ning, A. J. Labelle, K. Wei Chou, A. Amassian, E. H. Sargent; *Nature Nanotech.*, **2012**, *7*, 577-582
- 74) H-S. Kim, C-R. Lee, J-H. Im, K-B. Lee, T. Moehl, A. Marchioro, S-J. Moon, R. Humphry-Baker, J-H. Yum, J. E. Moser, M Grätzel, N-G. Park; *Scientific Reports* **2**, **2012**, 591
- 75) K. Sears, G. Fanchini, S. E. Watkins, C. P. Huynh, S. C. Hawkins; *Thin Solid Films*, **2013**, *531*, 525-529
- 76) A. J. Ferguson, J. L. Blackburn, N. Kopidakis; *Mat. Lett.*, **2013**, *90*, 115-125
- 77) T. Kietzke, “Recent Advances in Organic Solar Cells,” *Advances in OptoElectronics*, vol. 2007, Article ID 40285, **2007**
- 78) a) J. E. Anthony; *Chem. Mater.*, **2011**, *23*, 583-590; b) Y. Lin, Y. Lia, X. Zhan; *Chem. Soc. Rev.*, **2012**, *41*, 4245-4272;

- 79) J. Xue, B. P. Rand, S. Uchida, S. R. Forrest; *Adv. Mater.*, **2005**, *17*, 66-71
- 80) G. Wei, X. Xiao, S. Wang, J. D. Zimmerman, K. Sun, V. V. Diev, M. E. Thompson, S. R. Forrest; *Nano Lett.*, **2011**, *11*, 4261-4264
- 81) Z. Li, G. He, X. Wan, Y. Liu, J. Zhou, G. Long, Y. Zuo, M. Zhang, Y. Chen; *Adv. Energ. Mater.*, **2012**, *1*, 74-77; Y. Sun, G. C. Welch, W. L. Leong, C. J. Takacs, G. C. Bazan, A. J. Heeger; *Nature Mater.*, **2012**, *11*, 44-48
- 82) T. Higashihara, M. Ueda; *Macromol. Res.*, **2003**, Precision synthesis of tailor-made polythiophene-based materials and their application to organic solar cells
- 83) Y. Sun, C. Cui, H. Wang, Y. Li, *Adv. Energ. Mater.*, **2011**, *1*, 1058-1061
- 84) L. Dou, J. You, J. Yang, C-C. Chen, Y. He, S. Murase, T. Moriarty, K. Emery, G. Li, Y. Yang; *Nature Photonics*, **2012**, *6*, 180-185
- 85) M. Wang, F. Wudl; *J. Mater. Chem.*, **2012**, *22*, 24297-24314; Y. Li, Q. Guo, Z. Li, J. Pei, W. Tian; *Energy Environ. Sci.*, **2010**, *3*, 1427-1436
- 86) T. L. Chen, Y. Zhang, P. Smith, A. Tamayo, Y. Liu, B. Ma; *Appl. Mater. Interfaces*, **2011**, *3*, 2275-2280; S. Miyanishi, Y. Zhang, K. Tajima, K. Hashimoto; *Chem. Commun.*, **2010**, *46*, 6723-6725
- 87) B. Walker, A. B. Tamayo, X-D. Dang, P. Zalar, J. Hwa Seo, A. Garcia, M. Tantiwiwat, T-Q. Nguyen; *Adv. Funct. Mater.*, **2009**, *19*, 3063-3069
- 88) X. Yu, S. Eymur, V. Singh, B. Yang, M. Tonga, A. Bheemaraju, G. Cooke, C. Subramani, D. Venkataraman, R. J. Stanley, V. M. Rotello; *Phys. Chem. Chem. Phys.*, **2012**, *14*, 6749-6754
- 89) D. D. Kenning, K. A. Mitchell, T. R. Calhoun, M. R. Funfar, D. J. Sattler, S. C. Rasmussen; *J. Org. Chem.*, **2002**, *67*, 9073-9076
- 90) D. Milstein, J. K. Stille; *J. Am. Chem. Soc.*, **1978**, *100*, 3636-3638
- 91) S. Ram, R. E. Ehrenkafer; *Tet. Lett.*, **1984**, *25*, 3415-3418
- 92) a) K. Ramadas, N. Srinivasan; *Synth. Comm.*, **1992**, *22*, 3189-3195; b) C. Mangeney, J.-C. Lacroix, K. I. Chane-Ching, M. Jouini, F. Villain, S. Ammar, S. Ammar, N. Jouini, P.-C. Lacaze; *Chem. Eur. J.*, **2001**, *7*, 5029-5040
- 93) T. Fonseca, B. Gigantea, T. L. Gilchrist; *Tetrahedron*, **2001**, *57*, 1793-1799
- 94) P. Chattopdhyay, R. Rai, P. S. Pandey; *Synth. Comm.*, **2006**, *36*, 1857-1861
- 95) J.-B. Carroll, B. J. Jordan, H. Xu, B. Erdogan, L. Lee, L. Cheng, C. Tiernan, G. Cooke, V. M. Rotello; *Org. Lett.*, **2005**, *7*, 2551-2554
- 96) W. J. Ebenezer, M. G. Hutchings, K. Jones, D. A. Lambert, I. Watt; *Tet. Lett.*, **2007**, *48*, 1641-1643
- 97) C. M. Cardona, W. Li, A. E. Kaifer, D. Stockdale, G. C. Bazan; *Adv. Mater.*, **2011**, *23*, 2367-2371
- 98) J. Pommerehne, H. Vestweber, W. Guss, R. F. Mahrt, H. Bassler, M. Porsch, J. Daub; *Adv. Mater.*, **1995**, *7*, 551-554

- 99) Y-S. Byun, J-H. Kim, J. Baek Park, I-N. Kang, S-H. Jin, D-H. Hwan; *Synth. Met.*, **2013**, *168*, 23-30
- 100) M. Kivala, C. Boudon, J-P. Gisselbrecht, B. Enko, P. Seiler, I. B. Mueller, N. Langer, P. D. Jarowski, G. Gescheidt, F. Diederich; *Chem. Eur. J.*, **2009**, *15*, 4111-4123
- 101) W. R. Hertler, W. Mahler, L. R. Melby, J. S. Miller, R. E. Putscher, O. W. Webster; *Mol. Cryst. Liq. Cryst.*, **1989**, *171*, 205-216; O. W. Webster; *J. Polym. Sci. Part A: Polym. Chem.*, **2002**, *40*, 210-221
- 102) N. N. P. Moonen, C. Boudon, J-P. Gisselbrecht, P. Seiler, M. Gross, F. Diederich; *Angew. Chem. Int. Ed.*, **2002**, *41*, 3044-3047
- 103) N. N. P. Moonen, R. Gist, C. Boudon, J-P. Gisselbrecht, P. Seiler, T. Kawai, A. Kishioka, M. Gross, M. Irie, F. Diederich; *Org. Biomol. Chem.*, **2003**, *1*, 2032-2034
- 104) T. Michinobu, J. C. May, J. H. Lim, C. Boudon, J-P. Gisselbrecht, P. Seiler, M. Gross, I. Biaggio, F. Diederich; *Chem. Commun.*, **2005**, 737-739
- 105) a) T. Michinobu, C. Boudon, J-P. Gisselbrecht, P. Seiler, B. Frank, N. N. P. Moonen, M. Gross, F. Diederich; *Chem. Eur. J.*, **2006**, *12*, 1889-1905; b) M. Kivala, C. Boudon, J-P. Gisselbrecht, P. Seiler, M. Gross, F. Diederich; *Angew. Chem. Int. Ed.*, **2007**, *46*, 6357-6360; c) J. Lorenzo Alonso-Gómez, P. Schanen, P. Rivera-Fuentes, P. Seiler, F. Diederich; *Chem. Eur. J.*, **2008**, *14*, 10564-10568; d) M. Kivala, T. Stanoeva, T. Michinobu, B. Frank, G. Gescheidt, F. Diederich; *Chem. Eur. J.*, **2008**, *14*, 7638-7647
- 106) Y-L. Wu, P. D. Jarowski, W. B. Schweizer, F. Diederich; *Chem. Eur. J.*, **2010**, *16*, 202-211
- 107) X. Xu, S. Chen, G. Yu, C. Di, H. You, D. Ma, Y. Liu; *Adv. Mater.*, **2007**, *19*, 1281-1285
- 108) S. M. Hubig, T. M. Bockman, J. K. Kochi; *J. Am. Chem. Soc.*, **1996**, *118*, 3842-3851
- 109) S. Banerjee, F. Ali, P. K. Nayak, N. Agarwal; *Thin Solid Films*, **2012**, *520*, 2644-2650
- 110) A. Leliege, P. Blanchard, T. Rousseau, J. Roncali; *Org. Lett.*, **2011**, *12*, 3098-3101
- 111) a) Y. Morioka, N. Yoshizawa, J-I. Nishida, Y. Yamashita; *Chem. Lett.*, **2004**, *9*, 1190-1191; b) T. Michinobu; *J. Am. Chem. Soc.*, **2008**, *130*, 14074-14075; c) J. Xu, X. Liu, J. Lu, M. Zhu, C. Huang, W. Zhou, X. Yin, H. Liu, Y. Li, J. Ye; *Langmuir*, **2008**, *24*, 4231-4237; d) T. Shoji, S. Ito, K. Toyota, M. Yasunami, N. Morita; *Chem. Eur. J.*, **2008**, *14*, 8398-8408
- 112) G. Cooke, Y-M. Legrand, V. M. Rotello; *Chem. Commun.*, **2004**, 1088-1089
- 113) K. Sonogashira, Y. Tohda, N. Hagihara; *Tet. Lett.*, **1975**, *16*, 4467-4470

Redox active molecules with molecular electronics and synthetic applications

- 114) A. Komaromi, Z. Novak; *Chem. Commun.*, **2008**, 4968-4970
- 115) D. Seebach, E. J. Corey; *J. Org. Chem.*, **1975**, *40*, 231-237
- 116) A. Arlt, S. Benson, S. Schulthoff, B. Gabor, A. Fürstner; *Chem. Eur. J.*, **2013**, *19*, 3596-3608
- 117) X. Bugaut, F. Glorius; *Chem. Soc. Rev.*, **2012**, *41*, 3511-3522
- 118) M. Süßner, H. Plenio; *Angew. Chem. Int. Ed.*, **2005**, *44*, 6885-6888
- 119) C. A. Fleckenstein, H. Plenio; *Adv. Synth. Catal.*, **2006**, *348*, 1058-1062
- 120) J. Liu, P. He, J. Yan, X. Fang, J. Peng, K. Liu, Y. Fang; *Adv. Mater.*, **2008**, *20*, 2508-2511
- 121) M. A. Hempenius, C. Cirmi, F. Lo Savio, J. Song, G. J. Vancso; *Macromol. Rapid Commun.*, **2010**, *31*, 772-783
- 122) C. K. A. Gregson, V. C. Gibson, N. J. Long, E. L. Marshall, P. J. Oxford, A. J. P. White; *J. Am. Chem. Soc.*, **2006**, *128*, 7410-7411
- 123) O. Diels, K. Alder; *Liebigs Ann. Chem.*, **1928**, *460*, 98-122
- 124) A. F. Khan, S. K. Upadhyay; *Synthesis*, **2009**, *16*, 2773-2777
- 125) J. R. Parry; *Tetrahedron*, **1983**, *39*, 1215
- 126) J. Clayden, P. MacLellan; *Beilstein J. Org. Chem.*, **2011**, *7*, 582.
- 127) C. E. Hoyle, A. B. Lowe, C. N. Bowman; *Chem. Soc. Rev.*, **2010**, *39*, 1355-1387
- 128) C. E. Hoyle, C. N. Bowman; *Angew. Chem. Int. Ed.*, **2010**, *49*, 1540-1573
- 129) a) M. Belley, R. Zamboni; *J. Org. Chem.*, **1989**, *54*, 1230-1232; b) J. R. Cabrero-Antonino, A. Leyva-Pérez, A. Corma; *Adv. Synth. Catal.*, **2012**, *354*, 678-687
- 130) A. B. Lowe; *Polym. Chem.*, **2010**, *1*, 17-36; Q-F. Li, Y. Yang, A. Maleckis, G. Otting, X-C. Su; *Chem. Commun.*, **2012**, 2704-2706
- 131) H. E. Ensley, C. A. Parnell, E. J. Corey; *J. Org. Chem.*, **1978**, *43*, 1610-1612
- 132) E. J. Corey, H. E. Ensley; *J. Am. Chem. Soc.*, **1975**, *97*, 6908-6909
- 133) D. A. Evans, J. Bartroli, T. L. Shih; *J. Am. Chem. Soc.*, **1981**, *103*, 2127-2129
- 134) F. Van Meurs, F. W. Metselaar, A. J. A. Post, J. A. A. M. Van Rossum, A. M. Van Wijk, H. Van Bekkum; *J. Organomet. Chem.*, **1975**, *84*, C22-C24
- 135) V. I. Sokolov, L. L. Troitskaya, N. S. Khrushcheva, O. A. Reutov; *J. Organomet. Chem.*, **1989**, *378*, 227-233
- 136) A. K. Chatterjee, T-L. Choi, D. P. Sanders, R. H. Grubbs; *J. Am. Chem. Soc.*, **2003**, *125*, 11360-11370
- 137) G. L. Thomas, R. J. Spandl, F. G. Glansdorp, M. Welch, A. Bender, J. Cockfield, J. A. Lindsay, C. Bryant, D. F. J. Brown, O. Loiseleur, H. Rudyk, M. Ladlow, D. R. Spring; *Angew. Chem. Int. Ed.*, **2008**, *47*, 2808-2812 (see supporting information for procedure details)
- 138) D-J. Liaw, K-L. Wang, W-H. Chen; *Macromol. Symp.*, **2006**, 68-76

Redox active molecules with molecular electronics and synthetic applications

- 139) C. Pugh; *Macromol. Symp.*, **1994**, *77*, 325-337; H. Yang, F. Zhang, B-P. Lin, P. Keller, X-Q. Zhang, Y. Suna, L-X. Guo; *J. Mater. Chem. C*, **2013**, 1482-1490
- 140) A. S. Abd-El-Aziz, D. J. Winram, P. O. Shipman, L. Bichler; *Macromol. Rapid Commun.*, **2010**, *31*, 1992-1997
- 141) K. Tamura, N. Akutagawa, M. Satoh, J. Wada, T. Masuda; *Macromol. Rapid Commun.*, **2008**, *29*, 1944-1949
- 142) T. Katsumata, J. Qu, M. Shiotsuki, M. Satoh, J. Wada, J. Igarashi, K. Mizoguchi, T. Masuda; *Macromolecules*, **2008**, *41*, 1175-1183